DYNAMIC MODELING, CONTROL AND SIMULATION OF A PLANAR FIVE-LINK BIPEDAL WALKING SYSTEM

BY

CHUNG YING AMY CHAN

A Thesis
Submitted to the Faculty of Graduate Studies
in Partial Fulfillment of the Requirements
for the Degree of

MASTER OF SCIENCE

*****

Department of Mechanical & Industrial Engineering
The University of Manitoba
Winnipeg, Manitoba

THE UNIVERSITY OF MANITOBA

FACULTY OF GRADUATE STUDIES

*****

COPYRIGHT PERMISSION PAGE

Dynamic Modeling, Control and Simulation of a Planar Five-Link Bipedal Walking System

BY

Chung Ying Amy Chan

A Thesis/Practicum submitted to the Faculty of Graduate Studies of The University of Manitoba in partial fulfillment of the requirements of the degree of Master of Science

Abstract

The purpose of this thesis is to contribute to the development of dynamic modeling and control of bipedal locomotion. The locomotion aimed to be realized in this thesis is walking on a flat horizontal surface in the sagittal plane. Firstly, a planar five-link biped robot, which consists of an upper body and two legs, having five degrees of freedom is modeled. The equations of motion are then developed which describe the motion of the bipedal system. The walking motion includes the single support phase, the impact of the free end of the swing leg with the walking surface, and the support end exchange at the end of each step. Secondly, a systematic approach is presented to determine the joint angle profiles from a set of constraint functions for the biped to walk on a flat horizontal surface. Five new constraint functions are proposed in terms of the physical coherent parameters, one of which is to keep the total mechanical energy of the biped at constant. This constraint is meant to test the hypothesis that, given only potential energy at the beginning of the step, the swing leg can be carried over by gravity. One important finding in this study is that it is impossible to design a set of joint angle profiles to keep the mechanical energy constant during the whole step and, regardless of the walking speed, a certain amount of extra energy must be provided to the biped at the beginning of the step. It was further found that given an appropriate amount of energy at the beginning of the step, it is possible to have a set of joint angle profiles such that the swing leg is carried over without any further energy input. These sets of joint angle profiles are of special interest; bipedal models tracking these joint angle profiles are more energy-efficient, since the extra energy input at the beginning of the step may be provided by the strain energy release of the deformable foot. Lastly, motion control of

the bipedal locomotion system with various degrees of parametric uncertainty is studied through the application of the sliding mode control technique and the computed torque control technique. In this work, an integral term is used in the equation of the sliding surface. Through the simulation study, it has been found that this integral term plays an important role in improving the tracking performance of the control system. The sliding mode control algorithm is further modified to eliminate the well-known chattering problem at the discontinuity surface. It was found that the proposed sliding mode control is superior to the computed torque control, especially when parametric uncertainties are present in the system.

Acknowledgements

Foremost, I would like to express my heartfelt gratitude to my advisor, Dr. Christine Q. Wu, for giving me the opportunity to pursue graduate studies. Thank you for providing continuous guidance, patient, encouragement, and sincere appreciation throughout the course of this thesis.

Along with Dr. Wu, I would like to thank Dr. Steve Onyshko, Dr. A.B. Thornton-Trump, and Dr. Nariman Sepehri for providing me with the fundamental background knowledge in the areas of biomechanics, controls and robotics. I would also like to thank my committee members, Dr. Steve Onyshko and Dr. A.B. Thornton-Trump, for their careful review, comments and suggestions with regard to this thesis.

I would like to thank my fellow students in the Nonlinear Systems Research Laboratory for making the last two years enjoyable. I would also like to thank my sister and my friends for their endless support. My sincere appreciation also goes to Rob Rostecki for his careful review and editing of this thesis.

Last but not least, I would like to thank my dad and mom for their infinite love, wisdom, encouragement, support and many sacrifices. Thanks for imprinting the importance of education in my mind and thanks for your confidence in my ability. Without any of these I could not have accomplished my goals.

And to all the others whom I did not mention here who molded me in any way, your support did not go unnoticed. I would like to thank you all from the very bottom of my heart.

Table of Contents

List of Figures

List of Tables

Chapter 1

Introduction

1.1 General Introduction

1.1.1 Motivation

Biped robot is a class of legged robot that is designed to duplicate human type locomotion. For the biped robot there are two kinds of walking: static and dynamic. Static walking is a low speed movement where the system center of gravity is kept within the supporting plane of the foot. The dynamic effects in maintaining the postural stability are ignored (Miyazaki and Arimoto 1980). Dynamic walking, on the other hand, is a high speed movement. During certain time periods, the center of gravity is outside of the supporting plane (Miyazaki and Arimoto 1980). Normal human walking is a kind of dynamic bipedal locomotion. Natural walking is one of the most fundamental motions of the human body. It is a process by which a human moves oneself from one position to another position. Since walking is a learned process, it is not surprising that each individual walks with certain personal characteristics; however, the basic walking pattern is the same. In the process of normal and steady walking, the erect upper body moves forward with one leg supporting the whole body and the other leg swings forward. As

the upper body passes over the support leg, the swing leg has to move ahead of the upper body in preparation for landing on the walking surface and becoming the support leg.

With the availability of powerful computers, dynamic modeling has become a useful mathematical tool for engineers and mathematicians who are interested in analyzing bipedal locomotion to design devices of locomotion for the handicapped, finding the control laws of human walking and deriving the control algorithms of bipedal locomotion machines. In general, dynamic modeling of the bipedal locomotion system includes three parts: (1) development of the mathematical model, (2) designing the joint angle profiles and (3) developing control algorithms for motion regulation. In the following sections, the important aspects of this thesis are briefly highlighted.

1.1.2 Mathematical Model

The procedure for the mathematical modeling of the bipedal locomotion system includes the development of the structure of the complex kinematic model and the development of the dynamic equations of motion.

Human locomotion systems represent extremely complex dynamic systems both from the aspect of mechanical-structural complexity and control system complexity (Vukobratovic et al. 1990). To study this system and its motion requires certain simplifications. A practical bipedal walking machine or biped robot used to study human type locomotion is based on a considerably simplified version of human being. In order to construct the kinematic model of the biped for this study, certain simplifications and assumptions were made. Since in this study the motion of the biped is constrained in the sagittal plane, the biped is considered as a planar model. The sagittal plane is defined by

the vertical axis and the direction of locomotion. The planar bipedal model considered here is a multi-link mechanism that consists of five rigid links with five degrees of rotational freedom. The upper body of the planar bipedal model, which includes the head, arms and trunk, is considered as a massive rigid inverted pendulum. The swing motion of the arms and the motion between the thorax and pelvis are ignored. The upper body is connected to the two legs with two rotational joints. Each leg consists of two massive rigid links as a thigh and a shank. All links are connected with each other by rotational joints. The feet are considered to be massless and therefore, the dynamic structures of the feet are neglected.

Once the simplifications and assumptions of the kinematic model are made, the equations of motion for the locomotion system can be developed. The equations of motion are used as the basis to describe the motion of the bipedal model and for the development of the control algorithm. The single support phase, the effect of impact between the end of the swing leg and the walking surface, and the effect of support leg exchange are considered in this study when developing the equations of motion. A computer program is developed to handle the complex numerical analysis of the dynamic model.

1.1.3 Motion Planning

To design the joint angle profiles that describe human-like locomotion of the biped is another challenging problem. A well-structured approach of designing the joint angle profiles that ties the resulting gait patterns with the physically coherent parameters is desired. Hurmuzlu (1993a) developed a systematic approach that can be followed to

formulate objective functions. Such objective functions were cast in terms of step length, progression speed, maximum clearance of the swing leg, and the support knee bias that could be used to prescribe the gait of a planar five-link bipedal robot during the single support phase. Hurmuzlu's approach is utilized in this study. The objective functions are modified by replacing the constraint functions imposed on the swing leg used in Hurmuzlu's work (1993a) with a constraint function that keeps the mechanical energy as a constant. The intention of keeping the mechanical energy as a constant is to test the hypothesis that given only potential energy at the beginning of the step, the swing leg can be carried over by gravity. This question is answered by the investigation of the simulation results of the desired joint angle profiles.

A major challenge of using this systematic approach to obtain the joint angle profiles is solving a set of equations combined with differential and algebraic equations, which are from the constraint functions. There is no general way to solve this combination of differential and algebraic equations. Besides, in the process of generating the motion, there are two additional conditions imposed on the possible solution that make this problem extremely challenging. The repeatability of movement is a fundamental characteristic of bipedal walking. Only the joint angle profiles satisfying this repeatability condition, i.e., the equality of angles at the beginning and at the end of each step, are acceptable for bipedal locomotion. Another condition is related to the knee of the swing leg. Since there is no locking mechanism imposed on the knee of the swing leg, it is possible that at a certain period of time, in order to satisfy the constraint functions, the knee of the swing leg may bend backward. Walking with the knee bent

backward is not a desirable motion. Therefore, the joint angle profiles obtained must also ensure that the knee of the swing leg does not bend backward during the step.

1.1.4 Motion Control

To control the walking motion of the biped, control algorithms are applied. The success of the control action in tracking the prescribed motion can be measured by two factors: (1) the periodicity of the resulting gait patterns, and (2) the magnitude of the residual tracking error. It is important to note that the system response never coincides with the prescribed one throughout the step cycle for any control action. This is due to system uncertainties and the disturbance caused by the contact event. A successful controller is one that eliminates the uncertainties and disturbance rapidly during the early stage of each step.

The sliding mode control system is known to be highly insensitive to parametric uncertainty and disturbance. The basic idea of the sliding mode control is to transform the original system in one state space into a system in a new state space. A time-varying surface $r(t)$, which is also referred as a sliding surface, is defined in the new state space by equation $r = 0$. This equation represents a set of linear differential equations which has a unique solution that the tracking error is equal to zero. Thus, the problem of tracking the desired trajectories is reduced to that of keeping r at zero. Once the system trajectories lie in the sliding surface, the system trajectories follow the desired one. The control law, however, contains a discontinuous term. Due to the unavoidable delay in switching between the control laws, chattering occurs at the discontinuity surface. In addition, there is a reaching phase problem. In the reaching phase the system trajectories

are sensitive to parameter variations. It is a challenge to design a sliding mode control algorithm that can eliminate all of these problems. A sliding mode control law is derived in this study by replacing the discontinuous term with a continuous one to remove the chattering. Both the sliding mode control and the classical computed torque control are employed for the tracking control action in this study. The tracking performances of these two control techniques are investigated and compared as various degrees of parametric uncertainty exist in the bipedal locomotion system.

1.2 Literature Survey of Dynamic Modeling and Control of Biped Robot

The research conducted in this thesis falls into the area of dynamic modeling, control, and simulation of human and bipedal locomotion. There has long been an interest for engineers, physiologists and mathematicians in understanding bipedal and human locomotion. This is not only because of the desire to build biped robots to perform tasks which are dangerous or degrading to humans, but also to improve devices for humans who have either partially or completely lost their lower limb control. Since the 1970's, many investigators have prompted ongoing research efforts on this topic and many studies have been published.

Dynamic modeling of bipedal locomotion systems is a challenging problem that requires knowledge of multi-link mechanism, nonlinear dynamics, control theory, and stability analysis. The major problem associated with the modeling and control of bipedal locomotion is the large number of degrees of freedom and the highly coupled nonlinear dynamics involved in the locomotion system. For a human, there are more than 300 degrees of freedom involved in the complete skeletal activity. Just for natural human

walking, 20 or more degrees of freedom may be involved (Golliday and Hemami 1977). Such a system involves great dynamic complexity, even if it is idealized to a system of rigid bodies with simple torque generators acting at each joint. Therefore, to study the dynamics of bipedal locomotion systems, it is critical to select mechanical models having few degrees of freedom to keep the equations of motion at a manageable level, and yet having enough degrees of freedom to adequately describe the motions of interest.

The simplest model that can represent some bipedal locomotion activities is a single massive link modeled as an inverted pendulum. Two situations are concerned: (1) the base joint is fixed to the supporting ground, and (2) the base joint moves in space. Several studies addressing some aspects of the inverted pendulum problem for modeling bipedal locomotion system have been published by Hemami and his colleagues. Hemami and his colleagues used a massive inverted pendulum with the base joint fixed to the supporting ground to study the behavior of a body in standing position when no muscle dynamics was involved (Hemami et al. 1973, Golliday and Hemami 1976, Hemami and Camana 1976, Hemami and Golliday 1977). Torques applied at the base joint were equivalent to the ankle joint in human body and maintained the upright vertical position. Chow and Jacobson (1972), on the other hand, considered the postural stability of the upper body and the control of human locomotion with the use of an inverted pendulum. The upper body was modeled as a single link inverted pendulum with the prescribed base point moved only in the vertical direction. It was an important step in the development of a mathematical model of the human body. Wu et al. (1996, 1998) utilized the general single link inverted pendulum problem to model the human upper body during gait. Their mathematical model was developed with a base excited inverted pendulum could

be used to predict major features of the upper body dynamics and to synthesize the mechanisms of walking. However, as pointed out in their paper (Wu et al. 1998), the single inverted pendulum models are too simple to accurately describe a complete locomotion.

Multi-link planar models, with their great complexity, offer the opportunity to study bipedal locomotion and the related properties that are impossible to investigate with the single inverted pendulum model. Hemami and his colleagues have been the pioneering group in studying the postural stability and locomotion related problems of humans using multi-link bipedal models. For example, in the paper of Gubina et al. (1974) they have investigated a partially placed massive torso supported on two massless legs as their bipedal model. The legs were of variable length as a substitute for knee function. The approach of modeling legged locomotion with massless legs used for simplifying the complicated locomotion systems is questionable for bipeds since typically one third of the mass of a human is contained in the legs (Golliday and Hemami 1977). Simple movements such as side stepping in the frontal plane (Goddard et al. 1983), side sway, body sway and sliding foot (Hemami and Wyman 1979a, 1979b, Goddard et al. 1983, Iqbal et al. 1993) were also studied. The main thrust of Hemami's work had been directed toward developing proper methods to represent the equations of motion. Particular emphasis was placed on the incorporation of holonomic and nonholonomic constraints that arose from the interconnection of members and interaction with the environment. In Hemami and Wyman's paper (1979a), dynamic systems with constraints that were either maintained or deliberately violated were considered. The key step in the model was the derivation of the forces of constraint as the functions of the state and the

input of the system. Linearization of the differential equations of the system was used to simplify the complex models in these early studies. Linear feedback stability and control were used.

In the study of the dynamics of human locomotion, many models have been developed. One approach is the direct dynamic problem. In the direct dynamic problem, the moments applied to the system serve as the system inputs and the solutions found is the system kinematics. The study of human locomotion has been investigated by Onyshko and Winter (1980) through the direct dynamic problem. In their study, a model of a seven-link biped was used. Since there were differences between the mathematical model and the human body, the measured data of joint moments were adjusted before being applied to the link segment model to produce a desirable walking cycle. They claimed that no constraints regarding the trajectories of any of the segments had been assumed. They showed that a normal human walking cycle can be achieved and, with minor modification, typical gait patterns could also be achieved. Pandy and Berme (1988) approached the study of human locomotion from the same direction. In their planar model, a damped spring was placed between the hip joint and the support leg ankle to simulate the flexion-extension characteristic of the knee. In this study, the joint moments applied were chosen on the basis of trial and error, but the initial conditions were obtained directly from experimental gait data. Later, Pandy and Berme extended their planar model to a three-dimensional model (1989). The application of torques at the mechanical joints is corresponded to the muscle dynamics of human body that enables the changing of relative positions of mechanical links (Vukobratovic et al. 1990). In this way, gait can be achieved. Another approach used to study human locomotion is the

inverse dynamic problem. In the inverse dynamic problem, the kinematics data is used as the system inputs to find the forces and moments applied to the system. The purpose of solving the inverse dynamic problem in human locomotion is to obtain information on the joint moments and the reaction forces at the joints of human lower extremities (Siegler et al. 1982). The kinematics measurement is obtainable from gait experiment. This problem has been studied by several investigators. Thornton-Trump et al. (1975) determined the translational and angular accelerations of the limb segment from the gait data during normal locomotion. The moments about the joints of the hip and knees and the reaction forces from the floor were then calculated. The reaction forces from the floor and the knee moments were used in the design of an external prosthetic polycentric knee joint. The conventional method of utilizing the experimental kinematic data is by numerical filtering and differentiating techniques. However, numerical differentiating techniques applied to experimentally obtained data will magnify the inherent measurement errors. Chao and Rim (1973) proposed a method based on the mathematical theory of optimization to determine the moments applied at the joints in human lower extremities without the application of numerical differentiation on the measured displacement. Using this method, the results showed less sensitivity to the inherent errors in the measurements. Ladin and Wu (1991) estimated the joint forces and moments from the combination of position and acceleration measurements. The estimated joint forces were then compared to the actual joint forces measured by strain gauges.

Many investigators have been interested in studying bipedal robots. Miura and Shimoyama (1984) developed their three-link biped robots (Biper-3 and Biper-4) to walk

sideways, backward and forward and studied in both the sagittal and frontal planes. The results served as a basis for choosing the appropriate feedback control gains. Furusho and Masubuchi (1986, 1987) developed their reduced order model that could well approximate the original higher order model in almost all walking phases in the sagittal plane. This mathematical model served as the basis for developing their spatial mechanism. They built their first biped (Kenkyaku-1) with a torso and two-link legs with no feet to verify their numerical results experimentally. This model had a steel pipe attached to the lowest end of each leg in order to maintain the lateral balance. Later, this model was improved by adding two more links (Kenkyaku-2) to study the kicking action in the double-support phase (Furusho and Sano 1990). Furusho and Sano (1990) developed a nine-link biped (BLR-G2) which included the foot structure and was equipped with foot pressure and ankle torque sensors to provide information about the conditions of contact with the floor. Their work contributed toward the realization of smooth three-dimensional walking with the sole firmly gripping the floor. The mathematical models given in the above studies served as the basis for building active mechanisms for realization of artificial locomotion.

Another issue related to the modeling of bipedal walking that has often been ignored is impact. Impact occurs as a result of the contact of the free end with the environment. In such contact, the velocities of the upper body and the leg segments are subject to an instantaneous change. Impact and support end switching play a remarkable role in the stability and progression of the bipedal locomotion system (Hurmuzlu and Moskowitz 1987), which has been avoided by some locomotion studies. Vukobratovic et al. (1970, 1990) and Park and Kim (1998) imposed a condition that the velocities at the

beginning and at the end of the step are the same to avoid the effect of impact. Katoh and Mori (1984) avoided the impact effect by using dynamic constraint functions that yielded smooth foot landing. Hurmuzlu's studies (Hurmuzlu 1993a, 1993b, Hurmuzlu and Basdogan 1994) had focused on the dynamics and control of biped gait. Hurmuzlu and Moskowitz (1986) first introduced the idea of including impact and support end switching in locomotion systems. In Hurmuzlu and Moskowitz's work (1987), they demonstrated the effect of impact and support end switching in the locomotion system with a very simple model. The study conducted by Zheng and Hemami (1984) also confirmed that impact has a significant effect on the stability of bipedal systems, but their treatment of impact was not considered in the same context as Hurmuzlu and Moskowitz (1987). Tzafestas et al. (1996) developed a 5-link biped robot to study the forward walking motion in the sagittal plane. Their 5-link bipedal model consisted of a torso, two thighs and two shanks. These links were connected via four rotational joints, which were considered to be friction-free and driven by independent actuators. The advantage of their five-link model is that it has sufficiently few degrees of freedom to keep the equations of motion to a manageable level, while still having enough degrees of freedom to adequately describe the walking motion that includes the impact between the free end of the swing leg and the walking surface.

Design of joint angle profiles for bipedal robots to imitate human type locomotion is another challenging problem. Most of the previous studies did not consider or define a method to design the joint angle profile. For example, Furusho and Masubuchi (1986, 1987) verified their numerical results experimentally by using a walking machine that demonstrated several walking patterns. However, the method to specify the joint angle

profile was never presented. Katoh and Mori (1984) used coupled van der Pol's equations to prescribe the motion for their bipedal model with telescopic legs, but there was no direct relation established between the parameters in the equations and the resulting walking patterns. Bay and Hemami (1987) also used a set of van der Pol oscillators in a network which were configured and used to model the central pattern generator. With adjustments of the parameters in the coupled van der Pol oscillators, the model could be made to generate various kinematic trajectories in periodic wave patterns that were close to those of human walking gait. Similar to Katoh and Mori (1984), there was no direct relation established between the resulting gait patterns and the adjustable parameters. In the work of Lee et al. (1988), they divided the single support phase into five distinct states with manually selected reference angles at each time instant. The trajectory was then formulated by polynomial interpolation. Channon et al. (1992) also formulated their trajectories as a third order polynomial equation, the coefficients of which are obtained by numerically minimizing the energy cost function. In Tzafestas et al. (1996), the joint angle profiles were manually selected to fit certain constraints. In the work of Hemami and Farnsworth (1977), the prescribed trajectories of the ankle, hip and knee angles were the time functions obtained from a computer-television interface system. The television system was employed to monitor a person walking and the computer-linked system measured the angles and smoothed them by computing the Fourier harmonics of each angle. Likewise, Vukobratovic et al. (1980, 1990) used measured human walking data as the desired joint angle profile. However, a practical walking machine is considerably simpler than a human being. The validity of minimizing the dynamics of a system without a good knowledge of its internal structure

and strategies is questionable. All of the above approaches to the problem of prescribing the motion of bipedal machines appear to fall short in terms of possessing a well-defined structure to address the design process. Consequently, it is desirable to develop a well-structured parametric formulation that ties the objective functions to the resulting gait patterns. Such objective functions are cast in terms of physically coherent parameters such as step length, progression speed, etc. Hurmuzlu (1993a, 1993b) developed a systematic approach that can be followed to formulate objective functions, which could be used to prescribe the gait of a planar five-link bipedal robot during the single support phase. The objective functions for locomotion were formulated in terms of four basic quantities which completely characterized the motion of the biped during the single support phase. The four quantities are step length, progression speed, maximum clearance of the swing limb and stance knee bias. This method is a more natural approach for planning joint angle profiles. Silva and Machado (1998) used a similar method for their joint trajectory design.

Motion control of the bipedal robots is a challenging problem due to the high degree of complexity and the efficiency needed to maintain balance. In most of the early studies, the nonlinear bipedal systems were linearized about the upright position. Based on the linearized system, linear feedback stability and control were used (Golliday and Hemami 1976, Hemami and Farnsworth 1977, Hemami and Golliday 1977, Hemami and Wyman 1979a, Hemami et al. 1980, Goddard et al. 1983). In these works, pole assignment was used to compute the feedback control gain. Since bipedal locomotion systems are highly nonlinear, linear controllers are not suitable to handle such systems (Slotine and Li 1991).

Physiological studies have pointed out that the control of human walking has a hierarchical structure (Furusho and Masubuchi 1987). Hierarchical control has been used in robot control. The control structure most often used with robots consists of four levels. The highest level makes decisions on how the task imposed is to be accomplished. The strategic level divides the imposed operation into elementary movements. The tactical level distributes the elementary movement to the motion of each degree of freedom, and the executive level executes the imposed motion of each degree of freedom (Borovac et al. 1989). Miyazaki and Arimoto (1980) proposed a useful hierarchical control strategy for their low order model. The control algorithm consisted of two parts. In the first part, the control torques for slow motion were determined by the motion of the center of gravity. In the second part, control torques in high speed motion were determined to track the predefined trajectory. Furusho and Masubuchi (1986, 1987) utilized hierarchical control in their reduced order model. They adopted a local feedback at each joint as the lower level control. Borovac et al. (1989) constructed a hierarchical control with two levels. The first level was defined to control the system to follow the desired trajectories in the absence of any perturbation. The second level was defined to force the actual system state vector to the desired motion whenever a disturbance was present. A similar control structure with the use of force-feedback was presented by Vukobratovic and Stokic (1980) for the application of decentralized control. For real-time control of the bipedal system in their study, instead of performing the on-line calculations of new dynamic states based on solving differential equations representing the momentary equilibrium state of the system, only the deviations of moments where the dynamic reactions act in the system to support contact were calculated. The perturbing moments

were then transformed into control signals to stabilize the locomotion. Shih (1996) constructed a two-level hierarchical control structure for a bipedal walking robot with seven degrees of freedom. The trajectory planning for the walking pattern was executed at the upper level and the servo control for the planned trajectory was executed at the lower level. The servo control consisted of the computed gravity plus the proportional plus derivative (PD) control was set up to follow the planned trajectory to realize a stable walking motion. Furusho and Sano (1990) also used a hierarchical control structure in the experiment of their nine-link biped (BLR-G2). Their control was sensor-based. At the lower level, it provided feedback control for each DC servomotor. The control mode at the lower level could be switched to position, torque or free rotation mode depending on the switching signal from the higher level. At the higher level, the switching signal was generated by using sensor information and control switching algorithms. Their work focused on the role of force/torque control of the sole and ankle during dynamic walking. Their biped achieved smooth three-dimensional walking based on information obtained from various sensors.

Neural network control is another type of controller that is often used for motion regulation of bipedal locomotion. Neural network control is based on the mechanism of neuronal network. It consists of interconnected processing elements, a mechanism for producing the network's response, and a method to encode information (Holzreiter and Köhle 1993). A neural network can be trained with cases to produce a specific response to an input pattern and can learn to improve its performance. Holzreiter and Köhle (1993) presented a way to use neural networks for the classification of gait patterns, which was close to a statistical method. Asides from classifying gait patterns, the neural

network was used as multi-dimensional nonlinear transformation algorithms for the design of mathematical models. It was also useful for analysis of how different walking speeds and treatments affect the shape of a specific gait pattern. Rodrigues et al. (1996) tried to develop a self-learning controller for the bipedal locomotion system to study the possibility of controlling bipedal locomotion without giving any kind of information about the system dynamics and known walking patterns. A Genetic Algorithm (GA) was used as a search method to find the necessary torque in each joint to obtain a desired trajectory for the biped's upper body center of mass. Rodrigues et al. (1996) suggested that the neural network could be trained with a set of patterns of elementary motions obtained from the GA. In a series of real time experimental studies by Miller and his colleagues (1994, 1996, 1999), neural network learning was shown to be effective for dynamic control problems in bipedal robots. They developed the hardware of a cerebellar model arithmetic computer (CMAC) neural network design to provide submillisecond response and training times. Miller (1994) presented preliminary real-time results of a study on the application of on-line neural network learning to the problem of biped walking with dynamic balance. Low-level on-line learning control strategies using the CMAC neural network enabled the biped to balance during changes in standing posture and to link short steps without falling. Kun and Miller (1996) developed an adaptive dynamic balance scheme for a biped robot using neural control and tested the scheme on an experimental biped. The CMAC neural network was used for the adaptive control of side-to-side and front-to-back balance. Test results showed that the biped performance improved with neural network training. This balance scheme was proven able to control variable-speed gaits in a later study by Kun and Miller (1999).

An artificial neural network was used by Srinivasan et al. (1992) as a new approach to modeling rhythmic movement control. They suggested that human locomotion is a rhythmic movement and is generated by the nervous system. The central pattern generators are a group of neurons that, because of their synaptic connections and inherent properties, oscillatory output behavior results. A hierarchical neural network structure consisting of four modules with a pattern generator at the top was proposed. The artificial neural network was applied to the control of an active external orthosis for use by paraplegics (Guiraud 1994). This control method was flexible to customize the dynamics according to the patient's own limb. The author suggested that the control should be capable of adapting to each combination of patient and orthosis by learning the system's transfer function.

Other nonlinear control methods were developed. Katoh and Mori (1984) designed a nonlinear controller to assure asymptotic stability convergence to the stable limit cycle solutions of coupled van der Pol's equations. The advantage of this control method is that the bipedal locomotion can be controlled by adjusting only a few parameters in the van der Pol's equations. Cotsaftis and Vibet (1988) developed a direct nonlinear decoupling method (DNDM). Based on this method, a control law that gave decoupled control of a two-dimensional biped was derived only from the knowledge of the Lagrangian of the system. The use of DNDM in designing a two-dimensional biped is simple and efficient because the differential equations of the system are not required in the derivation of the control torque for driving the biped mechanism. The differential equation of the system, on the other hand, can be derived from the control algorithms.

Computed torque control is a classical nonlinear control based on the feedback linearization technique. This control technique requires the parameters in the dynamic model of the system to be exactly known for good control performance. Tzafestas et al. (1996) employed a pure computed torque control for the robust control of a five-link biped robot. In their work, the performance of the computed torque control technique was satisfactory when no parametric uncertainty existed in the system. They also showed that the computed torque control technique was superior to the simple local PD control. Chevallereau et al. (1998) used a modified computed torque control in which a physical constraint was taken into account. The physical constraint was the reaction force that prevented the foot from sliding or taking off. This method showed good performance for the bipedal walking in their study. A control method based on the computed torque control was presented by Park and Kim (1998). The computed torque controller applied on the swing leg was used to track the motion of the joint angle and the controller applied on the support leg was used to stabilize the error dynamics of the base link position. The simulation results of this study also showed that the computed torque controllers work very well. In Park and Chung's work (2000), they proposed a new hybrid control method, a combination of impedance control and computed torque control, to control biped robot locomotion. The impedance control was used for the swing leg and the computed torque control was used for the support leg. The simulation results showed that the proposed controller was superior to the pure computed torque controller, especially in reducing impact and stabilizing foot placement. They also showed that the proposed controller made the biped more robust in regard to parametric uncertainty. Another hybrid control was proposed by Vukobratovic and Timcenko (1996). This

hybrid approach combined the traditional model-based and fuzzy logic-based control techniques. The model-based decentralized control scheme was extended by fuzzy logic-based tuners for modifying parameters of the joint servo controllers. The simulation experiments demonstrated the suitability of this hybrid approach for improving the performance of the bipedal locomotion robot.

In physical systems, uncertainties regarding the values of parameters usually exist. Adaptive inverse dynamic based control is one of the nonlinear controllers used to deal with constant or slowly varying uncertainties. Adaptive control is an approach to estimate the uncertain parameters on-line based on the measured signals and to use the estimated parameters in the control input computation (Slotine and Li 1991). The effectiveness of this control method for bipedal locomotion was investigated using a kneeless biped (Yang 1994) and a five-link biped (Yang and Shahabuddin 1994). It was suggested that the difficulty of using such control for bipedal locomotion was in dealing with different sets of nonlinear dynamic equations for different phases, each of whose duration was usually very short. Satisfactory performances were obtained. The simulation results showed that the tracking errors were improved as compared to the initial setting and the performances were robust.

The sliding mode control technique has received considerable attention in the control of bipedal locomotion mainly because sliding model control systems are highly insensitive to parameter variations and disturbances (Slotine and Sastry 1983, Slotine 1984, Bailey and Arapostathis 1987, Paden and Sastry 1987, Slotine1991). It is more desirable than adaptive control for dealing with disturbances, quickly varying parameters, and unmodeled dynamics (Slotine and Li 1991). A sliding surface must be designed for

the sliding mode control law. The motion control problem is to get the system trajectories to track the desired trajectories, which is equivalent to maintaining the system trajectories on the sliding surface. Ideally, the classical sliding mode control method will result in perfect tracking of the desired trajectory. However, there are important drawbacks in this method. Due to the unavoidable delay in switching between control laws at the discontinuity surface, trajectories' chattering rather than sliding on the surface is resulted. Chattering is generally undesirable in practice, since it involves extremely high control activity, and may excite high-frequency unmodeled dynamics (Slotine and Sastry 1983). Another drawback is the reaching phase, a phase in which the trajectories starting from the given initial condition off the sliding surface tend toward the sliding surface. The trajectories in this phase are sensitive to parameter variations. Tzafestas and his colleagues (1996) have investigated the robustness of the biped system through sliding mode control. They further demonstrated that sliding mode control is superior to computed torque control and local PD control for bipedal locomotion when parametric uncertainty exists in the system. A sliding mode control law with a saturation function replacing the discontinuous term was used in Tzafestas et al. (1996). The same control law had been used in Slotine et al. (1983, 1984, 1991) to smooth out the chattering. This control law maintained the system's trajectories close to the sliding surface within a thin boundary layer instead of on the surface. Chang and Hurmuzlu (1992, 1993) developed a sliding mode control for a five-link bipedal robot without a reaching phase. A sliding mode control law with the discontinuous term replaced by a saturation function was also used. In addition, Chang and Hurmuzlu modified the vector of tracking error and redefined the sliding surface. For arbitrary initial conditions, the modified tracking errors

were zero. Thus, the initial state of the system lay on the new sliding domain leading to the elimination of the reaching phase. The simulation results verified that such a controller was capable of achieving steady gait. Lee et al. (1988) developed a control scheme for controlling dynamic walking in the sagittal and the frontal plane independently. The Model Following plus Variable Structure Systems (sliding mode control) technique was developed to control dynamic walking in the sagittal plane, while the Nonlinear Feedback plus Modified α-Computed Torque technique was developed to control dynamic walking in the frontal plane. Simulation results showed that the proposed algorithms could achieve stable and steady walking and could achieve trajectory tracking in the presence of modeling errors.

1.3 Objectives of This Thesis

The goal of this thesis is to contribute to the development of the dynamic modeling and control of a five-link bipedal locomotion system walking on a flat horizontal surface. The dynamic modeling of such a bipedal locomotion system starts with the development of the mathematical model that describes the motion of the bipedal locomotion system. A kinematic bipedal model that consists of five rigid links, which are connected by four pure rotational joints, is used in this study. The bipedal locomotion system has five degrees of rotational freedom with the motion in the sagittal plane. The first objective is to develop the mathematical model that describes a complete walking motion. Such a model includes the single support phase, the impact with the walking surface phase, and the support end exchange phase. The second objective is to present a systematic methodology for designing the joint angle profiles which can prescribe the

motion of walking on a flat horizontal surface for the planar five-link biped. New constraint functions are developed from the kinematic relations of the bipedal model for generating the joint angle profiles. The modeling is completed with the application of control algorithms to regulate the motion of the biped to follow the prescribed motion. The third objective is to improve the traditional sliding mode control algorithm so that the chattering problem and the reaching phase problem are eliminated and, at the same time, good tracking performance can be obtained. The tracking performance of the sliding mode control technique is to be compared to the performance of the computed torque control technique in both situations where parametric uncertainty is absent or present in the system. The development of a good computer program is a very important part of this thesis because all the information of the behavior of the bipedal locomotion system and the performance of the control algorithms are provided by the computer simulation results.

1.4 Thesis Organization

The remaining chapters in this thesis are organized as follows. Chapter 2 outlines the mathematical model development of the five-link biped robot in the sagittal plane. The methodology for developing the equations of motion, which is based on Largrangian formulation, is presented in detail. Chapter 3 presents the methodology for planning joint angle profiles of the five-link biped robot. The joint angle profiles of the five-link biped robot are generated to prescribe walking on a flat horizontal surface. Chapter 4 deals with the motion control strategy. The development of sliding mode control and computed torque control are presented in detail. Chapter 5 presents two major simulation

results. One result is the desired joint angle profiles designed using the methodology developed in Chapter 3. Another results are the outputs of the simulation study with the sliding mode control and computed torque control applied to the bipedal locomotion system to regulate the motion. The robustness of each of the two control techniques is investigated as various degrees of parametric uncertainty exist in the system. The final conclusion and the future work recommendation are presented in Chapter 6.

Chapter 2

Mathematical Model of the Five-Link Biped Robot

2.1 Introduction

This chapter outlines the methodology employed to develop the equations of motion that can describe the walking motion of a five-link biped robot. Brief background information about mathematical modeling of a biped robot is given in Section 2.2. The kinematic model of a five-link biped robot in the sagittal plane is introduced in Section 2.3. The five-link biped robot consists of five rigid links that are connected by four purely rotational joints with one degree of rotational freedom each. The detailed procedure for the derivation of the equations of motion is presented. In Section 2.4, the equations of motion are developed through the standard procedure of Lagrangian formulation. Three phases are included in the mathematical model of the biped robot walking on a flat horizontal surface during one walking step: (1) the "single support" phase, (2) the "impact with walking surface" phase, and (3) the "support end exchange" phase. In this section, two sets of equations of motion are developed, which fully describe the locomotion during the single support phase and the impact with walking surface phase. The techniques for handling the impact of the free end of the swing leg

with the walking surface at the completion of each step and the support end exchange are also presented.

2.2 Background Information

Mathematical modeling of a bipedal locomotion system has been a challenging problem for many researchers. This is mainly due to the dynamic complexity of linkage systems with many degrees of freedom (Gubina et al. 1974). The dynamic behavior of a bipedal locomotion system is described in terms of the time rate of change of the linkage configuration in relation to the joint torques. This relationship can be expressed by a set of differential equations, called equations of motion. For a human walking motion, 20 or more degrees of freedom may be involved. This is difficult to handle mathematically. Hence, it is critical to select kinematic models having sufficiently few degrees of freedom to keep the equations of motion to a manageable level, and yet having enough degrees of freedom to adequately describe the motion. It is sufficient for studies of the dynamics of posture to employ a mechanical model of inverted pendulums with no more than three degrees of freedom (torso, thigh, and shank) (Golliday and Hemami 1977). However, when locomotion is considered, many more degrees of freedom that arise from the motion of the two legs and their associated segments are involved. Bipedal locomotion generally consists of alternately placing the foot of each leg against the surface so that the leg can support and drive the bipedal body forward. By observing natural human walking, two main phases comprise one walking cycle. During the support phase, the foot is on the walking surface, whereas during the swing phase the foot is no longer in contact with the walking surface and is swinging forward in preparation for the next

contact. The support phase can be subdivided into three separate phases: (1) first double support, when both feet are in contact with the ground, (2) single leg support, where one foot is swinging through space and the other foot is in contact with the ground, and (3) second double support, when both feet are again in contact with the ground (Vaughan et al. 1992). For normal walking motion, there is a natural symmetry between the left side and the right. Thus the first double support for one leg is the second double support for another leg. The five-link bipedal model studied in this thesis is a simplified model that is sufficient to describe walking motion in the sagittal plane. Similar five-link bipedal models were also studied by Furusho and Masubuchi (1986, 1987), Cotsaftis and Vibet (1988), Lee et al. (1988), Chang and Hurmuzlu (1992), Hurmuzlu (1993a, 1993b), and Tzafestas et al. (1996). In this study, the walking motion of the five-link biped robot is in the sagittal plane and only includes the single support phase, the impact with walking surface phase, and the support end exchange phase. To simplify the analysis, the double support phase is not included in the walking motion.

The equations of motion describing the dynamics of the bipedal locomotion system can be developed by utilizing the Lagrangian formulation or the Newton-Euler formulation. The Newton-Euler formulation is derived directly by interpreting the Newton's Second Law of Motion, which describes dynamic systems in terms of force and momentum. The equations of motion incorporate all the forces and moments acting on the individual links, including the coupling forces and moments between links. Therefore, additional arithmetic operations are required to eliminate these terms in order to obtain explicit relations between the joint torques and the resultant motion in terms of joint displacements. Lagrangian formulation describes the system's dynamic behavior in

terms of work and energy using generalized coordinates, which reduces the number of equations needed to describe the motion. Lagrangian formulation has the advantage that only the kinetic and potential energies of the system are required to be computed and all the workless forces and constraint forces can be automatically eliminated (Murray et al. 1994). The resultant equations are generally compact and provide a closed-form expression in terms of joint torques and joint displacements. Furthermore, the derivation of the Lagrangian formulation is more systematic than the Newton-Euler formulation (Asada and Slotine 1986). The principle of Lagrangian formulation has been employed to develop the equations of motion describing the dynamics of the bipedal locomotion system since the 1970's, for example, in Gubina et al. (1974), Hemami and Golliday (1977), Hemami and Wyman (1979a, 1979b), Miyazaki and Arimoto (1980), Onyshko and Winter (1980), Furusho and Sano (1990), and Tzafestas et al. (1996). The Lagrangian formulation is employed in this thesis to develop the equations of motion describing the dynamics of the locomotion system.

2.3 The Kinematic Model of the Five-Link Biped Robot

The kinematic model of the five-link biped robot is briefly presented in this section. The biped robot studied here is modeled for walking on a flat horizontal plane surface only. The five-link bipedal model employed to investigate dynamic walking is shown in Figure 2.1. This bipedal model consists of five rigid links, one link for the upper body (link 3) and two links for the thighs, (link 2 and link 4), and the two links for the shanks, (link 1 and link 5). These links are connected to one another by four purely rotational joints; two joints at the hip and two joints at the knees. These rotational joints

are considered to be frictionless and are driven by independent motors. To simplify our analysis, the following assumptions of the model are made:

(1) The feet of the bipedal model are massless.

(2) There is point contact between the tip of the support leg and the walking surface.

(3) The left side and the right side of the bipedal model are symmetric.

(4) The bipedal model is constrained in the sagittal plane.

(5) There is sufficient friction between the foot and the walking surface to prevent slippage.

Although we neglected the dynamic of the feet by assuming massless feet and point contact between the tip of the lower limb and the walking surface, we still allow the biped to apply torque at the ankles to increase or decrease its speed during walking.

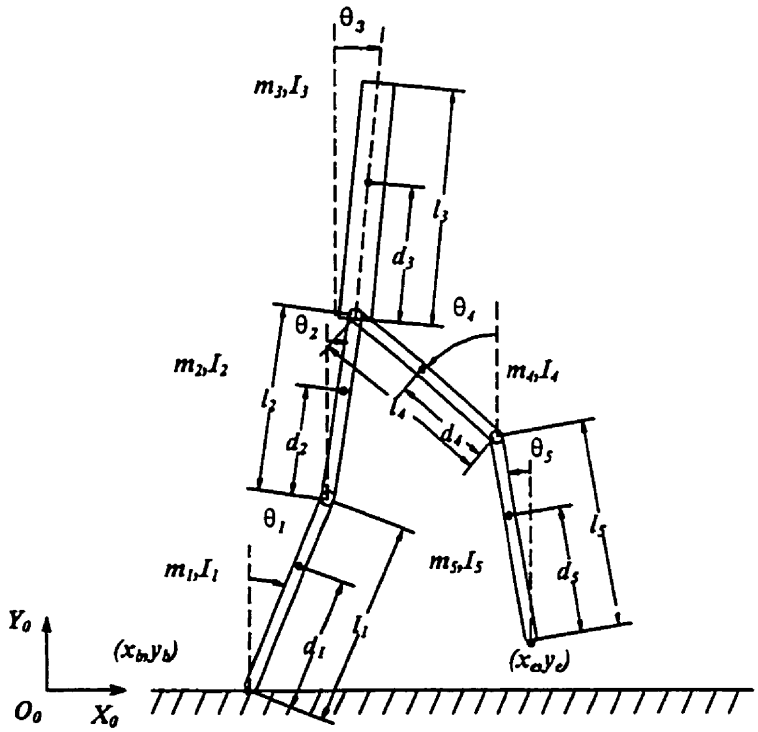

Figure 2.1 Five-Link Biped Robot

The parameters that are shown in Figure 2.1 are as follows:

m_i - mass of link i

l_i - length of link i

d_i - distance between the center of mass and the lower joint of link i

I_i - moment of inertia of link i with respect to the axis which passes through the center of mass of link i and perpendicular to the sagittal plane.

θ_i - angle of link i with respect to the vertical

(x_e, y_e) - the position of the tip of the swing leg

(x_b, y_b) - the position of the point of support

O_o-X_o-Y_o - the fixed coordinate frame

According to the kinematic relationship between links shown in Figure 2.1 (note the reference directions for all angles), the position and the velocity of the free end of the swing leg can be defined. The position of the free end is formulated as

$$\begin{aligned} x_e &= x_b + \ell_1 \sin\theta_1 + \ell_2 \sin\theta_2 + \ell_4 \sin\theta_4 + \ell_5 \sin\theta_5 \\ y_e &= y_b + \ell_1 \cos\theta_1 + \ell_2 \cos\theta_2 + \ell_4 \cos\theta_4 + \ell_5 \cos\theta_5 \end{aligned} \tag{2.1}$$

and the velocity of the free end is

$$v_e = \begin{Bmatrix} \dot{x}_e \\ \dot{y}_e \end{Bmatrix} = \begin{pmatrix} \ell_1 \cos\theta_1 \\ -\ell_1 \sin\theta_1 \end{pmatrix} \dot{\theta}_1 + \begin{pmatrix} \ell_2 \cos\theta_2 \\ -\ell_2 \sin\theta_2 \end{pmatrix} \dot{\theta}_2 + \begin{pmatrix} \ell_4 \cos\theta_4 \\ \ell_4 \sin\theta_4 \end{pmatrix} \dot{\theta}_4 + \begin{pmatrix} \ell_5 \cos\theta_5 \\ \ell_5 \sin\theta_5 \end{pmatrix} \dot{\theta}_5 \tag{2.2}$$

According to the kinematic relationship between links, the coordinate of the center of mass (cgx, cgy) of the bipedal model and the coordinate of the center of mass (xc_i, yc_i) of each link i can also be presented as the following:

$$\begin{aligned} cgx &= \frac{m_1 xc_1 + m_2 xc_2 + m_3 xc_3 + m_4 xc_4 + m_5 xc_5}{m_1 + m_2 + m_3 + m_4 + m_5} \\ cgy &= \frac{m_1 yc_1 + m_2 yc_2 + m_3 yc_3 + m_4 yc_4 + m_5 yc_5}{m_1 + m_2 + m_3 + m_4 + m_5} \end{aligned} \tag{2.3}$$

and

$$
\begin{aligned}
xc_1 &= d_1 \sin\theta_1 \\
yc_1 &= d_1 \cos\theta_1 \\
xc_2 &= \ell_1 \sin\theta_1 + d_2 \sin\theta_2 \\
yc_2 &= \ell_1 \cos\theta_1 + d_2 \cos\theta_2 \\
xc_3 &= \ell_1 \sin\theta_1 + \ell_2 \sin\theta_2 + d_3 \sin\theta_3 \\
yc_3 &= \ell_1 \cos\theta_1 + \ell_2 \cos\theta_2 + d_3 \cos\theta_3 \\
xc_4 &= \ell_1 \sin\theta_1 + \ell_2 \sin\theta_2 + (\ell_4 - d_4)\sin\theta_4 \\
yc_4 &= \ell_1 \cos\theta_1 + \ell_2 \cos\theta_2 - (\ell_4 - d_4)\cos\theta_4 \\
xc_5 &= \ell_1 \sin\theta_1 + \ell_2 \sin\theta_2 + \ell_4 \sin\theta_4 + (\ell_5 - d_5)\sin\theta_5 \\
yc_5 &= \ell_1 \cos\theta_1 + \ell_2 \cos\theta_2 - \ell_4 \cos\theta_4 - (\ell_5 - d_5)\cos\theta_5
\end{aligned}
\tag{2.4}
$$

The linear velocity of the center of mass of each link is represented as follows:

$$
\begin{aligned}
vc_1 &= \begin{pmatrix} d_1 \cos\theta_1 \\ -d_1 \sin\theta_1 \end{pmatrix} \dot{\theta}_1 \\
vc_2 &= \begin{pmatrix} \ell_1 \cos\theta_1 \\ -\ell_1 \sin\theta_1 \end{pmatrix} \dot{\theta}_1 + \begin{pmatrix} d_2 \cos\theta_2 \\ -d_2 \sin\theta_2 \end{pmatrix} \dot{\theta}_2 \\
vc_3 &= \begin{pmatrix} \ell_1 \cos\theta_1 \\ -\ell_1 \sin\theta_1 \end{pmatrix} \dot{\theta}_1 + \begin{pmatrix} \ell_2 \cos\theta_2 \\ -\ell_2 \sin\theta_2 \end{pmatrix} \dot{\theta}_2 + \begin{pmatrix} d_3 \cos\theta_3 \\ -d_3 \sin\theta_3 \end{pmatrix} \dot{\theta}_3 \\
vc_4 &= \begin{pmatrix} \ell_1 \cos\theta_1 \\ -\ell_1 \sin\theta_1 \end{pmatrix} \dot{\theta}_1 + \begin{pmatrix} \ell_2 \cos\theta_2 \\ -\ell_2 \sin\theta_2 \end{pmatrix} \dot{\theta}_2 + \begin{pmatrix} (\ell_4 - d_4)\cos\theta_4 \\ (\ell_4 - d_4)\sin\theta_4 \end{pmatrix} \dot{\theta}_4 \\
vc_5 &= \begin{pmatrix} \ell_1 \cos\theta_1 \\ -\ell_1 \sin\theta_1 \end{pmatrix} \dot{\theta}_1 + \begin{pmatrix} \ell_2 \cos\theta_2 \\ -\ell_2 \sin\theta_2 \end{pmatrix} \dot{\theta}_2 + \begin{pmatrix} \ell_4 \cos\theta_4 \\ \ell_4 \sin\theta_4 \end{pmatrix} \dot{\theta}_4 + \begin{pmatrix} (\ell_5 - d_5)\cos\theta_5 \\ (\ell_5 - d_5)\sin\theta_5 \end{pmatrix} \dot{\theta}_5
\end{aligned}
\tag{2.5}
$$

2.4 Equations of Motion

The locomotion of the biped walking on a flat horizontal surface is constrained in the sagittal plane. One complete gait cycle of walking in the forward direction, which is considered for modeling in this study, includes four stages: (1) left or right leg is in contact with the walking surface supporting the whole body while the other leg swings in the forward walking direction, (2) the swing leg then comes into sudden contact with the walking surface at the completion of the swinging motion and becomes the support leg, (3) the leg, which was the swing leg, is now the support leg carrying the weight of the

whole body and the other leg swings forward, and (4) this swing leg then comes into sudden contact with the walking surface and becomes the support leg again. This gait cycle repeats to transport the upper body from one position to another position. As mentioned previously, by assuming the left side and right side of the bipedal model to be symmetric, the walking motion can be simplified. One step is considered to be half of a gait cycle. The walking motion of one step is divided into three distinct phases: the "single support" phase, the "impact with walking surface" phase and the "support end exchange" phase.

2.4.1 Single Support Phase

The single support phase is a continuous forward motion during which the biped robot has one leg (the support leg) in contact with the walking surface carrying all the weight of the biped's body and one leg (the swing leg) swinging in the air in the forward walking direction. The friction of the ground is assumed to be sufficiently large so that no slippage at the support end with the walking surface can be ensured. A dynamic model with one leg (the support leg) attached to the walking surface is employed to develop a set of equations of motion during the single support phase. The constraints of x_b and y_b are constant and $\dot{x}_b = \dot{y}_b = 0$ are valid during this phase. The configuration of the dynamic model is shown on Figure 2.2. It has to be noticed that the positive direction of angles θ_1, θ_2 and θ_3 is defined as clockwise from the vertical and the positive direction of angles θ_4 and θ_5 is defined as counter-clockwise from the vertical.

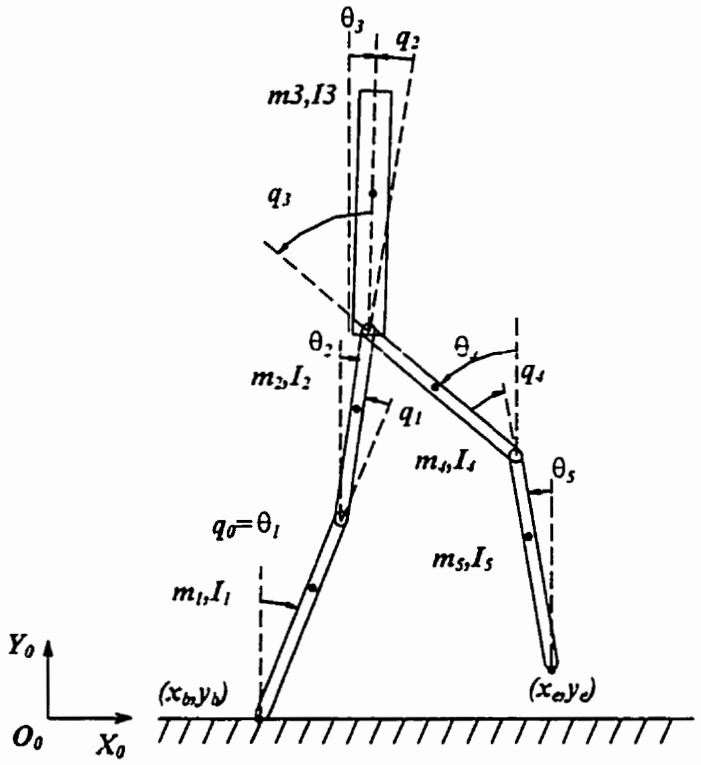

Figure 2.2 Biped with One Support Leg

The derivation of the equations of motion for the open kinematic chain used to describe the motion of the biped robot in this single support phase follows the standard procedure of Lagrangian formulation (Murray et al. 1994). The Lagrangian formulation of the five-link system is given by the difference between kinetic and potential energies:

$$L = K - P \tag{2.6}$$

The potential energy is given by:

$$P = \sum_{i=1}^{5} P_i \qquad \text{with} \quad P_i = m_i \cdot g \cdot yc_i \tag{2.7}$$

where

g is the gravitational acceleration (g=9.81 m/sec^2)

and yc_i is determined from equation (2.4).

The kinetic energy is given by:

$$K = \sum_{i=1}^{5} K_i \qquad \text{with} \quad K_i = \frac{1}{2} m_i v c_i^{\,2} + \frac{1}{2} I_i \dot{\theta}_i^{\,2} \tag{2.8}$$

Substituting yc_i from equation (2.4) into equation (2.7) and vc_i from equation (2.5) into equation (2.8), and applying some dynamic manipulation, the kinetic energy and potential energy for each link are formulated as follows:

Link 1

$$\begin{aligned} K_1 &= \frac{1}{2}(I_1 + m_1 d_1^{\,2})\dot{\theta}_1^{\,2} \\ P_1 &= m_1 g d_1 \cos\theta_1 \end{aligned} \tag{2.9}$$

Link 2

$$\begin{aligned} K_2 &= \frac{1}{2}\left[I_2 + m_2 d_2^{\,2}\right]\dot{\theta}_2^{\,2} + \frac{1}{2} m_2 \ell_1^{\,2}\dot{\theta}_1^{\,2} + m_2 \ell_1 d_2 \cos(\theta_1 - \theta_2)\dot{\theta}_1\dot{\theta}_2 \\ P_2 &= m_2 g(\ell_1 \cos\theta_1 + d_2 \cos\theta_2) \end{aligned} \tag{2.10}$$

Link 3

$$\begin{aligned} K_3 &= \frac{1}{2}\left[I_3 + m_3 d_3^{\,2}\right]\dot{\theta}_3^{\,2} + \frac{1}{2} m_3[\ell_1^{\,2}\dot{\theta}_1^{\,2} + \ell_2^{\,2}\dot{\theta}_2^{\,2} + 2\ell_1\ell_2 \cos(\theta_1 - \theta_2)\dot{\theta}_1\dot{\theta}_2 \\ &\quad + 2\ell_1 d_3 \cos(\theta_1 - \theta_3)\dot{\theta}_1\dot{\theta}_3 + 2\ell_2 d_3 \cos(\theta_2 - \theta_3)\dot{\theta}_2\dot{\theta}_3] \\ P_3 &= m_3 g(\ell_1 \cos\theta_1 + \ell_2 \cos\theta_2 + d_3 \cos\theta_3) \end{aligned} \tag{2.11}$$

Link 4

$$\begin{aligned} K_4 &= \frac{1}{2}\left[I_4 + m_4(\ell_4 - d_4)\right]\dot{\theta}_4^{\,2} + \frac{1}{2} m_4[\ell_1^{\,2}\dot{\theta}_1^{\,2} + \ell_2^{\,2}\dot{\theta}_2^{\,2} + 2\ell_1\ell_2 \cos(\theta_1 - \theta_2)\dot{\theta}_1\dot{\theta}_2 \\ &\quad + 2\ell_1(\ell_4 - d_4)\cos(\theta_1 + \theta_4)\dot{\theta}_1\dot{\theta}_4 + 2\ell_2(\ell_4 - d_4)\cos(\theta_2 + \theta_4)\dot{\theta}_2\dot{\theta}_4] \\ P_4 &= m_4 g(l_1 \cos\theta_1 + l_2 \cos\theta_2 - (\ell_4 - d_4)\cos\theta_4) \end{aligned} \tag{2.12}$$

Link 5

$$\begin{aligned} K_5 &= \frac{1}{2}\left[I_5 + m_5(\ell_5 - d_5)^2\right]\dot{\theta}_5^{\,2} + \frac{1}{2} m_5[\ell_1^{\,2}\dot{\theta}_1^{\,2} + \ell_2^{\,2}\dot{\theta}_2^{\,2} + \ell_4^{\,2}\dot{\theta}_4^{\,2} + 2\ell_1\ell_2 \cos(\theta_1 - \theta_2)\dot{\theta}_1\dot{\theta}_2 \\ &\quad + 2\ell_1\ell_4 \cos(\theta_1 + \theta_4)\dot{\theta}_1\dot{\theta}_4 + 2\ell_1(\ell_5 - d_5)\cos(\theta_1 + \theta_5)\dot{\theta}_1\dot{\theta}_5 + 2\ell_2\ell_4 \cos(\theta_2 + \theta_4)\dot{\theta}_2\dot{\theta}_4 \\ &\quad 2\ell_2(\ell_5 - d_5)\cos(\theta_2 + \theta_5)\dot{\theta}_2\dot{\theta}_5 + 2\ell_4(\ell_5 - d_5)\cos(\theta_4 - \theta_5)\dot{\theta}_4\dot{\theta}_5] \\ P_5 &= m_5 g(\ell_1 \cos\theta_1 + \ell_2 \cos\theta_2 - \ell_4 \cos\theta_4 - (\ell_5 - d_5)\cos\theta_5) \end{aligned} \tag{2.13}$$

The Lagrangian equation of motion is in the form as follows:

$$\frac{d}{dt}\left\{\frac{\partial L}{\partial \dot{q}_i}\right\} - \frac{\partial L}{\partial q_i} = T_i \tag{2.14}$$

The detailed procedure of formulating the Lagrangian equation of motion can be found in Appendix I. Equation (2.14) can be rearranged into the following standard form:

$$\underline{D}(\underline{\theta})\ddot{\underline{\theta}} + \underline{h}(\underline{\theta},\dot{\underline{\theta}})\dot{\underline{\theta}} + \underline{G}(\underline{\theta}) = T_\theta \tag{2.15}$$

where

$$\underline{\theta} = [\theta_1, \theta_2, \theta_3, \theta_4, \theta_5]^T$$

$$\underline{T}_\theta = [T_{\theta 1}, T_{\theta 2}, T_{\theta 3}, T_{\theta 4}, T_{\theta 5}]^T$$

Each term in equation (2.15) is formulated as follows:

$$\underline{D}(\underline{\theta}) = D_{ij}(\underline{\theta}) \quad (i, j = 1,2,\ldots 5) \tag{2.16}$$

where

$$\begin{aligned}
D_{11} &= I_1 + m_1 d_1^{\,2} + (m_2 + m_3 + m_4 + m_5)\ell_1^{\,2} \\
D_{12} &= [m_2 \ell_1 d_2 + (m_3 + m_4 + m_5)\ell_1 \ell_2]\cos(\theta_1 - \theta_2) \\
D_{13} &= [m_3 \ell_1 d_3]\cos(\theta_1 - \theta_3) \\
D_{14} &= [m_4 \ell_1 (\ell_4 - d_4) + m_5 \ell_1 \ell_4]\cos(\theta_1 + \theta_4) \\
D_{15} &= [m_5 \ell_1 (\ell_5 - d_5)]\cos(\theta_1 + \theta_5)
\end{aligned}$$

$$\begin{aligned}
D_{21} &= D_{12} \\
D_{22} &= I_2 + m_2 d_2^{\,2} + (m_3 + m_4 + m_5)\ell_2^{\,2} \\
D_{23} &= [m_3 \ell_2 d_3]\cos(\theta_2 - \theta_3) \\
D_{24} &= [m_4 \ell_2 (\ell_4 - d_4) + m_5 \ell_2 \ell_4]\cos(\theta_2 + \theta_4) \\
D_{25} &= [m_5 \ell_2 (\ell_5 - d_5)]\cos(\theta_2 + \theta_5)
\end{aligned}$$

$$\begin{aligned}
D_{31} &= D_{13} \\
D_{32} &= D_{23} \\
D_{33} &= I_3 + m_3 d_3^{\,2} \\
D_{34} &= D_{35} = 0
\end{aligned}$$

$$\begin{aligned}
D_{41} &= D_{14} \\
D_{42} &= D_{24} \\
D_{43} &= D_{34} \\
D_{44} &= I_4 + m_4 (\ell_4 - d_4)^2 + m_5 \ell_4^{\,2} \\
D_{45} &= [m_5 \ell_4 (\ell_5 - d_5)]\cos(\theta_4 - \theta_5)
\end{aligned}$$

$$
\begin{aligned}
D_{51} &= D_{15} \\
D_{52} &= D_{25} \\
D_{53} &= D_{35} \\
D_{54} &= D_{45} \\
D_{55} &= I_5 + m_5(\ell_5 - d_5)^2
\end{aligned}
$$

$$
\underline{h}(\underline{\theta}, \dot{\underline{\theta}})\dot{\underline{\theta}} = col\left[\sum_{1\,(j\neq i)}^{5} h_{ijj}\dot{\theta}_j^{\,2}\right] \tag{2.17}
$$

$$
\begin{aligned}
h_{122} &= [m_2\ell_1 d_2 + (m_3 + m_4 + m_5)\ell_1\ell_2]\sin(\theta_1 - \theta_2) \\
h_{133} &= [m_3\ell_1 d_3]\sin(\theta_1 - \theta_3) \\
h_{144} &= -[m_4\ell_1(\ell_4 - d_4) + m_5\ell_1\ell_4]\sin(\theta_1 + \theta_4) \\
h_{155} &= -[m_5\ell_1(\ell_5 - d_5)]\sin(\theta_1 + \theta_5)
\end{aligned}
$$

$$
\begin{aligned}
h_{211} &= -h_{122} \\
h_{233} &= [m_3\ell_2 d_3]\sin(\theta_2 - \theta_3) \\
h_{244} &= -[m_4\ell_2(\ell_4 - d_4) + m_5\ell_2\ell_4]\sin(\theta_2 + \theta_4) \\
h_{255} &= -[m_5\ell_2(\ell_5 - d_5)]\sin(\theta_2 + \theta_5)
\end{aligned}
$$

$$
\begin{aligned}
h_{311} &= -h_{133} \\
h_{322} &= h_{233} \\
h_{344} &= h_{355} = 0
\end{aligned}
$$

$$
\begin{aligned}
h_{411} &= h_{144} \\
h_{422} &= h_{244} \\
h_{433} &= 0 \\
h_{455} &= [m_5\ell_4(\ell_5 - d_5)]\sin(\theta_4 - \theta_5)
\end{aligned}
$$

$$
\begin{aligned}
h_{511} &= h_{155} \\
h_{522} &= h_{255} \\
h_{533} &= 0 \\
h_{544} &= -h_{455}
\end{aligned}
$$

$$
\begin{aligned}
G_1 &= -[m_1 d_1 + m_2\ell_1 + m_3\ell_1 + m_4\ell_1 + m_5\ell_1]g\sin\theta_1 \\
G_2 &= -[m_2 d_2 + m_3\ell_2 + m_4\ell_2 + m_5\ell_2]g\sin\theta_2 \\
G_3 &= -[m_3 d_3]g\sin\theta_3 \\
G_4 &= [m_4(\ell_4 - d_4) + m_5\ell_4]g\sin\theta_4 \\
G_5 &= [m_5(\ell_5 - d_5)]g\sin\theta_5
\end{aligned} \tag{2.18}
$$

The equation of motion (2.15) is further modified into equation (2.19) using the relative angle for the control purpose.

$$
\underline{D}_q(\underline{q})\ddot{\underline{q}} + \underline{h}_q(\underline{q}, \dot{\underline{q}})\dot{\underline{q}} + \underline{G}_q(q) = \underline{T}_q \tag{2.19}
$$

where $\underline{D}_q(q)$ is the 5×5 symmetric, positive definite inertia matrix, $\underline{h}_q(q, \dot{q})\dot{q}$ is the 5×1

vector of centripetal and Coriolis torques, $\underline{G}_q(q)$ is the 5×1 vector representing gravitational torques, and $\underline{T}_q$ is the 5×1 vector of control torque applied at each joint. The relative angles (q_i) between links are used instead of the absolute angle θ_i of each link (see Figure 2.2). The relationship between the relative angles (q_i) and the absolute angles (θ_i) is as follows:

$$q_0 = \theta_1 \qquad q_1 = \theta_1 - \theta_2 \qquad q_2 = \theta_2 - \theta_3$$
$$q_3 = \theta_3 + \theta_4 \qquad q_4 = \theta_4 - \theta_5$$

The detail modification of the equations of motion (2.19) can be found in Appendix II. The same set of equations of motion is used for both the left leg support, as well as the right leg support.

2.4.2 Impact with Walking Surface Phase

At the completion of each step, the swing leg (leading leg in contact) comes into a sudden contact (impact) with the walking surface. The angular velocity of each joint will be subjected to jump discontinuities. The support end of the biped is then transferred to the tip of the swing leg and the support leg (trailing leg in contact) leaves the walking surface immediately. That is the moment the biped robot is not supported by either leg. The constraints of x_b and y_b are constant and $\dot{x}_b = \dot{y}_b = 0$, which were valid in the single support phase, are violated. This implies that neither of the equations of motion (2.15) nor (2.19) can be used here. The dynamic model developed for the single support phase cannot apply to this phase. The biped robot is so treated as both legs are in the air and another set of equations of motion must be derived. The dynamic model of the biped with both legs in the air is shown in Figure 2.3. To fully describe the configuration and

the position of the biped, in addition to θ_i (i=1, 2...5), the coordinates x_b and y_b at the end of the trailing leg of the bipedal model are also needed.

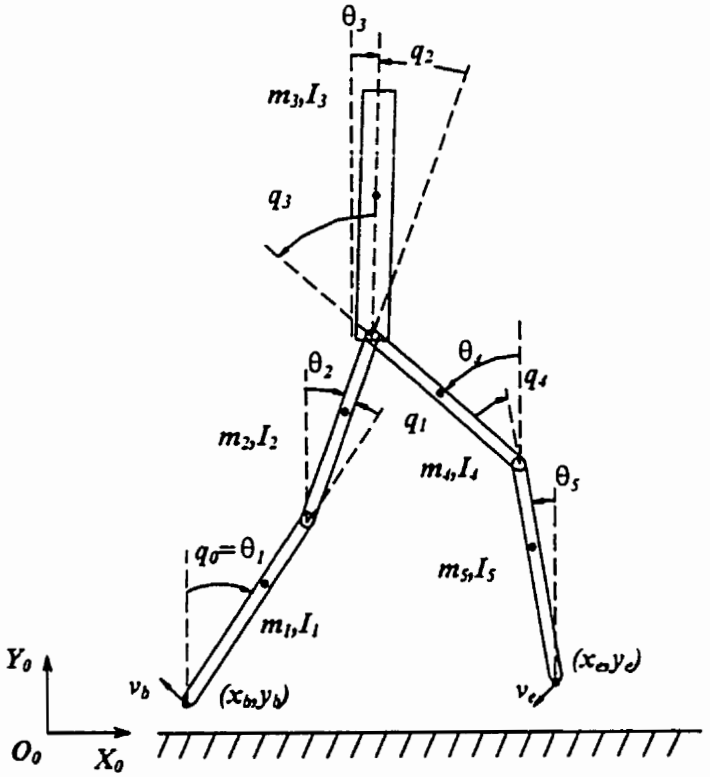

Figure 2.3 Biped with Both Legs in Air

From the configuration of the biped robot in Figure 2.3, the coordinate and the velocity of the center of mass of each link are as follows:

$$
\begin{aligned}
xc_1 &= x_b + d_1 \sin\theta_1 \\
yc_1 &= y_b + d_1 \cos\theta_1 \\
xc_2 &= x_b + \ell_1 \sin\theta_1 + d_2 \sin\theta_2 \\
yc_2 &= y_b + \ell_1 \cos\theta_1 + d_2 \cos\theta_2 \\
xc_3 &= x_b + \ell_1 \sin\theta_1 + \ell_2 \sin\theta_2 + d_3 \sin\theta_3 \\
yc_3 &= y_b + \ell_1 \cos\theta_1 + \ell_2 \cos\theta_2 + d_3 \cos\theta_3 \\
xc_4 &= x_b + \ell_1 \sin\theta_1 + \ell_2 \sin\theta_2 + (\ell_4 - d_4)\sin\theta_4 \\
yc_4 &= y_b + \ell_1 \cos\theta_1 + \ell_2 \cos\theta_2 - (\ell_4 - d_4)\cos\theta_4 \\
xc_5 &= x_b + \ell_1 \sin\theta_1 + \ell_2 \sin\theta_2 + \ell_4 \sin\theta_4 + (\ell_5 - d_5)\sin\theta_5 \\
yc_5 &= y_b + \ell_1 \cos\theta_1 + \ell_2 \cos\theta_2 - \ell_4 \cos\theta_4 - (\ell_5 - d_5)\cos\theta_5
\end{aligned}
\tag{2.20}
$$

and

$$
\begin{aligned}
vc_1 &= \begin{pmatrix} \dot{x}_b \\ \dot{y}_b \end{pmatrix} + \begin{pmatrix} d_1 \cos\theta_1 \\ -d_1 \sin\theta_1 \end{pmatrix} \dot{\theta}_1 \\
vc_2 &= \begin{pmatrix} \dot{x}_b \\ \dot{y}_b \end{pmatrix} + \begin{pmatrix} \ell_1 \cos\theta_1 \\ -\ell_1 \sin\theta_1 \end{pmatrix} \dot{\theta}_1 + \begin{pmatrix} d_2 \cos\theta_2 \\ -d_2 \sin\theta_2 \end{pmatrix} \dot{\theta}_2 \\
vc_3 &= \begin{pmatrix} \dot{x}_b \\ \dot{y}_b \end{pmatrix} + \begin{pmatrix} \ell_1 \cos\theta_1 \\ -\ell_1 \sin\theta_1 \end{pmatrix} \dot{\theta}_1 + \begin{pmatrix} \ell_2 \cos\theta_2 \\ -\ell_2 \sin\theta_2 \end{pmatrix} \dot{\theta}_2 + \begin{pmatrix} d_3 \cos\theta_3 \\ -d_3 \sin\theta_3 \end{pmatrix} \dot{\theta}_3 \\
vc_4 &= \begin{pmatrix} \dot{x}_b \\ \dot{y}_b \end{pmatrix} + \begin{pmatrix} \ell_1 \cos\theta_1 \\ -\ell_1 \sin\theta_1 \end{pmatrix} \dot{\theta}_1 + \begin{pmatrix} \ell_2 \cos\theta_2 \\ -\ell_2 \sin\theta_2 \end{pmatrix} \dot{\theta}_2 + \begin{pmatrix} (\ell_4 - d_4)\cos\theta_4 \\ (\ell_4 - d_4)\sin\theta_4 \end{pmatrix} \dot{\theta}_4 \\
vc_5 &= \begin{pmatrix} \dot{x}_b \\ \dot{y}_b \end{pmatrix} + \begin{pmatrix} \ell_1 \cos\theta_1 \\ -\ell_1 \sin\theta_1 \end{pmatrix} \dot{\theta}_1 + \begin{pmatrix} \ell_2 \cos\theta_2 \\ -\ell_2 \sin\theta_2 \end{pmatrix} \dot{\theta}_2 + \begin{pmatrix} \ell_4 \cos\theta_4 \\ \ell_4 \sin\theta_4 \end{pmatrix} \dot{\theta}_4 + \begin{pmatrix} (\ell_5 - d_5)\cos\theta_5 \\ (\ell_5 - d_5)\sin\theta_5 \end{pmatrix} \dot{\theta}_5
\end{aligned}
\tag{2.21}
$$

Following the same procedure as for the single support phase, the kinetic energy and the potential energy equations for each link can be determined as follows:

Link 1

$$
\begin{aligned}
K_1 &= \frac{1}{2}(I_1 + m_1 d_1^{\,2})\dot{\theta}_1^{\,2} + \frac{1}{2} m_1 [\dot{x}_b^{\,2} + \dot{y}_b^{\,2} + 2 d_1 \dot{\theta}_1 (\dot{x}_b \cos\theta_1 - \dot{y}_b \sin\theta_1)] \\
P_1 &= m_1 g (y_b + d_1 \cos\theta_1)
\end{aligned}
\tag{2.22}
$$

Link 2

$$
\begin{aligned}
K_2 &= \frac{1}{2}\left[I_2 + m_2 d_2^{\,2}\right]\dot{\theta}_2^{\,2} + \frac{1}{2} m_2 (\ell_1^{\,2}\dot{\theta}_1^{\,2} + 2\ell_1 \dot{\theta}_1 (\dot{x}_b \cos\theta_1 - \dot{y}_b \sin\theta_1) \\
&\quad + 2 d_2 \dot{\theta}_2 (\dot{x}_b \cos\theta_2 - \dot{y}_b \sin\theta_2) + 2\ell_1 d_2 \cos(\theta_1 - \theta_2)\dot{\theta}_1 \dot{\theta}_2) + \frac{1}{2} m_2 (\dot{x}_b^{\,2} + \dot{y}_b^{\,2}) \\
P_2 &= m_2 g (y_b + \ell_1 \cos\theta_1 + d_2 \cos\theta_2)
\end{aligned}
\tag{2.23}
$$

Link 3

$$
\begin{aligned}
K_3 &= \frac{1}{2}\left[I_3 + m_3 d_3^{\,2}\right]\dot{\theta}_3^{\,2} + \frac{1}{2} m_3 [\ell_1^{\,2}\dot{\theta}_1^{\,2} + \ell_2^{\,2}\dot{\theta}_2^{\,2} + 2\ell_1\ell_2 \cos(\theta_1 - \theta_2)\dot{\theta}_1\dot{\theta}_2 \\
&\quad + 2\ell_1 d_3 \cos(\theta_1 - \theta_3)\dot{\theta}_1\dot{\theta}_3 + 2\ell_2 d_3 \cos(\theta_2 - \theta_3)\dot{\theta}_2\dot{\theta}_3] \\
&\quad + \frac{1}{2} m_3 [\dot{x}_b^{\,2} + \dot{y}_b^{\,2} + 2\ell_1 \dot{\theta}_1 (\dot{x}_b \cos\theta_1 - \dot{y}_b \sin\theta_1) + 2\ell_2 \dot{\theta}_2 (\dot{x}_b \cos\theta_2 - \dot{y}_b \sin\theta_2) \\
&\quad + 2 d_3 \dot{\theta}_3 (\dot{x}_b \cos\theta_3 - \dot{y}_b \sin\theta_3)] \\
P_3 &= m_3 g (y_b + \ell_1 \cos\theta_1 + \ell_2 \cos\theta_2 + d_3 \cos\theta_3)
\end{aligned}
\tag{2.24}
$$

Link 4

$$K_4 = \frac{1}{2}\left[I_4 + m_4(\ell_4 - d_4)^2\right]\dot{\theta}_4^2 + \frac{1}{2}m_4[\ell_1^2\dot{\theta}_1^2 + \ell_2^2\dot{\theta}_2^2 + 2\ell_1\ell_2\cos(\theta_1 - \theta_2)\dot{\theta}_1\dot{\theta}_2$$
$$+ 2\ell_1\ell_4\cos(\theta_1 + \theta_4)\dot{\theta}_1\dot{\theta}_4 + 2\ell_2(\ell_4 - d_4)\cos(\theta_2 + \theta_4)\dot{\theta}_2\dot{\theta}_4]$$
$$+ \frac{1}{2}m_4[\dot{x}_b^2 + \dot{y}_b^2 + 2\ell_1\dot{\theta}_1(\dot{x}_b\cos\theta_1 - \dot{y}_b\sin\theta_1) + 2\ell_2\dot{\theta}_2(\dot{x}_b\cos\theta_2 - \dot{y}_b\sin\theta_2)$$
$$+ 2(\ell_4 - d_4)\dot{\theta}_4(\dot{x}_b\cos\theta_4 + \dot{y}_b\sin\theta_4)]$$
$$P_4 = m_4 g(y_b + \ell_1\cos\theta_1 + \ell_2\cos\theta_2 - (\ell_4 - d_4)\cos\theta_4) \qquad (2.25)$$

Link 5

$$K_5 = \frac{1}{2}\left[I_5 + m_5(\ell_5 - d_5)^2\right]\dot{\theta}_5^2 + \frac{1}{2}m_5[\ell_1^2\dot{\theta}_1^2 + \ell_2^2\dot{\theta}_2^2 + \ell_4^2\dot{\theta}_4^2 + 2\ell_1\ell_2\cos(\theta_1 - \theta_2)\dot{\theta}_1\dot{\theta}_2$$
$$+ 2\ell_1\ell_4\cos(\theta_1 + \theta_4)\dot{\theta}_1\dot{\theta}_4 + 2\ell_1(\ell_5 - d_5)\cos(\theta_1 + \theta_5)\dot{\theta}_1\dot{\theta}_5 + 2\ell_2\ell_4\cos(\theta_2 + \theta_4)\dot{\theta}_2\dot{\theta}_4$$
$$2\ell_2(\ell_5 - d_5)\cos(\theta_2 + \theta_5)\dot{\theta}_2\dot{\theta}_5 + 2\ell_4(\ell_5 - d_5)\cos(\theta_4 - \theta_5)\dot{\theta}_4\dot{\theta}_5]$$
$$+ \frac{1}{2}m_5[\dot{x}_b^2 + \dot{y}_b^2 + 2\ell_1\dot{\theta}_1(\dot{x}_b\cos\theta_1 - \dot{y}_b\sin\theta_1) + 2\ell_2\dot{\theta}_2(\dot{x}_b\cos\theta_2 - \dot{y}_b\sin\theta_2)$$
$$+ 2\ell_4\dot{\theta}_4(\dot{x}_b\cos\theta_4 + \dot{y}_b\sin\theta_4) + 2(\ell_5 - d_5)\dot{\theta}_5(\dot{x}_b\cos\theta_5 + \dot{y}_b\sin\theta_5)]$$
$$P_5 = m_5 g(y_b + \ell_1\cos\theta_1 + \ell_2\cos\theta_2 - \ell_4\cos\theta_4 - (\ell_5 - d_5)\cos\theta_5) \qquad (2.26)$$

The equations of motion are derived by substituting equations (2.22) to (2.26) into the Lagrangian equation of motion (2.27).

$$\frac{d}{dt}\left\{\frac{\partial K}{\partial\dot{\theta}_{ai}}\right\} - \frac{\partial K}{\partial\theta_{ai}} + \frac{\partial P}{\partial\theta_{ai}} = T_{ai} \qquad (2.27)$$

By rearranging the equation (2.27), the equations of motion can be written into the following standard from:

$$\underline{D}_a(\underline{\theta}_a)\ddot{\underline{\theta}}_a + \underline{h}_a(\underline{\theta}_a, \dot{\underline{\theta}}_a)\dot{\underline{\theta}}_a + \underline{G}_a(\underline{\theta}_a) = \underline{T}_a \qquad (2.28)$$

where $\theta_a=[\theta_1\ \theta_2\ \theta_3\ \theta_4\ \theta_5\ x_b\ y_b]$, θ_i, (i=1,2,...,5) represents the angle of each link with respect to the vertical, and (x_b, y_b) is the position of the point of support.

Each term in equation (2.28) is derived as follows:

$D_{aij} = D_{ij}$ $(i, j = 1,2,\ldots,5)$ (from equation (2.16))

$$
\begin{aligned}
D_{a16} &= [m_1 d_1 + (m_2 + m_3 + m_4 + m_5)\ell_1]\cos\theta_1 \\
D_{a17} &= -[m_1 d_1 + (m_2 + m_3 + m_4 + m_5)\ell_1]\sin\theta_1 \\
D_{a26} &= [m_2 d_2 + (m_3 + m_4 + m_5)\ell_2]\cos\theta_2 \\
D_{a27} &= -[m_2 d_2 + (m_3 + m_4 + m_5)\ell_2]\sin\theta_2 \\
D_{a36} &= [m_3 d_3]\cos\theta_3 \\
D_{a37} &= -[m_3 d_3]\sin\theta_3 \\
D_{a46} &= [m_4(\ell_4 - d_4) + m_5\ell_4]\cos\theta_4 \\
D_{a47} &= [m_4(\ell_4 - d_4) + m_5\ell_4]\sin\theta_4 \\
D_{a56} &= [m_5(\ell_5 - d_5)]\cos\theta_5 \\
D_{a57} &= [m_5(\ell_5 - d_5)]\sin\theta_5
\end{aligned}
\tag{2.29}
$$

$$
D_{a61} = D_{a16} \quad D_{a62} = D_{a26} \quad D_{a63} = D_{a36}
$$
$$
D_{a64} = D_{a46} \quad D_{a65} = D_{a56}
$$
$$
D_{a66} = (m_1 + m_2 + m_3 + m_4 + m_5)
$$
$$
D_{a67} = 0
$$
$$
D_{a71} = D_{a17} \quad D_{a72} = D_{a27} \quad D_{a73} = D_{a37}
$$
$$
D_{a74} = D_{a47} \quad D_{a75} = D_{a57}
$$
$$
D_{a76} = 0
$$
$$
D_{a77} = (m_1 + m_2 + m_3 + m_4 + m_5)
$$

$$
h_{a7} = \sum_{j=1}^{7} h_{a7jj} \text{ where } j \neq 7
$$
$$
h_{a711} = -[m_1 d_1 + (m_2 + m_3 + m_4 + m_5)\ell_1]\dot{\theta}_1^{\,2}\cos\theta_1
$$
$$
h_{a722} = -[m_2 d_2 + (m_3 + m_4 + m_5)\ell_2]\dot{\theta}_2^{\,2}\cos\theta_2
$$
$$
h_{a733} = -[m_3 d_3]\dot{\theta}_3^{\,2}\cos\theta_3
$$
$$
h_{a744} = [m_4(\ell_4 - d_4) + m_5\ell_4]\dot{\theta}_4^{\,2}\cos\theta_4
$$
$$
h_{a755} = [m_5(\ell_5 - d_5)]\dot{\theta}_5^{\,2}\cos\theta_5
$$
$$
h_{a766} = 0
$$
$$
\underline{h}_a(\underline{\theta}_a, \dot{\underline{\theta}}_a)\dot{\underline{\theta}}_a = col[h_{ai}] \quad (i = 1,2,\ldots,7) \tag{2.30}
$$
$$
h_{ai} = h_i \quad (i = 1,2,\ldots,5) \qquad \text{(from equation (2.17))}
$$

$$
h_{a6} = \sum_{j=1}^{7} h_{a6jj} \text{ where } j \neq 6
$$
$$
h_{a611} = -[m_1 d_1 + (m_2 + m_3 + m_4 + m_5)\ell_1]\dot{\theta}_1^{\,2}\sin\theta_1
$$
$$
h_{a622} = -[m_2 d_2 + (m_3 + m_4 + m_5)\ell_2]\dot{\theta}_2^{\,2}\sin\theta_2
$$
$$
h_{a633} = -[m_3 d_3]\dot{\theta}_3^{\,2}\sin\theta_3
$$
$$
h_{a644} = -[m_4(\ell_4 - d_4) + m_5\ell_4]\dot{\theta}_4^{\,2}\sin\theta_4
$$
$$
h_{a655} = -[m_5(\ell_5 - d_5)]\dot{\theta}_5^{\,2}\sin\theta_5
$$
$$
h_{a677} = 0
$$

$$
G_{ai} = G_i \quad (i = 1,2\ldots,5) \qquad \text{(from equation (2.18)}
$$
$$
G_{a6} = 0 \tag{2.31}
$$
$$
G_{a7} = (m_1 + m_2 + m_3 + m_4 + m_5)g
$$

$$T_{ai} = T_{\theta i} \quad (i = 1,2\ldots,5)$$
$$T_{a6} = T_{a7} = 0 \tag{2.32}$$

The detailed derivation of the above equations of motion (2.28) can be found in Appendix III. The equations of motion (2.28) are used for the calculation of the instantaneous changes of joint angular velocities at the moment when the free end of the swing leg collides with the walking surface.

During the single support phase, the free end of the swing leg is moving in the forward direction. It gets ahead of the body and comes into sudden contact with the walking surface at the moment of the completion of each step. At this instant, the impact phase takes place. This is assumed to take place in an infinitely small time interval and to be perfectly plastic. Perfectly plastic is defined as the situation in which the tip of the swing leg does not leave the walking surface after impact with the walking surface and the velocity $\underline{v}_e$ of the tip of the swing leg immediately becomes zero. Due to the collision with the walking surface, there are sudden changes in the angular velocity of each joint. It is therefore necessary to compute the new joint velocities each time just after each collision between the free end and the walking surface. It is assumed that there are no changes in the angle displacements of the joints.

The equation representing the impact can be formulated by the following procedure. Let $\underline{x}_e$ be the position of the free end of the swing leg, with respect to the fixed coordinate frame, which comes into contact with the walking surface. We can express it as

$$\underline{x}_e = \underline{x}_e(\theta) \tag{2.33}$$

where $\theta = [\theta_1,\ldots,\theta_n]^T$ is the vector of generalized coordinates of the system.

If $\underline{x}_{contact}$ is the contact point, the impact will occur when

$$\underline{x}_e(\theta)=\underline{x}_{contact} \tag{2.34}$$

This represents an external constraint to the motion, which implies that a generalized constraint force F is introduced into the system (Tzafestas et al. 1996),

$$\underline{F}_\delta = \left[\frac{\partial \underline{x}_e}{\partial \underline{\theta}_a}\right]^T \underline{\lambda} = \underline{J}_a{}^T \underline{\lambda} \tag{2.35}$$

where $\underline{J}_a$ is the Jacobian and $\underline{\lambda}$ is a suitable column vector of Lagrange multipliers. The equations of motion just before the impact are the same as (2.28)

$$\underline{D}_a(\underline{\theta}_a)\ddot{\underline{\theta}}_a + \underline{h}_a(\underline{\theta}_a,\dot{\underline{\theta}}_a)\dot{\underline{\theta}}_a + \underline{G}_a(\underline{\theta}_a) = \underline{T}_a$$

and the equations of motion just after the impact are

$$\underline{D}_a(\underline{\theta}_a)\ddot{\underline{\theta}}_a + \underline{h}_a(\underline{\theta}_a,\dot{\underline{\theta}}_a)\dot{\underline{\theta}}_a + \underline{G}_a(\underline{\theta}_a) = \underline{T}_a + \underline{F}_\delta \tag{2.36}$$

Integrating the equation (2.36) over the infinitely small time interval during the impact $[t_0, t_0+\Delta t]$ (t_0 is the instant of impact).

$$\lim_{\Delta t\to 0}\int_{t_0}^{t_0+\Delta t}\underline{D}_a(\underline{\theta}_a)\ddot{\underline{\theta}}_a dt + \lim_{\Delta t\to 0}\int_{t_0}^{t_0+\Delta t}[\underline{h}_a(\underline{\theta}_a,\dot{\underline{\theta}}_a)\dot{\underline{\theta}}_a + \underline{G}_a(\underline{\theta}_a) - \underline{T}_a]dt = \lim_{\Delta t\to 0}\int_{t_0}^{t_0+\Delta t}\underline{F}_\delta\, dt \tag{2.37}$$

as $\Delta t \to 0$

$$\lim_{\Delta t\to 0}\int_{t_0}^{t_0+\Delta t}[\underline{h}_a(\underline{\theta}_a,\dot{\underline{\theta}}_a)\dot{\underline{\theta}}_a + \underline{G}_a(\underline{\theta}_a) - \underline{T}_a]dt \to 0$$

and so the equation (2.37) becomes

$$\underline{D}_a(\underline{\theta}_a)\Delta\dot{\underline{\theta}} = \int_{t_0}^{t_0+\Delta t}\underline{F}_\delta\, dt = \underline{J}_a{}^T\int_{t_0}^{t_0+\Delta t}\underline{\lambda}\, dt \tag{2.38}$$

Since the relative velocity $\Delta\underline{v}_e = \underline{v}_e(t_0+\Delta t) - \underline{v}_e(t_0)$ between the free end and the

walking surface can be measured, it can be used for the computation of $\Delta\underline{\dot{\theta}}$. First of all we have to find the relation between $\Delta\underline{\dot{\theta}}$ and $\Delta\underline{v}_e$. We have

$$\underline{v}_e = \underline{J}_a \underline{\dot{\theta}}_a \tag{2.39}$$

and so

$$\underline{v}_e - \underline{v}_{contact} = \underline{J}_a \underline{\dot{\theta}}_a - \underline{v}_{contact} \tag{2.40}$$

If the point with which the biped comes into contact is not moving ($v_{contact}$=0), then we have

$$\underline{J}_a[\underline{\dot{\theta}}_a(t_0+\Delta t) - \underline{\dot{\theta}}_a(t_0)] = \underline{v}_e(t_0+\Delta t) - \underline{v}_e(t_0) \Rightarrow \underline{J}_a \Delta\underline{\dot{\theta}} = \Delta\underline{v}_e \tag{2.41}$$

Therefore, from (2.35), (2.38) and (2.41), we can obtain

$$\underline{J}_a \Delta\underline{\dot{\theta}} = \underline{J}_a \left[\underline{D}_a^{-1}(\underline{\theta}_a) \cdot \underline{J}_a^T \cdot \int_{t_0}^{t_0+\Delta t} \underline{\lambda}\, dt \right] = \Delta\underline{v}_e \tag{2.42}$$

Hence

$$\int_{t_0}^{t_0+\Delta t} \underline{\lambda}\, dt = \left[\underline{J}_a \underline{D}_a^{-1} \underline{J}_a^T \right]^{-1} \Delta\underline{v}_e$$

The equation for calculating the instantaneous changes in the angular velocities $\Delta\dot{\theta}$, of the links of the biped robot at the moment of impact between the free end and the walking surface is formulated from the equations of motion (2.28) of the dynamic model with both legs in the air. From the above formulation, the impact formula can be represented by the following equation:

$$\Delta\underline{\dot{\theta}} = \underline{D}_a^{-1} \cdot \underline{J}_a^T \cdot (\underline{J}_a \cdot \underline{D}_a^{-1} \cdot \underline{J}_a^T)^{-1} \cdot (\Delta\underline{v}_e) \tag{2.43}$$

where

$\Delta\underline{\dot{\theta}} = \underline{\dot{\theta}}_{after} - \underline{\dot{\theta}}_{before}$

$\Delta\underline{v}_e = \underline{v}_{e\,after} - \underline{v}_{e\,before}$

$\underline{D}_a$ is the 7×7 inertia matrix defined in the equations of motion (2.28), and $\underline{J}_a$ is the 2×7 Jacobian matrix of the biped in the air which is given as the following:

$$\underline{J}_a = \frac{\partial \underline{x}_e}{\partial \underline{\theta}_a} \tag{2.44}$$

Where $\underline{x}_e$ is the position vector $[x_e, y_e]^T$ of the free end

$$\begin{aligned}
J_a(1,1) &= \ell_1 \cos\theta_1 & J_a(2,1) &= -\ell_1 \sin\theta_1 \\
J_a(1,2) &= \ell_2 \cos\theta_2 & J_a(2,2) &= -\ell_2 \sin\theta_2 \\
J_a(1,3) &= 0 & J_a(2,3) &= 0 \\
J_a(1,4) &= \ell_4 \cos\theta_4 & J_a(2,4) &= \ell_4 \sin\theta_4 \\
J_a(1,5) &= \ell_5 \cos\theta_5 & J_a(2,5) &= \ell_5 \sin\theta_5 \\
J_a(1,6) &= 1 & J_a(2,6) &= 0 \\
J_a(1,7) &= 0 & J_a(2,7) &= 1
\end{aligned}$$

Since the velocity $\underline{v}_e$ of the free end becomes zero immediately after the impact with the walking surface,

$$\Delta \underline{v}_e = -\underline{v}_{e\,before} \tag{2.45}$$

Therefore, equation (2.43) becomes

$$\dot{\underline{\theta}}_{after} = \dot{\underline{\theta}}_{before} + \underline{D}_a^{-1} \cdot \underline{J}_a^T \cdot (\underline{J}_a \cdot \underline{D}_a^{-1} \cdot \underline{J}_a^T)^{-1} \cdot (-\underline{v}_{e\,before}) \tag{2.46}$$

where $\dot{\underline{\theta}}_{before}$ and $\dot{\underline{\theta}}_{after}$ are the velocities of the links just before and just after the impact. It should be remarked here again that the angular displacements of the joints during the time interval of the impact do not change.

2.4.3 Support End Exchange Phase

Simultaneously, as the free end collides with the walking surface, the end of the support leg leaves the walking surface immediately and the support end transfers to the end of the swing leg that comes into contact with the walking surface. An instantaneous

exchange of support from one end to another end takes place. The duration of this whole process is assumed to be the same as the duration of the impact of the free end with the walking surface. During the instantaneous exchange of support leg, individual angular displacements and velocities do not physically change. Since the roles of the swing and support leg will be exchanged, in order to use the same set of equations of motion of the single support phase for both legs, the numbering of links has to be relabeled. Such renumbering causes discontinuities in the angular displacements and velocities. The re-labeling scheme is as follows:

Link 1 $\Leftrightarrow$ Link 5 Link 2 $\Leftrightarrow$ Link 4 Link 3 does not change

These lead to the following changes:

$$\theta_1(0) = -\theta_5(T), \quad \theta_2(0) = -\theta_4(T), \quad \theta_3(0) = \theta_3(T)$$
$$\theta_4(0) = -\theta_2(T), \quad \theta_5(0) = -\theta_1(T)$$

$$\dot{\theta}_1(0) = -\dot{\theta}_{after\,5}(T), \quad \dot{\theta}_2(0) = -\dot{\theta}_{after\,4}(T), \quad \dot{\theta}_3(0) = \dot{\theta}_{after\,3}(T)$$
$$\dot{\theta}_4(0) = -\dot{\theta}_{after\,2}(T), \quad \dot{\theta}_5(0) = -\dot{\theta}_{after\,1}(T)$$

where

$\underline{\theta}(0)$ and $\underline{\dot{\theta}}(0)$ is the initial conditions of next step

$\underline{\theta}(T)$ is the terminal posture of the completion of each step before switching support leg, and

$\underline{\dot{\theta}}_{after}(T)$ is the angular velocities after impact at the completion of each step.

The following transformation matrix is formed from the above relationships to describe the effect on the angular displacements and the angular velocities immediately before and after the switching.

$$\begin{bmatrix} q_0 \\ q_1 \\ q_2 \\ q_3 \\ q_4 \\ \dot{q}_1 \\ \dot{q}_2 \\ \dot{q}_3 \\ \dot{q}_4 \\ \dot{q}_5 \end{bmatrix}_{after\ switching} = \begin{bmatrix} 1 & -1 & -1 & -1 & 1 & 0 & 0 & 0 & 0 & 0 \\ 0 & 0 & 0 & 0 & 1 & 0 & 0 & 0 & 0 & 0 \\ 0 & 0 & 0 & -1 & 0 & 0 & 0 & 0 & 0 & 0 \\ 0 & 0 & -1 & 0 & 0 & 0 & 0 & 0 & 0 & 0 \\ 0 & 1 & 0 & 0 & 0 & 0 & 0 & 0 & 0 & 0 \\ 0 & 0 & 0 & 0 & 0 & 1 & -1 & -1 & -1 & 1 \\ 0 & 0 & 0 & 0 & 0 & 0 & 0 & 0 & 0 & 1 \\ 0 & 0 & 0 & 0 & 0 & 0 & 0 & 0 & -1 & 0 \\ 0 & 0 & 0 & 0 & 0 & 0 & 0 & -1 & 0 & 0 \\ 0 & 0 & 0 & 0 & 0 & 0 & 1 & 0 & 0 & 0 \end{bmatrix} \begin{bmatrix} q_0 \\ q_1 \\ q_2 \\ q_3 \\ q_4 \\ \dot{q}_1 \\ \dot{q}_2 \\ \dot{q}_3 \\ \dot{q}_4 \\ \dot{q}_5 \end{bmatrix}_{before\ switching} \tag{2.47}$$

The new angular displacements and angular velocities calculated from the above equation are used as the initial conditions for the next step.

2.5 Summary

This chapter presented the methodology for the derivation of equations of motion to describe the locomotion of a biped robot walking on a flat horizontal surface. A five-link kinematic model of the biped robot was developed which has sufficiently few degrees of freedom to keep the equations of motion to a manageable level, while having enough degrees of freedom to approximately describe the locomotion. The complete walking motion in one step being studied includes three phases: the "single support" phase, the "impact with walking surface" phase, and the "support end exchange" phase. The equations of motion for the single support phase were developed by using the bipedal model with one support leg and the equations of motion for the impact phase were developed by using the bipedal model with both legs in the air. Instantaneous sharp changes in the angular velocities occurred during the impact between the free end of the swing leg and the walking surface at the completion of each step. Simultaneously, the

support end transferred from the end of the support leg to the end of the swing leg, which came into contact with the walking surface. The roles of the two legs were exchanged. Techniques for handling the impact with the walking surface and the exchange of support end were also presented in this chapter.

Chapter 3

Joint Angle Profiles Planning for the Five-Link Biped Robot Walking on a Flat Horizontal Surface

3.1. Introduction

Joint angle profiles planning for a bipedal locomotion system is the generation of a set of joint angle movements at each time instant that leads to a desired walking motion. In this chapter, the methodology used to design the joint angle profiles as the prescribed walking motion of the five-link biped robot is presented. The joint angle profiles planned are aimed at realizing the walking motion of the five-link bipedal robot on a flat horizontal surface in the sagittal plane during the single support phase only and can be used for tracking of the control system. Hurmuzlu (1993a) developed a systematic approach to formulate constraint functions that can be used to synthesize a five-element bipedal automaton. These constraint functions were cast in terms of physically coherent parameters of human gait and used as objective functions by a controller. In the following section, Hurmuzlu's approach is adapted to formulate constraint functions in terms of the kinematic relations between links; these constraint functions are then used to generate the profiles of joint displacements, velocities and accelerations of the five-link biped robot. We improve the constraint functions by replacing the constraints imposed on the swing leg used in Hurmuzlu's work (1993a) with the constraint of keeping the total

mechanical energy of the bipedal robot constant. Five dynamic constraint functions are defined by overall walking speed, the support knee bias and upright posture of the upper body. The last constraint function is defined to keep the mechanical energy as a constant. The purpose of this constraint is to test the hypothesis that given only potential energy at the beginning of the step, the swing leg can be carried over by gravity. The bipedal walking motion realized by the desired joint angle profiles has certain characteristics of human walking. Since repeatability of movements is a fundamental characteristic of bipedal walking, it is very important that the designed profiles of joint angles ensure the realization of the repeatability condition for steady and continuous walking. That means the equality of the joint angles at the beginning and at the end of each step. Only the set of joint angle profiles satisfying this condition is acceptable for bipeds.

3.2 Joint Angle Profiles Planning

Generally speaking, the joint angle profiles of the support leg, the upper body and the free swing leg are not unique. The objective in designing the joint angle profiles is to obtain an acceptable walking motion such that the biped robot can transport the whole body across the walking surface safely. The constraint functions formulated in the following section are for the purpose of generating joint angle profiles of the bipedal locomotion across a flat horizontal surface.

3.2.1 Constraint Functions

Five dynamic constraint functions are developed in this section. The constraint functions, which can be used to prescribe a specific locomotion of the planar five-link

biped robot during the single support phase, are formulated as kinematic relations. It should be mentioned here that, in order to simplify the mathematical presentation, the number of constraint functions is equal to the number of generalized coordinates of the biped robot. The five constraint functions can be described as the following:

(1) The erect body posture

One of the basic aspects for bipedal walking is to always maintain the upper body of the biped robot at the upright position. That means that the net rotation of the upper body is kept zero at all the time ($\theta_3(t) = 0$). This is valid as long as normal walking motion is considered (Winter 1991). The following equation enforces this condition:

$$S_1 = \theta_3 = 0$$

Since we have the relationship that

$$\theta_3 = q_0 - q_1 - q_2$$

S_1 can be expressed in terms of the relative angles

$$S_1 = q_0 - q_1 - q_2 = 0 \tag{3.1}$$

(2) The overall progression speed

The overall progression speed is defined as the linear velocity of the center of mass of the upper body in the forward walking direction (i.e., the positive x-direction). The steady progression speed is maintained by

$$\dot{x}c_3 = V_p$$

where $\dot{x}c_3$ is the velocity of the center of mass of the upper body in the x-direction and V_p is the desired progression speed. This selection of progression speed gives us some freedom to control the overall walking speed of the biped robot. We have

$$\dot{x}c_3 = \ell_1 \cdot \cos(q_0) \cdot \dot{q}_0 + \ell_2 \cdot \cos(q_0 - q_1) \cdot (\dot{q}_0 - \dot{q}_1) + d_3 \cos(q_0 - q_1 - q_2) \cdot (\dot{q}_0 - \dot{q}_1 - \dot{q}_2)$$

From the above kinematic relations of the 5-link biped robot, the following constraint function is obtained

$$S_2 = \ell_1 \cdot \cos(q_0) \cdot \dot{q}_0 + \ell_2 \cdot \cos(q_0 - q_1) \cdot (\dot{q}_0 - \dot{q}_1) + d_3 \cos(q_0 - q_1 - q_2) \cdot (\dot{q}_0 - \dot{q}_1 - \dot{q}_2) - V_p = 0 \tag{3.2}$$

(3) The bias of the knee of the support leg

For a human knee joint, a locking mechanism is embraced which allows the knee to bend in one direction only and lock at certain positions. This mechanism is very important for the support leg since it carries the weight of the whole body. Lacking this mechanism, the support knee has a tendency to collapse. However, the five-link biped robot does not have this locking mechanism included in the model to prevent the knee of the support leg from bending backward and to prevent the links from collapsing. In order to obtain a human like gait pattern, the knee of the support leg (q_1) has to be fixed at a certain angular position during the single support phase. This constraint function is given by

$$S_3 = q_1 - \sigma = 0 \tag{3.3}$$

where σ is the bias angle.

(4) The coordination of the support leg and swing leg motion

For normal continuous walking, the biped robot is moving forward in the positive x-direction. The free swing leg also has to move in the same forward walking direction. In order to specify the walking direction, the following must be set.

$$x_T = 2xc_3$$

where, with respect to the fixed coordinate frame, x_T is the x-coordinate of the tip of the swing leg and xc_3 is the x-coordinate of the center of mass of the upper body. This relation implies that the center of the upper body is always about the center with respect to the tips of the two legs. This relation also implies that the tip of the swing leg moves at twice the speed of the center of mass of the upper body in the positive x-direction. We have

$$x_t = \ell_1 \sin(q_0) + \ell_2 \sin(q_0 - q_1) + \ell_4 \sin(-q_0 + q_1 + q_2 + q_3) + \ell_5 \sin(-q_0 + q_1 + q_2 + q_3 - q_4)$$

and

$$xc_3 = \ell_1 \sin(q_0) + \ell_2 \sin(q_0 - q_1) + d_3 \sin(q_0 - q_1 - q_2)$$

From the above kinematic relation, the constraint function is obtained as

$$\begin{aligned} S_4 = {} & \ell_1 \sin(q_0) + \ell_2 \sin(q_0 - q_1) + 2d_3 \sin(q_0 - q_1 - q_2) - \ell_4 \sin(-q_0 + q_1 + q_2 + q_3) \\ & - \ell_5 \sin(-q_0 + q_1 + q_2 + q_3 - q_4) = 0 \end{aligned} \tag{3.4}$$

(5) Constant mechanical energy

Mechanical energy is defined as the energy state of any link or the whole biped robot system at an instant in time. Mechanical energy comprises translational kinetic energy, rotational energy, and potential energy (V=K+P). This constraint function, which keeps the mechanical energy of the whole body constant, is formulated by setting

$$\dot{V} = 0$$

where $\dot{V}$ is the time derivative of the mechanical energy and is defined as

$$\dot{V} = \frac{dV}{dt} = \frac{\partial V}{\partial x_i} \dot{x}_i$$

and

$$x_i = [q_0, q_1, q_2, q_3, q_4, \dot{q}_0, \dot{q}_1, \dot{q}_2, \dot{q}_3, \dot{q}_4]$$

Since, mechanical energy is comprised of translational kinetic energy, rotational kinetic energy and potential energy,

$$V_i = K_i + P_i \quad (i=1,\ldots 5)$$

The total kinetic energy including the translational and rotational kinetic energy of each link is as follows:

$$K = \sum_{i=1}^{5} K_i$$

with

$$K_i = \frac{1}{2} m_i v c_i^2 + \frac{1}{2} I_i \dot{\theta}_i^2$$

The potential energy of each link is as the following:

$$P = \sum_{i=1}^{5} P_i$$

with

$$P_i = m_i \cdot g \cdot yc_i$$

where g=9.81 m/sec^2 (acceleration of gravity)

The zero reference for the potential energy is set at the ground level of the walking surface in the fixed coordinate frame. The detailed derivation of the kinetic energy and the potential energy of each link can be found in Section 2.4.1 and the detailed derivation of $\dot{V}$ can be found in Appendix IV.

The constraint function is represented in the following form:

$$S_5 = \frac{\partial V}{\partial x_i} \dot{x}_i = 0$$

where

$$x_i = \{q_0, q_1, q_2, q_3, q_4, \dot{q}_0, \dot{q}_1, \dot{q}_2, \dot{q}_3, \dot{q}_4\} \text{ and } \dot{x}_i = \{\dot{q}_0, \dot{q}_1, \dot{q}_2, \dot{q}_3, \dot{q}_4, \ddot{q}_0, \ddot{q}_1, \ddot{q}_2, \ddot{q}_3, \ddot{q}_4\}$$

Therefore,

$$S_5 = \begin{bmatrix} \frac{\partial V}{\partial q_0} & \frac{\partial V}{\partial q_1} & \frac{\partial V}{\partial q_2} & \frac{\partial V}{\partial q_3} & \frac{\partial V}{\partial q_4} & \frac{\partial V}{\partial \dot{q}_0} & \frac{\partial V}{\partial \dot{q}_1} & \frac{\partial V}{\partial \dot{q}_2} & \frac{\partial V}{\partial \dot{q}_3} & \frac{\partial V}{\partial \dot{q}_4} \end{bmatrix} \cdot \begin{bmatrix} \dot{q}_0 \\ \dot{q}_1 \\ \dot{q}_2 \\ \dot{q}_3 \\ \dot{q}_4 \\ \ddot{q}_0 \\ \ddot{q}_1 \\ \ddot{q}_2 \\ \ddot{q}_3 \\ \ddot{q}_4 \end{bmatrix} = 0 \qquad (3.5)$$

By solving equations (3.1) to (3.5), a set of joint angle profiles can be found and can be used as the desired trajectories for tracking control.

3.2.2 Approach for Solving the Constraint Functions

The problem we deal with here is to find the corresponding joint displacements, velocities and accelerations for a desired motion. Once the constraint equations are solved, the desired motion can be achieved by moving each joint to the determined values. This problem involves solving the above constraint equations. The constraint equations, i.e., equations (3.1) to (3.5), developed in Section 3.2.1 are a combination of differential and algebraic equations. Since the set of differential and algebraic equations is very inconvenient to handle in analytical form, the equations are therefore solved in numerical form. Solving a set of equations consisting of differential and algebraic equations (DAE) alone is a very challenging problem. There is no general method to solve such a set of differential and algebraic equations. In addition, the solution set of the angular displacements, velocities and accelerations of joints obtained from solving the

DAE problem must also satisfy another two extra conditions. Firstly, the repeatability condition which requires that the configuration of the biped obtained at the end of each step must be very close to the configuration at the beginning of each step, and secondly, the knee of the swing leg does not bend backward.

By observing the five constraint functions, in equations (3.1), (3.2) and (3.3) only the relative angles of the support leg are involved. Therefore, we can solve the equations (3.1), (3.2) and (3.3) together to obtain the motion of the support leg first. Equations (3.1) and (3.3) are algebraic equations and equation (3.2) is a differential equation. In order to solve them together we need to obtain the time derivatives of these three equations. The detailed derivation of the time derivatives of equations (3.1), (3.2) and (3.3) can be found in Appendix V. Now we have three unknowns of angular displacements, three unknowns of angular velocities and three unknowns of angular accelerations involved in equations (3.1), (3.2) and (3.3) and their time derivatives, i.e., nine equations. Instead of solving S=0, $\dot{S}=0$, and $\ddot{S}=0$, we adapted the following procedure (Hurmuzlu 1993b) to solve the equations numerically.

The constraint functions S_1, S_2 and S_3, in equations (3.1), (3.2) and (3.3), can be written as

$$S=[S_1,\ldots S_3]^T$$

Let that

$$\dddot{S} := C_1\ddot{S} + C_2\dot{S} + C_3S = 0 \tag{3.6}$$

where C_1, C_2 and C_3 are 3 × 3 matrices containing the parameters designed as below. If S_i is a holonomic constraint, the ith row of C_1 is set to c_i where c_1={1, 0, 0, ..., 0}, c_2={0, 1, 0, ..., 0}, etc. If the constraint is nonholonomic, the ith row of C_1 is set to 0 and the ith row of C_2 is set to c_i. The matrices C_2 and C_3 are diagonal and contain selected

parameters such that the solution set of S is asymptotically stable about the origin (i.e., $S_t \rightarrow 0$ as $t \rightarrow 0$) (Hurmuzlu 1993b). Since we used equation (3.6), the joint angle profiles obtained will only satisfy equation (3.6) instead of the equations (3.1) to (3.5) and their time derivatives individually.

The matrices, C_1, C_2 and C_3, for equation (3.6) are chosen as follows:

$$C_1 = \text{diag}\{\ 1,\ 0,\ 1\ \} \qquad C_2 = \text{diag}\{\ \alpha, 1, \alpha\ \} \qquad C_3 = \text{diag}\{\ \beta, \lambda, \beta\ \}$$

where

$$\lambda_{1,2} = -\frac{\alpha}{2} \pm \sqrt{\frac{\beta^2}{4} - \alpha\beta} \quad (\beta > 4\alpha > 0)$$

Now the second order differential equation $\ddot{\tilde{S}}$ (3.6) can be solved. The expressions of the angular displacements, velocities and accelerations at $t > t_0$ are obtained in terms of S_t, the initial values of the angular displacements, velocities, accelerations and the initial time t_0.

Now using equations (3.1), (3.2), (3.3) and their time derivatives, the following expressions are obtained:

$$q_1 = S_3 + \sigma \tag{3.7}$$

$$q_0 = \arctan\left(\frac{\ell_2 \sin(q_1)}{\ell_1 + \ell_2 \cos(q_1)}\right) + \arcsin\left(\frac{\int_{t_0}^{t} S_2\, dt - \eta_1(t)}{\sqrt{[\ell_1 + \ell_2 \cos(q_1)]^2 + [\ell_2 \sin(q_1)]^2}}\right) \tag{3.8}$$

$$q_2 = q_0 - q_1 - S_1 \tag{3.9}$$

where

$$\eta_1(t) = -Vp(t - t_0) - \ell_1 \sin(q_0(t_0)) - \ell_2 \sin(q_0(t_0) - q_1(t_0)) - d_3 \sin(S_1(t_0)) + d_3 \sin(S_1)$$

$$\dot{q}_1 = \dot{S}_3 \tag{3.10}$$

$$\dot{q}_0 = \frac{\dot{S}_2 + Vp - d_3\cos(S_1)\dot{S}_1 + \ell_2\cos(q_0 - q_1)\dot{q}_1}{\ell_1\cos(q_0) + \ell_2\cos(q_0 - q_1)} \tag{3.11}$$

$$\dot{q}_2 = \dot{q}_0 - \dot{q}_1 - \dot{S}_1 \tag{3.12}$$

$$\ddot{q}_1 = \ddot{S}_3 \tag{3.13}$$

$$\ddot{q}_0 = \frac{\eta_2(t)}{(\ell_1\cos(q_0) + \ell_2\cos(q_0 - q_1))^2} \tag{3.14}$$

$$\ddot{q}_2 = \ddot{q}_0 - \ddot{q}_1 - \ddot{S}_1 \tag{3.15}$$

where

$$\eta_2(t) = \ddot{S}_2 - d_3\cos(S_1)\ddot{S}_1 + d_3\sin(S_1)\dot{S}_1^2 + \ell_2\cos(q_0 - q_1)\ddot{q}_1 + \ell_2\sin(q_0 - q_1)(\dot{q}_0 - \dot{q}_1)\dot{q}_1 + [l_1\sin(q_0)\dot{q}_0 + l_2\sin(q_0 - q_1)(\dot{q}_0 - \dot{q}_1)] * [S_2 + Vp - d_3\cos(S_1)\dot{S}_1 + l_2\cos(q_0 - q_1)\dot{q}_1]$$

Substituting the numerical solutions of S_1, S_2, S_3 and their time derivatives into equations (3.7) to (3.15), we can obtain the values of the angular displacements, velocities and accelerations associated with the support leg.

In order to obtain the motion of the swing leg, we developed two approaches to do so. The first approach is to derive the time derivative of equation (3.4) twice to obtain $\ddot{S}_4 = 0$. With the solution obtained from equations (3.7) to (3.15), $\ddot{S}_4 = 0$ and $S_5 = 0$ (i.e., equation (3.5)) are solved simultaneously. The time derivatives of S_4 can be found in Appendix V. The second approach is to let

$$C_1\ddot{S}_4 + C_2\dot{S}_4 + C_3S_4 = 0 \tag{3.16}$$

where

C_1=1, C_2=α and C_3=β

and simultaneously solve with S_5=0 (i.e., equation (3.5)).

Thus the numerical solutions for the angular displacements (q_3 and q_4), velocities and accelerations associated with the swing leg can be obtained. The two approaches are used to solve this problem numerically. Since the joint angle profiles obtained from the second approach are better than the first approach in satisfying the two extra conditions, which are the repeatability condition and the condition that the knee of the swing leg does not bend backward, the second approach is chosen for obtaining the desired joint angel profiles.

3.3 Summary

The methodology used for planning the joint angle profiles as the prescribed walking motion of the five-link biped robot during the single support phase in the sagittal plane was presented in this chapter. Five constraint functions were formulated as the kinematic relations between links that would be used to generate the profiles of joint displacements, velocities and accelerations for the bipedal walking. The difficulty of solving the constraint functions was addressed. The five constraint functions were a combination of differential and algebraic equations. Solving the differential algebraic equations together was challenging. In addition, the solutions had to satisfy the repeatability condition and the condition that the knee of the swing leg cannot bend backward. That made the problem even harder to solve. The approach used for solving the differential algebraic equations was presented. The prescribed human-like walking motion generated through this method should match the motion described by the five constraint functions, and should satisfy the repeatability condition and the condition that the knee does not bend backward.

Chapter 4

Motion Control of the Five-Link Biped Robot Walking on a Flat Horizontal Surface

4.1 Introduction

In this chapter, the motion control problem is considered. Given the nonlinear dynamic system of the biped and given a set of desired angle profiles for the joints, a control technique is applied to the system for choosing the input joint torques such that, from any initial state, the movement of each joint follows the desired joint angle profiles and the tracking errors tend to zero. In Section 4.2, brief background information about linear and nonlinear control techniques is given. Uncertainties usually exist in models of physical systems. A control technique that can account for uncertainties existing in the system is practically useful. In Section 4.3, the problem of parametric uncertainty is presented. Physical parameters of the five-link biped robot, including the link masses, the link moments of inertia, the link lengths, and the positions of the centers of mass, are the sources of uncertainties considered in this study. Two nonlinear control techniques are employed for tracking control of the bipedal locomotion system. In Section 4.3, the traditional computed torque control technique is presented and in Section 4.4, the sliding mode control technique with a modified control law is presented.

4.2 Background Information

The control strategy in this study is based on motion tracking during the forward walking motion of the five-link biped robot. The equations of motion (2.19) developed in Chapter 2 describe the dynamic motion of the biped during the single support phase. The terms $\underline{h}_q(\underline{q},\underline{\dot{q}})\underline{\dot{q}}$ and $\underline{G}_q(\underline{q})$ include centripetal, Coriolis, and gravitational torques, which are highly nonlinear and their effects increase drastically as the angular velocities of the biped increase. One approach to controller synthesis is to design a linear controller based on the linear approximation of the nonlinear system. Linear approximation of a bipedal locomotion system has been used in some studies (Gubina et al. 1974, Golliday and Hemami 1977, Hemami and Wyman 1979a, 1979b, Furusho and Masubuchi 1986 and 1987). The nonlinear elements are linearized by assuming that the system is operating within a very close neighborhood of some operating points and an approximate model is derived with a linear relationship between the input and output of the system. A state feedback control law is then used to control the linearized system. According to Slotine and Li (1991), linear control method is not suitable for controlling nonlinear system, such as bipedal locomotion system. The reason behind this is that linear control law neglects all the nonlinear forces associated with the motion. The nonlinearities in the system cannot be compensated properly and, as a result, the accuracy of the trajectory tracking is reduced (Slotine and Li 1991). This can be demonstrated easily in robot motion control problems as the speed of motion increases. Nonlinear dynamic forces are involved, such as Coriolis and centripetal forces, and vary as the square of speed. The linearized control system neglects these forces and the controller's accuracy quickly degrades (Slotine and Li 1991). Besides, linear control law is based on the assumption that the system state

remains in the close neighborhood of some operating point. As a result, biped robots can only walk with a very small swing angle. For a larger swing angle, i.e., larger step length, biped robots will fall before they can complete one step. Therefore, linear control law is not suitable for the bipedal locomotion system considered in this study. Recently, researchers are more interested in the development and application of nonlinear control. Feedback linearization technique can be used for nonlinear control design. The main idea is to algebraically transform a nonlinear system dynamics into a partially or fully linear one, so that linear control techniques can be applied (Slotine and Li 1991). This is achieved by exact state transformations and feedback that is different from linear approximations of the dynamics. A conceptually simple nonlinear control called computed torque control, which is based on the feedback linearization technique, can fully compensate the nonlinear forces in the nonlinear system and lead to high accuracy control for a very large range of robot speeds. Computed torque control requires full-state feedback and perfect knowledge of the system parameters. Due to the latter requirement, this controller becomes practically limited since most physical systems contain uncertainties. Uncertainty can be classified into two major sources: parametric uncertainty and unmodeled dynamics. The only type of uncertainty that is considered in this thesis is parametric uncertainty. Sliding mode control is one class of the robust control technique that can account for uncertainties. Nonlinearities are intentionally introduced into the control law that tolerate the parametric uncertainty to make it robust. Sliding mode control has been successfully applied to robot motion control systems (Chang and Hurmuzlu 1992, Tzafestas et al. 1996). The sliding mode control law presented in this chapter is designed based on the sliding mode control technique.

4.3 Parametric Uncertainty

Modeling of nonlinear systems is usually imprecise. Two major sources, namely, parametric uncertainty and unmodeled dynamics, contribute to imprecision in the system. Parametric uncertainty stems from the uncertainty about the actual system. For example, the physical parameters of the system are not known exactly. Unmodeled dynamics comes from assumptions incorporated in the system during modeling in order to simplify the presentation of the system dynamics (Slotine and Li 1991). In this thesis, only parametric uncertainty is considered.

The parametric uncertainties considered are the uncertainties of the physical parameters of the biped. These physical parameters include the mass (m), the length (l) and the moment of inertia (I) of each link, and as well as the position of the center of mass of each link (d) with respect to the end of the link. Although the uncertainties of those physical parameters are not known, we assume that the bounds of the values of those parameters are known. For example, the masses of the links are known with uncertainty $e_m \times 100\%$ (where $0 \le e_m < 1$). Similarly, let e_I, e_l and e_d be the uncertainties in the link moment of inertia (I), the link length (l) and the position of center of mass (d) with respect to the end of the link, respectively. Due to the presence of parametric uncertainties, the terms $\underline{D}_\theta(\theta)$, $\underline{h}_\theta(\theta,\dot{\theta})\dot{\theta}$ and $\underline{G}_\theta(\theta)$ in equation (2.15) are estimated as $\hat{\underline{D}}_\theta(\theta)$, $\hat{\underline{h}}_\theta(\theta,\dot{\theta})\dot{\theta}$ and $\hat{\underline{G}}_\theta(\theta)$. The bounds between the actual terms and the estimated terms are defined as follows. These bounds are used to calculate the estimated terms, which will be used in designing the control algorithms when facing the above parametric uncertainties.

$$\Delta \underline{D}_\theta = \hat{\underline{D}}_\theta - \underline{D}_\theta$$

$$\Delta \underline{h}_\theta = \hat{\underline{h}}_\theta \dot{\theta} - \underline{h}_\theta \dot{\theta}$$

and

$$\Delta \underline{G}_\theta = \hat{\underline{G}}_\theta - \underline{G}_\theta$$

Incorporating these uncertainties, e_m, e_I, e_l and e_d, $\Delta \underline{D}_\theta$, $\Delta \underline{h}_\theta$ and $\Delta \underline{G}_\theta$ can be computed using equations (2.16), (2.17) and (2.18) as follows:

$$\Delta \underline{D}_\theta = \Delta D_{ij} \quad (i, j = 1,2,\ldots,5)$$

where

$$\begin{aligned}
\Delta D_{11} &= e_I I_1 + m_1 d_1^2[(1+e_m)(1+e_d)^2 - 1] + (m_2 + m_3 + m_4 + m_5)\ell_1^2[(1+e_m)(1+e_l)^2 - 1] \\
\Delta D_{12} &= \{m_2 \ell_1 d_2[(1+e_m)(1+e_l)(1+e_d) - 1] \\
&\quad + (m_3 + m_4 + m_5)\ell_1 \ell_2[(1+e_m)(1+e_l)^2 - 1]\}\cos(\theta_1 - \theta_2) \\
\Delta D_{13} &= \{m_3 \ell_1 d_3[(1+e_m)(1+e_l)(1+e_d) - 1]\}\cos(\theta_1 - \theta_3) \\
\Delta D_{14} &= \{m_4 \ell_1 (\ell_4 - d_4)[(1+e_m)(1+e_l)(1+e_{ld4}) - 1] \\
&\quad + m_5 \ell_1 \ell_4[(1+e_m)(1+e_l)^2 - 1]\}\cos(\theta_1 + \theta_4) \\
\Delta D_{15} &= \{m_5 \ell_1 (\ell_5 - d_5)[(1+e_m)(1+e_l)(1+e_{ld5}) - 1]\}\cos(\theta_1 + \theta_5)
\end{aligned}$$

$$\begin{aligned}
\Delta D_{21} &= \Delta D_{12} \\
\Delta D_{22} &= e_I I_2 + m_2 d_2^2[(1+e_m)(1+e_d)^2 - 1] + (m_3 + m_4 + m_5)\ell_2^2[(1+e_m)(1+e_l)^2 - 1] \\
\Delta D_{23} &= \{m_3 \ell_2 d_3[(1+e_m)(1+e_l)(1+e_d) - 1]\}\cos(\theta_2 - \theta_3) \\
\Delta D_{24} &= \{m_4 \ell_2 (\ell_4 - d_4)[(1+e_m)(1+e_l)(1+e_{ld4}) - 1] \\
&\quad + m_5 \ell_2 \ell_4[(1+e_m)(1+e_l)^2 - 1]\}\cos(\theta_2 + \theta_4) \\
\Delta D_{25} &= \{m_5 \ell_2 (\ell_5 - d_5)[(1+e_m)(1+e_l)(1+e_{ld5}) - 1]\}\cos(\theta_2 + \theta_5)
\end{aligned}$$

$$\begin{aligned}
\Delta D_{31} &= \Delta D_{13} \\
\Delta D_{32} &= \Delta D_{23} \\
\Delta D_{33} &= e_I I_3 + m_3 d_3^2[(1+e_m)(1+e_d)^2 - 1] \\
\Delta D_{34} &= \Delta D_{35} = 0
\end{aligned}$$

$$\begin{aligned}
\Delta D_{41} &= \Delta D_{14} \\
\Delta D_{42} &= \Delta D_{24} \\
\Delta D_{43} &= \Delta D_{34} \\
\Delta D_{44} &= e_I I_4 + m_4(\ell_4 - d_4)^2[(1+e_m)(1+e_{ld4})^2 - 1] + m_5 \ell_4^2[(1+e_m)(1+e_l)^2 - 1] \\
\Delta D_{45} &= \{m_5 \ell_4 (\ell_5 - d_5)[(1+e_m)(1+e_l)(1+e_{ld5}) - 1]\}\cos(\theta_4 - \theta_5)
\end{aligned}$$

$$\begin{aligned}
\Delta D_{51} &= \Delta D_{15} \\
\Delta D_{52} &= \Delta D_{25} \\
\Delta D_{53} &= \Delta D_{35} \\
\Delta D_{54} &= \Delta D_{45} \\
\Delta D_{55} &= e_I I_5 + m_5(\ell_5 - d_5)^2[(1+e_m)(1+e_{ld5})^2 - 1]
\end{aligned}$$

$$\Delta \underline{h}(\underline{\theta},\dot{\underline{\theta}})\dot{\underline{\theta}} = col\left[\sum_{1(j\neq i)}^{5}\Delta h_{ij}\dot{\theta}_j^{\,2}\right]$$

where

$$\begin{aligned}
\Delta h_{122} &= \{m_2\ell_1 d_2[(1+e_m)(1+e_l)(1+e_d)-1] \\
&\quad +(m_3+m_4+m_5)\ell_1\ell_2[(1+e_m)(1+e_l)^2-1]\}\sin(\theta_1-\theta_2) \\
\Delta h_{133} &= \{m_3\ell_1 d_3[(1+e_m)(1+e_l)(1+e_d)-1]\}\sin(\theta_1-\theta_3) \\
\Delta h_{144} &= -\{m_4\ell_1(\ell_4-d_4)[(1+e_m)(1+e_l)(1+e_{ld4})-1] \\
&\quad +m_5\ell_1\ell_4[(1+e_m)(1+e_l)^2-1]\}\sin(\theta_1+\theta_4) \\
\Delta h_{155} &= -\{m_5\ell_1(\ell_5-d_5)[(1+e_m)(1+e_l)(1+e_{ld5})-1]\}\sin(\theta_1+\theta_5)
\end{aligned}$$

$$\begin{aligned}
\Delta h_{211} &= -\Delta h_{122} \\
\Delta h_{233} &= \{m_3\ell_2 d_3[(1+e_m)(1+e_l)(1+e_d)-1]\}\sin(\theta_2-\theta_3) \\
\Delta h_{244} &= -\{m_4\ell_2(\ell_4-d_4)(1+e_m)(1+e_l)(1+e_{ld4})-1] \\
&\quad +m_5\ell_2\ell_4[(1+e_m)(1+e_l)^2-1]\}\sin(\theta_2+\theta_4) \\
\Delta h_{255} &= -\{m_5\ell_2(\ell_5-d_5)[(1+e_m)(1+e_l)(1+e_{ld5})-1]\}\sin(\theta_2+\theta_5)
\end{aligned}$$

$$\begin{aligned}
\Delta h_{311} &= -\Delta h_{133} \\
\Delta h_{322} &= \Delta h_{233} \\
\Delta h_{344} &= \Delta h_{355} = 0
\end{aligned}$$

$$\begin{aligned}
\Delta h_{411} &= \Delta h_{144} \\
\Delta h_{422} &= \Delta h_{244} \\
\Delta h_{433} &= 0 \\
\Delta h_{455} &= \{m_5\ell_4(\ell_5-d_5)[(1+e_m)(1+e_l)(1+e_{ld5})-1]\}\sin(\theta_4-\theta_5)
\end{aligned}$$

$$\begin{aligned}
\Delta h_{511} &= \Delta h_{155} \\
\Delta h_{522} &= \Delta h_{255} \\
\Delta h_{533} &= 0 \\
\Delta h_{544} &= -\Delta h_{455}
\end{aligned}$$

and

$$\begin{aligned}
\Delta G_1 &= -\{m_1 d_1[(1+e_m)(1+e_d)-1]+(m_2+m_3+m_4+m_5)\ell_1[(1+e_m)(1+e_l)-1]\}g\sin\theta_1 \\
\Delta G_2 &= -\{m_2 d_2[(1+e_m)(1+e_d)-1]+(m_3+m_4+m_5)\ell_2[(1+e_m)(1+e_l)-1]\}g\sin\theta_2 \\
\Delta G_3 &= -\{m_3 d_3[(1+e_m)(1+e_d)-1]\}g\sin\theta_3 \\
\Delta G_4 &= \{m_4(\ell_4-d_4)[(1+e_m)(1+e_{ld4})-1]+m_5\ell_4[(1+e_m)(1+e_l)-1]\}g\sin\theta_4 \\
\Delta G_5 &= \{m_5(\ell_5-d_5)[(1+e_m)(1+e_{ld5})-1]\}g\sin\theta_5
\end{aligned}$$

The terms, e_{ld4} and e_{ld5} in the above equations can be defined as

$$e_{ldi} = \frac{\ell_i e_l - d_i e_d}{\ell_i - d_i} \qquad (i = 4, 5)$$

Since the equations of motion are in terms of the relative angle (q_i) between links instead of the absolute angle θ_i of each link, we have to transform the terms $\Delta\underline{D}_\theta$, $\Delta\underline{h}_\theta$ and $\Delta\underline{G}_\theta$ into $\Delta\underline{D}_q$, $\Delta\underline{h}_q$ and $\Delta\underline{G}_q$. The transformation method we employed in Chapter 2 can be used here. $\Delta\underline{D}_q$, $\Delta\underline{h}_q$ and $\Delta\underline{G}_q$ are in the following form:

$$\Delta\underline{D}_q(q) = \Delta D_q(i,j) \qquad (i,j = 1,2\ldots,5) \tag{4.1}$$

$$\begin{aligned}
\Delta D_q(i,1) &= \Delta A_{i1} + \Delta A_{i2} + \Delta A_{i3} - \Delta A_{i4} - \Delta A_{i5} \\
\Delta D_q(i,2) &= -\Delta A_{i2} - \Delta A_{i3} + \Delta A_{i4} + \Delta A_{i5} \\
\Delta D_q(i,3) &= -\Delta A_{i3} + \Delta A_{i4} + \Delta A_{i5} \\
\Delta D_q(i,4) &= \Delta A_{i4} + \Delta A_{i5} \\
\Delta D_q(i,5) &= -\Delta A_{i5}
\end{aligned}$$

where

$$\begin{aligned}
\Delta A_{1j} &= \Delta D_{1j} + \Delta D_{2j} + \Delta D_{3j} - \Delta D_{4j} - \Delta D_{5j} \\
\Delta A_{2j} &= -\Delta D_{2j} - \Delta D_{3j} + \Delta D_{4j} + \Delta D_{5j} \\
\Delta A_{3j} &= -\Delta D_{3j} + \Delta D_{4j} + \Delta D_{5j} \\
\Delta A_{4j} &= \Delta D_{4j} + \Delta D_{5j} \\
\Delta A_{5j} &= -\Delta D_{5j}
\end{aligned}$$

$$\Delta\underline{h}_q = [\Delta h_{q0}, \Delta h_{q1}, \Delta h_{q2}, \Delta h_{q3}, \Delta h_{q4}]^T \tag{4.2}$$

where

$$\begin{aligned}
\Delta h_{q0} &= \Delta h_1 + \Delta h_2 + \Delta h_3 - \Delta h_4 - \Delta h_5 \\
\Delta h_{q1} &= -\Delta h_2 - \Delta h_3 + \Delta h_4 + \Delta h_5 \\
\Delta h_{q2} &= -\Delta h_3 + \Delta h_4 + \Delta h_5 \\
\Delta h_{q3} &= \Delta h_4 + \Delta h_5 \\
\Delta h_{q4} &= -\Delta h_5
\end{aligned}$$

$$\Delta\underline{G}_q = [\Delta G_{q0}, \Delta G_{q1}, \Delta G_{q2}, \Delta G_{q3}, \Delta G_{q4}]^T \tag{4.3}$$

where

$$\begin{aligned}
\Delta G_{q0} &= \Delta G_1 + \Delta G_2 + \Delta G_3 - \Delta G_4 - \Delta G_5 \\
\Delta G_{q1} &= -\Delta G_2 - \Delta G_3 + \Delta G_4 + \Delta G_5 \\
\Delta G_{q2} &= -\Delta G_3 + \Delta G_4 + \Delta G_5 \\
\Delta G_{q3} &= \Delta G_4 + \Delta G_5 \\
\Delta G_{q4} &= -\Delta G_5
\end{aligned}$$

The bounds, $\Delta\underline{D}_q$, $\Delta\underline{h}_q$ and $\Delta\underline{G}_q$, between the actual and the estimated terms are thus defined. These bounds will be used in designing the control algorithm for motion tracking as physical parameters such as the link masses, link lengths, link moments of inertia and positions of center of mass are uncertain.

4.4 Computed Torque Control

Computed torque control is a traditional nonlinear control method based on the feedback linearization technique which cancels the nonlinearities of the system dynamics and obtains a simple input-output relation. The computed torque control law for the tracking control purpose has the following structure:

$$\underline{T}_q = \underline{D}_q(\underline{q})\underline{u} + \underline{h}_q(\underline{q},\dot{\underline{q}})\dot{\underline{q}} + \underline{G}_q(\underline{q}) \tag{4.4}$$

The structure of this control law is similar to the structure of the equations of motion (2.16) developed in Chapter 2. Substituting this control law (4.4) into equations of motion (2.16), we can obtain

$$\underline{D}_q(\underline{q})\ddot{\underline{q}} = \underline{D}_q(\underline{q})\underline{u} \tag{4.5}$$

$D_q(q)$ is assumed to be positive definite, and therefore it is invertible. Thus we have

$$\ddot{\underline{q}} = \underline{u} \tag{4.6}$$

The nonlinear terms involved in the system are eliminated. The equation (4.6) represents a set of five decoupled second order differential equations, each of which can be controlled by a linear control law. The proportional plus derivative (PD) control is a suitable control law for use in controlling the decoupled second order differential equations (4.6). The PD control law can be represented in the following form:

$$\underline{u} = \ddot{\underline{q}}_d - \underline{K}_D \cdot \dot{\underline{e}} - \underline{K}_P \cdot \underline{e} \tag{4.7}$$

where $e_j = q_j(t) - q_{dj}(t) \quad (j = 0,1,\ldots,4)$

q_{dj} is the desired angle profile of each joint. $\underline{K}_D$ and $\underline{K}_P$ are 5×5 diagonal control gain matrices, (i.e. $\underline{K}_D = diag[K_{Dj}]$ and $\underline{K}_P = diag[K_{Pj}]$). They are positive definite (i.e. $\underline{K}_{Dj} > 0$ and $\underline{K}_{Pi} > 0$). Substituting equation (4.7) into equation (4.6), the closed-loop equation of the error $e(t)$ can be obtained,

$$\ddot{\underline{e}} + \underline{K}_D \cdot \dot{\underline{e}} + \underline{K}_P \cdot \underline{e} = 0 \tag{4.8}$$

This is a linear differential equation that governs the error between the actual joint angle profiles and the desired joint angle profiles. It shows that the error tends to zero as time goes to infinity (i.e. $t \to \infty$). The block diagram of the closed-loop control system is shown in Figure 4.1.

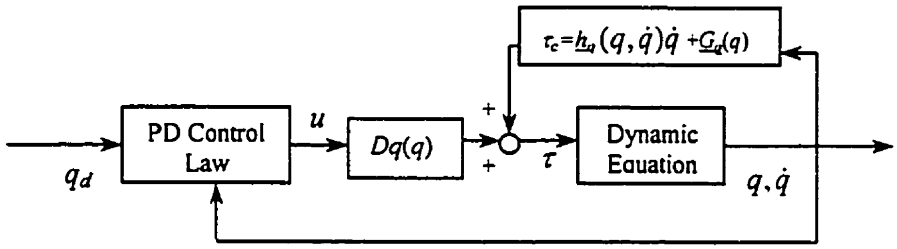

Figure 4.1 Block Diagram of the Closed-Loop Control System

The control gain matrices $\underline{K}_D$ and $\underline{K}_P$ are the parameters that can be adjusted to affect the system response. If λ is the natural frequency of the closed-loop system, the control gain matrices can be set as

$$\underline{K}_D = diag[2\lambda], \underline{K}_P = diag[\lambda^2] \tag{4.9}$$

The control gain matrices are chosen to obtain a critically damped closed-loop performance. The natural frequency λ should be chosen as sufficiently large in order to

get a fast system response, but, at the same time, it should not be too large in order to avoid excitation of the possibly unmodeled high frequency characteristics in the system.

As shown in equation (4.6), the nonlinear terms of the system dynamics are completely eliminated. This is true only if the physical parameters of the actual system are known exactly. In most of the physical systems, however, degrees of parametric uncertainty usually exist. When the parameter uncertainties exist in the biped system, the terms, $\underline{D}_q(q)$ $\underline{h}_q(q,\dot{q})\,\dot{q}$ and $\underline{G}_q(q)$, are not available exactly but can be estimated from equation (4.1) to (4.3). Instead of equation (4.4), one can only use the following control law:

$$\underline{T}_q = \hat{\underline{D}}_q(\underline{q})\underline{u} + \hat{\underline{h}}_q(\underline{q},\underline{\dot{q}})\underline{\dot{q}} + \hat{\underline{G}}_q(\underline{q}) \tag{4.10}$$

and instead of equation (4.6), the following equation is obtained

$$\underline{\ddot{q}} = (\underline{D}_q^{-1}\hat{\underline{D}}_q)\underline{u} + \underline{D}_q^{-1}(\hat{\underline{h}}_q\underline{\dot{q}} + \hat{\underline{G}}_q - \underline{h}_q\underline{\dot{q}} - \underline{G}_q) \tag{4.11}$$

It is obvious that equation (4.11) is not a linear equation. The nonlinearities are not cancelled exactly between the modeled system dynamics and the actual system dynamics. The control system is actually coupled and nonlinear. Trying to control the system with a linear control law will result in poor performance. The fact that no robustness is guaranteed in the presence of parameter uncertainty or unmodeled dynamics and is a major disadvantage of computed torque control.

4.5 Sliding Mode Control

Sliding model control is one class of robust nonlinear control that is designed based on consideration of both the modeled dynamic system and the presence of uncertainties in the model. The typical structure of a sliding mode control consists of a

nominal part similar to a computed torque control law and an additional part aimed at dealing with uncertainties in the model. The tracking control problem is to get the system angle profiles of the joint $(q,\dot{q})$ to track the desired joint angle profiles $(q_d,\dot{q}_d)$. This is equivalent to keeping the system trajectories remaining on the sliding surface. In order to do so, we have to define a time-varying surface $r(t)$. Subsequently, a control law is developed to direct the system trajectories toward the sliding surface. Firstly, the vector of the tracking error e is defined as

$$e = \underline{q} - \underline{q}_d$$
$$\dot{e} = \underline{\dot{q}} - \underline{\dot{q}}_d$$

A time-varying surface $r(t)$ for the second order system (2.19) (i.e., n=2) is defined as

$$r(t) = \left(\frac{d}{dt} + \lambda\right)^{n-1} e$$
$$= \dot{e} + \lambda e$$

If an integral term is used, a term $\int_0^t e\,dt'$ becomes the variable of interest instead of e.

The system is now considered to be third-order (i.e., n=3) (Slotine and Li 1991) and the time-varying surface $r(t)$ becomes

$$r = \left(\frac{d}{dt} + \lambda\right)^2 \left(\int_0^t e(t')\,dt'\right)$$
$$= \dot{e} + 2\lambda e + \lambda^2 \int_0^t e(t')dt' \qquad (4.12)$$

and

$$\dot{r} = \ddot{e} + 2\lambda\dot{e} + \lambda^2 e \qquad (4.13)$$

where λ is a diagonal matrix of positive gains given by λ=diag[λ_1, λ_2, ...λ_n].

As the time-varying surface $r(t)$=0, it becomes the sliding surface. For the traditional sliding mode control, the control algorithm is developed as the following to direct the system trajectories toward the sliding surface and to account for the presence of modeling imprecision.

$$\underline{T}_q = \underline{\hat{T}}_q - \underline{\eta}\,\mathrm{sgn}(r) \tag{4.14}$$

This algorithm is discontinuous across the sliding surface due to the signum function in equation (4.14). This control algorithm has been proven to attract those system trajectories that start off the sliding surface to move towards the surface and those that start on the surface to remain on it (Slotine and Sastry 1983). However, there is a shortcoming to this method. Due to the unavoidable small time delay in switching between control laws at the discontinuity surface, trajectories chatter around the sliding surface instead of sliding on it. Since chattering involves high control activity and may excite the high-frequency unmodelled dynamics in the system, it is undesirable in practice and has to be removed. Instead of the discontinuous control algorithm (4.14), we have developed a continuous control algorithm which can eliminate this chattering.

The control algorithm has the form

$$\underline{T}_q = \underline{\hat{T}}_q - \underline{\eta}\tanh(\alpha r) \tag{4.15}$$

where

$$\underline{\eta} = [\eta_1\ \eta_2 \cdots \eta_n]^T$$

The equation of motion (2.19) is in the following form

$$\underline{D}_q(\underline{q})\ddot{\underline{q}} + \underline{h}_q(\underline{q},\dot{\underline{q}})\dot{\underline{q}} + \underline{G}_q(\underline{q}) = \underline{T}_q$$

and the time derivative of the sliding surface $r(t)$ (4.13) can be rearranged as follows:

$$\begin{aligned}\dot{r} &= \ddot{e} + 2\lambda\dot{e} + \lambda^2 e \\ &= \ddot{\underline{q}} - \ddot{\underline{q}}_d + 2\lambda\dot{e} + \lambda^2 e \\ &= -\underline{D}_q^{-1}(\underline{h}_q(\underline{q},\dot{\underline{q}})\dot{\underline{q}} + \underline{G}_q(\underline{q})) + \underline{D}_q^{-1}\underline{T}_q - \ddot{\underline{q}}_d + 2\lambda\dot{e} + \lambda^2 e\end{aligned} \tag{4.16}$$

The best approximation $\hat{\underline{T}}_q$ of the control law that will achieve $\dot{r} = 0$ in equation (4.16) is

$$\hat{\underline{T}}_q = \hat{\underline{D}}_q(\underline{q})(\ddot{\underline{q}}_d - 2\lambda\dot{e} - \lambda^2 e) + \hat{\underline{h}}_q(\underline{q},\dot{\underline{q}}) + \hat{\underline{G}}_q(\underline{q}) \tag{4.17}$$

Instead of keeping trajectories on the surface $r(t)=0$, the control algorithm maintains the trajectories close to the surface within a thin boundary layer. Once the system trajectories move into the boundary layer, they will remain inside the boundary layer. The parameter α in equation (4.15) is the inverse of the boundary layer thickness with $\varepsilon=1/(\alpha\lambda^{n-1})$. Now we are not tracking for a "perfect" performance but tracking to within a guaranteed precision, $|e^{(i)}|\leq 2\lambda^i\varepsilon$ (Slotine and Li 1991).

4.5.1 Stability Analysis of the Sliding Model Control Algorithm

Before we study the stability of the control system, the following assumptions and preliminaries must be made:

1. The inertia matrix $\underline{D}_q>0$, i.e., $\underline{D}_q$ is positive definite.
2. The matrix $(\dot{\underline{D}}_q - 2\underline{h}_q)$ is skew-symmetric (Slotine and Li 1991). Hence,

$$x^T(\dot{\underline{D}}_q - 2\underline{h}_q)x = 0$$

3. Properties of the Euclidean norm

$$\|x\| \leq \sum_{i=1}^{n}|x|$$

and

$$x^T A \leq \|x\|\|A\|$$

4. For any $x \neq 0$, and any positive α

$$x_i[\tanh(\alpha x_i)] > 0$$

and

$$x_i[\tanh(\alpha x_i)] = | x_i | [\tanh(\alpha | x_i |)]$$

where tanh(.) is a function defined as

$$\tanh(x) = \frac{e^{x} - e^{-x}}{e^{x} + e^{-x}}$$

tanh(.) is a smooth sigmoidal function that switches about zero to force the state to converge to zero.

5. The equation of motion (2.19) developed in Chapter 2 has the form of

$$\underline{D}_q(\underline{q})\ddot{\underline{q}} + \underline{h}_q(\underline{q}, \dot{\underline{q}})\dot{\underline{q}} + \underline{G}_q(q) = \underline{T}_q$$

We define a value v which is related to r

$$v = \dot{\underline{q}} - r = \dot{\underline{q}}_d - 2\lambda e - \lambda^2 \int_0^t e(t')dt' \tag{4.18}$$

$$\dot{v} = \ddot{\underline{q}} - \dot{r} = \ddot{\underline{q}}_d - 2\lambda \dot{e} - \lambda^2 e \tag{4.19}$$

Therefore, equation (2.19) can be rewritten as

$$\underline{D}_q(\underline{q})\dot{r} + \underline{h}_q r = \underline{T}_q - \Delta \tag{4.20}$$

where Δ is given as

$$\Delta = \underline{D}_q \dot{v} + \underline{h}_q v + \underline{G}_q \tag{4.21}$$

The attractiveness of the boundary can be proven using Lyapunov's direct method. Consider the Lyapunov function candidate given by

$$V = \frac{1}{2} r^T \underline{D}_q r \tag{4.22}$$

where V is positive definite and $V \rightarrow \infty$ as $\|r\| \rightarrow \infty$.

Using the above assumptions and preliminaries, the derivative of V along the trajectory of the solutions of (4.20), is given by

$$\begin{aligned}
\dot{V} &= \frac{1}{2} r^T \underline{\dot{D}}_q r + r^T \underline{D}_q \dot{r} \\
&= \frac{1}{2} r^T (\underline{\dot{D}}_q - 2\underline{h}_q) r + r^T (\underline{T}_q - \Delta) \\
&= -\sum_{i=1}^{n} r_i \eta_i \tanh(\alpha r_i) + \sum_{i=1}^{n} r_i (\hat{\underline{T}}_q - \Delta_i) \\
&\le -\sum_{i=1}^{n} |r_i| \eta_i \tanh(\alpha |r_i|) + \sum_{i=1}^{n} |r_i| |\Delta_i - \hat{\underline{T}}_q| \qquad (4.23) \\
&\le -\left[\sum_{i=1}^{n} |r_i| \eta_i (\tanh(\alpha |r_i|) - \mu_i) \right]
\end{aligned}$$

where $\mu_i = \dfrac{|\Delta_i - \hat{\underline{T}} q|}{\eta_i}, \quad 0 \le \mu_i \le 1$

It is clear that in order to guarantee $\dot{V} < 0$, the following condition must be satisfied.

$$\tanh(\alpha_i |r_i|) - \mu_i \ge 0, i = 1, 2, \ldots, n$$

Thus, $\dot{V} < 0$ for all

$$|r_i| \ge \frac{1}{2\alpha_i} \ln\left[\frac{1+\mu_i}{1-\mu_i}\right] = \beta_i$$

By increasing the value of α_i it is possible to find the bound of β_i. Therefore, r is also bounded. Similarly to the discussion in Slotine and Li (1991), the parameter β_i indicates the thickness of the boundary layer within which the control discontinuity is smoothed out. From the above analysis, the control algorithm guarantees the attractiveness of the boundary layer and discontinuity is eliminated. The initial conditions can be arbitrarily chosen so that the system trajectories are started inside the boundary and will stay inside the boundary due to its attractiveness. Therefore, no reaching phase problem will occur.

4.6 Summary

In this chapter, two nonlinear control techniques were presented. The traditional computed torque control technique is a conceptually simple nonlinear control technique. Computed torque is developed based on a feedback linearization technique that can fully compensate the nonlinear forces in the dynamic system and lead to high accuracy control for a very large range of robot speeds. The major disadvantage of this technique is that no robustness can be guaranteed in the presence of parametric uncertainty in the system. The traditional sliding mode control technique, on the other hand, is developed based on the consideration of parametric uncertainty. Nonlinearities are intentionally introduced into the control law that tolerates the parametric uncertainty, making the system robust. However, the system is known to chatter. A sliding mode control algorithm with the discontinuous term replaced by a continuous term was presented in this chapter, which guaranteed the tracking error to be within a certain precision and eliminated the chattering problem and the reaching phase problem.

Chapter 5

Simulation Results

5.1 Introduction

In this chapter, the results of a simulation study are presented for the planar five-link biped walking on a flat horizontal surface. The simulation study contains two parts. The first part is determination of the desired joint angle profiles based on the systematic approach discussed in Chapter 3. These joint angle profiles will be used as the desired joint angle profiles for motion regulation. Some insights into energy input during walking are also investigated. The second part is motion control using the computed torque control technique and the sliding mode control technique.

In Section 5.2, the results of the desired angle profile of each joint during walking on a flat horizontal surface in the single support phase are presented. The desired joint angle profiles are determined by the five constraint functions developed in Chapter 3, namely, (1) the erect body posture, (2) the overall progression speed, (3) the bias of the knee of the support leg, (4) the coordination of the support leg and swing leg motion, and (5) constant mechanical energy. Furthermore, a set of acceptable joint angel profiles must satisfy the repeatability condition and the condition that the knee of the swing leg

does not bend backward. Four different progression speeds with the same bias angles are selected to be studied and the results are presented.

In Section 5.3, the simulation study of motion control is presented. The goal of motion control is to realize a steady stable gait of the biped walking on a flat horizontal surface. A comparison of the tracking performance of the computed torque control and the sliding mode control is investigated. This section also demonstrates the capability of the two control techniques to control the bipedal locomotion system with the presence of parametric uncertainties. The theoretical expectation is that the sliding mode control technique is superior to the computed torque control technique, when parametric uncertainties exist in the system. The reason for this expectation is that sliding mode control is designed based on the consideration of both the modeled dynamic system and the presence of uncertainties in the model. Nonlinearities are intentionally introduced into the control law that tolerate parametric uncertainty to make the system robust. This theoretical expectation will be investigated through the study of the simulation results presented in Section 5.3.

5.2 The Results of the Joint Angle Profiles Planning

By using the methodology for joint angle profiles planning discussed in Chapter 3, the desired joint angle profiles for the motion of the five-link biped walking on a flat horizontal surface can be obtained from the five constraint functions. Intensive numerical simulations were carried out to generate different sets of joint angle profiles with different progression speeds (V_p). When generating the joint angle profiles, the repeatability condition, which requires that the posture of the biped robot at the end of the

step be very close to the initial posture, has to be considered. As mentioned in Chapter 3, the constraint functions S_1, S_2 and S_3 (i.e., equations (3.1) to (3.3)) are decoupled from the other two constraint functions. Therefore, the joint angle profiles for the supporting leg and the upper body can be determined first. Subsequently, the joint angle profiles of the swing leg can be determined from the remaining constraints, S_4 and S_5 (i.e., equations (3.4) and (3.5)). During the intensive numerical simulations, it was often found that either the knee of the swing leg would bend backward or the end states would not be close enough to the initial states to ensure the start of the next step. Walking with the knee bent backward is not desirable and such joint angle profiles are not acceptable. As well, the condition of repeatability must be satisfied in order to initiate the next step. Therefore, the acceptable joint angle profiles must be those that (1) satisfy the constraint functions presented in Section 3.2.1, (2) are repeatable and (3) do not cause the knee of the swing leg to be bent backward. Such requirements make the determination of the acceptable joint angle profiles highly challenging. In the simulation study, four different progression speeds with the same bias angles were used. For each walking speed, a set of joint angular displacements and velocities were obtained. Also, from the simulation results of the four different progression speeds, the hypothesis of giving only potential energy at the beginning of the step so that the swing leg can be carried over without extra energy input is investigated.

5.2.1 Simulation Study of the Joint Angle Profiles Design

The values of the parameters m_i, I_i, l_i and d_i of the five-link biped robot are listed in Table 5.1 and are used for generating joint angle profiles and, later, motion regulation.

Link		Mass, m_i (kg)	Moment of inertia, I_i (kg-m^2)	Length, l_i (m)	Location of center of mass, d_i (m)
1,4	Shank	2.23	3.30×10^{-2}	0.332	0.189
2,5	Thigh	5.28	3.30×10^{-2}	0.302	0.236
3	Upper Body	14.79	3.30×10^{-2}	0.486	0.282

Table 5.1 Parameters of the biped robot

The four cases with their progression speeds are as follows:

1). V_p = 0.5596 m/sec (slow walking speed)

2). V_p = 1.11306 m/sec (moderate walking speed 1)

3). V_p = 1.11354 m/sec (moderate walking speed 2)

4). V_p = 1.4502 m/sec (fast walking speed)

The bias angle of the knee of the support leg is set as 0.1 radian for all cases and the initial posture of the biped with the following angular displacements is used for all cases.

$$q_0 = -0.1642 \text{ radian} \quad q_1 = 0.1 \text{ radian} \quad q_2 = -0.2642 \text{ radian}$$

$$q_3 = -0.1642 \text{ radian} \quad q_4 = 0.1 \text{ radian}$$

The initial angular velocities at each joint are zero,

i.e., $\dot{q}_0 = \dot{q}_1 = \dot{q}_2 = \dot{q}_3 = \dot{q}_4 = 0$ radian / sec

This set of initial conditions indicates that all energy in the five-link bipedal system is in the form of potential energy. The kinetic energy is zero at the beginning of the step. Following the procedure outlined in Chapter 3, the parameters α, β and γ, contained in the matrices, C_1, C_2 and C_3 (defined in equation (3.6)), for all simulations of four different walking speeds are chosen such that the solution set of S_i (defined in equation (3.6)) is asymptotically stable about the origin. The values of α, β and γ, are shown below:

$$\alpha = 13.0 \qquad \beta = 52.02 \qquad \lambda = -5.99$$

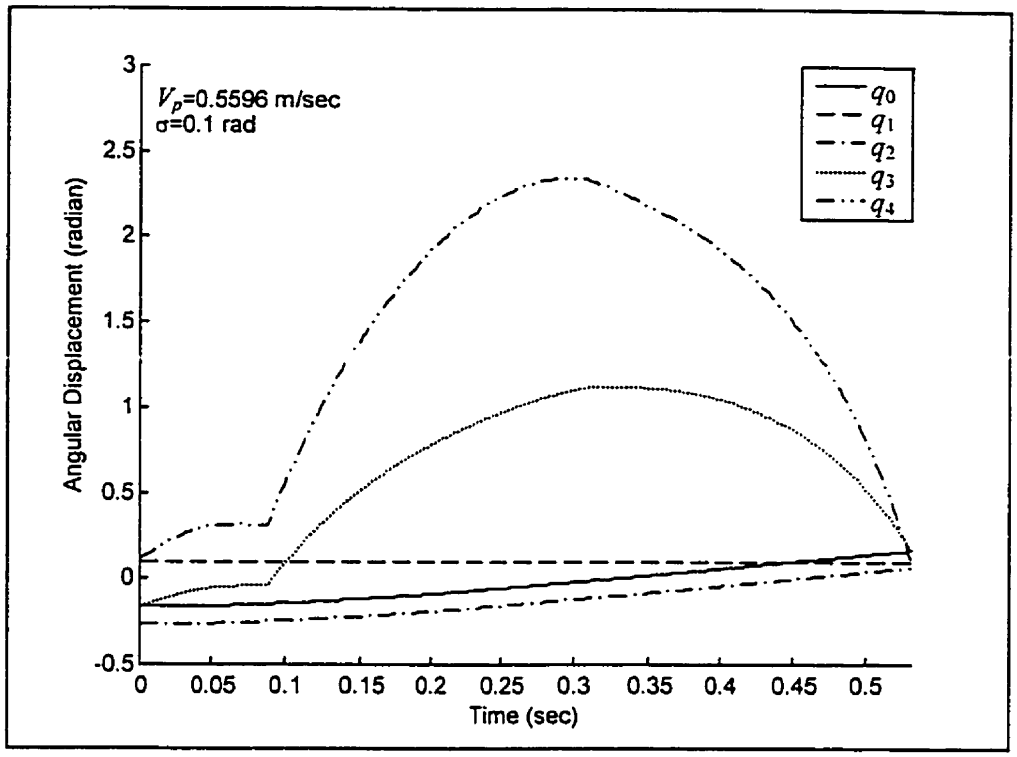

Figure 5.1 Angular displacements of Joints for Case 1.

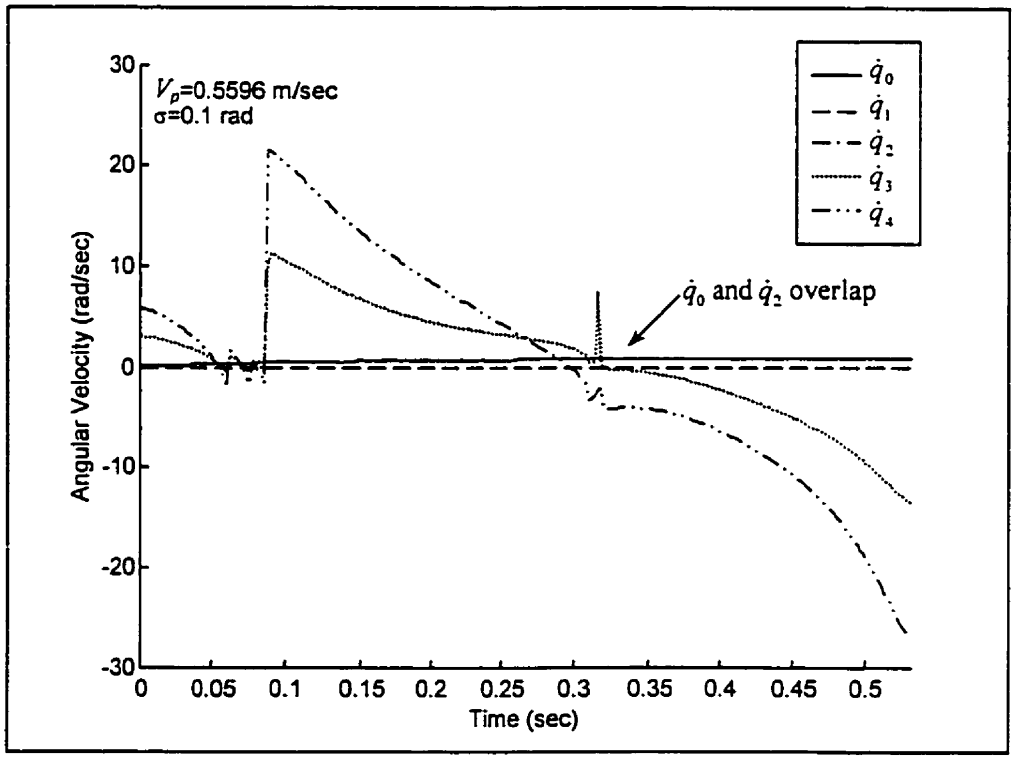

Figure 5.2 Angular Velocities of Joints for Case 1.

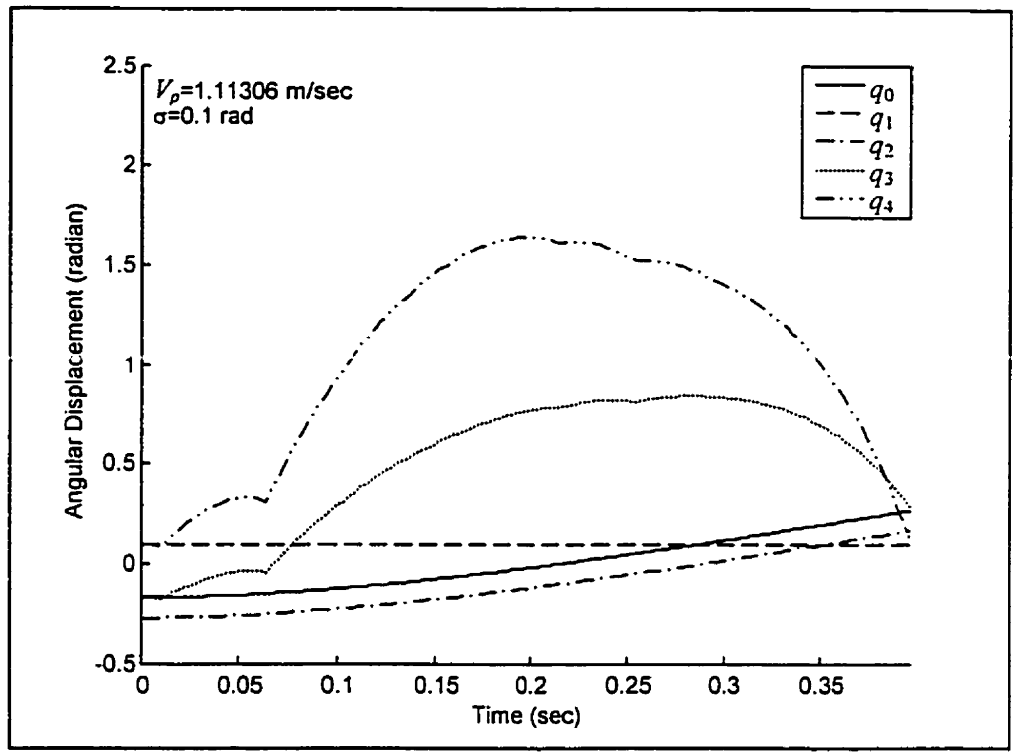

Figure 5.3 Angular Displacements of Joints for Case 2.

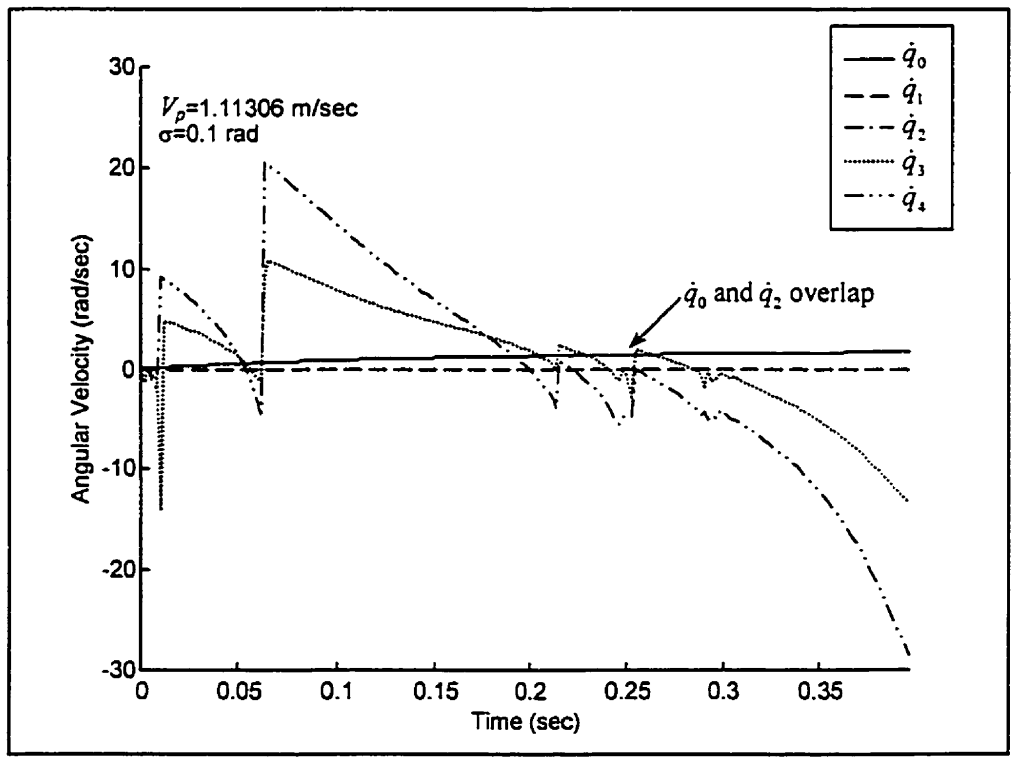

Figure 5.4 Angular Velocities of Joints for Case 2.

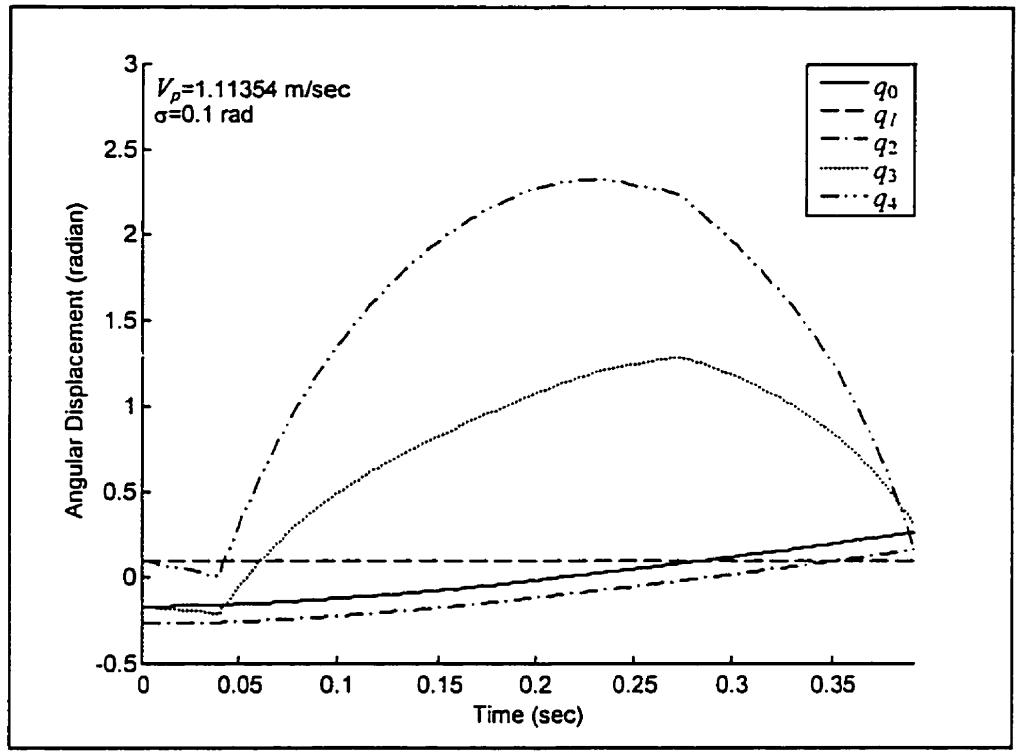

Figure 5.5 Angular Displacements of Joints for Case 3.

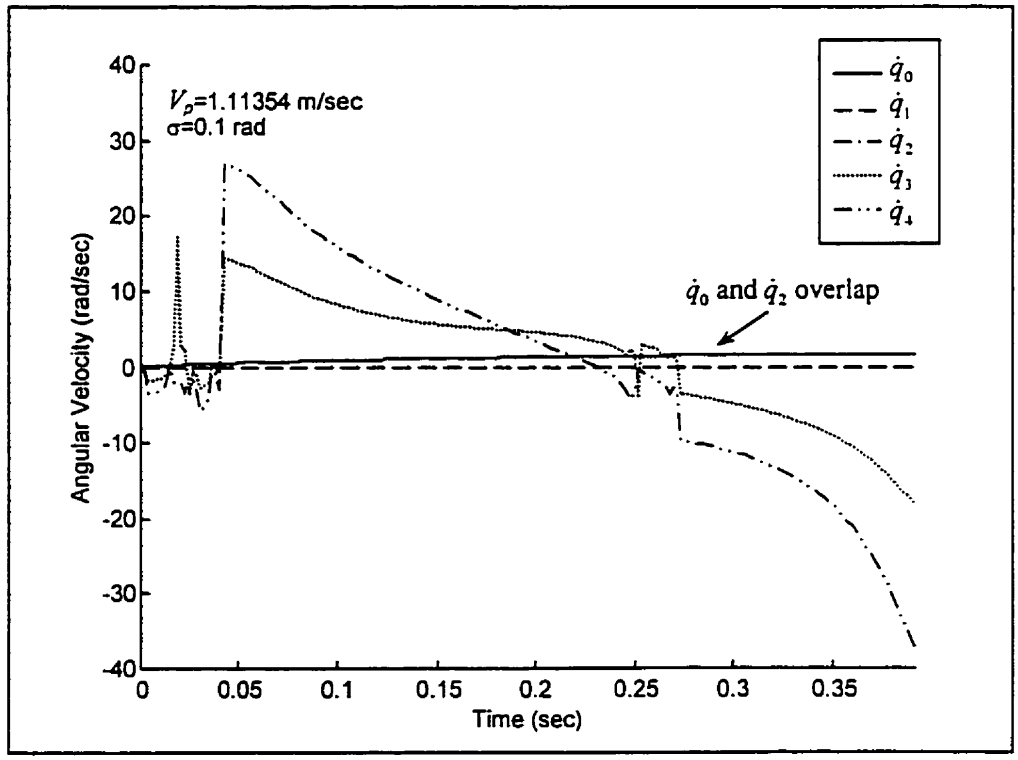

Figure 5.6 Angular Velocities of Joints for Case 3.

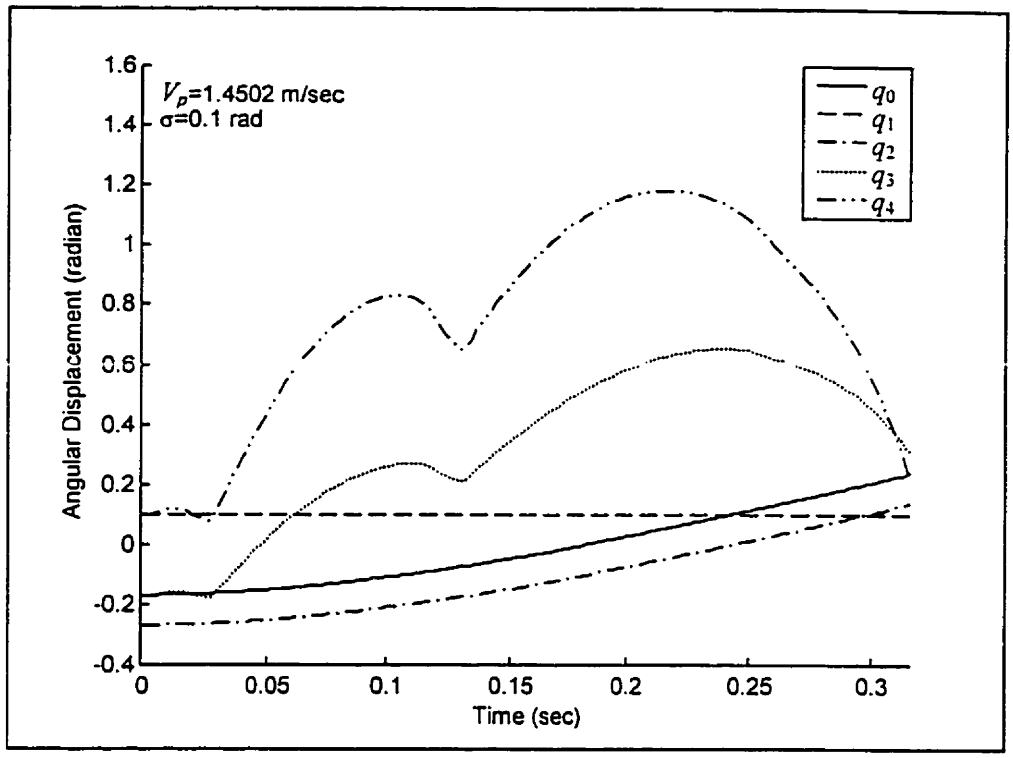

Figure 5.7 Angular Displacements of Joints for Case 4.

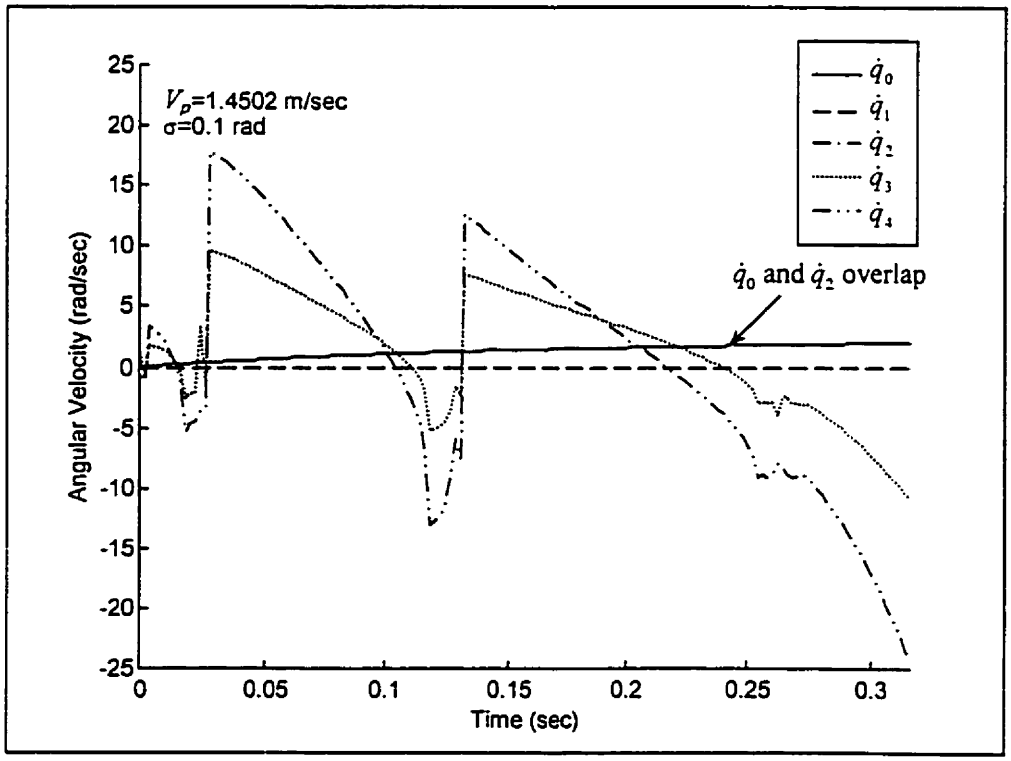

Figure 5.8 Angular Velocities of Joints for Case 4.

The discussions of the simulation results of the joint angle profiles design are presented here in two parts. The first discussion concerns the angular displacement profiles and the angular velocity profiles of all five joints, while the second discussion concerns the energy profiles corresponding to the four different speeds. Figures 5.1 to 5.8 show the profiles of the angular displacements and velocities of all five joints versus time for one step obtained for the four cases. It should be mentioned in here that the numerical solution obtained from solving the constraint functions is very sensitive to the choice of the initial conditions and parameters. The joint angle profiles presented here are the best and acceptable results in that they generated the walking motion that is prescribed by the all five constraint functions shown in equations (3.1) to (3.5), and they also satisfied the repeatability condition and the condition that the knee of the swing leg does not bend backward. The angular displacements and velocities of q_0, q_1 and q_2 show the motion of the support leg and those of q_3 and q_4 show the motion of the swing leg for one step. From Figures 5.1 to 5.8, it can be seen that the joint angle profiles are different with different progression speeds but the patterns are similar.

The simulation results for the fast walking speed is used here as an example for further discussion of the desired joint angle profiles. Note that similar observations can be made for those with other walking speeds. Figure 5.9 shows the stick figure of the five-link biped with the walking motion obtained from the fast walking case, where V_p=1.4502 m/sec. From this figure, one can observe the overall motion of the biped during the single support phase. The solid line represents the support leg and the upper body and the dash line represents the swing leg.

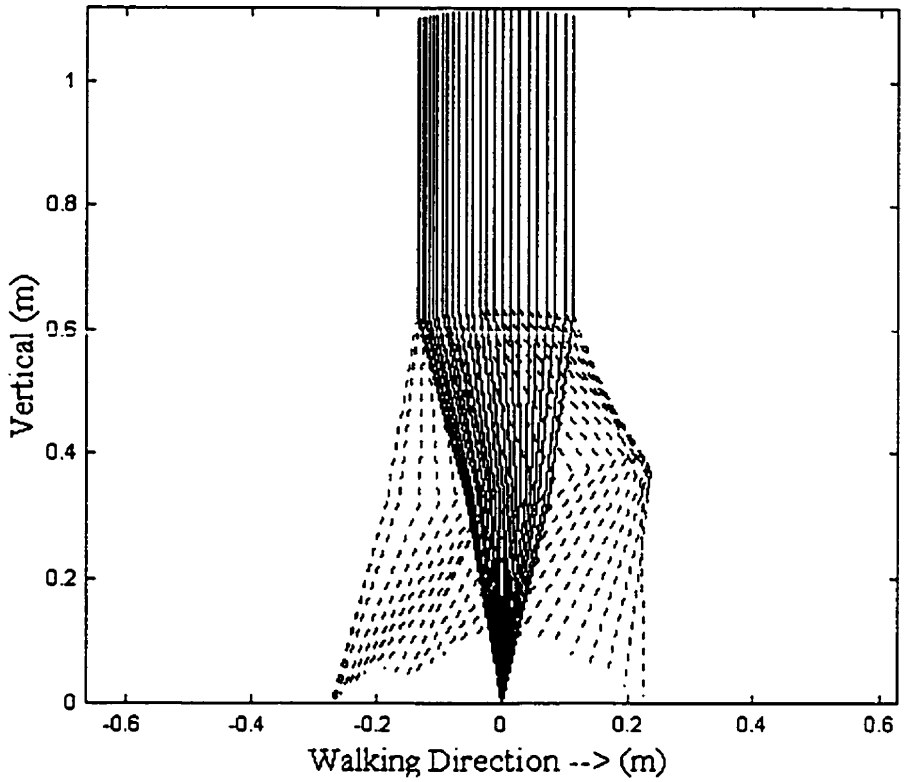

Figure 5.9 Stick Figure of the Walking Motion of the Five-Link Biped

The support leg, with its tip as the support, propels the upper body forward in the walking direction. The upper body is maintained at the upright position and moves forward with the speed gradually increasing from zero at the start of the step to the desired progression speed. The knee joint (q_1) of the support leg is kept constant, which is equal to the bias angle (σ), throughout the single support phase. This guarantees that the knee will not collapse or bend backward. The swing leg leaves the walking surface at the beginning of the step and swings forward. At the end of the step the swing leg comes back on the walking surface. It can be seen from the stick figure that the knee of the swing leg does not bend backward. The stick figure also shows that the position of the upper body is always between the tips of the two legs.

From the above discussion, it shows that the walking motion resulting from the fast walking case (V_p=1.4502 m/sec) corresponds to the motion described by the constraint functions and approximates to natural walking. As can be seen in Figure 5.9, the ending posture of the biped is close to the starting posture. The configuration of joints of the ending posture (i.e. the starting posture for the next step) are as follows:

$$q_0 = -0.114 \text{ radian}$$

$$q_1 = 0.172 \text{ radian}$$

$$q_2 = -0.286 \text{ radian}$$

$$q_3 = -0.141 \text{ radian}$$

$$q_4 = 0.100 \text{ radian}$$

A close initial and end configuration indicates that this set of joint angle profiles also satisfies the repeatability condition. Therefore, we selected this set of joint angle profiles obtained with the fast walking speed (V_p=1.4502 m/sec) to be used later as the desired joint angle profiles for the motion control.

We next discuss the observations from the mechanical energy profiles for the walking being studied. The question we would like to address is: given only potential energy at the initiation of the step, is it possible for the swing leg to be carried through the step without extra energy input? This question can be answered by investigating the mechanical energy profiles from the numerical simulation results. Figures 5.10 to 5.13 show the mechanical energy profiles of the biped robot during the single support phase of the four cases. These four figures show that, with the other four constraints (i.e., equations (3.1) to (3.4)) satisfied, it is not possible to keep the energy constant during the whole step. Therefore, extra energy must be inputted to the bipedal system regardless of

the walking speed. Figures 5.10 to 5.13 show that regardless of the walking speed, energy input is required at the beginning of the step. Such an energy input causes a sudden increase in angular velocities at the joints of the swing leg (see Figures 5.2, 5.4, 5.6 and 5.8 for details). That means that a sudden input of energy is needed for the swing leg at the beginning of the step to initialize the step regardless of the walking speed. Such an initial energy input may be provided by the actuators or by the natural strain energy release of the deformable feet of the bipedal model. Depending on the walking speed, there might be a need for a second energy input. Such energy input occurs approximately when the support leg, swing leg and the upper body are around the upright position. Figures 5.2, 5.4, 5.6 and 5.8 show that the levels of angular velocities increase are lower for the slow walking case than for the fast walking case. Figures 5.10 to 5.13 also show that the second energy input is necessary for the fast walking case. This extra energy input is needed to move the swing leg ahead of the gravity center of the upper body at the mid point of the tip of the two legs (i.e., satisfying constraint function S_4). For slow walking, such an energy input may not be necessary. Energy input is proportional to the walking speed, i.e., higher walking speed demands higher total energy input.

It is interesting to note that for the slow and moderate walking speeds, it is possible to design a set of joint angle profiles such that, with a proper initial energy input, the swing leg can be carried through the step without extra energy input. This finding is important from the viewpoint of development of bipedal robots. The biped that follows such a set of joint angle profiles is more energy efficient since the initial energy can be provided by the strain energy release of the deformable foot.

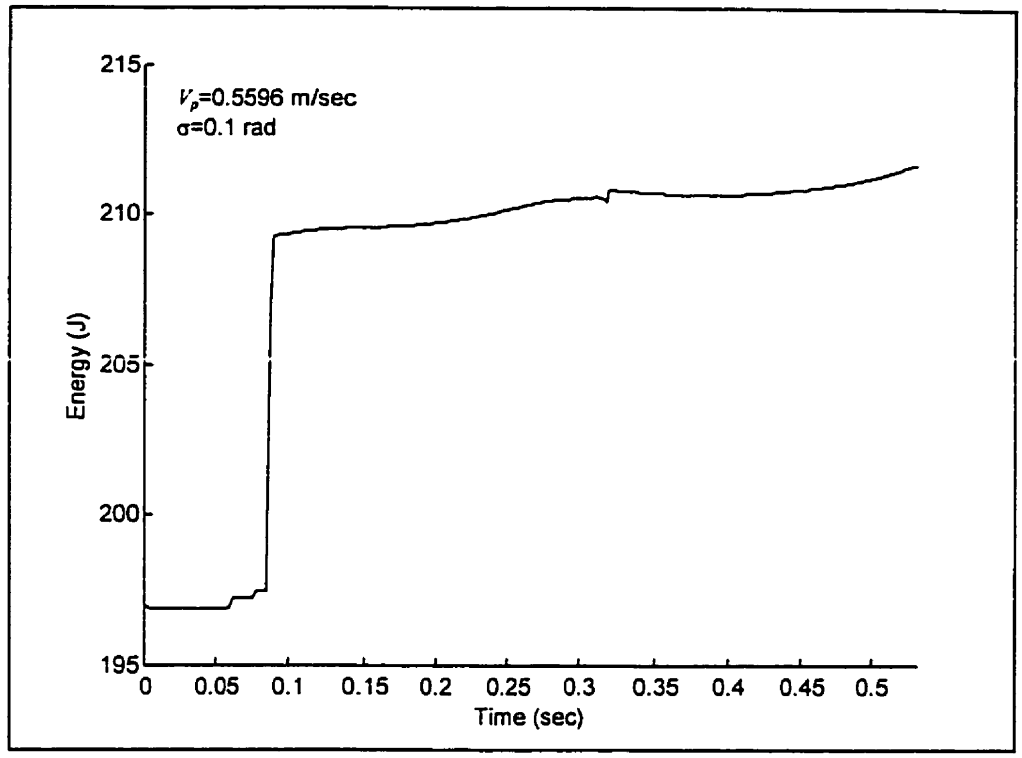

Figure 5.10 Mechanical Energy of Case 1

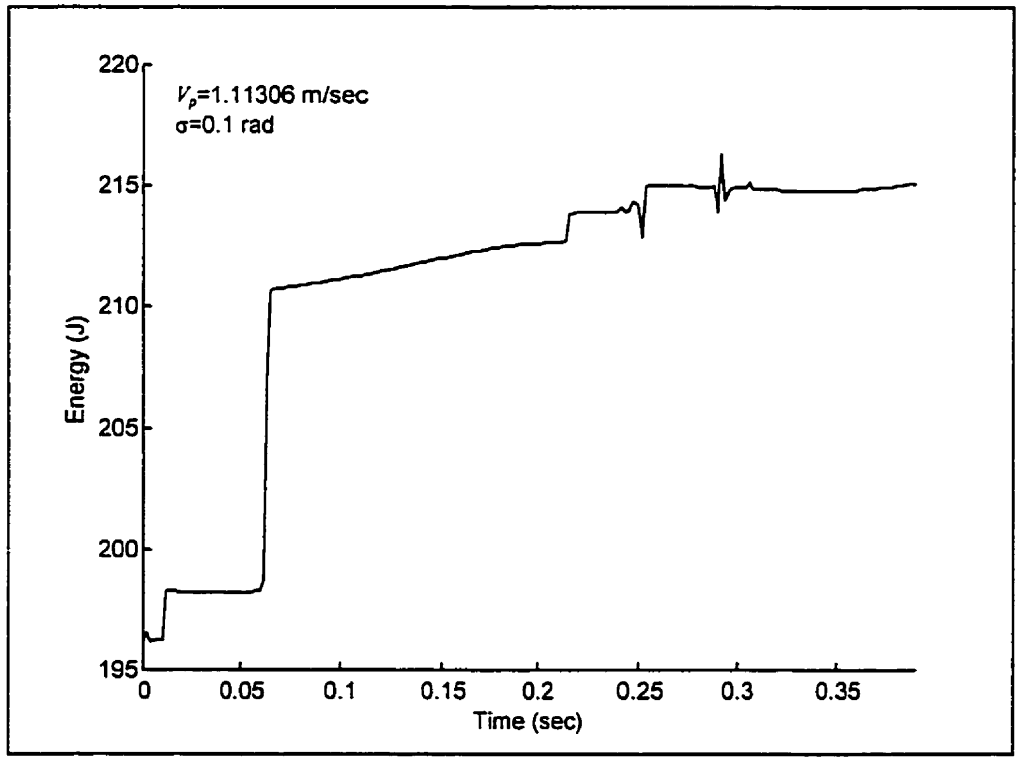

Figure 5.11 Mechanical Energy of Case 2

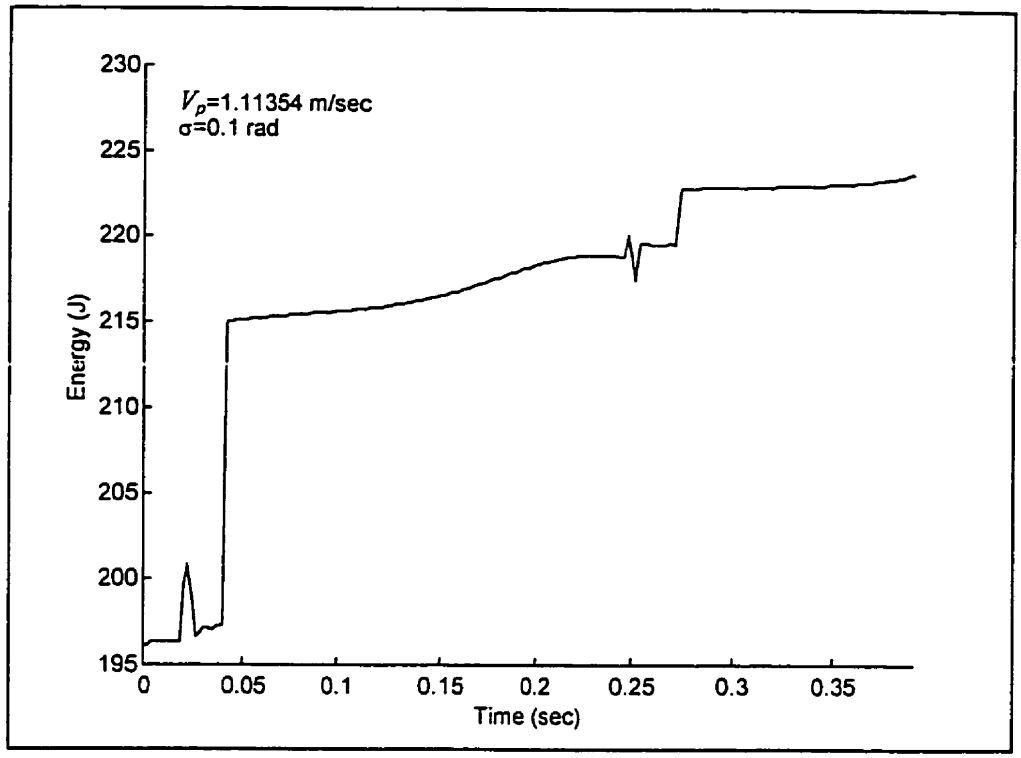

Figure 5.12 Mechanical Energy of Case 3

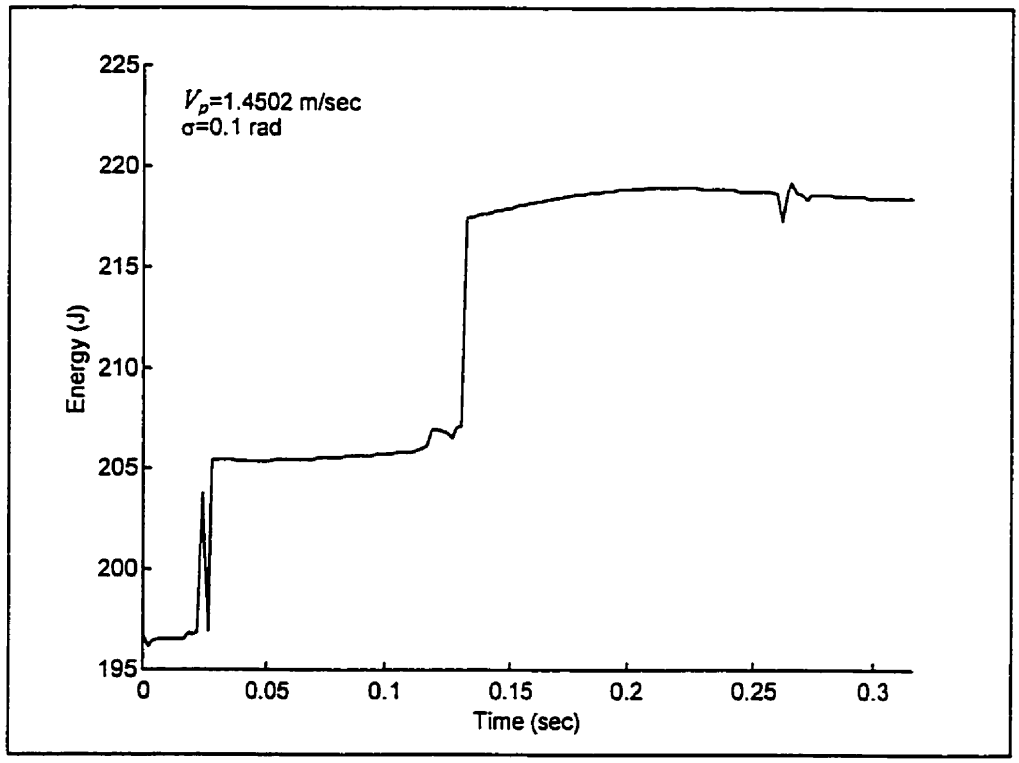

Figure 5.13 Mechanical Energy of Case 4

5.3 Simulation Results of the Motion Control

In this section, the results of the simulation study of the motion control are presented for the case where the five-link biped is walking on a flat horizontal surface. Computed torque control and sliding mode control techniques were applied for motion control. The tracking performances of these two techniques were compared for various degrees of parametric uncertainty existing in the system. The computed torque control technique requires an exact knowledge of the system parameters. When this is not the case, it is believed that the computed torque control is expected to be not as robust as the sliding mode control. This expectation was investigated by the results shown in this section.

The five-link biped robot studied here is shown in Figure 2.1. The values of the parameter m_i, I_i, l_i and d_i are listed in Table 5.1. A set of joint angle profiles obtained from Section 5.1 with walking speed of 1.4502 m/sec was used as the desired joint angle profiles. The objective of this simulation study was to investigate the performance of the sliding mode control and the performance of the computed torque control as the degree of the parametric uncertainties (e_m, e_I, e_l and e_d) (see detailed definition of e_m, e_I, e_l and e_d in Section 4.3) increase. Three cases were studied here:

Case 1. No uncertainty ($e_m = e_I = e_l = e_d = 0\%$)

Case 2. 40% uncertainty ($e_m = e_I = 0.4$ (40%) and $e_l = e_d = 0.1$ (10%))

Case 3. 200% uncertainty ($e_m = e_I = 2$ (200%) and $e_l = e_d = 0.1$ (10%))

For Case 1 (No uncertainty), the physical parameters of the biped, such as link masses, moments of inertia, lengths and positions of the centers of mass, are exactly known. For Case 2 and Case 3, dominating parametric uncertainties are present in the mass and

moment of inertia parameters and smaller uncertainties are present in the geometric parameters. The parametric uncertainties of each link are assumed to be the same. All the simulation results were carried out with time step T_s=0.002sec and are shown in graphical form.

In Case 1 (No uncertainty), computed torque control and sliding mode control techniques were applied. For the computed torque control law, the control gain matrices $\underline{K_D}$ and $\underline{K_P}$ (shown in equation (4.7)) needed to be adjusted to obtain good tracking performance. Since we set $\underline{K_D}$=diag[2λ] and $\underline{K_P}$=diag[λ^2] (shown in equation (4.9)), there was only one parameter (λ) to adjust, where λ was chosen to be 80 in this case for the best tracking performance. For the sliding mode control law, the parameters λ and α (shown in equations (4.15) and (4.17)) needed to be adjusted. The best tracking results were obtained with the choice of λ = 18 and α = 0.2. Figures 5.14 to 5.18 show the angular displacement of each joint (i.e., q_0, q_1, q_2, q_3 and q_4). The solid line represents the result obtained with the sliding mode control law applied. The dashed line represents the result obtained with the computed torque control law applied. The dotted line represents the desired joint angle profile. Figures 5.14a to 5.18a show the angular displacements of the first three steps and Figures 5.14b to 5.18b show the angular displacements from the seventh to tenth step. The time period of one step was approximately 0.32 sec. The discontinuity appearing at the end of each step is due to the renumbering of links to incorporate the switching of the roles of support and swing leg. It should be noted here that the ending posture and the starting posture of the biped from the set of desired joint angle profiles were not exactly the same. Even though the control law performs a perfect tracking, there will be a large error occurring at the beginning of

each step. A similar problem has been found in other related work (Tzafestas et al. 1996). Therefore, similarly to other such study, all discussions presented here only consider the period of time during the step (i.e., away from the beginning of each step). One can observe that the simulated joint angle profiles of the computed torque control and the sliding mode control followed the desired joint angle profiles quite closely at the beginning. However, after a few steps, the simulated joint angle profiles of the computed torque control were deviated from the desired joint angle profiles. The tracking performance was evaluated in terms of the total of the absolute values of the error $e(t)$, where $e(t)$ is the difference between the simulated angular displacement and the desired angular displacement of each joint. The equation of the tracking error can be represented by (Tzafestas et al. 1996)

$$|e(t)|=|e_0(t)|+|e_1(t)|+|e_2(t)|+|e_3(t)|+|e_4(t)| \tag{5.1}$$

Figure 5.19 shows the tracking errors of the results obtained through the sliding mode control and the computed torque control. The overall tracking error of the sliding mode control, which is shown by a solid line in Figure 5.19, was lower than that of the computed torque control, which is shown by a dashed line. The tracking errors near the switching of support and swing leg were neglected due to the reason discussed earlier. The average tracking error of the computed torque control was about 0.0331 radians, while the average tracking error of the sliding mode control was only about 0.018 radians. The tracking error obtained from the computed torque control was almost twice that obtained from the sliding mode control. Figures 5.20a to 5.24a show the control torque of each joint. Again, in these figures the solid line represents the results of the sliding mode control and the dashed line represents the results of the computed torque

control. Figures 5.20b to 5.24b show the control torques within one step. The control torques of both the sliding mode control and the computed torque control were comparable and within a reasonable range. This means that the control torques applied to the joints of the biped were similar for the sliding mode control and the computed torque control. Thus, with the comparable of control torques, the sliding mode control showed better tracking performance than the computed torque control in this case.

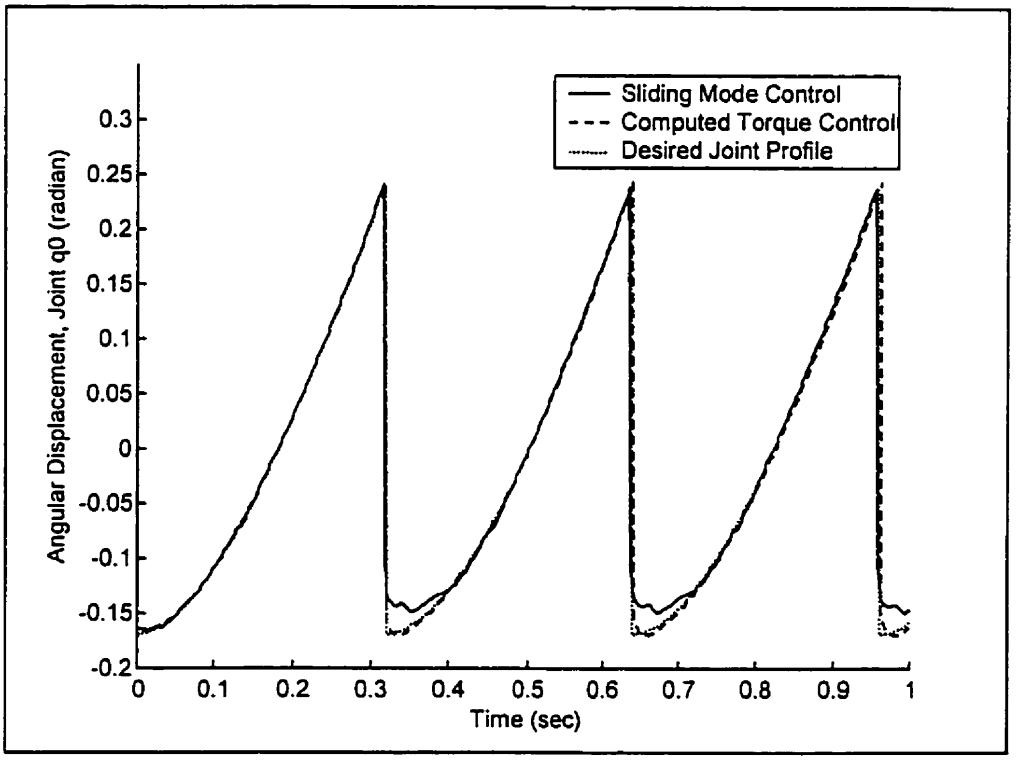

Figure 5.14a Angular Displacement (q_0) of Step 1 to 3 for Case 1

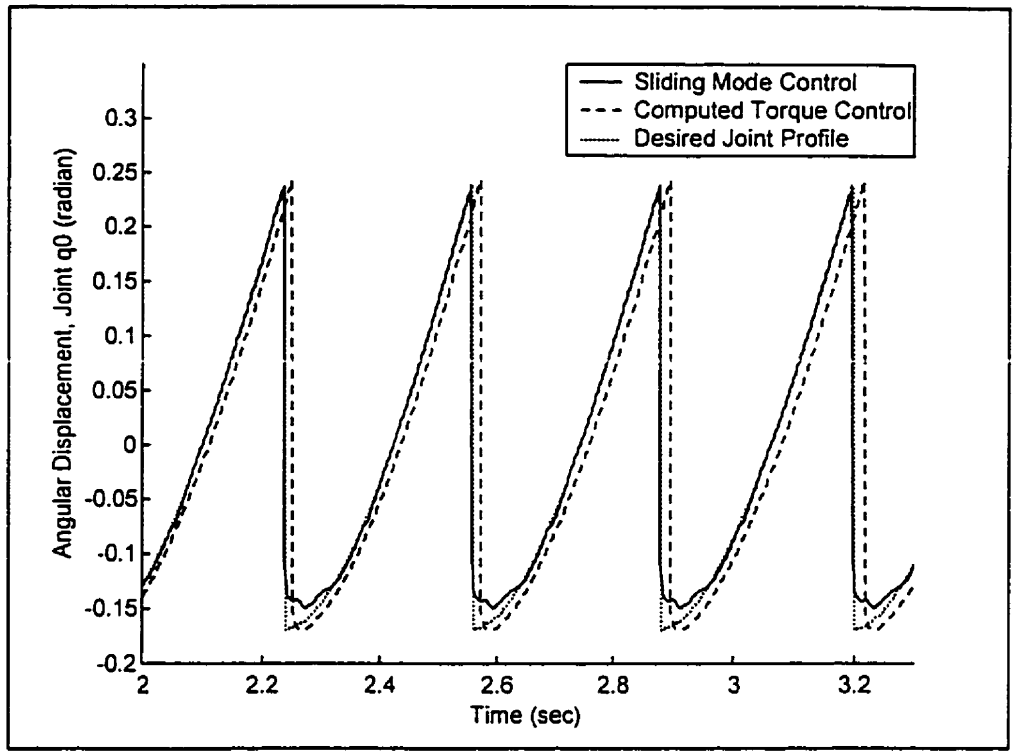

Figure 5.14b Angular Displacement (q_0) of Step 7 to 10 for Case 1

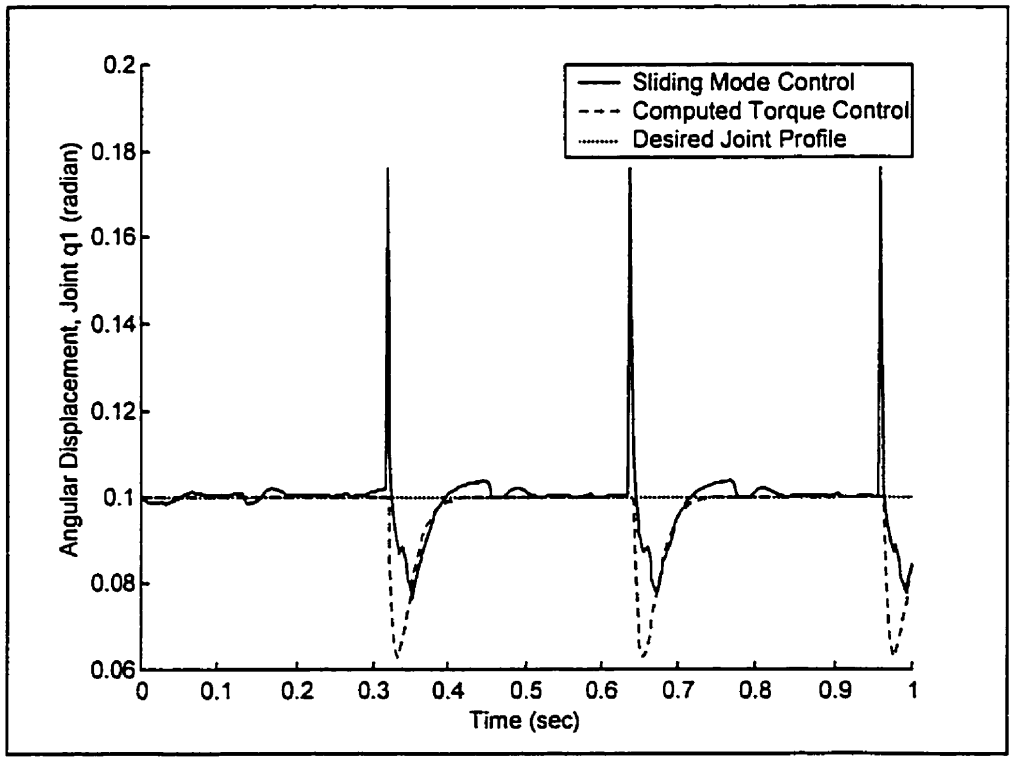

Figure 5.15a Angular Displacement (q_1) of Step 1 to 3 for Case 1

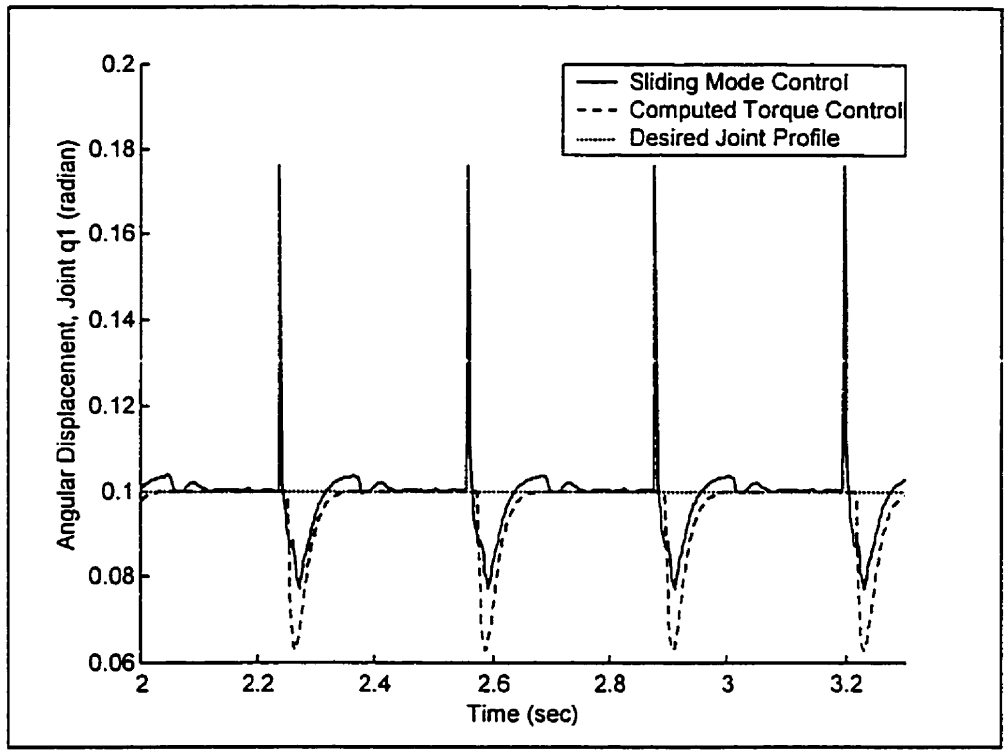

Figure 5.15b Angular Displacement (q_1) of Step 7 to 10 for Case 1

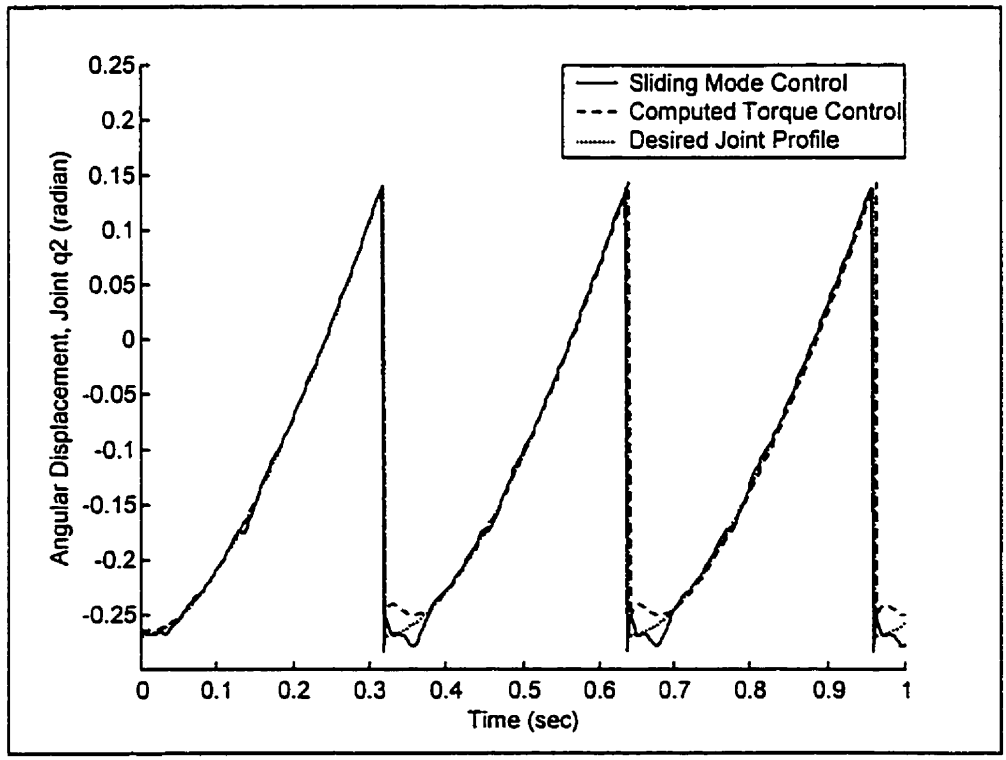

Figure 5.16a Angular Displacement (q_2) of Step 1 to 3 for Case 1

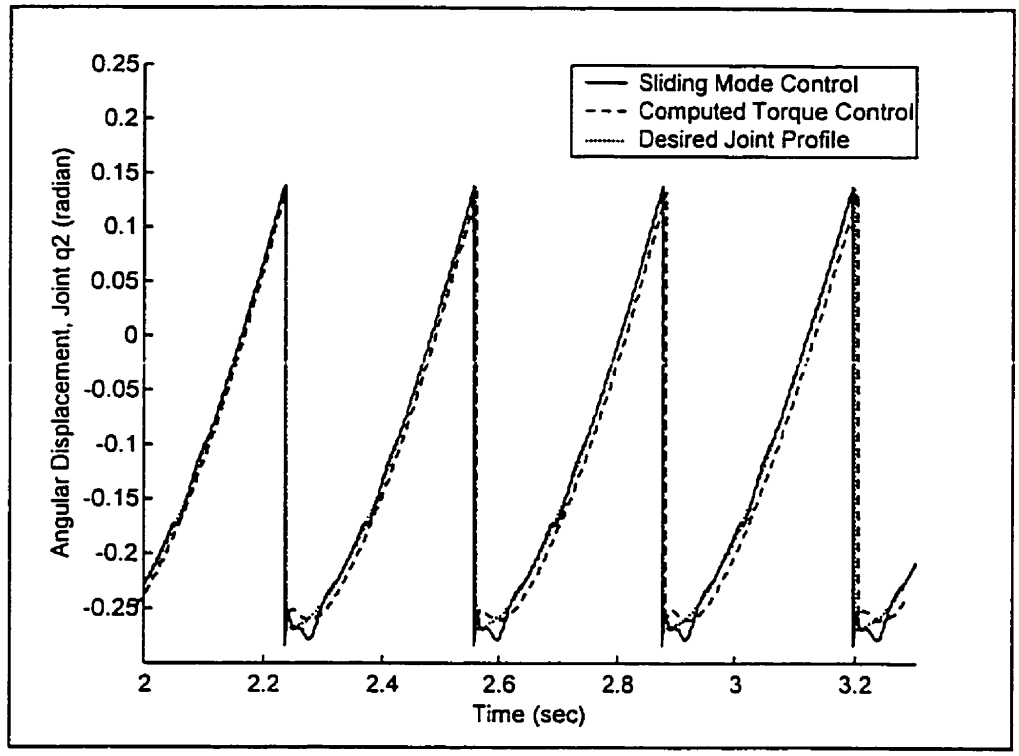

Figure 5.16b Angular Displacement (q_2) of Step 7 to 10 for Case 1

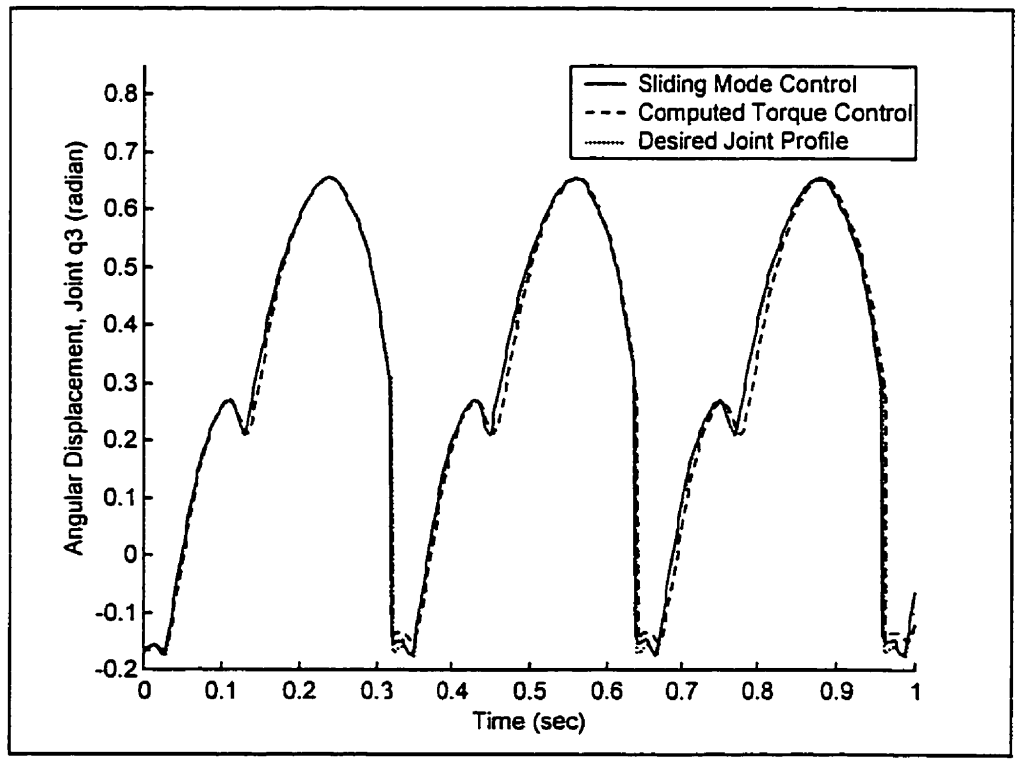

Figure 5.17a Angular Displacement (q_3) of Step 1 to 3 for Case 1

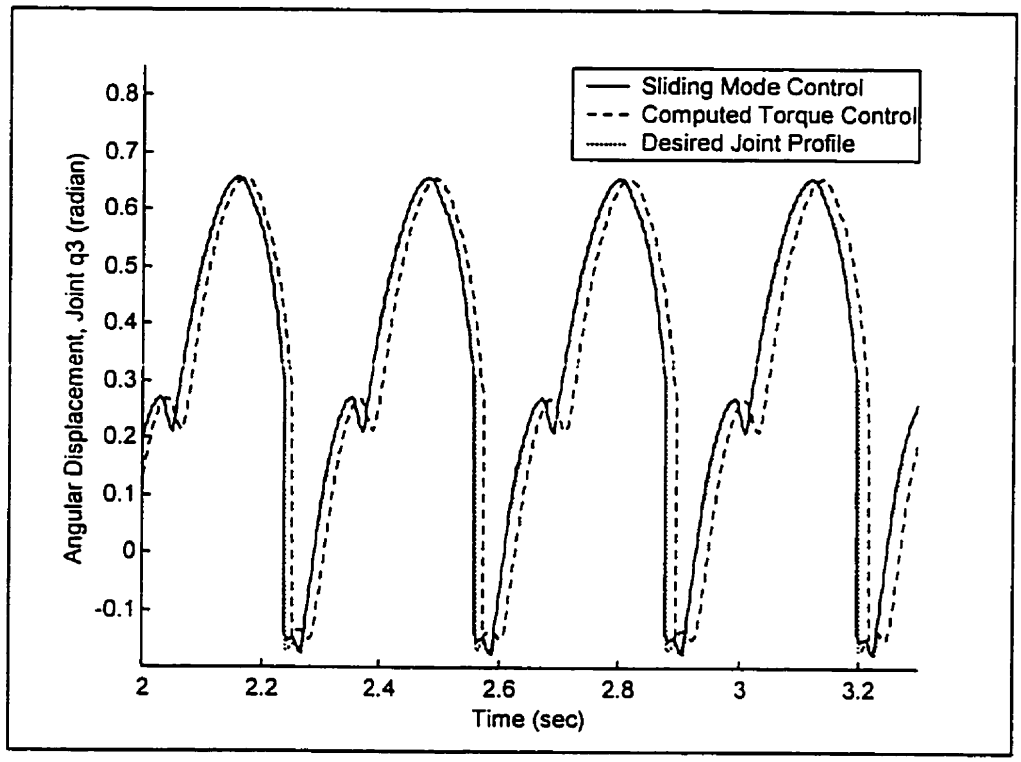

Figure 5.17b Angular Displacement (q_3) of Step 7 to 10 for Case 1

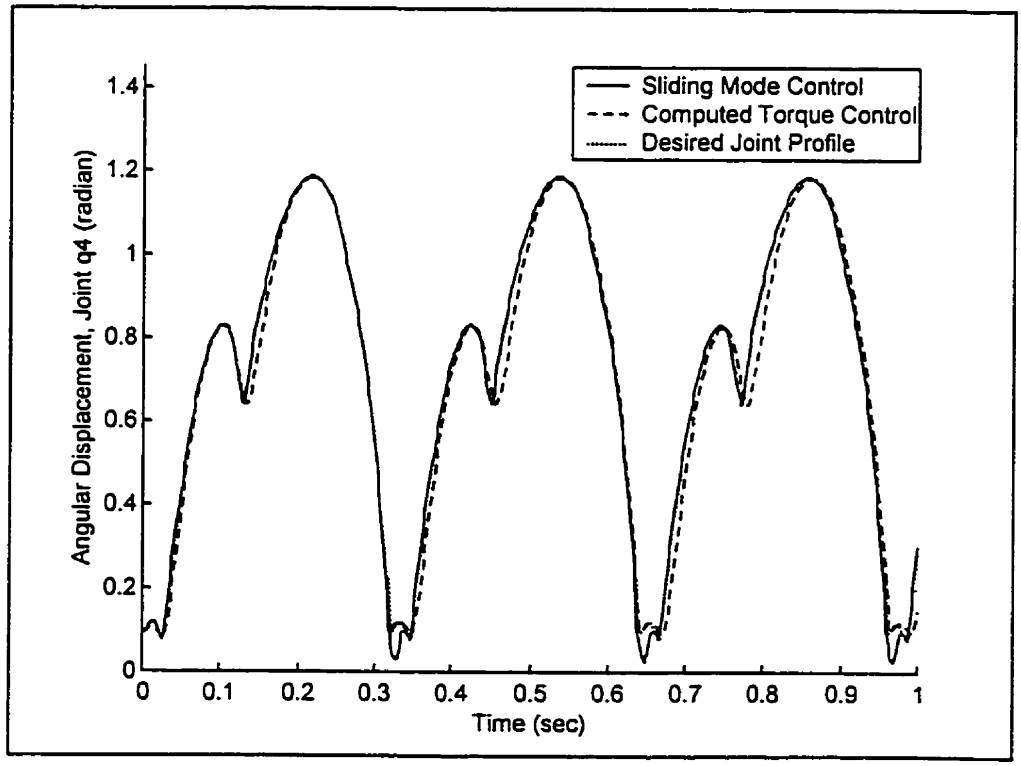

Figure 5.18a Angular Displacement (q_4) of Step 1 to 3 for Case 1

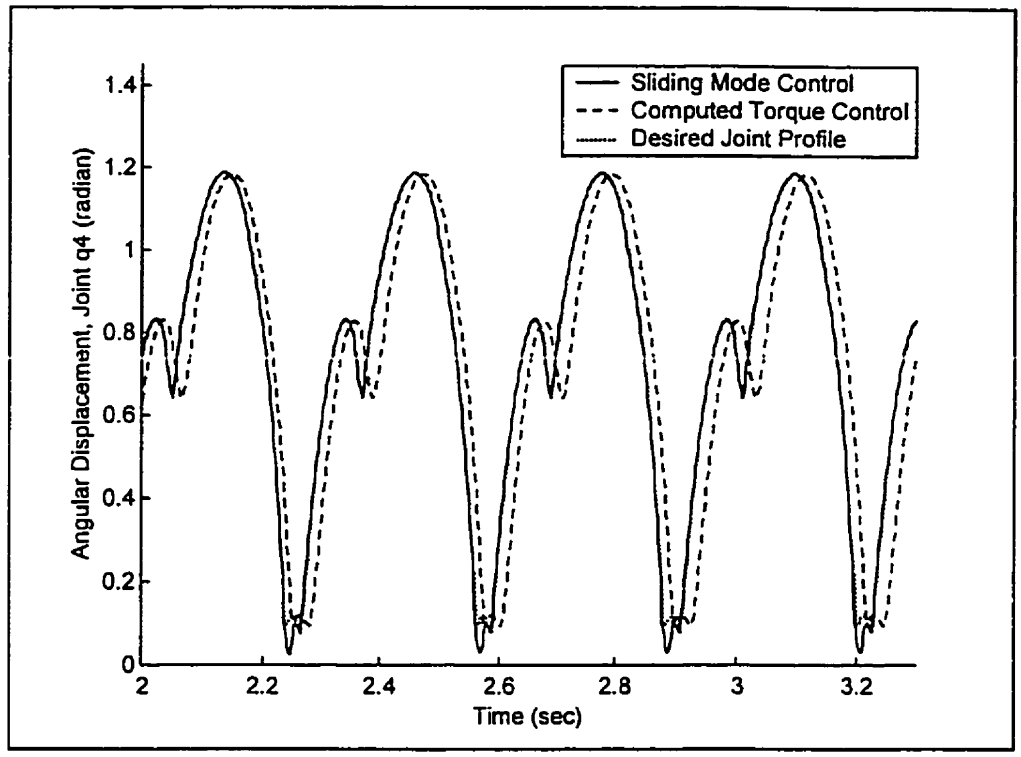

Figure 5.18b Angular Displacement (q_4) of Step 7 to 10 for Case 1

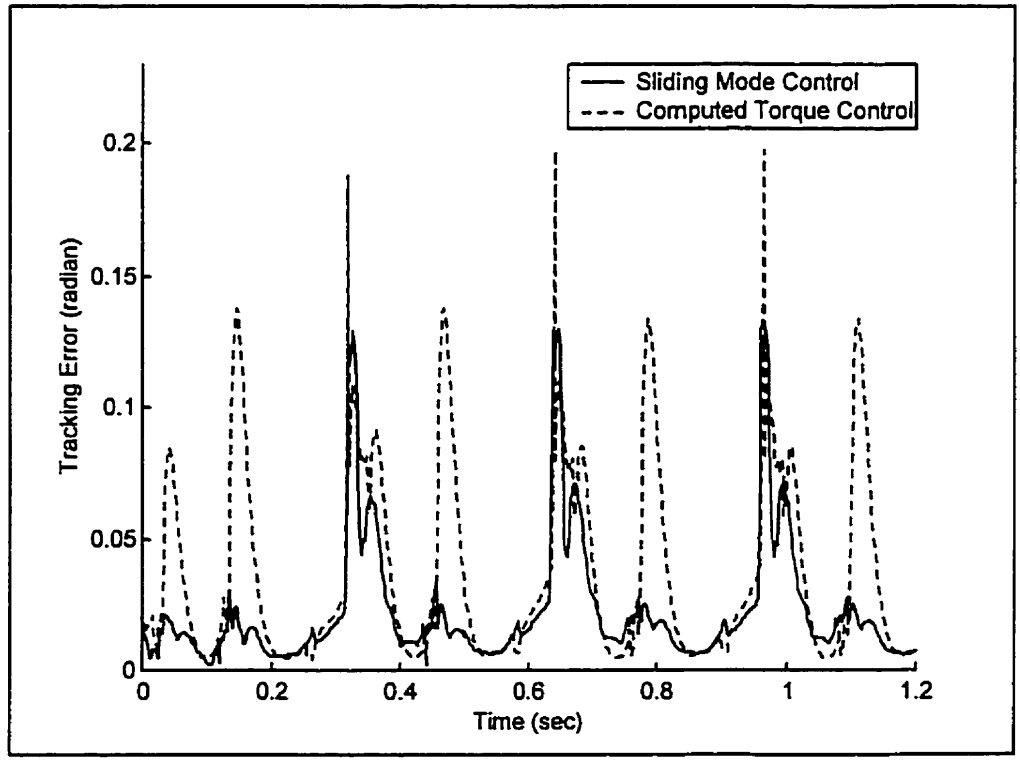

Figure 5.19 Tracking Error of Case 1

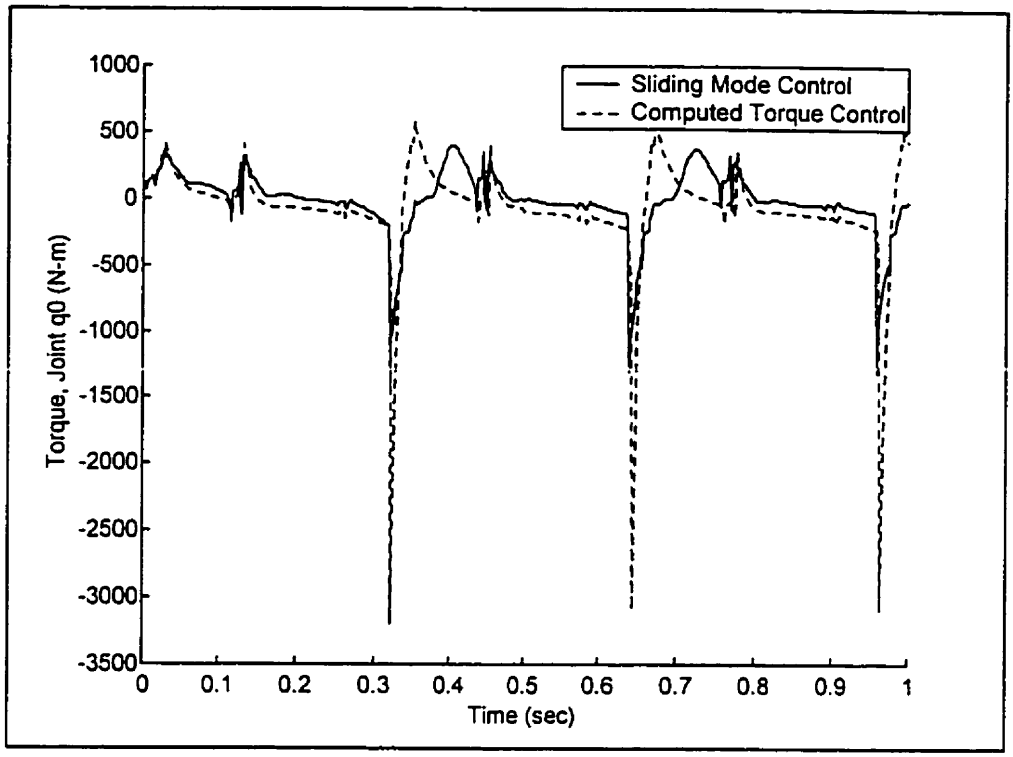

Figure 5.20a Control Torque at q_0 of Case 1

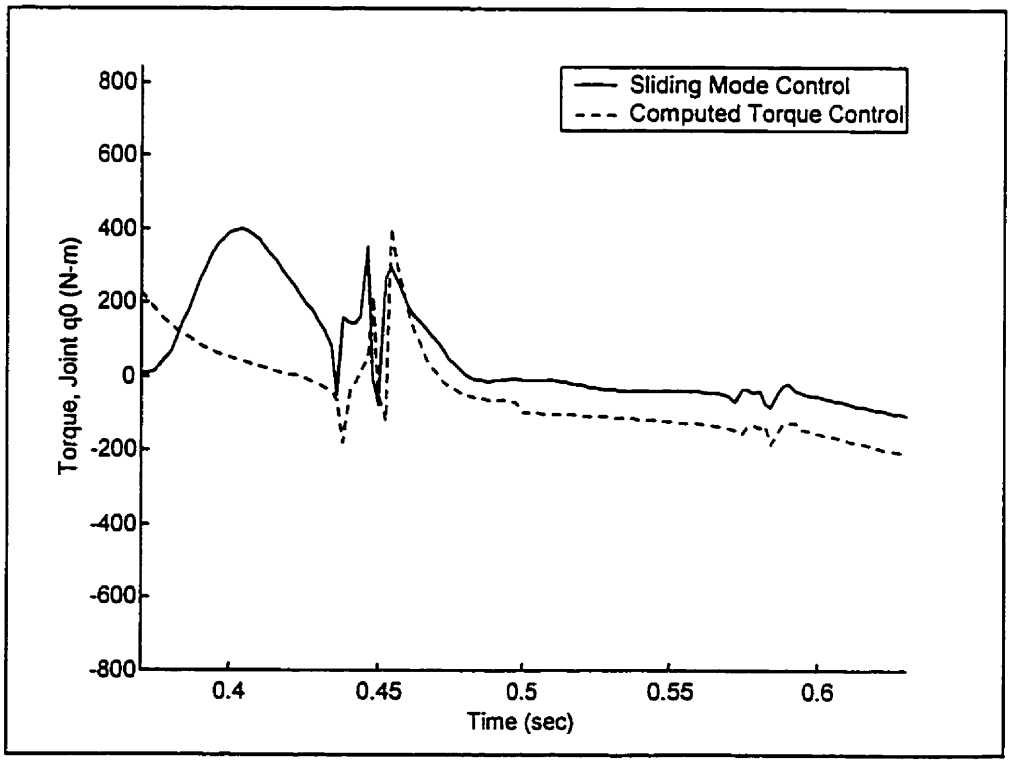

Figure 5.20b Control Torque at q_0 of Case 1 within One Step

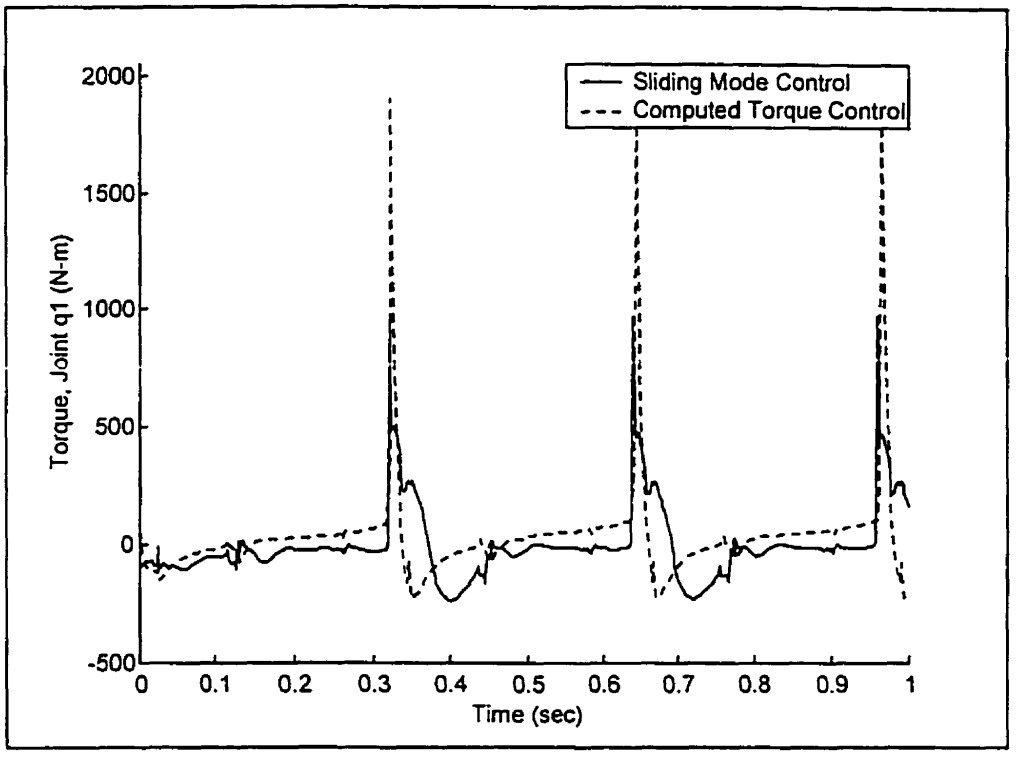

Figure 5.21a Control Torque at q_1 of Case 1

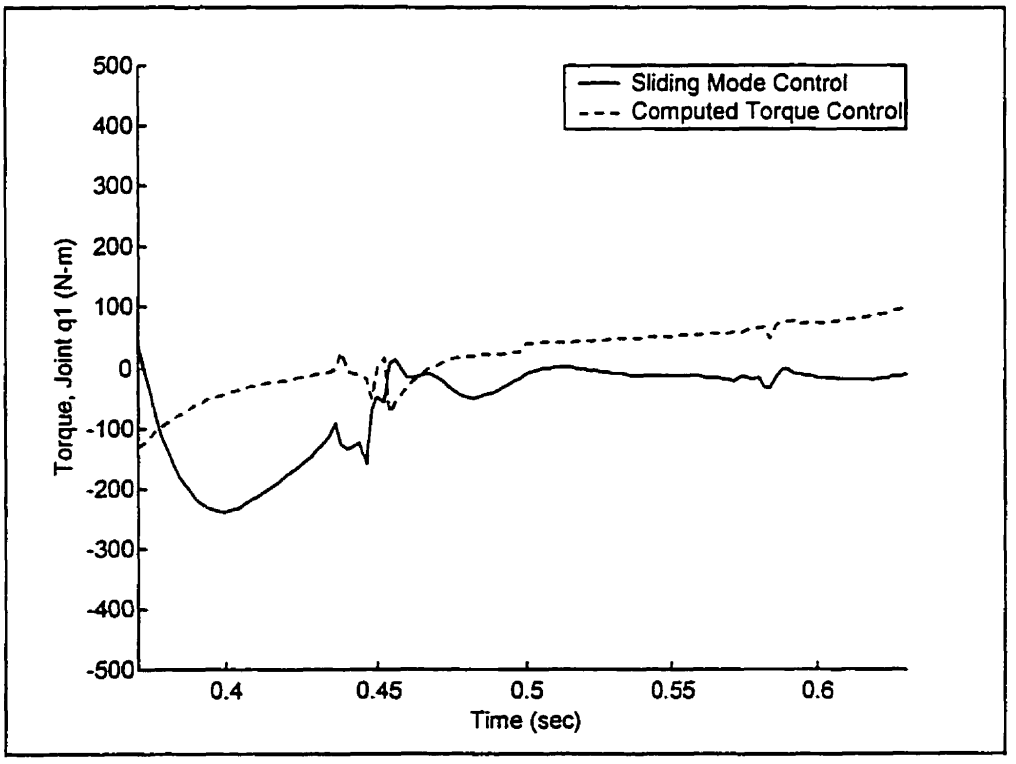

Figure 5.21b Control Torque at q_1 of Case 1 within One Step

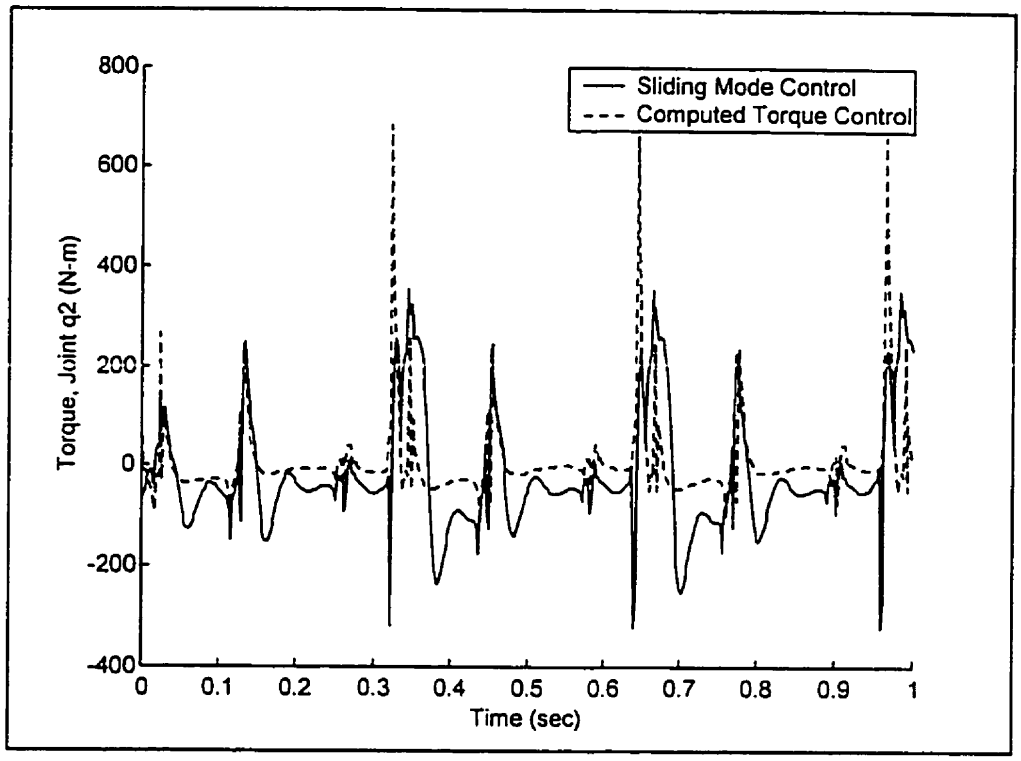

Figure 5.22a Control Torque at q_2 of Case 1

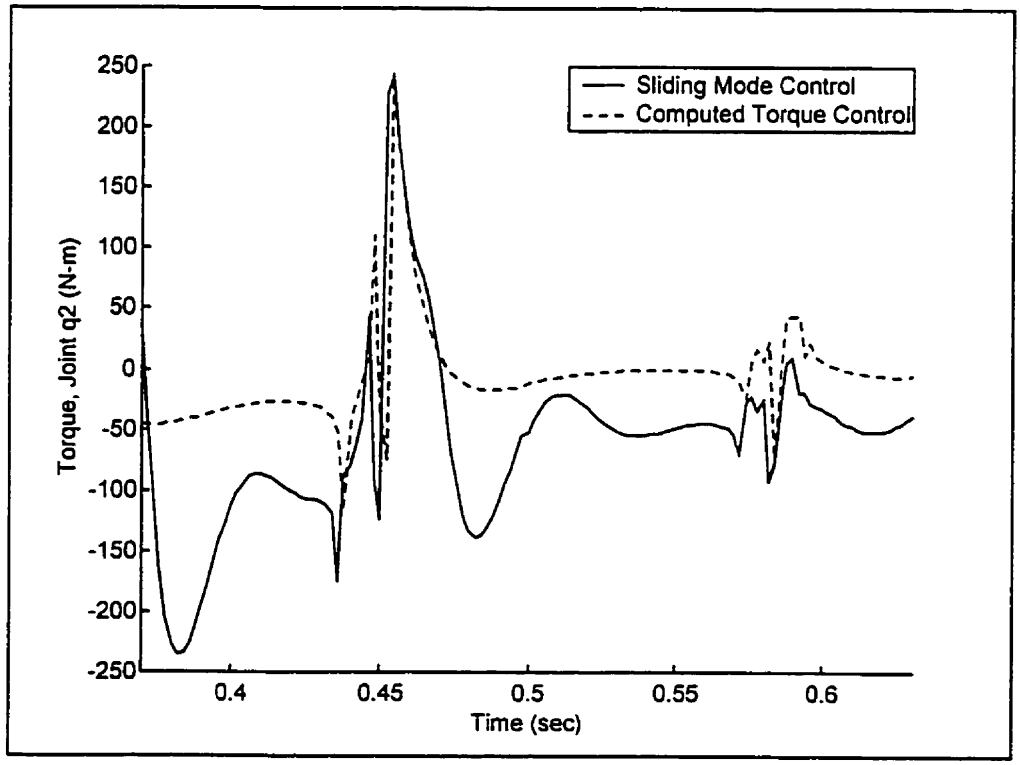

Figure 5.22b Control Torque at q_2 of Case 1 within One Step

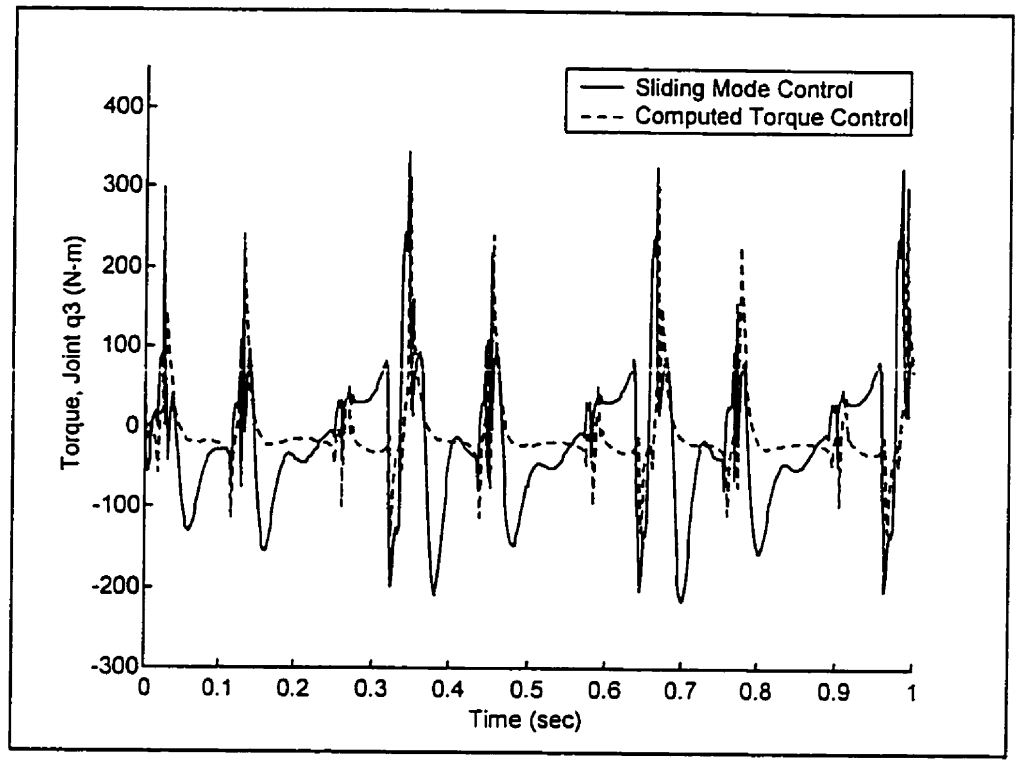

Figure 5.23a Control Torque at q_3 of Case 1

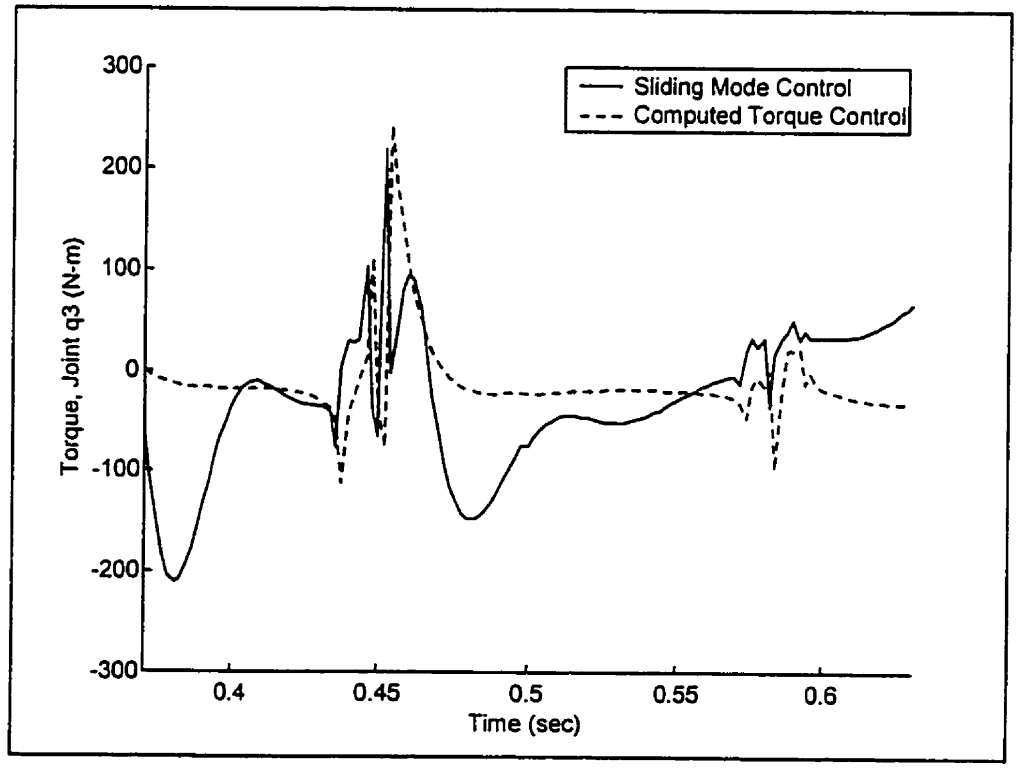

Figure 5.23b Control Torque at q_3 of Case 1 within One Step

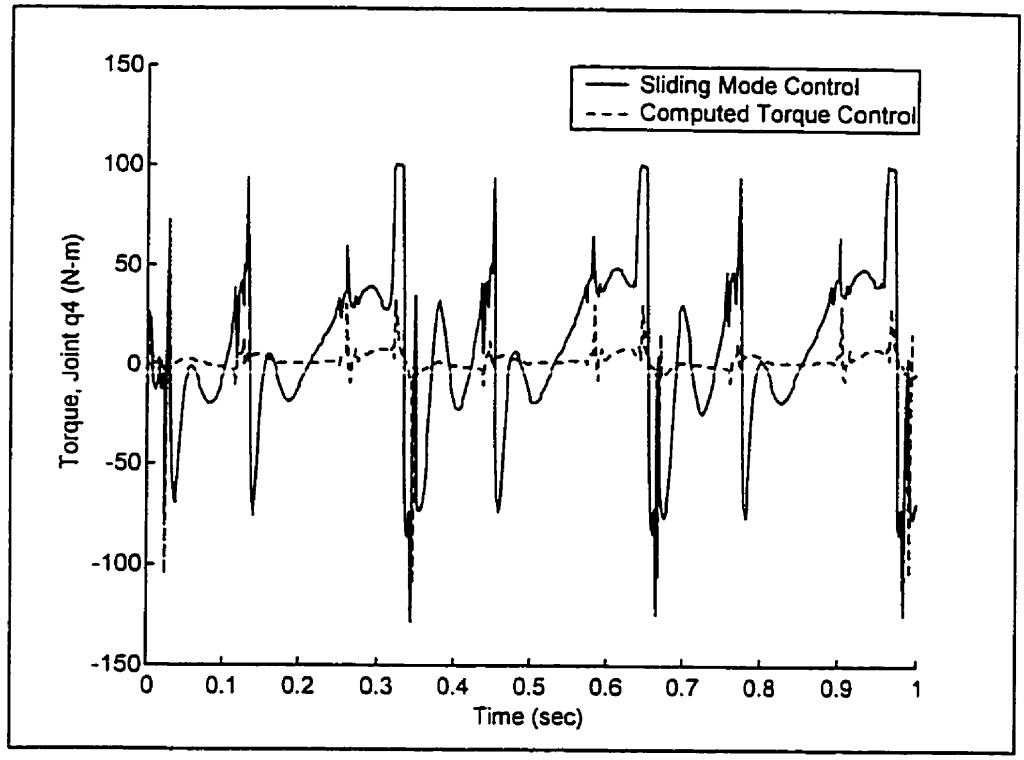

Figure 5.24a Control Torque at q_4 of Case 1

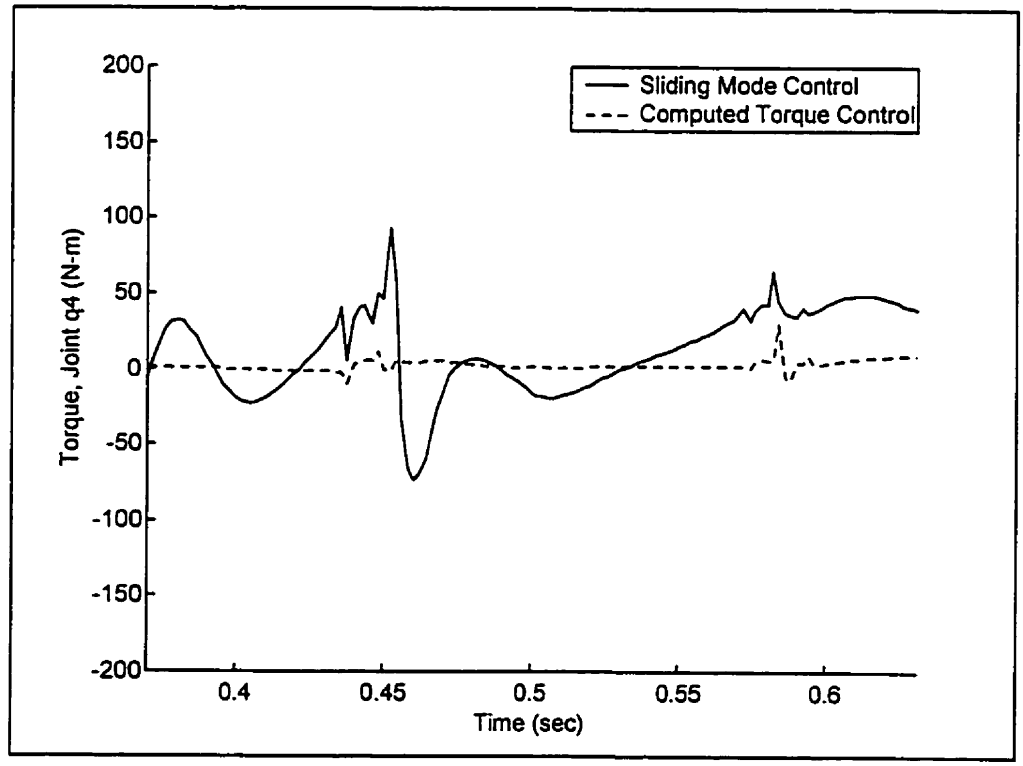

Figure 5.24b Control Torque at q_4 of Case 1 within One Step

In Case 2, as the parametric uncertainties increased to $e_m = e_l = 0.4$ and $e_l = e_d = 0.1$, simulation results were obtained through both the sliding mode control and the computed torque control. For the computed torque control, the best tracking performance results were obtained with the choice of $\lambda = 80$. For the sliding mode control, the best tracking performance results were obtained with the choice of $\lambda = 15$ and $\alpha = 0.2$. Figures 5.25a to 5.29a show the angular displacement of each joint of the first three steps and Figures 5.25b to 5.29b show the angular displacements from the seventh to tenth step. The simulation results showed that the simulated joint angle profiles of both the sliding mode control and the computed torque control followed the desired joint angle profiles closely. The simulated joint angle profiles obtained through the computed torque control differed slightly from the desired one, especially the profiles of q_3 and q_4. The tracking errors for both the sliding mode control and computed torque control are shown in Figure 5.30. Even though both increased, the average tracking error of the computed torque control (about 0.0386 radians) was still higher than that of the sliding mode control (about 0.0195 radians). Figures 5.31a to 5.35a show the control torque of each joint and Figures 5.31b to 5.35b show the control torques within one step. In this case, the control torques from the sliding mode control and computed torque control were comparable. Nevertheless, the sliding mode control again showed better tracking performance than the computed torque control as the control torques applied to the joints through such two control techniques were similar.

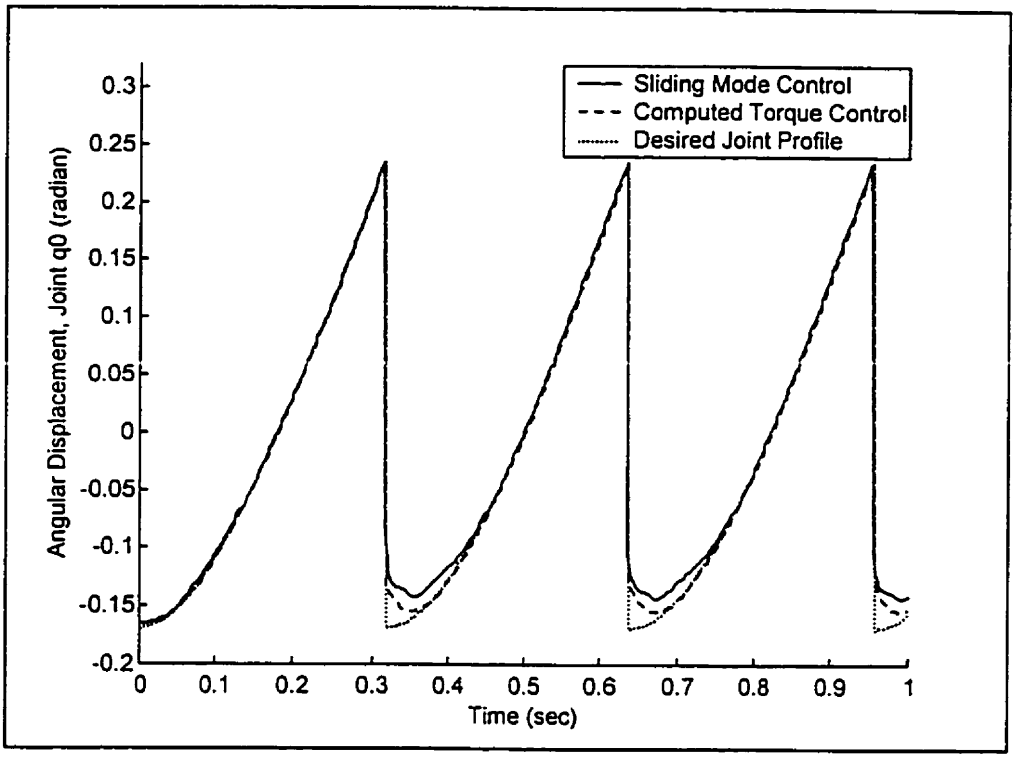

Figure 5.25a Angular Displacement (q_0) of Step 1 to 3 for Case 2

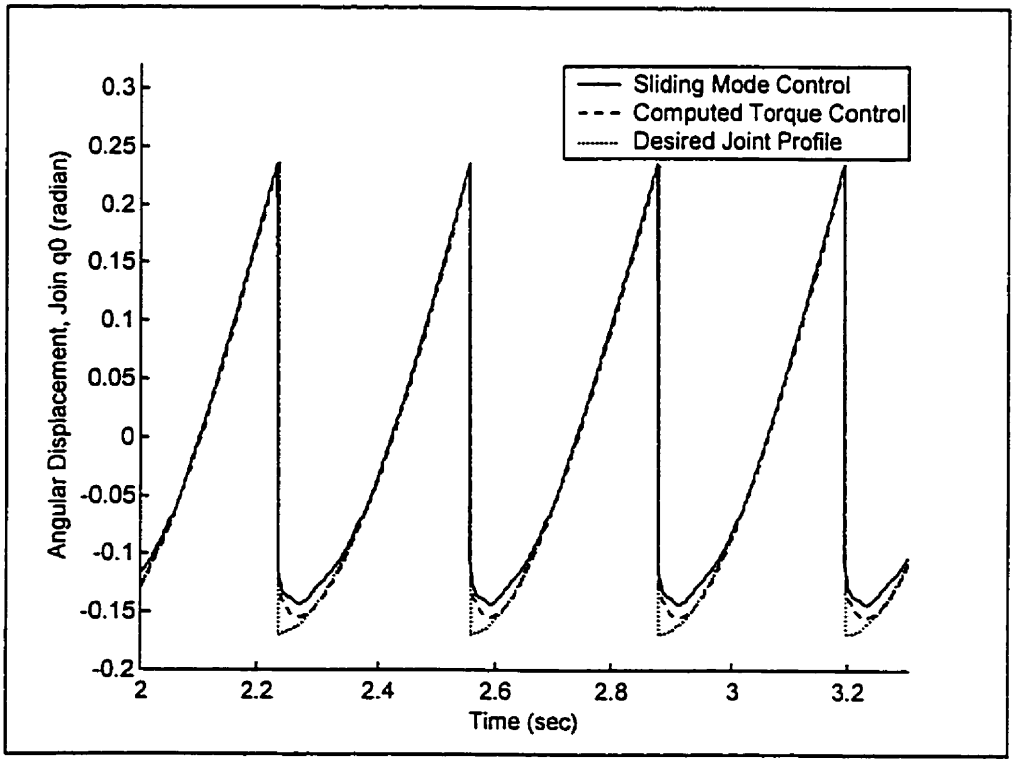

Figure 5.25b Angular Displacement (q_0) of Step 7 to 10 for Case 2

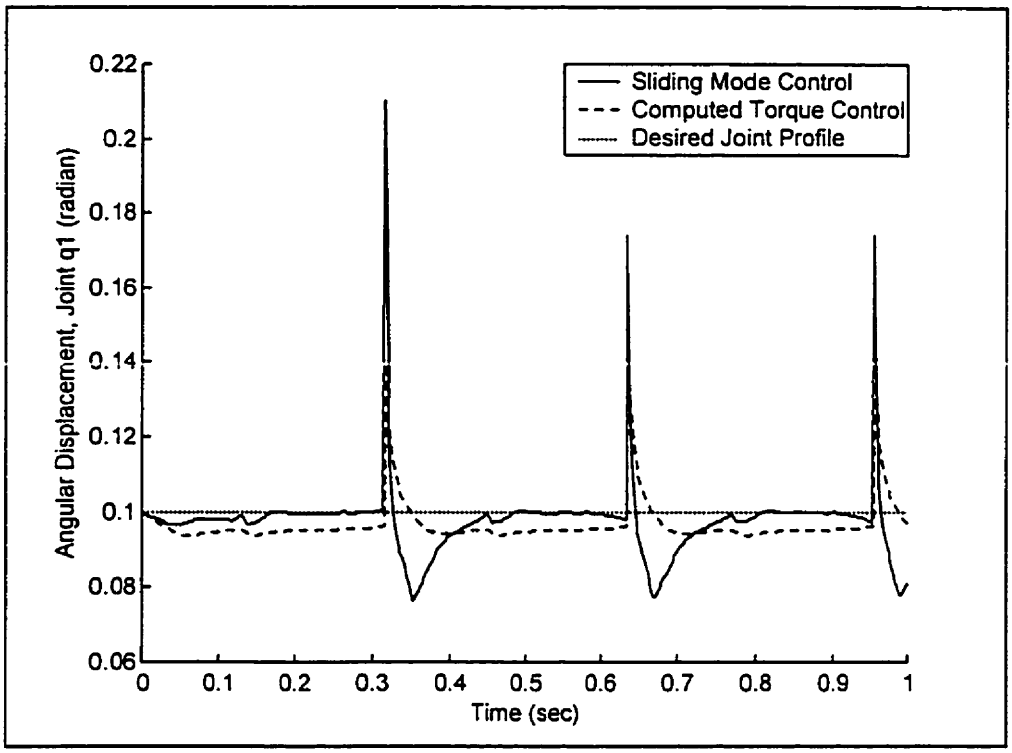

Figure 5.26a Angular Displacement (q_1) of Step 1 to 3 for Case 2

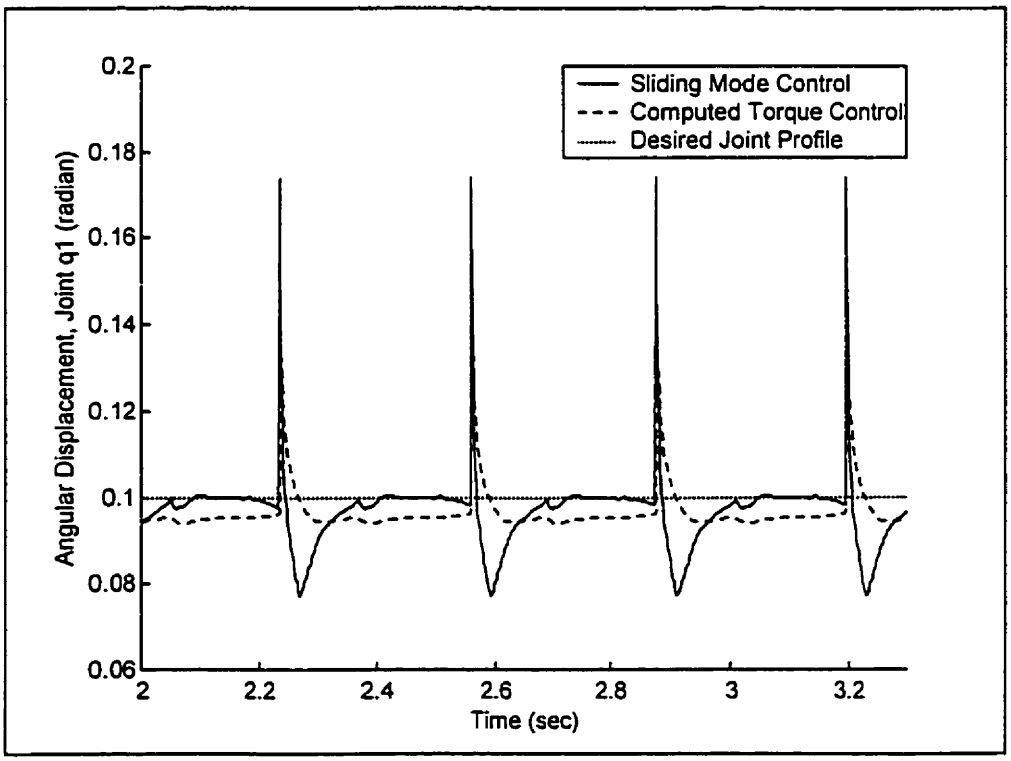

Figure 5.26b Angular Displacement (q_1) of Step 7 to 10 for Case 2

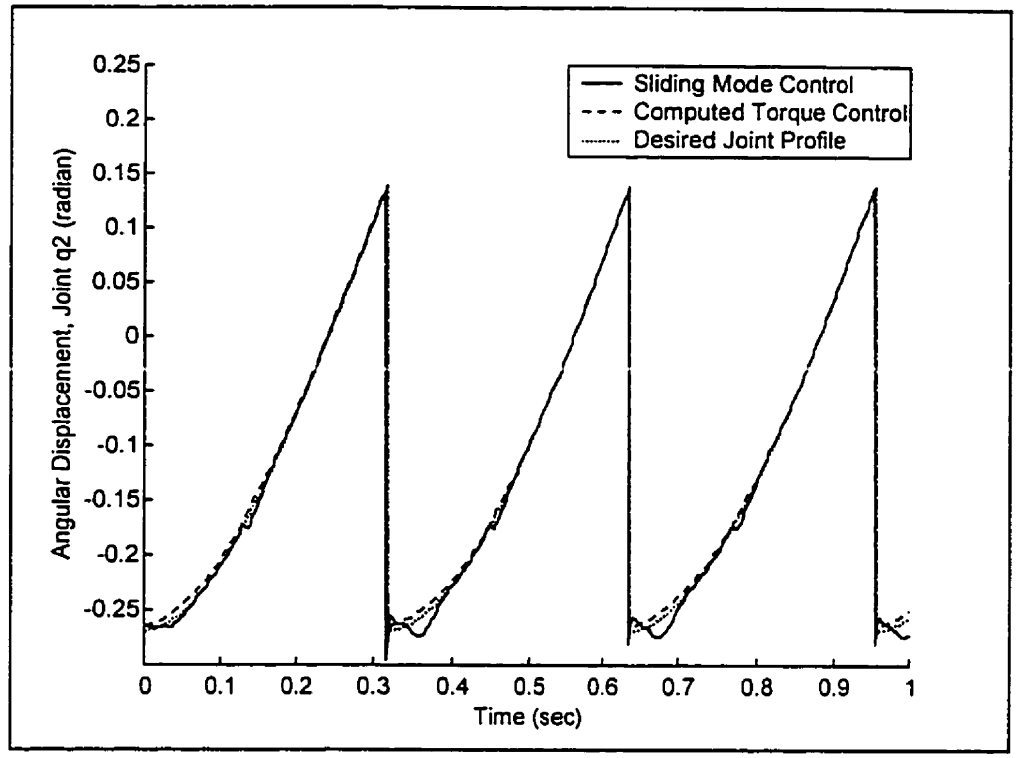

Figure 5.27a Angular Displacement (q_2) of Step 1 to 3 for Case 2

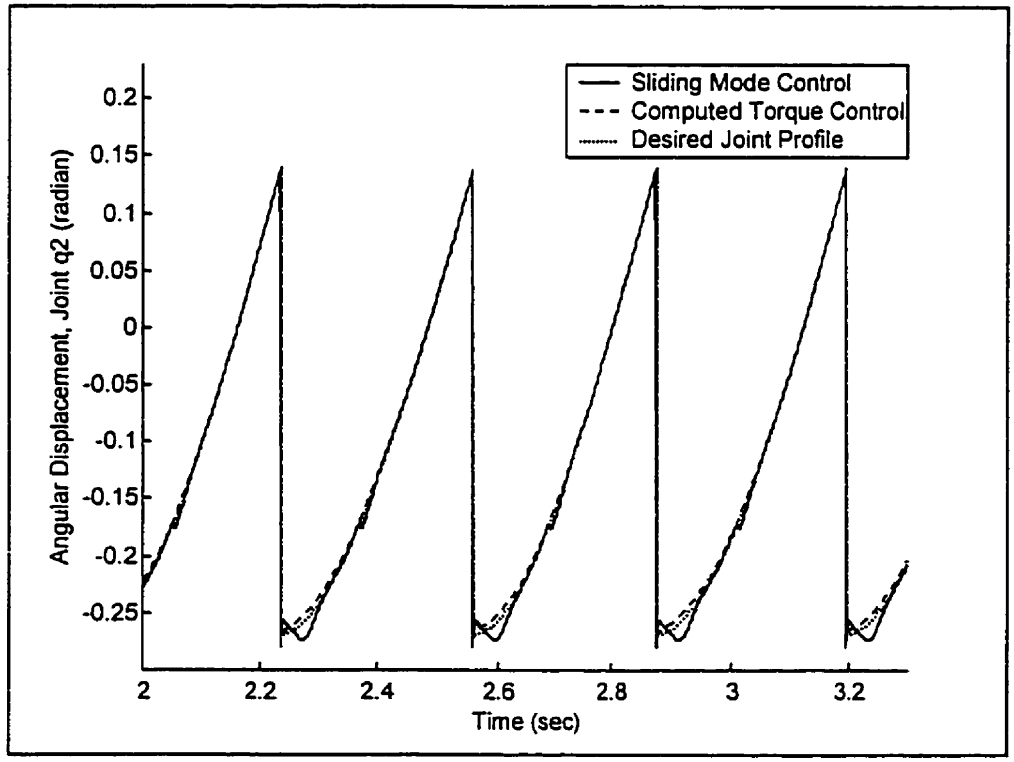

Figure 5.27b Angular Displacement (q_2) of Step 7 to 10 for Case 2

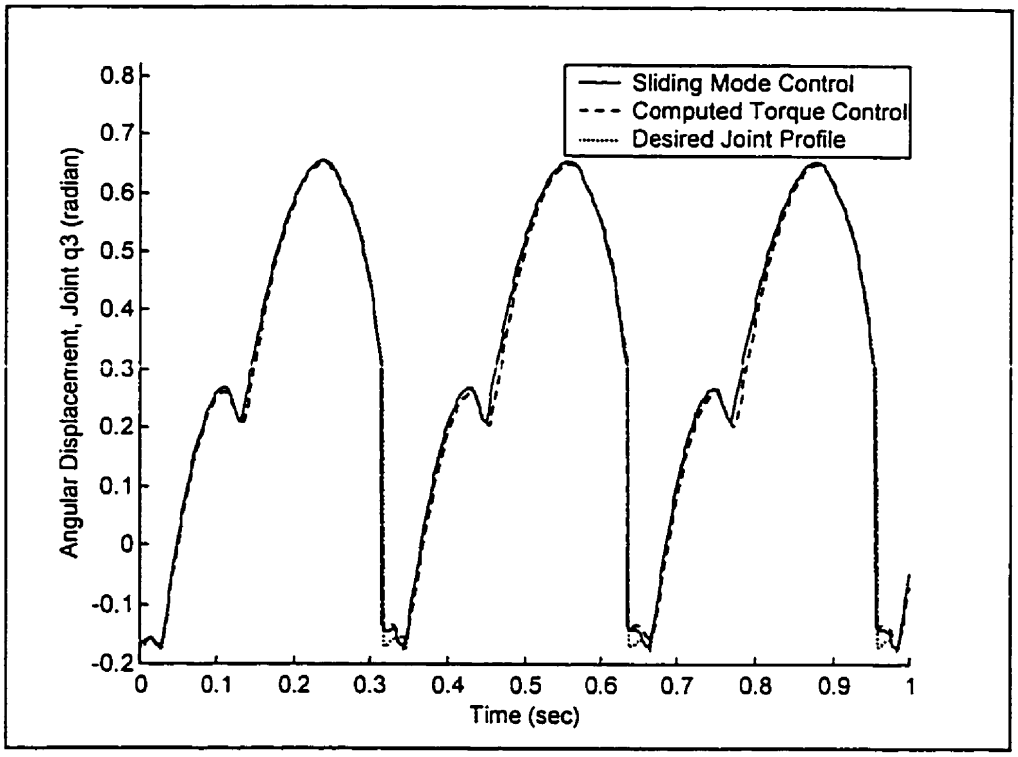

Figure 5.28a Angular Displacement (q_3) of Step 1 to 3 for Case 2

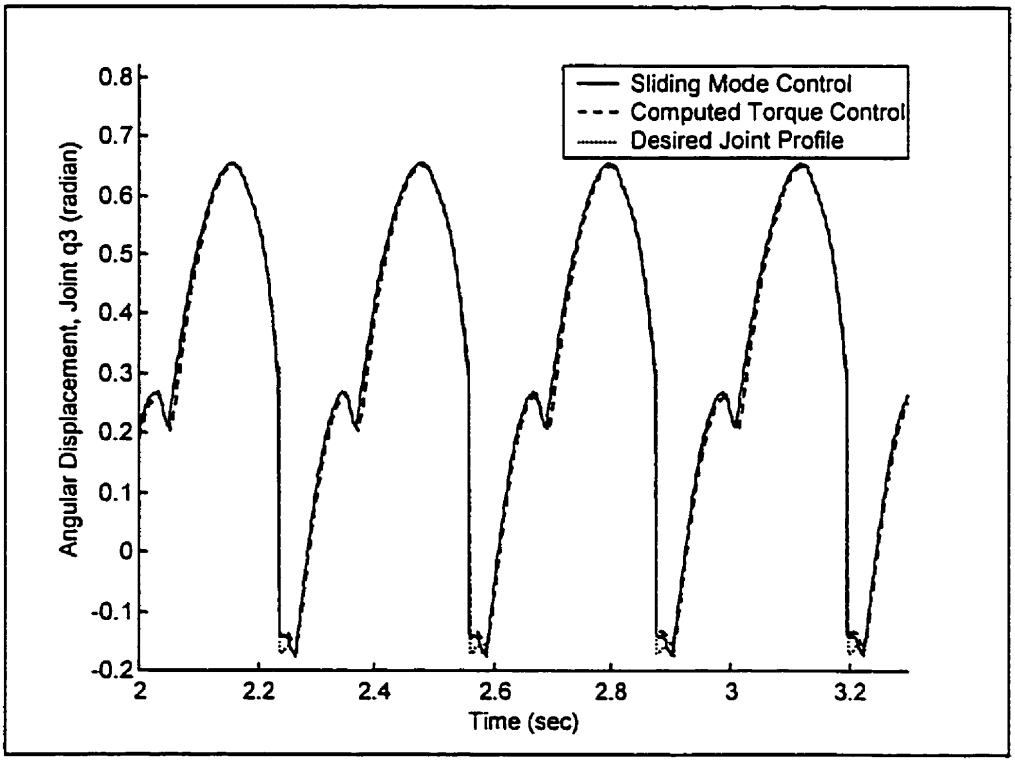

Figure 5.28b Angular Displacement (q_3) of Step 7 to 10 for Case 2

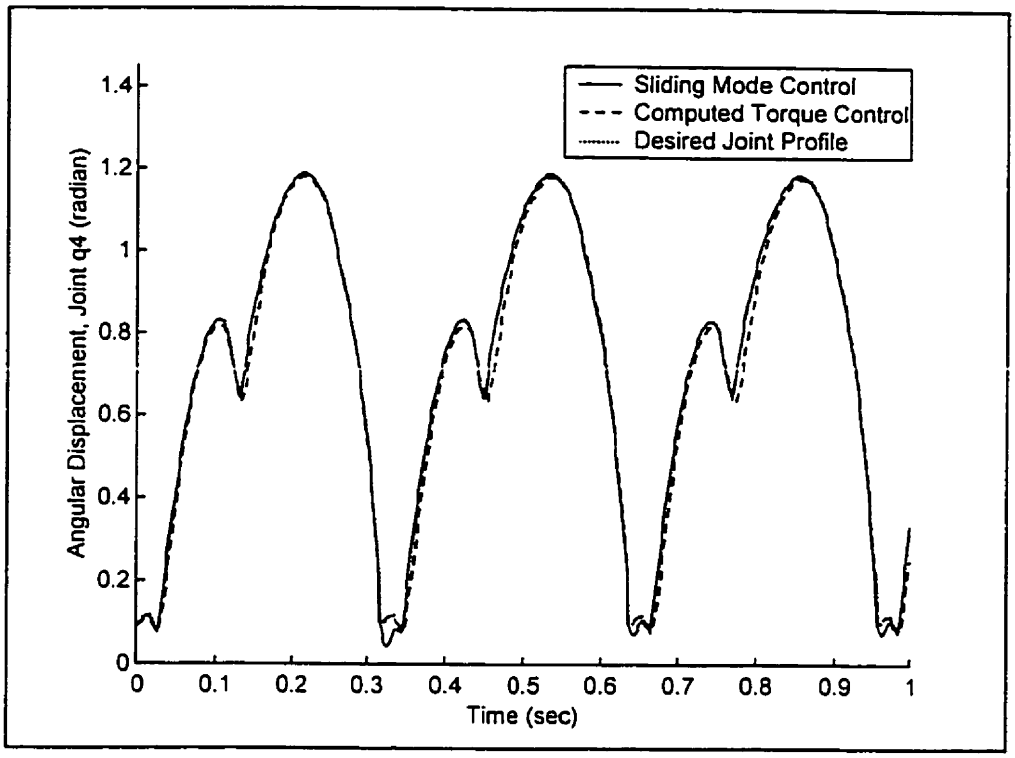

Figure 5.29a Angular Displacement (q_4) of Step 1 to 3 for Case 2

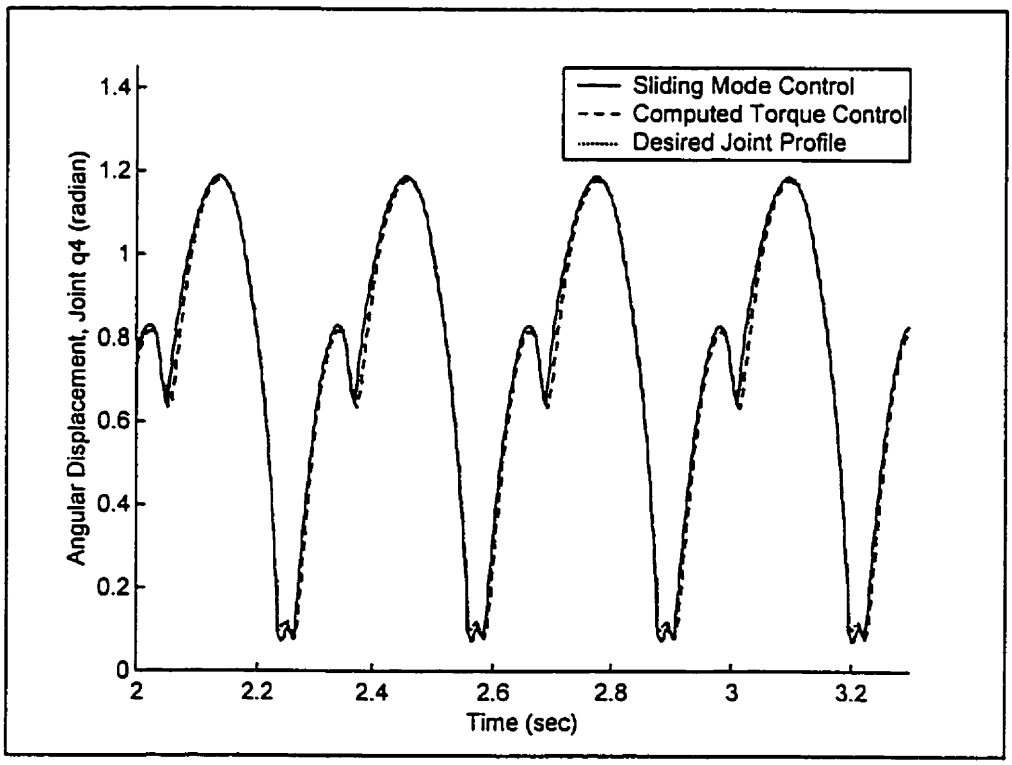

Figure 5.29b Angular Displacement (q_4) of Step 7 to 10 for Case 2

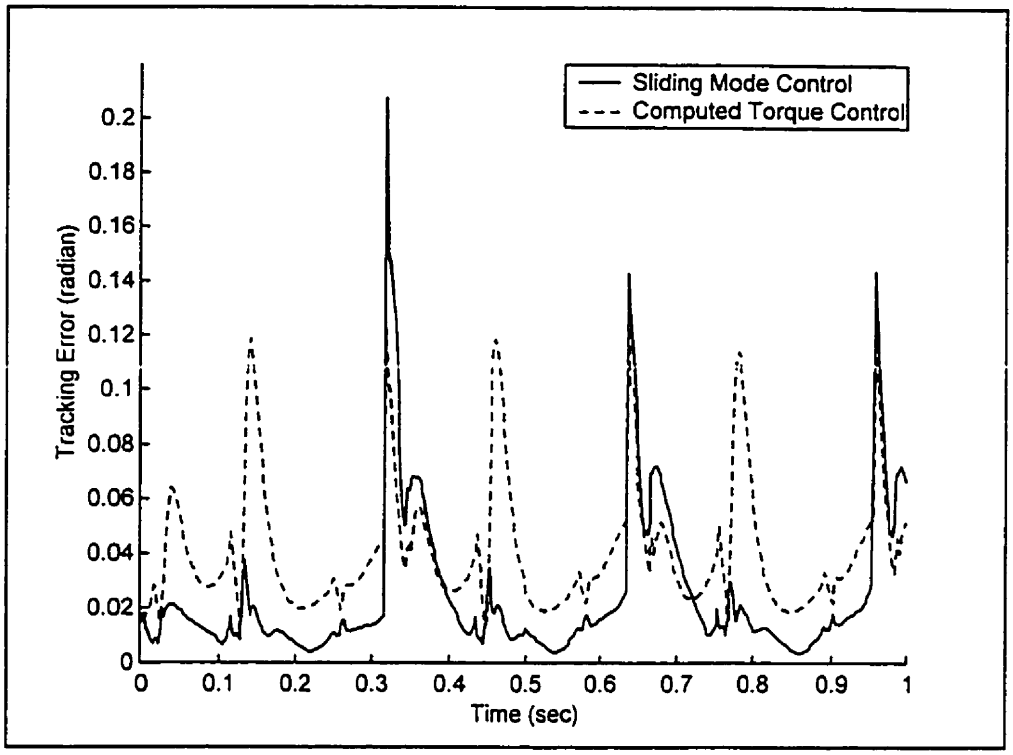

Figure 5.30 Tracking Error of Case 2

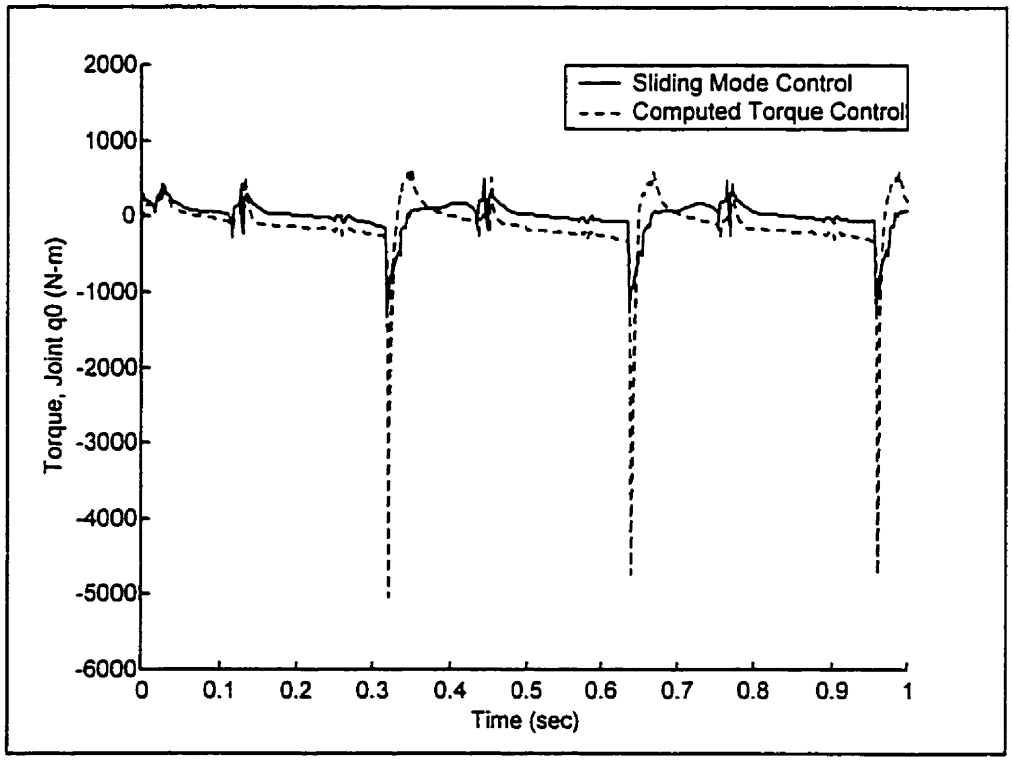

Figure 5.31a Control Torque at q_0 of Case 2

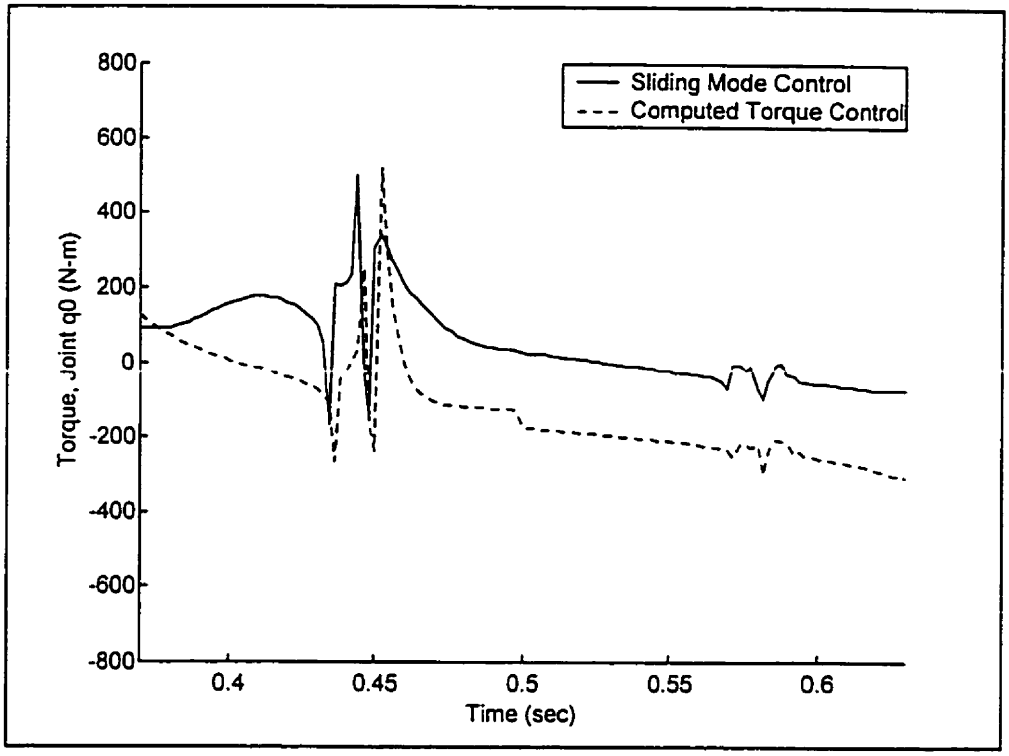

Figure 5.31b Control Torque at q_0 of Case 2 within One Step

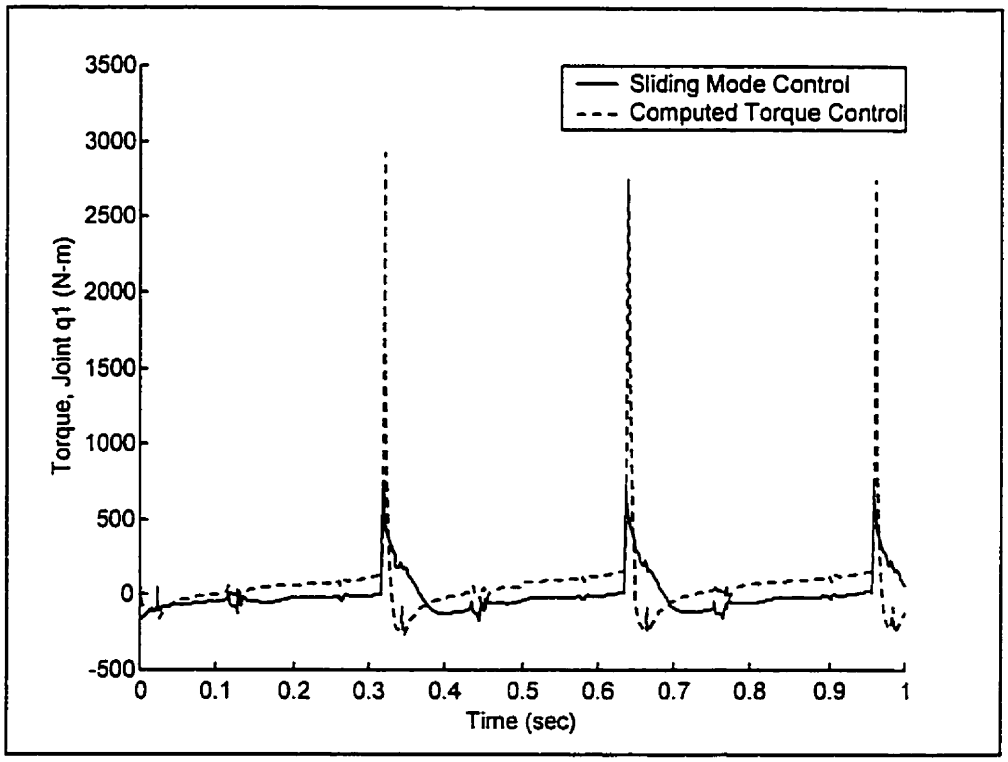

Figure 5.32a Control Torque at q_1 of Case 2

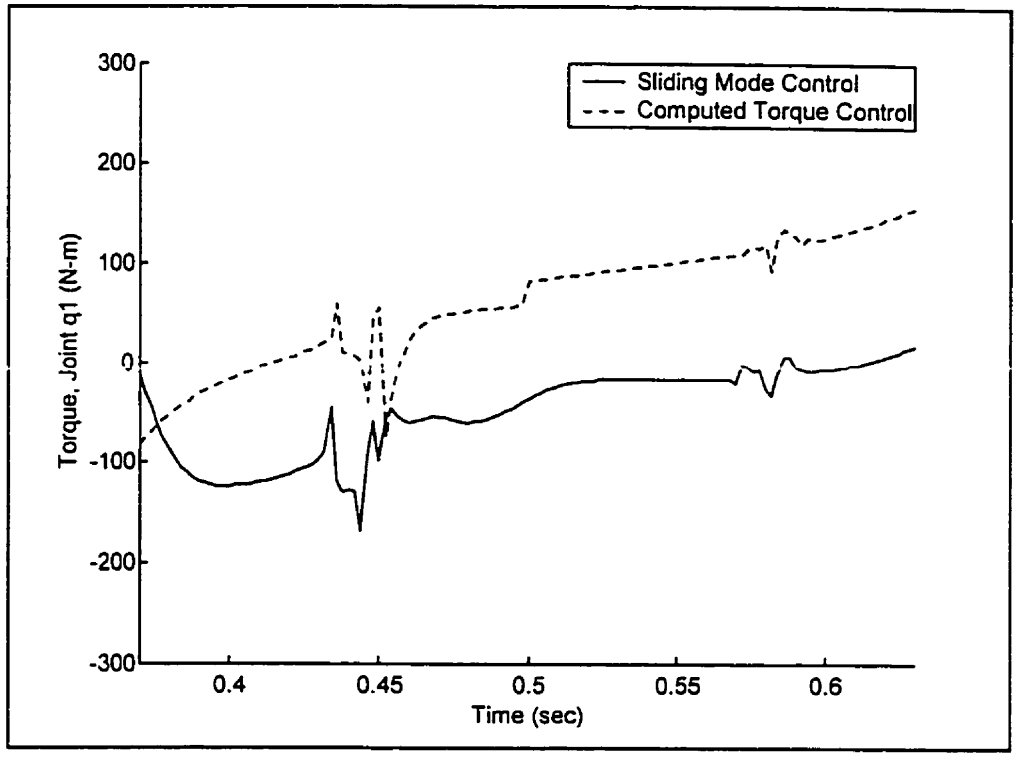

Figure 5.32b Control Torque at q_1 of Case 2 within One Step

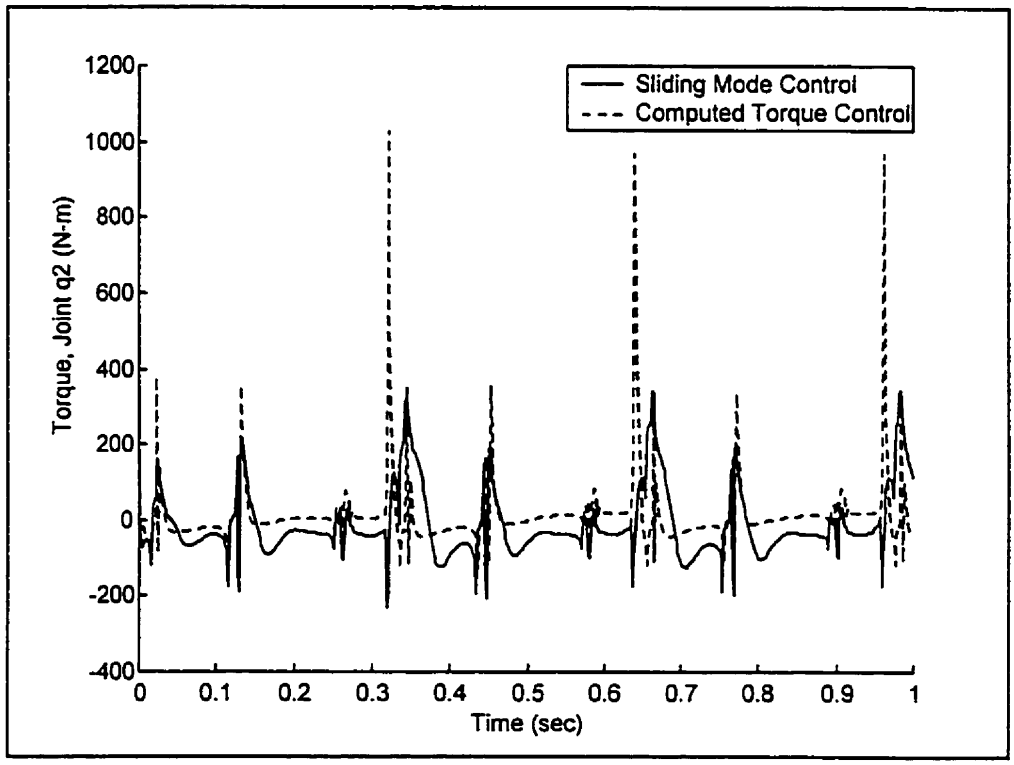

Figure 5.33a Control Torque at q_2 of Case 2

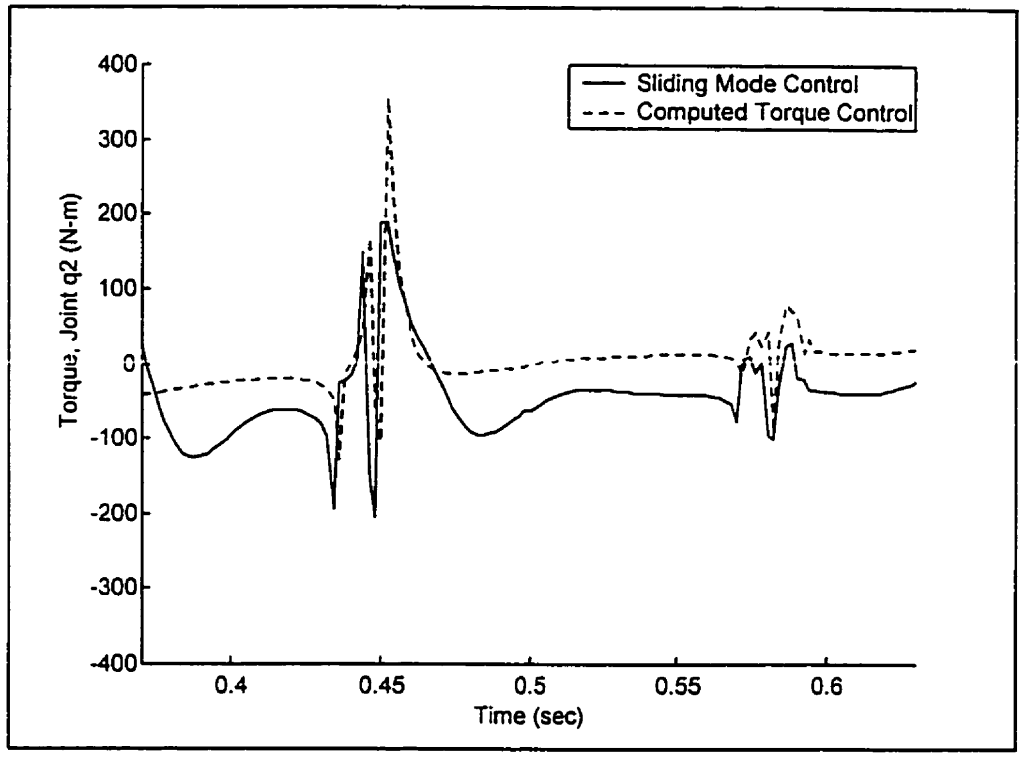

Figure 5.33b Control Torque at q_2 of Case 2 within One Step

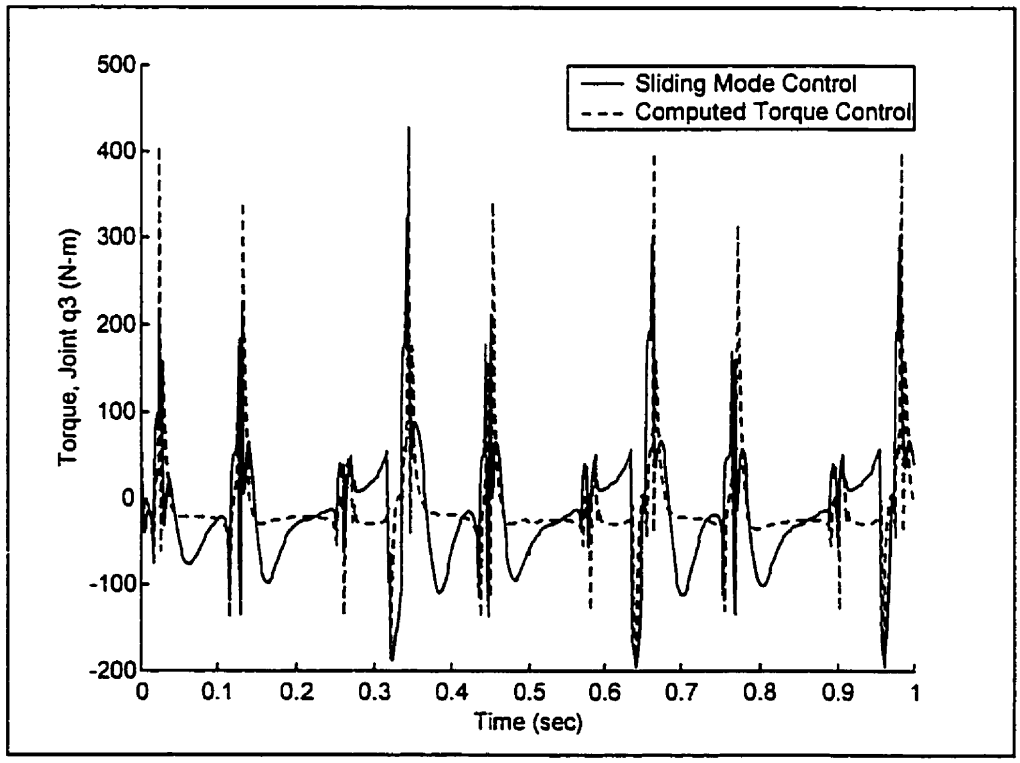

Figure 5.34a Control Torque at q_3 of Case 2

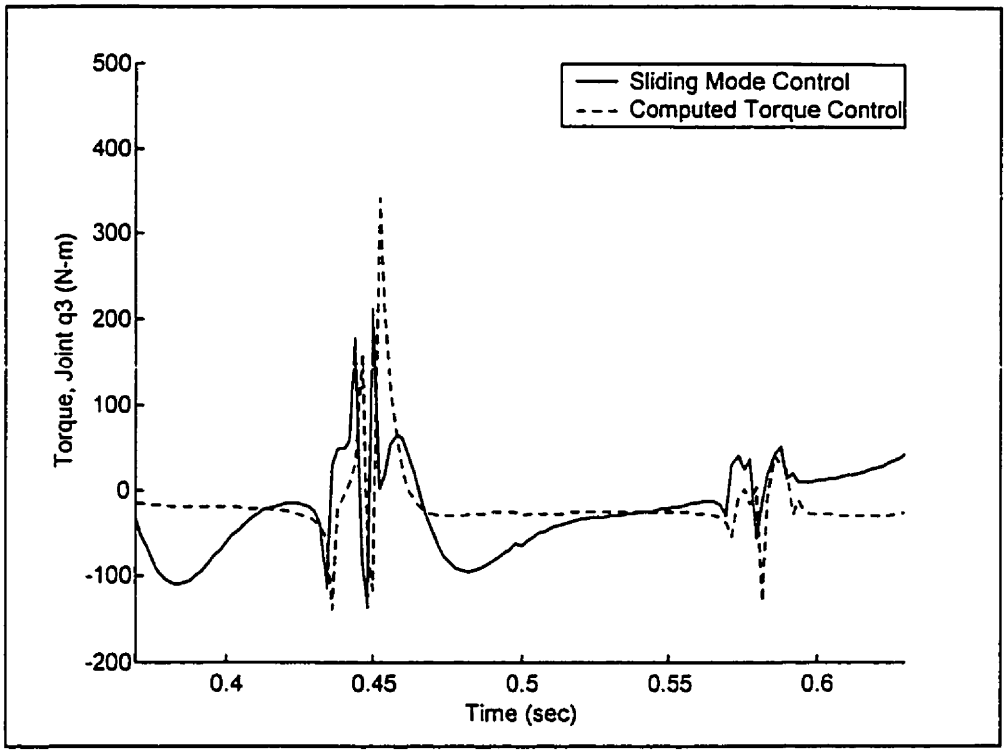

Figure 5.34b Control Torque at q_3 of Case 2 within One Step

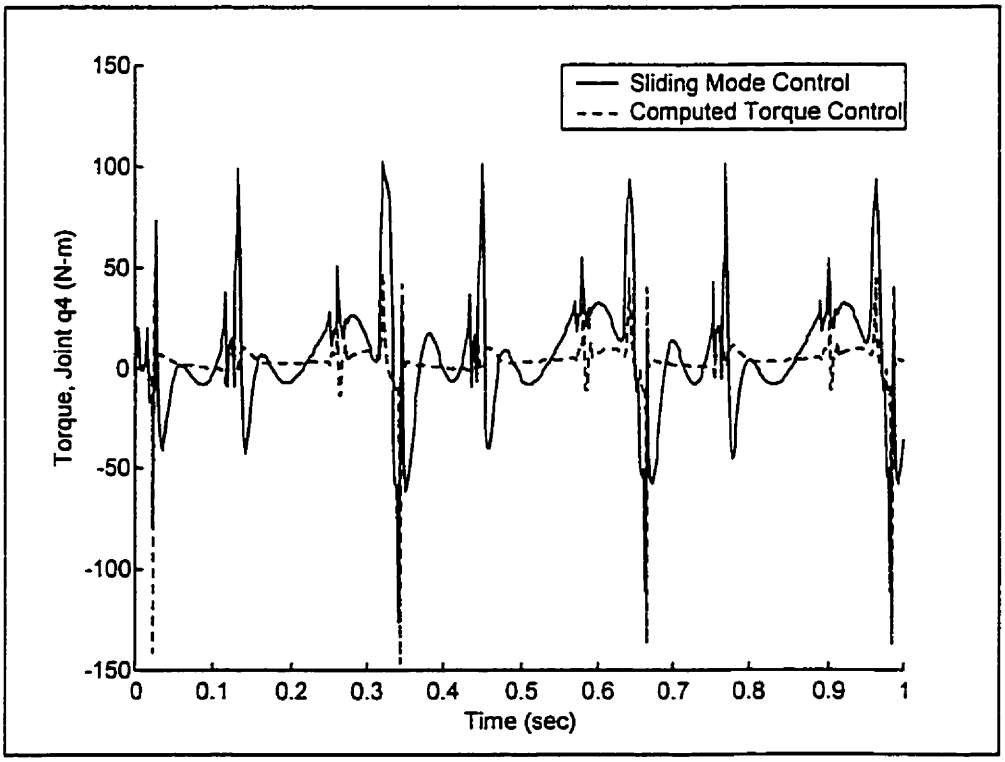

Figure 5.35a Control Torque at q_4 of Case 2

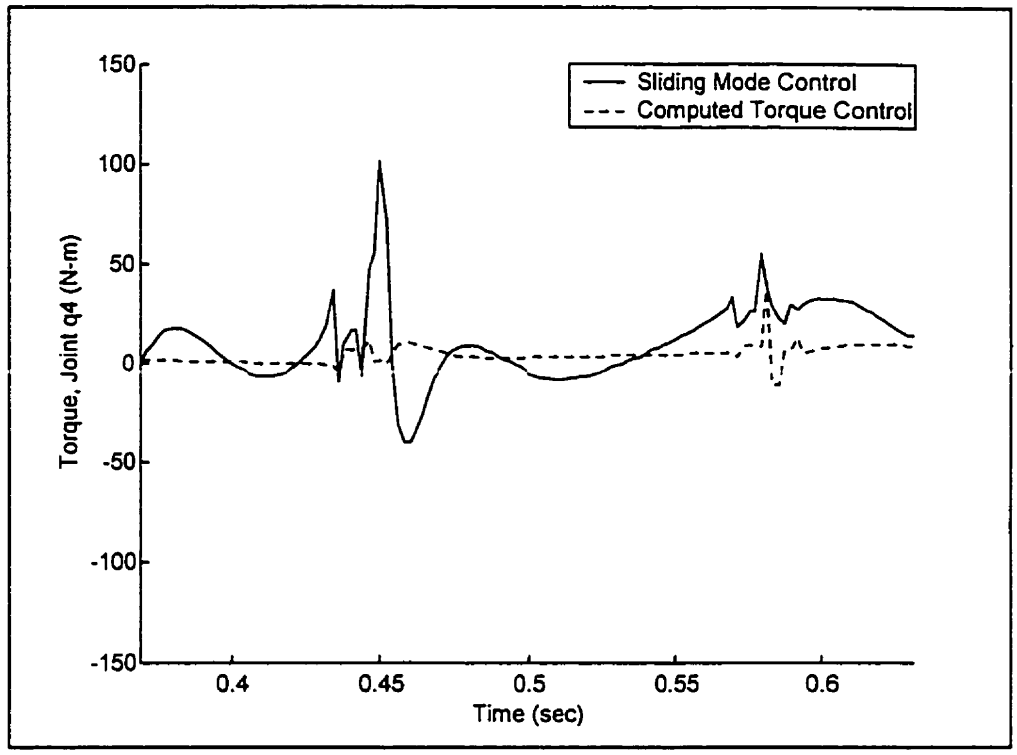

Figure 5.35b Control Torque at q_4 of Case 2 within One Step

For the last case (200% uncertainty), the parametric uncertainties were increased significantly ($e_m = e_I = 2$ and $e_I = e_d = 0.1$). Since the parameters of mass and moment of inertia were the primary sources of uncertainty, we kept the uncertainty in the geometrical parameters (e_I and e_d) the same as in Case 2 (40% uncertainty) and increased the uncertainty in e_m and e_I significantly. A similar arrangement can been found in Tzafestas et al. (1996). For the computed torque control, the best results were obtained with $\lambda = 80$. For the sliding mode control, the best results were obtained with $\lambda = 15$ and $\alpha = 0.2$. The simulated joint angle profiles obtained through the sliding mode control and the computed torque control and the desired joint angle profiles are shown in Figures 5.36a to 5.40a for the first three steps and in Figures 5.36b to 5.40b for the seventh to tenth step. The tracking errors obtained for the two control laws are shown in Figure

5.41. The control torques are shown in Figures 5.42a to 5.46a and the control torques within one step are shown in Figures 5.42b to 5.46b. The control torques of the sliding mode control and the computed torque control were comparable. One can observe that by applying the similar control torques to the system, the simulated joint angle profiles obtained through the computed torque control had higher tracking error than the sliding mode control throughout the step. The average tracking error of the computed torque control was about 0.049 radians, while the average tracking error of the sliding mode control was only about 0.037 radians. In this case, the sliding mode control again showed better performance than the control torque control.

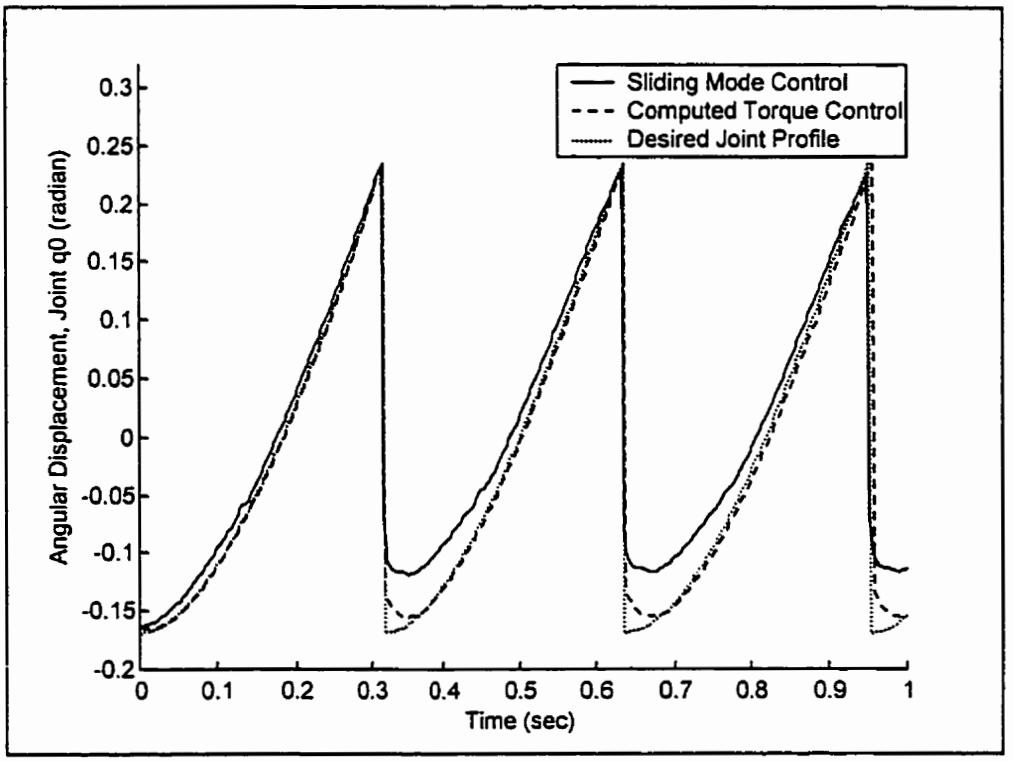

Figure 5.36a Angular Displacement (q_0) of Step 1 to 3 for Case 3

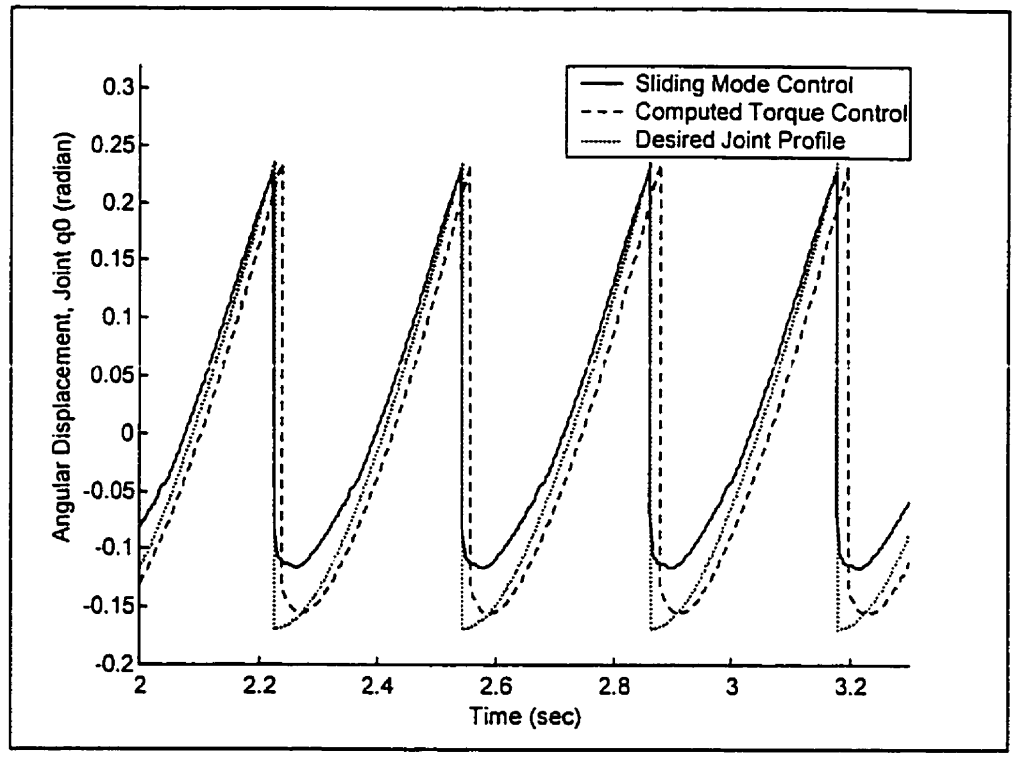

Figure 5.36b Angular Displacement (q_0) of Step 7 to 10 for Case 3

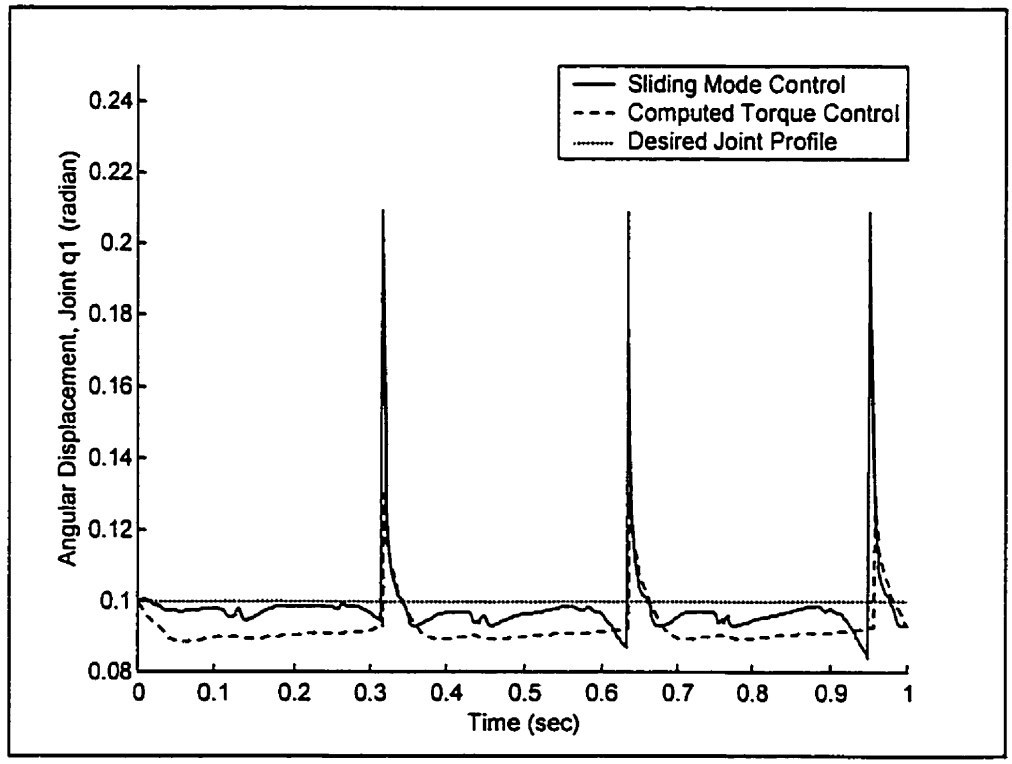

Figure 5.37a Angular Displacement (q_1) of Step 1 to 3 for Case 3

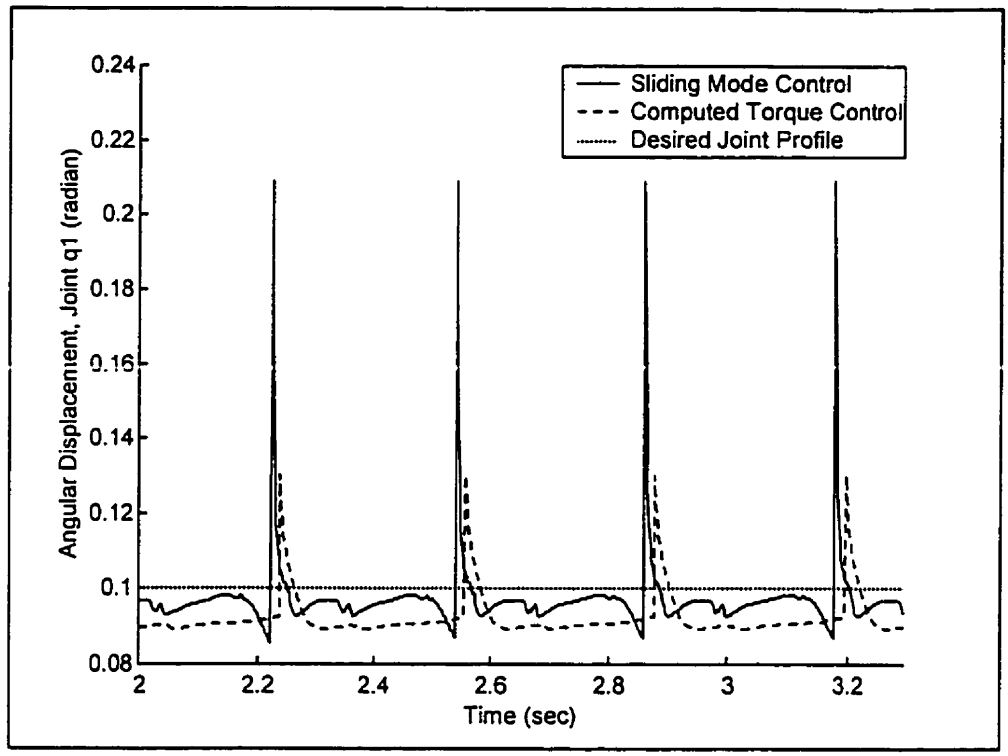

Figure 5.37b Angular Displacement (q_1) of Step 7 to 10 for Case 3

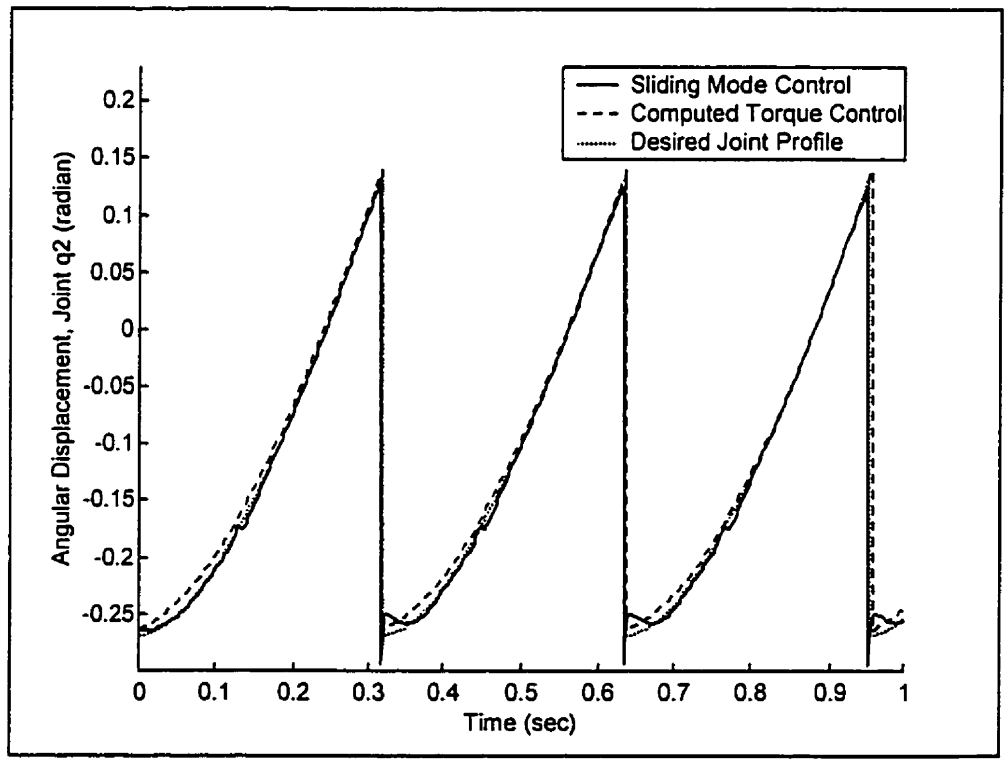

Figure 5.38a Angular Displacement (q_2) of Step 1 to 3 for Case 3

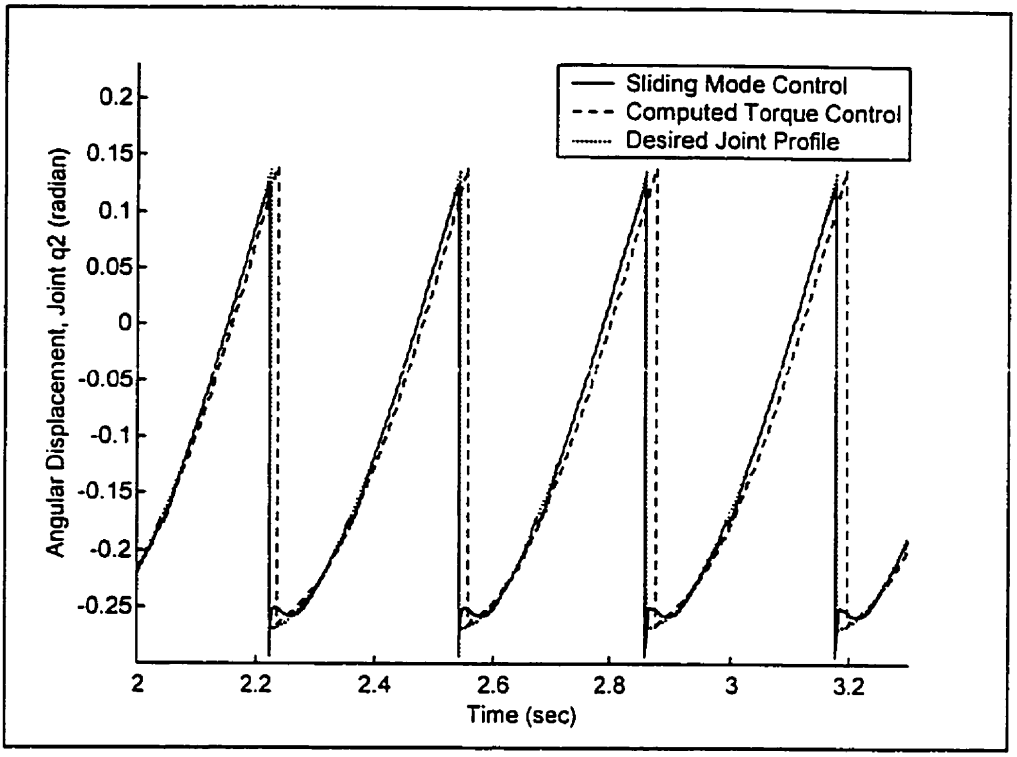

Figure 5.38b Angular Displacement (q_2) of Step 7 to 10 for Case 3

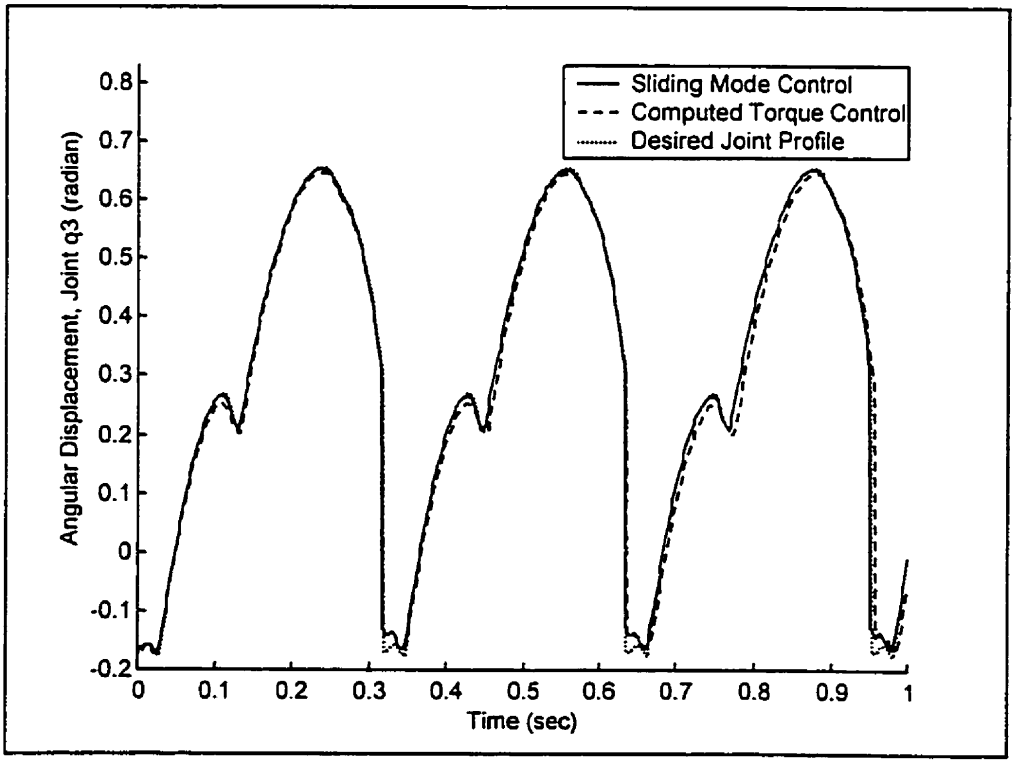

Figure 5.39a Angular Displacement (q_3) of Step 1 to 3 for Case 3

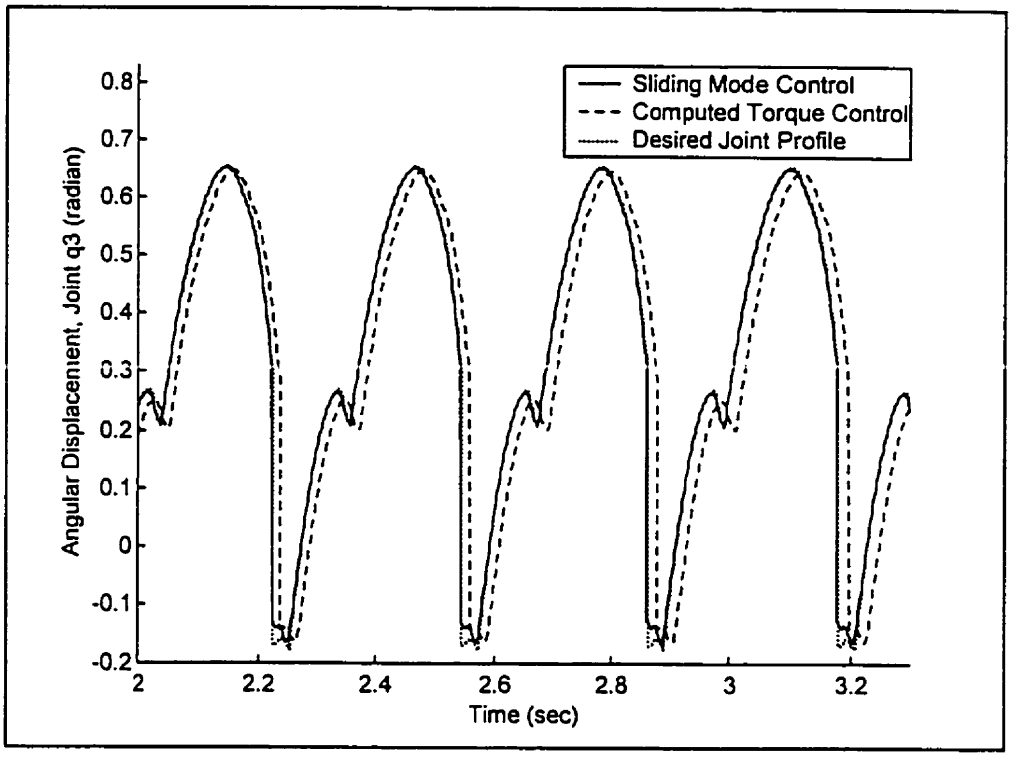

Figure 5.39b Angular Displacement (q_3) of Step 7 to 10 for Case 3

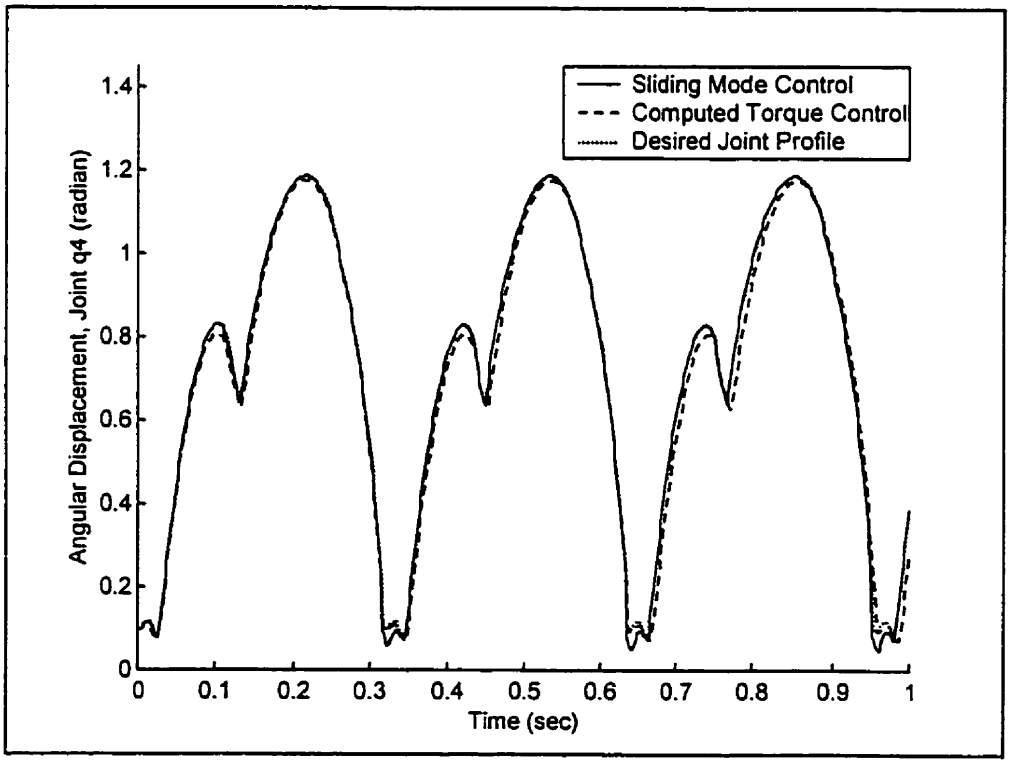

Figure 5.40a Angular Displacement (q_4) of Step 1 to 3 for Case 3

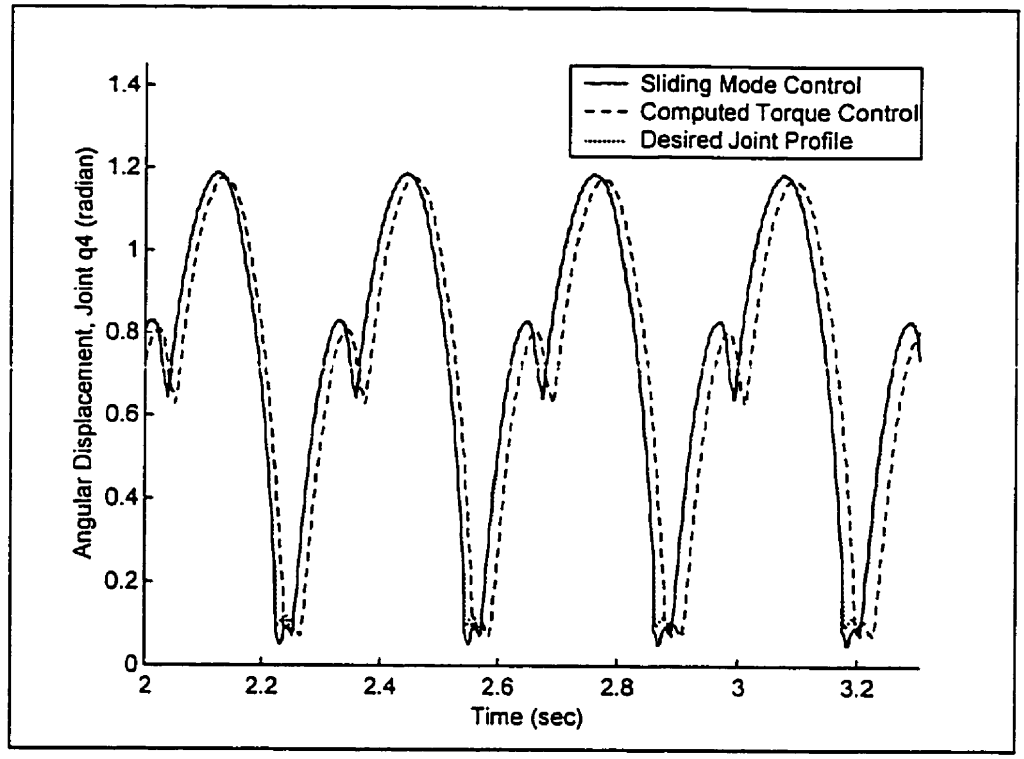

Figure 5.40b Angular Displacement (q_4) of Step 7 to 10 for Case 3

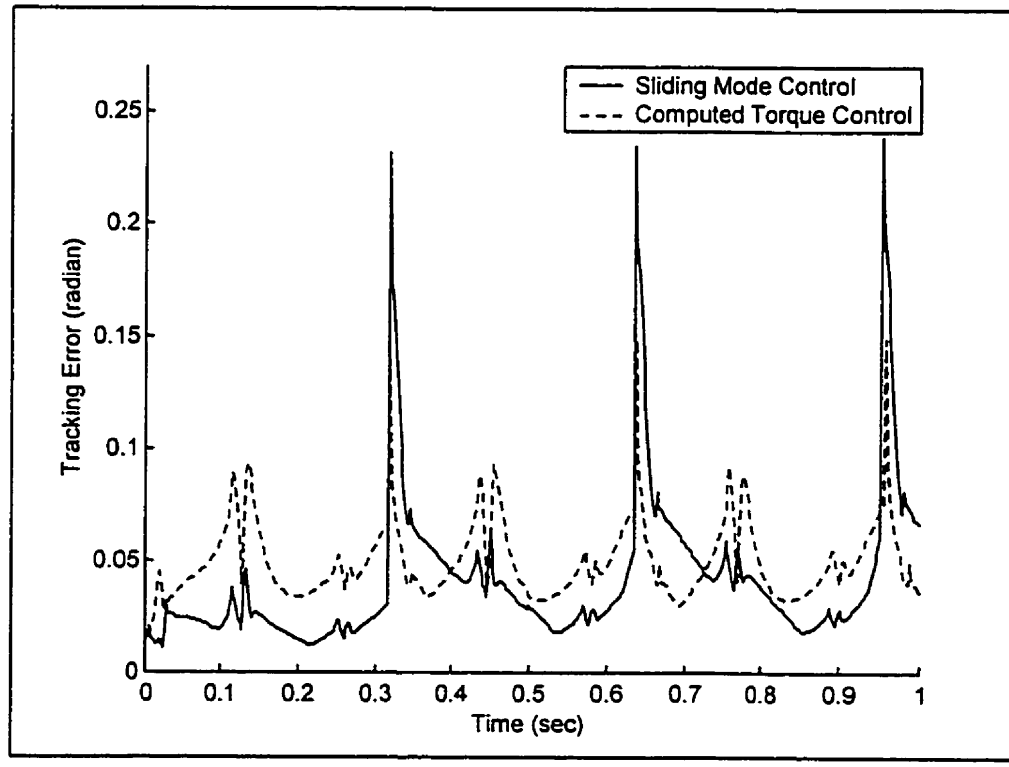

Figure 5.41 Tracking Error of Case 3

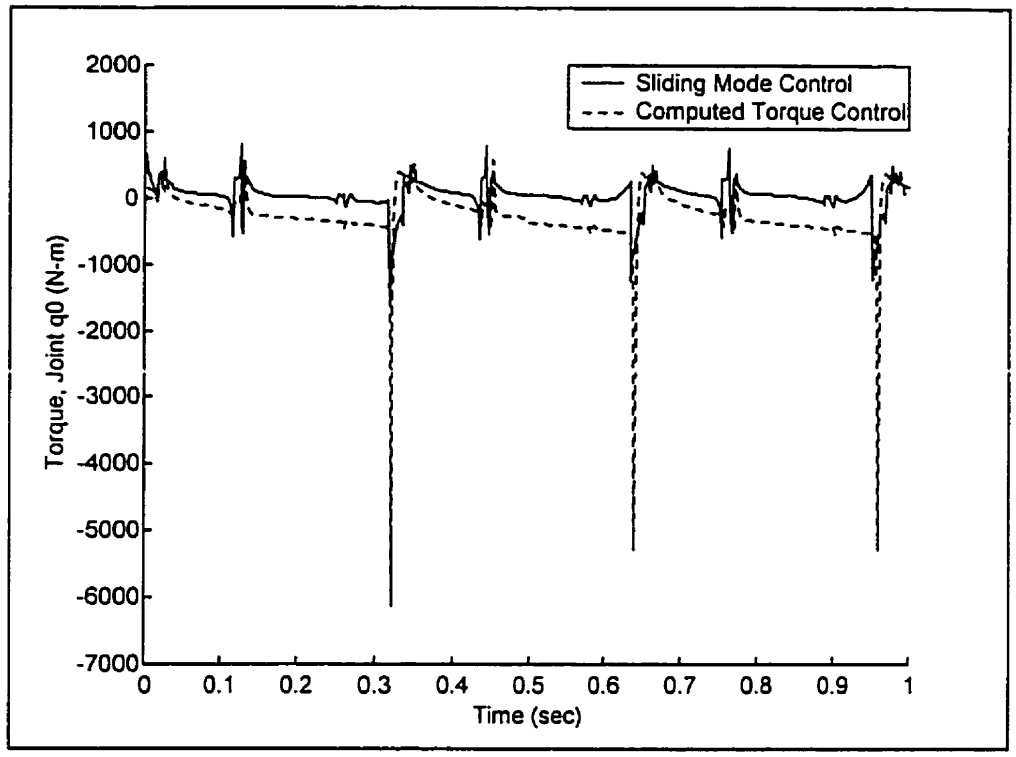

Figure 5.42a Control Torque at q_0 of Case 3

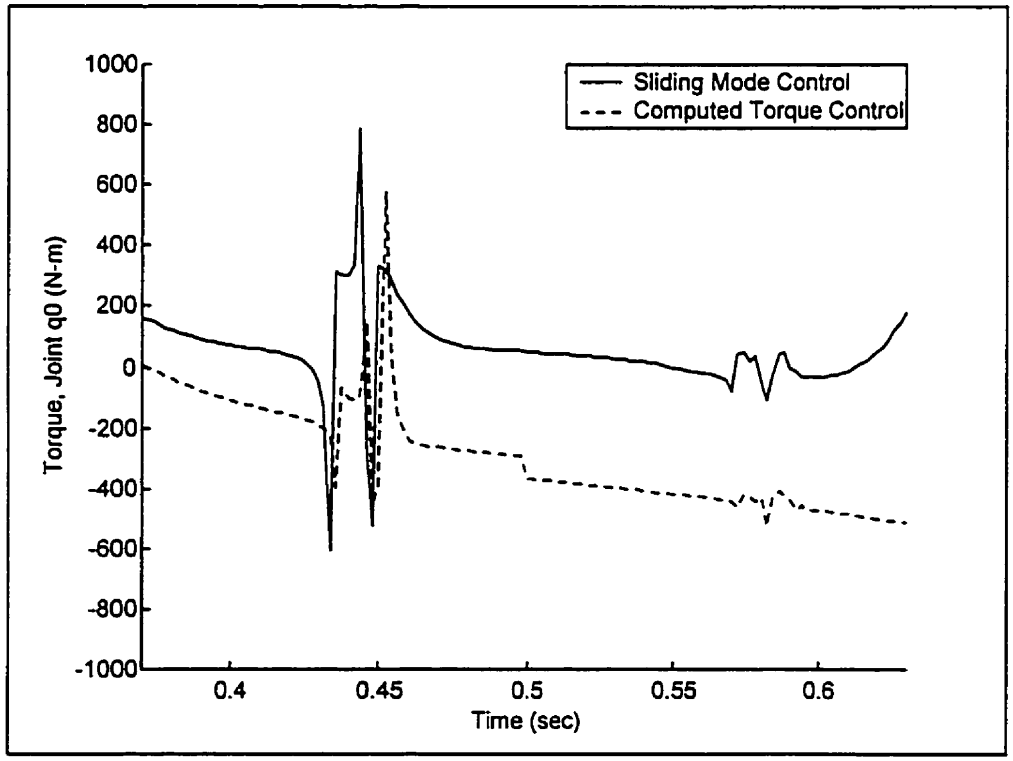

Figure 5.42b Control Torque at q_0 of Case 3 within One Step

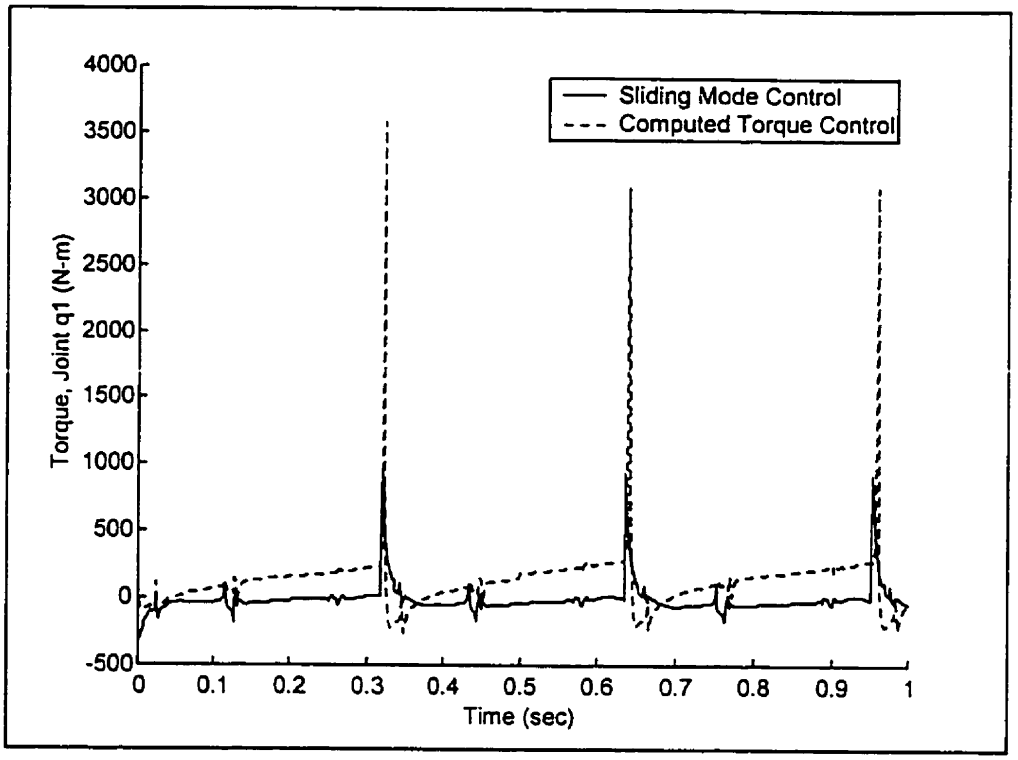

Figure 5.43a Control Torque at q_1 of Case 3

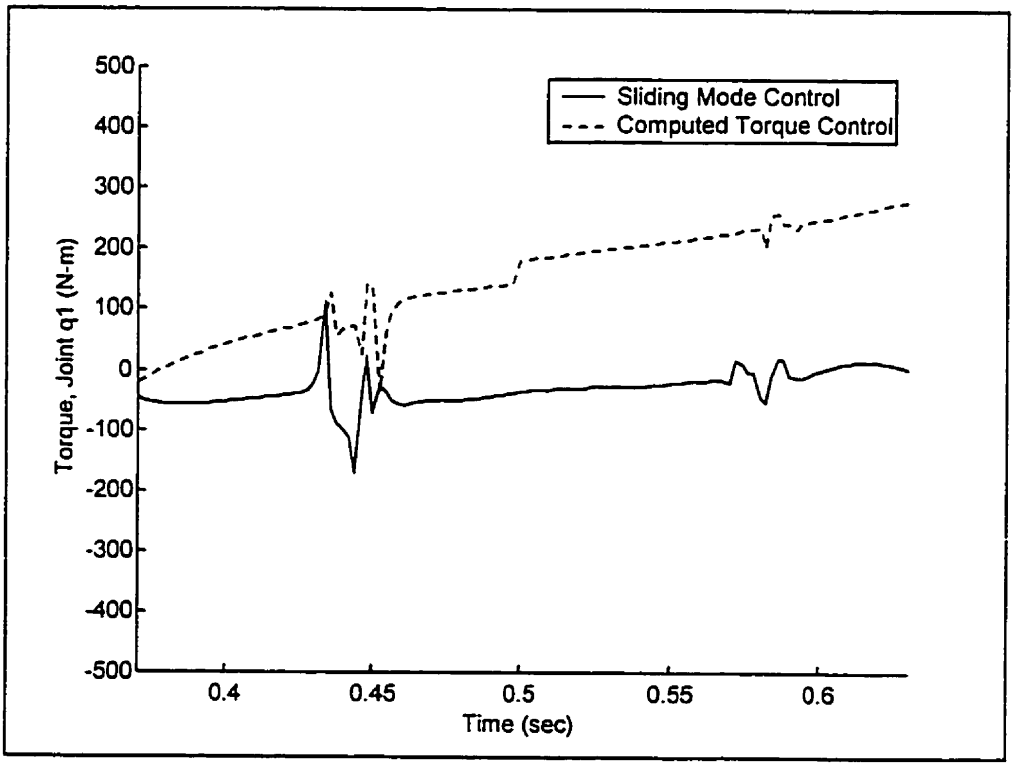

Figure 5.43b Control Torque at q_1 of Case 3 within One Step

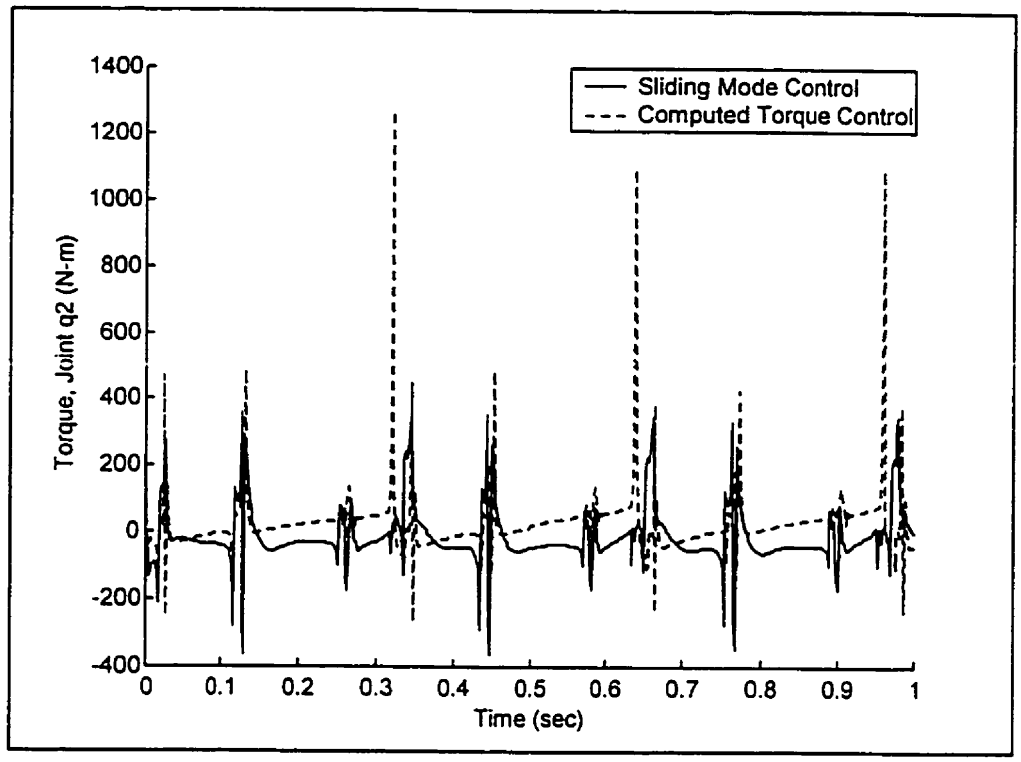

Figure 5.44a Control Torque at q_2 of Case 3

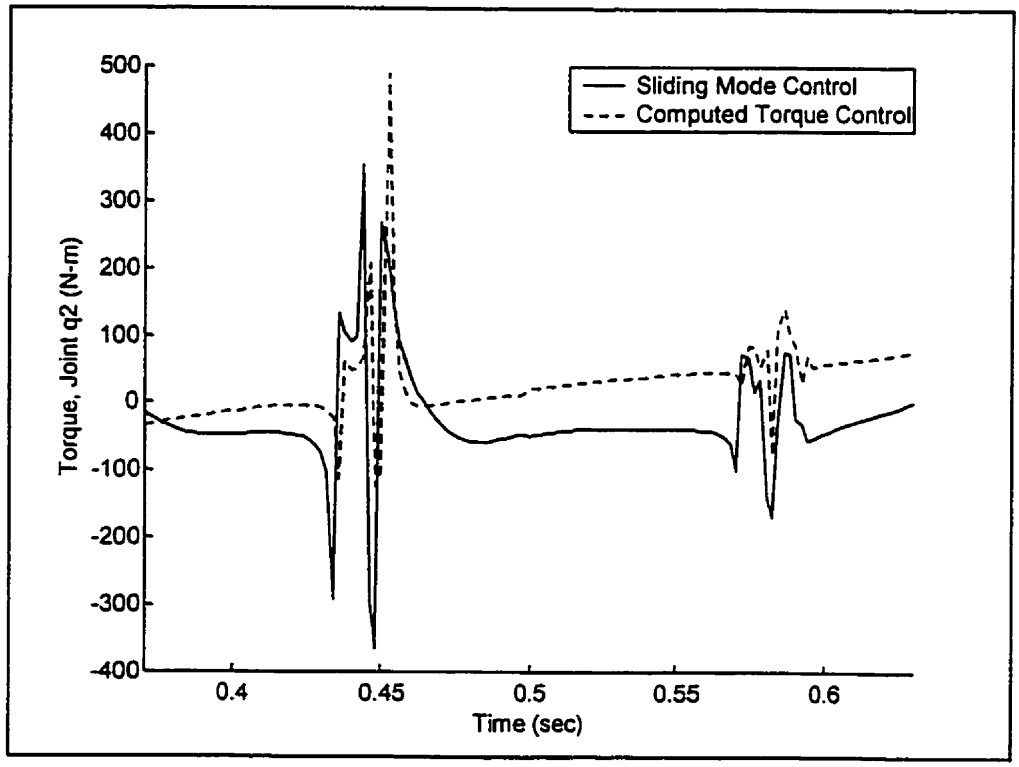

Figure 5.44b Control Torque at q_2 of Case 3 within One Step

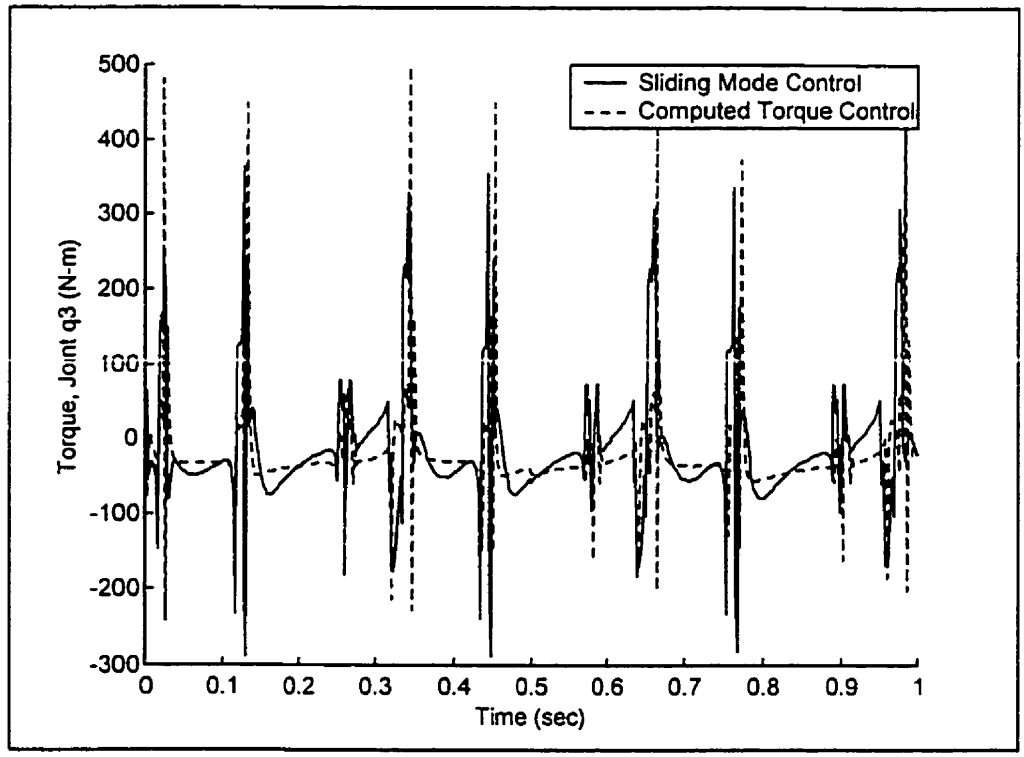

Figure 5.45a Control Torque at q_3 of Case 3

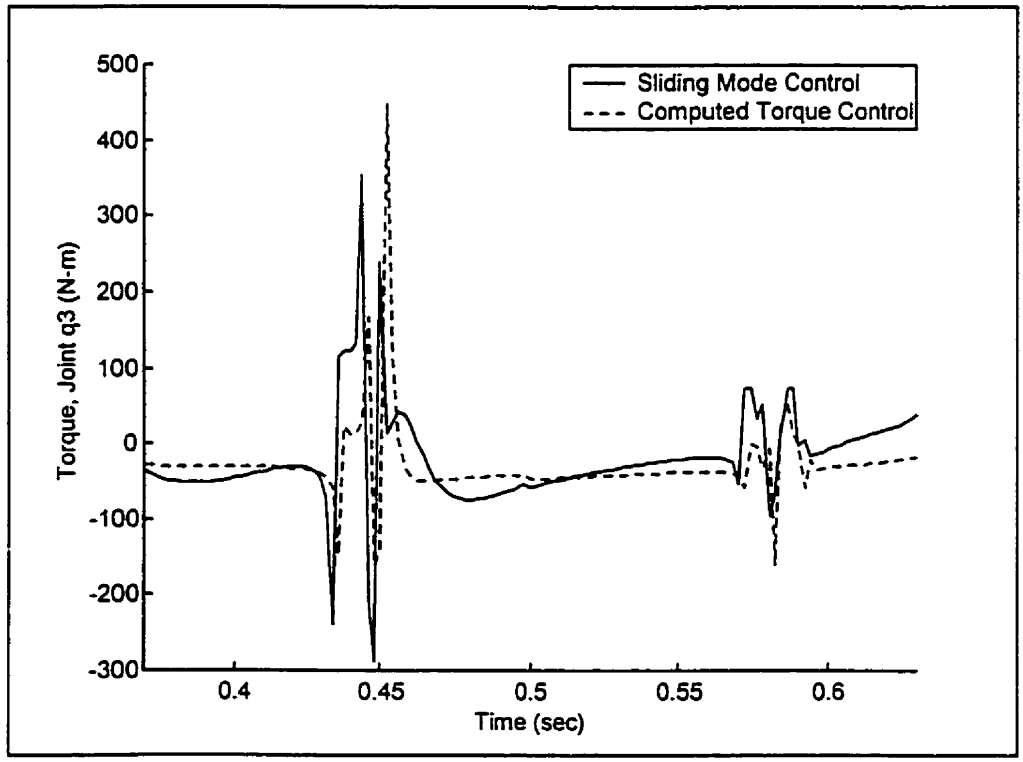

Figure 5.45b Control Torque at q_3 of Case 3 within One Step

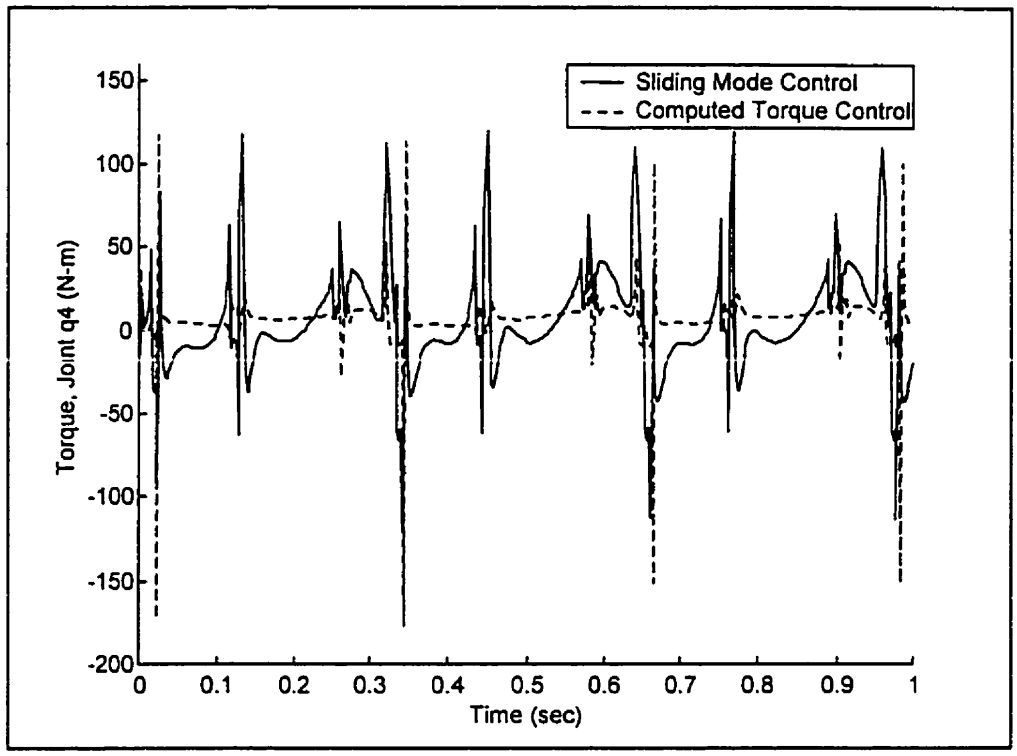

Figure 5.46a Control Torque at q_4 of Case 3

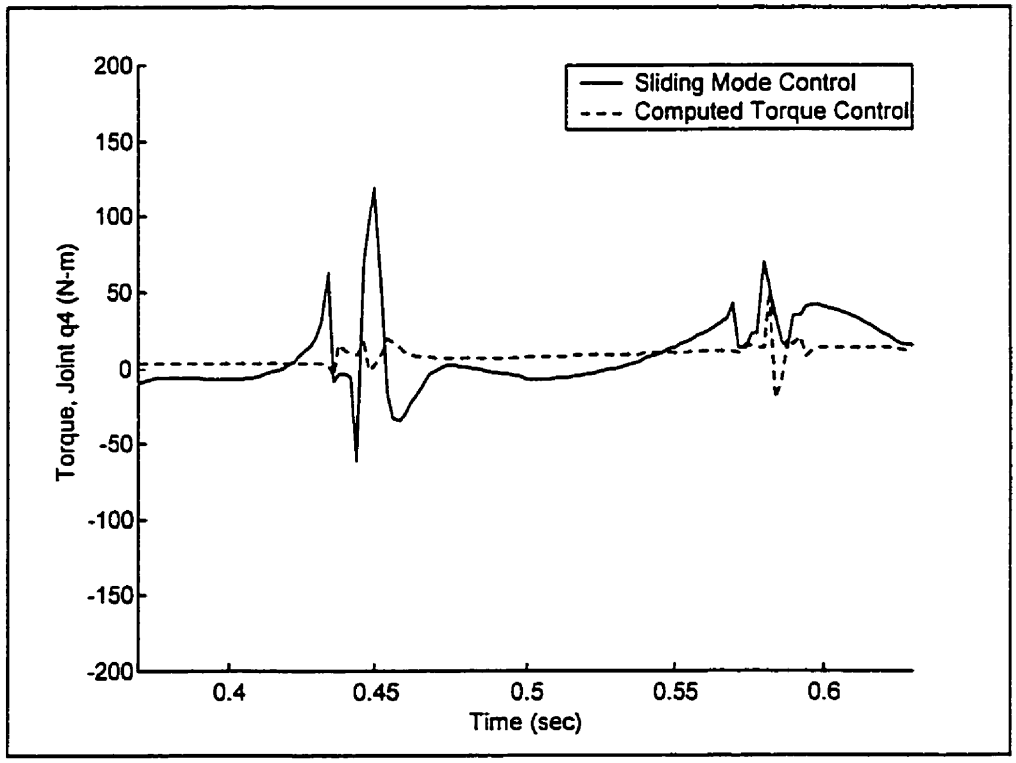

Figure 5.46b Control Torque at q_4 of Case 3 within One Step

From the results of the three cases presented above, the sliding mode control technique showed much better tracking performance than the computed torque control, especially when large parametric uncertainties existed in the system. Based on observing the plots resulted from the three cases, the computed torque control was not as robust as the sliding mode control. This verified the theoretically expected superiority of the sliding mode control over the computed torque control in the presence of parametric uncertainties.

5.4 Summary

In this chapter, two major results were presented. In Section 5.2, the results of the joint angle profiles planning were presented. Through the methodology presented in Chapter 3, the desired joint angle profiles for the motion of the biped walking on a flat horizontal surface were obtained from the five constraint functions. The acceptable joint angle profiles must be those that (1) satisfy the constraint functions presented in Section 3.2.1, (2) are repeatable, and (3) do not cause the knee of the swing leg to be bent backward. Such requirements made the determining of the acceptable joint angel profiles highly challenging. The simulation results of the four cases with different progression speeds were studied. The hypothesis of constant energy was investigated. The results of the simulation study on the energy profiles showed that (1) extra energy must be inputted to the bipedal system being studied at the beginning of the step regardless of the walking speed, (2) depending on the walking speed, there may be a need for a second energy input, and (3) energy input is proportional to the walking speed. For the system being studied, the second energy input was required for fast walking, while for slow and

moderate walking, with the proper initial energy input, no extra energy was required to carry the swing leg through the step.

In Section 5.3, the simulation study of tracking control was presented. The tracking performances of the sliding mode control and computed torque control were investigated as various degrees of parametric uncertainty in the system were considered. From the results presented in Section 5.3, the tracking performed through the sliding mode control technique was much better than that through computed torque control. The superiority of the sliding mode control technique over the computed torque control technique was strengthened when large parametric uncertainties were present in the system. This verified the theoretical expectation that sliding mode control is more preferable than computed torque control in the presence of parametric uncertainty. During the intensive numerical simulation, we found that, when compared with the conventional sliding surfaces used by most sliding mode control systems, the tracking performance of the sliding mode control was improved by designing the sliding surface with the integral term (see details in Section 4.4). The simulation results showed that replacing the discontinuous term with the continuous term in the sliding mode control algorithm smoothed out the chattering around the sliding surface and, at the same time, good tracking performance was obtained. The simulation results also showed that no reaching phase problem occurred with the use of this sliding mode control algorithm.

Chapter 6

Conclusions

6.1 Conclusions

In this thesis, dynamic modeling and control of a planar bipedal walking system were studied. The locomotion goal for the bipedal system to realize in this thesis was walking on a flat horizontal surface in the sagittal plane. The dynamic modeling of bipedal locomotion consists of the following three parts: (1) development of mathematical model which approximates the motion of the locomotion system, (2) design of the joint angle profiles for the desired walking motion that are used for tracking control, and (3) application of the control algorithms for regulating the motion. Contributions have been made to each part and are detailed below.

(1) Development of mathematical model:

A bipedal model of locomotion system is a complex linkage system due to the dynamic complexity with many degrees of freedom. A planar five-link kinematic model was used in this study as the biped robot. This bipedal model, consisted of five rigid links that were connected to one another by four purely rotational joints, had five degrees of freedom. The mathematical model developed in this study described a complete walking motion which included the single support phase, the effect of the impact between

the swing leg and the walking surface at the completion of each step, and the effect of the support end exchange. The impact effect was incorporated into the model by formulating an impact equation to compute the new joint velocities just after each collision between the free end of the swing leg and the walking surface. At the same instant as the impact occurs, the end of the support leg leaves the walking surface and the support end transfers to the tip of the swing leg that comes into contact with the walking surface. The effect of this instantaneous exchange of support from one end to another end was incorporated through re-labeling the numbering of links. A transformation matrix was formed to describe the effect on the angular displacements and angular velocities due to this re-labeling.

The advantage of the dynamic model developed in this thesis over other models is that it has enough degrees of freedom to approximate the walking motion in the sagittal plane and, at the same time, has sufficiently few degrees of freedom to keep the equations of motion to a manageable level. Renumbering of links reduced the derivation process of equations of motion by half, since the same set of equations of motion for the single support phase can be used for both the left and right leg supports. Furthermore, the impact between the swing leg and the walking surface at the contact instant is also included in the proposed model. The impact has been considered important for bipedal walking, yet it has been neglected in most of the bipedal models.

(2) Joint angle profiles planning

A systematic approach to determining joint angle profiles, developed by Hurmuzlu (1993a), was adapted in this study. Five new constraint functions were defined from the physically coherent parameters of bipedal walking, which were upright

posture of the upper body, the overall walking speed, the support knee bias, static stability, and keeping the mechanical energy of the whole system as a constant. The last constraint was used to test the hypothesis that, given only potential energy at the beginning of the step, the swing leg can be carried over by gravity. The five constraint functions led to a set of combined differential and algebraic equations, which had to be solved to obtain the joint angle profiles of the biped. In addition, two extra conditions must be satisfied for the acceptable joint angle profiles. One is the repeatability condition, which require that the configuration of the biped obtained at the end of each step be very close to the configuration at the beginning of each step. Another condition is that the knee of the swing leg could not bend backward. The above constraint equations and the two extra conditions made determining joint angle profiles highly challenging. After carrying out intensive numerical simulations, four set of acceptable joint angle profiles with four different progression speeds were obtained.

Through the numerical simulations, the question of giving only potential energy at the initiation of the step whether it is possible for the swing leg to be carried through the step without extra energy input was explored. It was found that, with the other four constraint functions satisfied, it was impossible to keep the energy constant during the whole step. Regardless of the walking speed, a certain amount of energy must be input to the biped at the beginning of the step. Depending on the walking speed, a second energy input might be needed. The simulation results showed that for fast walking, the second energy input was required at the instant when the swing leg, supporting leg and the upper body were close to the vertical. This energy is required to move the swing leg ahead of the upper body so that the gravity center of the upper body is located at the mid point

between the tips of the swing leg and the supporting leg (Constraint 4). For walking with slow or moderate speed, the second energy input was not necessary. These findings are important for the development of bipedal robots and prosthesis design. They indicate that a set of joint angle profiles can be designed where, with a proper initial energy input, no extra energy is required to carry the swing leg through the step. The biped that follows such a set of joint angle profiles is more energy efficient since the initial energy can be provided by the strain energy release of deformable foot.

(3) Motion control

Sliding mode control has been designed in this study to regulate the motion of the five-link biped robot. An integral term was used in designing the sliding surface. The advantage of using the integral term in the sliding surface is that the system trajectories converge to the sliding surface faster. Simulation results showed that the tracking performance of the proposed sliding mode control was significantly improved as compared to conventional sliding model control without using the integral term in the sliding surface.

The response for the classical sliding mode control system is known to chatter around the sliding surface. In order to overcome the chattering problem, our control algorithm was further improved by replacing the discontinuous term with a continuous one. The chatting problem was eliminated, however this replacement did not come without a price. Instead of keeping trajectories on the sliding surface, the control algorithm maintained the trajectories close to the surface within a thin boundary layer. Through the Lyapunov stability analysis, it was proven that the control algorithm can

guarantee the attractiveness of the boundary layer and the control algorithm can maintain the trajectories close to the surface within a thin boundary layer.

In this thesis, the tracking performances of the sliding mode control and the computed torque control were compared as various degrees of parametric uncertainty existed in the system. It was found that the sliding mode control technique was more effective than the computed torque control technique when parametric uncertainties existed in the bipedal system. The superiority of the sliding mode control over the computed torque control was strengthened when large parametric uncertainties were present. This finding agrees with previous work of Tzafestas et al. (1996).

In summary, contributions have been made in the following three areas. (1) A dynamic model of a bipedal robot was developed. Such a model has several advantages. It has sufficient degrees of freedom to approximate the bipedal walking, and it is still simple enough to keep the equations of motion to a manageable level. Impact is also included in the proposed model, which has been neglected by most of the existing models. (2) Joint angle profiles are designed based on a set of new constraint functions proposed in this thesis. One advantage of the proposed constraint functions is to consider energy as one of the factors. This is an important step towards designing joint angle profiles that minimize the energy during walking. Such an optimization is highly desirable for the development of bipedal robots. (3) A modified sliding mode control law was designed in this work. The performance of the proposed sliding mode control and classical computed torque control were compared. It was found that the proposed sliding mode control was superior to the computed torque control especially when there were parametric uncertainties present in the system.

6.2 Future Works

The results obtained in this thesis are only a first step in the development of dynamic models of bipedal locomotion systems. In the future, work can be extended in different directions. The planar five-link biped system can be extended to a three-dimensional system to include motion in the frontal plane. By including the analysis of the motion and balance in the frontal plane, not only normal gait, but also pathological gait can be studied. The five-link bipedal model can also be extended to a model with seven or more links to include the dynamics of feet. Double support phase can also be included in the analysis. Since minimization of energy is a basic characteristic of human natural walking (Winter et al. 1976), the methodology of joint angle profiles planning can be extended to design the prescribed motion with optimization of energy. Discrete mapping technique can be employed to facilitate the joint angle profiles design process. In the area of motion control, the performance of different nonlinear control techniques can be explored, such as adaptive control and neural network control.

References

Asada, H., and Slotine, J.-J. E., 1986, Robot Analysis and Control, *John Wiley and Sons, New York.*

Bailey, E., and Apapostathis, A., 1987, Simple Sliding Mode Control Scheme Applied to Robot Manipulators, *International Journal of Control*, Vol. 45, No. 4, April 1987, pp. 1197-1209.

Bay, J.S., and Hemami, H., 1987, Modeling of a Neural Pattern Generator with Coupled Nonlinear Oscillators, *IEEE Transactions on Biomedical Engineering*, Vol. BME-34, No. 4, Appril 1987, pp. 297-306.

Borovac, B., Vukobratovic, M., and Surla, D., 1989, An approach to Biped Control Synthesis, *Robotica (1989)*, Vol. 7, pp. 231-241.

Chang, T.-H., and Hurmuzlu, Y., 1992, Trajectory Tracking in Robotic Systems using Variable Structure Control without a Reaching Phase, *Proceedings of the American Control Conference*, June 1992, v 2, pp. 1505-1509.

Chang, T.-H., and Hurmuzlu, Y., 1993, Sliding Control without Reaching Phase and its Application to Bipedal Locomotion, *Journal of Dynamic Systems, Measurement, and Control*, September 1993, Vol. 115, pp. 447-455.

Channon, P.H., Hopkins, S.H., and Pham, D.T., 1992, Derivation of Optimal Walking Motions for a Bipedal Walking Robot, *Robotica (1992)*, Vol. 10, pp. 165-172.

Chao, E.Y.-S., and Rim, K., 1973, Application of Optimization Principles in Determining the Applied Moments in Human Leg Joints During Gait, *Journal of Biomechanics*, Vol. 6, pp. 497-510.

Chevallereau, C., Formal'sky, A., and Perrin, B., 1998, Low Energy Cost Reference Trajectories for a Biped Robot, *Proceedings of the 1998 IEEE International Conference on Robotics and Automation*, pp. 1398-1403.

Chow, C.K., and Jacobson, D.H., 1972, Further Studies of Human Locomotion: Postural Stability and Control, *Mathematical Biosciences*, Vol. 15, pp. 93-108.

Cotsaftis, M., and Vibet, C., 1988, Control Law Decoupling for 2-D Biped Walking System, *IEEE Engineering in Medicine and biology Magazine*, Vol. 7, No. 3, September 1988, pp. 41-45.

Furusho, J., and Masubuchi, M., 1986, Control of a Dynamical Biped Locomotion System for Steady Walking, *Journal of Dynamic Systems, Measurement, and Control*, June 1986, Vol. 108, pp. 111-118.

Furusho, J., and Masubuchi, M., 1987, A Theoretically Motivated Reduced Order Model for the Control of Dynamic Biped Locomotion, *Journal of Dynamic Systems, Measurement, and Control*, June 1987, Vol. 109, pp. 155-163.

Furusho, J., and Sano, A., 1990, Sensor-Based Control of a Nine-Link Biped, *The International Journal of Robotics Research*, Vol. 9, No. 2, April 1990, 83-98.

Goddard, R.E. Jr., Hemami, H., and Weimer, F.C., 1983, Biped Side Step in the Frontal Plane, *IEEE Transactions on Automatic Control*, Vol. AC-28, No. 2, February 1983, pp. 179-187.

Golliday, C.L. Jr., and Hemami, H., 1976, Postural Stability of the Two-Degree-of-Freedom Biped by General Linear Feedback, *IEEE Transactions on Automatic Control*, February 1976, pp. 74-79.

Golliday, C.L. Jr., and Hemami, H., 1977, An Approach to Analyzing Biped Locomotion Dynamics and Designing Robot Locomotion Controls, *IEEE Transactions on Automatic Control*, Vol. AC-22, No. 6, December 1977, pp. 963-972.

Gubina, F., Hemami, H., and McGhee, R.B., 1974, On the Dynamic Stability of Biped Locomotion, *IEEE Transactions on Biomedical Engineering*, Vol. BME-21, No. 2, March 1974, pp.102-108.

Guiraud, D., 1994, Application of an Artificial Neural Network to the Control of an Active External Orthosis of the Lower Limb, *Medical and Biological Engineering and Computing*, Vol. 32, pp. 610-614.

Hemami, H., and Camana, P.C., 1976, Nonlinear Feedback in Simple Locomotion Systems, *IEEE Transactions on Automatic Control*, December 1977, pp. 855-860.

Hemami, H., and Farnsworth, R.L., 1977, Postural and Gait Stability of a Planar Five Link Biped by Simulation, *IEEE Transactions on Automatic Control*, Vol. 22, No. 3, June 1977, pp. 452-458.

Hemami, H., and Golliday, C. Jr., 1977, The Inverted Pendulum and Biped Stability, *Mathematical Bioscience*, Vol. 34, pp. 95-110.

Hemami, H., Robinson, C.S., and Ceranowicz, A.Z., 1980, Stability of Planar Biped Models by Simultaneous Pole Assignment and Decoupling, *Int. J. Systems Sci.*, Vol. 11, No. 1, pp. 65-75.

Hemami, H., Weimer, F.C., and Koozekanani, S.H., 1973, Some Aspects of the Inverted Pendulum Problem for Modeling of Locomotion Systems, *IEEE Transactions on Automatic Control*, December 1973, pp.658-661.

Hemami, H., and Wyman, B.F., 1979, Modeling and Control of Constrained Dynamic Systems with Application to Biped Locomotion in the Frontal Plane, *IEEE Transactions on Automatic Control*, Vol. AC-24, No. 4, August 1979, pp.526-535.

Hemami, H., and Wyman, B.F., 1979, Indirect Control of the Forces of Constraint in Dynamic Systems, *Journal of Dynamic Systems, Measurement, and Control*, December 1979, Vol. 101, pp. 355-360.

Holzreiter, H.S., and Köhle, M.E., 1993, Assessment of Gait Patterns Using Neural Networks, *Journal of Biomechanics*, Vol. 26, No. 6, pp. 645-651.

Hurmuzlu Y., 1993, Dynamics of Bipedal Gait: Part I - Objective Functions and the Contact Event of a Planar Five-Link Biped, *Journal of Applied Mechanics*, Vol. 60, pp. 331-336.

Hurmuzlu, Y., 1993, Dynamics of Bipedal Gait: Part II - Stability Analysis of a Planar Five-Link Biped, *Journal of Applied Mechanics*, Vol. 60, pp. 337-343.

Hurmuzlu, Y., and Basdogan, C., 1994, On the Measurement of Dynamic Stability of Human Locomotion, *Journal of Biomechanical Engineering*, Vol. 116, pp. 30-36.

Hurmuzlu, Y., and Moskowitz, G.D., 1986, The Role of Impact in the Stability of Bipedal Locomotion, *Dynamics and Stability of Systems*, Vol. 1, No. 3, pp. 217-234.

Hurmuzlu, Y., and Moskowitz, G.D., 1987, Bipedal Locomotion Stabilized by Impact and Switching: I. Two- and Three- Dimensional, Three-Element Models, *Dynamics and Stability of Systems*, Vol. 2, No. 2, pp. 73-96.

Iqbal, K., Hemami, H., and Simon, S., 1993, Stability and Control of a Frontal Four-Link Biped System, *IEEE Transactions on Biomedical Engineering*, Vol. 40, No. 10, October 1993, pp. 1007-1018.

Katoh, R., and Mori, M., 1984, Control Method of Biped Locomotion Giving Asymptotic Stability of Trajectory, *Automatica*, Vol. 20, No. 4, pp. 405-414.

Kun, A.L., and Miller, W.T., 1996, Adaptive Dynamic Balance of a Biped Robot Using Neural Networks, *Proceedings of the 1996 IEEE International Conference on Robotics and Automation*, pp. 240-245.

Kun, A.L., and Miller, W.T., 1999, Control of Variable-Speed Gaits for a Biped Robot, *IEEE Robotics and Automation Magazine*, Vol. 6, No. 3, pp. 19-29.

Ladin, Z., and Wu, G., 1991, Combining Position and Acceleration Measurements for Joint Force Estimation, *Journal of Biomechanics*, Vol. 24, No. 12, pp. 1173-1187.

Lee, T.-T., Jeng, P.L., and Gruver, W.A., 1988, Control of a 5-Link Biped Robot for Steady Walking, *Third International Symposium on Intelligent Control 1988*, August 1988, pp. 484-489.

Miller, W.T., 1994, Real-Time Neural Network Control of a Biped Walking Robot, *IEEE Control Systems*, Vol. 14, No. 1, pp. 41-48.

Miura, H., and Shimoyama, I., 1984, Dynamic Walk of a Biped, *The International Journal of Robotics Research*, Vol. 3, No. 2, Summer 1984, pp. 60-74.

Miyazaki, F., and Arimoto, S., 1980, A Control Theoretic Study on Dynamical Biped Locomotion, *Journal of Dynamic Systems, Measurement, and Control*, December 1980, Vol. 102, pp. 233-239

Murray, R.M., Li, Z., and Sastry S.S., 1994, A Mathematical Introduction to Robotic Manipulation, *CRC Press, Boca Raton, Florida.*

Onyshko, S., and Winter, D.A., 1980, A Mathematical Model for the Dynamics of Human Locomotion, *Journal of Biomechanics*, Vol. 13, pp. 361-368.

Paden, B.E., and Sastry, S.S., 1987, Calculus for Computing Filippov's Differential Inclusion with Application to the Variable Structure Control of Robot Manipulators, *IEEE Transactions on Circuits and Systems*, Vol. 3, No. 1, January 1987, pp. 73-82.

Pandy, M.G., and Berme, N., 1988, A Numerical Method for Simulating the Dynamics of Human Walking, *Journal of Biomechanics*, Vol. 21, No. 12, pp. 1043-1051.

Pandy, M.G., and Berme, N., 1989, Quantitative Assessment of Gait Determinants During Single Stance via a Three-Dimensional Model - Part 1. Normal Gait, *Journal of Biomechanics*, Vol. 22, No. 6/7, pp. 717-724.

Park, J.H., and Chung, H., 2000, Hybrid Control of Biped Robots to Increase Stability in Locomotion, *Journal of Robotic Systems*, Vol. 17, No. 4, pp.187-197.

Park, J.H., and Kim, K.D., 1998, Biped Robot Walking Using Gravity-Compensated Inverted Pendulum Mode and Computed Torque Control, *Proceedings of the 1998 IEEE International Conference on Robotics and Automation*, pp. 3528-3533.

Rodrigues, L., Prado, M., Tavares, P., da Silva, K., and Rosa, A., 1996, Simulation and Control of Biped Locomotion - GA Optimization, *Proceedings of the IEEE Conference on Evolutionary Computation*, pp. 390-395.

Shih, C.-L., 1996, The Dynamics and Control of a Biped Walking Robot with Seven Degrees of Freedom, *Journal of Dynamic Systems, Measurement, and Control*, Vol. 118, December 1996, pp. 683-690.

Siegler, S., Seliktar, R., and Hyman, W., 1982, Simulation of Human Gait with the Aid of a Simple Mechanical Model, *Journal of Biomechanics*, Vol. 15, No. 6, pp. 415-452.

Silva, F.M., and Tenreiro Machado, J.A., 1998, Towards Efficient Biped Robots, *Proceedings of the 1998 IEEE/RSJ International Conference on Intelligent Robots and Systems*, pp. 394-399.

Slotine, J.J., 1984, Sliding Controller Design for Non-Linear Systems, *International Journal of Control*, Vol. 40, No. 2, pp. 421-434.

Slotine, J.-J., and Li, W., 1991, Applied Nonlinear Control, *Prentice Hall, New Jersey.*

Slotine, J.J., and Sastry, S.S., 1983, Tracking Control of Non-Linear Systems using Sliding Surfaces, with Application to Robot Manipulators, *International Journal of Control*, Vol. 38, No. 2, pp. 465-492.

Srinivasan, S., Gander, R.E., and Wood, H.C., 1992, A Movement Pattern Generator Model Using Artificial Neural Networks, *IEEE Transactions on Biomedical Engineering*, Vol. 39, No. 7, July 1992, pp. 716-722.

Thornton-Trump, A.B., and Daher, R., 1975, The Prediction of Reaction Forces From Gait Data, *Journal of Biomechanics*, Vol. 8, pp. 173-178.

Tzafestas, S., Raibert, M., and Tzafestas, C., 1996, Robust Sliding-mode Control Applied to a 5-Link Biped Robot, *Journal of Intelligent and Robotic Systems*, Vol. 15, pp. 67-133.

Vaughan, C.L., Davis, B.L., and O'Connor, J.C., 1992, Dynamics of Human Gait, *Human Kinetics Publishers, Champaign, Illinois.*

Vukobratovic, M., Borovac, B., Surla, D., and Stokic, D., 1990, Scientific Fundamentals of Robotics 7: Biped Locomotion Dynamics, Stability, Control and Application, *Springer-Verlag, New York.*

Vukobratovic, M., and Frank, A.A., 1970, On the Stability of Biped Locomotion, *IEEE Transactions on Bio-Medical Engineering*, Vol. BME-17, No. 1, January 1970, pp. 25-36.

Vukobratovic M., and Stokic, D., 1980, Significance of Force-Feedback in Controlling Artificial Locomotion-Manipulation Systems, *IEEE Transactions on Bio-Medical Engineering*, Vol. BME-27, No. 12, December 1980, pp. 705-713.

Vukobratovic, M., Timcenko, O., 1996, Experiments with Nontraditional Hybrid Control Technique of Biped Locomotion Robots, *Journal of Intelligent and Robotic System*, Vol. 16, No. 1, pp. 25-43.

Winter, D.A., The Biomechanicas and Motor Control of Human Gait: Normal, Elderly and Pathological, 2nd Editon, *Waterloo Biomechanics*, 1991.

Winter, D.A., Quanbury, A.O., and Reimer, G.D., 1976, Analysis of Instantaneous Energy of Normal Gait, *Journal of Biomechanics*, Vol. 9, pp. 253-257.

Wu, Q., 1996, Lyapunov Stability Analysis of a Class of Base-Excited Inverted Pendulums with Application to Bipedal Locomotion Systems, *University of Manitoba Ph.D. Thesis.*

Wu, Q., Thornton-Trump, A.B., and Sepehri, N., 1998, Lyapunov Stability Control of Inverted Pendulums with General Base Point Motion, *International Journal of Non-Linear Mechanics*, Vol. 33, No. 5, pp. 801-818.

Yang, J.-S., 1994, A Control Study of a Kneeless Biped Locomotion System, *Journal of The Franklin Institute Engineering and Applied Mathematics*, Vol. 331B, No. 2, pp. 125-143.

Yang, J.-S., and Shahabuddin, A., 1994, Trajectory Planning and Control, for a Five-Degree-of-Freedom Biped Locomotion System, *Proceedings of the American Control Conference*, June 1994, pp.3105-3109.

Zheng, Y.-F., and Hemami, H., 1984, Impact Effects of Biped Contact with the Environment, *IEEE Transactions on Systems, Man, and Cybernetics*, Vol. SMC-14, No. 3, May/June 1984, pp. 437-443.

Appendix I

Derivation of the Five-Link Biped Dynamic Model with Single Leg Support

The equations of motion for the single support phase are derived by applying the Lagrangian formulation. The Lagrangian formulation is given as

$$L = K - P$$

and the Lagranian equation of motion is in the form:

$$\frac{d}{dt}\left\{\frac{\partial L}{\partial \dot{q}_i}\right\} - \frac{\partial L}{\partial q_i} = T_i.$$

which can be rearranged as

$$\frac{d}{dt}\left\{\frac{\partial K}{\partial \dot{\theta}_i}\right\} - \frac{\partial K}{\partial \theta_i} + \frac{\partial P}{\partial \theta_i} = T_i$$

Each term in this equation is derived as follows:

$$\begin{aligned}
\frac{d}{dt}\left(\frac{\partial K}{\partial \dot{\theta}_1}\right) = {} & [I_1 + m_1 d_1^{\,2} + m_2 \ell_1^{\,2} + m_3 \ell_1^{\,2} + m_4 \ell_1^{\,2} + m_5 \ell_1^{\,2}]\ddot{\theta}_1 \\
& + [m_2 \ell_1 d_2 + m_3 \ell_1 \ell_2 + m_4 \ell_1 \ell_2 + m_5 \ell_1 \ell_2]\cos(\theta_1 - \theta_2)\ddot{\theta}_2 \\
& + [m_3 \ell_1 d_3]\cos(\theta_1 - \theta_3)\ddot{\theta}_3 \\
& + [m_4 \ell_1 (\ell_4 - d_4) + m_5 \ell_1 \ell_4]\cos(\theta_1 + \theta_4)\ddot{\theta}_4 \\
& + [m_5 \ell_1 (\ell_5 - d_5)]\cos(\theta_1 + \theta_5)\ddot{\theta}_5 \\
& - [m_2 \ell_1 d_2 + m_3 \ell_1 \ell_2 + m_4 \ell_1 \ell_2 + m_5 \ell_1 \ell_2]\sin(\theta_1 - \theta_2)\dot{\theta}_1\dot{\theta}_2 \\
& + [m_2 \ell_1 d_2 + m_3 \ell_1 \ell_2 + m_4 \ell_1 \ell_2 + m_5 \ell_1 \ell_2]\sin(\theta_1 - \theta_2)\dot{\theta}_2^{\,2} \\
& - [m_3 \ell_1 d_3]\sin(\theta_1 - \theta_3)\dot{\theta}_1\dot{\theta}_3 \\
& + [m_3 \ell_1 d_3]\sin(\theta_1 - \theta_3)\dot{\theta}_3^{\,2} \\
& - [m_4 \ell_1 (\ell_4 - d_4) + m_5 \ell_1 \ell_4]\sin(\theta_1 + \theta_4)\dot{\theta}_1\dot{\theta}_4 \\
& - [m_4 \ell_1 (\ell_4 - d_4) + m_5 \ell_1 \ell_4]\sin(\theta_1 + \theta_4)\dot{\theta}_4^{\,2} \\
& - [m_5 \ell_1 (\ell_5 - d_5)]\sin(\theta_1 + \theta_5)\dot{\theta}_1\dot{\theta}_5 \\
& - [m_5 \ell_1 (\ell_5 - d_5)]\sin(\theta_1 + \theta_5)\dot{\theta}_5^{\,2}
\end{aligned}$$

$$\frac{d}{dt}\left(\frac{\partial K}{\partial \dot{\theta}_2}\right) = [I_2 + m_2 d_2^{\,2} + m_3 \ell_2^{\,2} + m_4 \ell_2^{\,2} + m_5 \ell_2^{\,2}]\ddot{\theta}_2$$
$$+ [m_2 \ell_1 d_2 + m_3 \ell_1 \ell_2 + m_4 \ell_1 \ell_2 + m_5 \ell_1 \ell_2]\cos(\theta_1 - \theta_2)\ddot{\theta}_1$$
$$+ [m_3 \ell_2 d_3]\cos(\theta_2 - \theta_3)\ddot{\theta}_3$$
$$+ [m_4 \ell_2 (\ell_4 - d_4) + m_5 \ell_2 \ell_4]\cos(\theta_2 + \theta_4)\ddot{\theta}_4$$
$$+ [m_5 \ell_2 (\ell_5 - d_5)]\cos(\theta_2 + \theta_5)\ddot{\theta}_5$$
$$+ [m_2 \ell_1 d_2 + m_3 \ell_1 \ell_2 + m_4 \ell_1 \ell_2 + m_5 \ell_1 \ell_2]\sin(\theta_1 - \theta_2)\dot{\theta}_1\dot{\theta}_2$$
$$- [m_2 \ell_1 d_2 + m_3 \ell_1 \ell_2 + m_4 \ell_1 \ell_2 + m_5 \ell_1 \ell_2]\sin(\theta_1 - \theta_2)\dot{\theta}_2^{\,2}$$
$$- [m_3 \ell_2 d_3]\sin(\theta_2 - \theta_3)\dot{\theta}_2\dot{\theta}_3$$
$$+ [m_3 \ell_2 d_3]\sin(\theta_2 - \theta_3)\dot{\theta}_3^{\,2}$$
$$- [m_4 \ell_2 (\ell_4 - d_4) + m_5 \ell_2 \ell_4]\sin(\theta_2 + \theta_4)\dot{\theta}_2\dot{\theta}_4$$
$$- [m_4 \ell_2 (\ell_4 - d_4) + m_5 \ell_2 \ell_4]\sin(\theta_2 + \theta_4)\dot{\theta}_4^{\,2}$$
$$- [m_5 \ell_2 (\ell_5 - d_5)]\sin(\theta_2 + \theta_5)\dot{\theta}_2\dot{\theta}_5$$
$$- [m_5 \ell_2 (\ell_5 - d_5)]\sin(\theta_2 + \theta_5)\dot{\theta}_5^{\,2}$$

$$\frac{d}{dt}\left(\frac{\partial K}{\partial \dot{\theta}_3}\right) = [I_3 + m_3 d_3^{\,2}]\ddot{\theta}_3$$
$$+ [m_3 \ell_1 d_3]\cos(\theta_1 - \theta_3)\ddot{\theta}_1$$
$$+ [m_3 \ell_2 d_3]\cos(\theta_2 - \theta_3)\ddot{\theta}_2$$
$$+ [m_3 \ell_1 d_3]\sin(\theta_1 - \theta_3)\dot{\theta}_1\dot{\theta}_3$$
$$- [m_3 \ell_1 d_3]\sin(\theta_1 - \theta_3)\dot{\theta}_1^{\,2}$$
$$+ [m_3 \ell_2 d_3]\sin(\theta_2 - \theta_3)\dot{\theta}_2\dot{\theta}_3$$
$$- [m_3 \ell_2 d_3]\sin(\theta_2 - \theta_3)\dot{\theta}_2^{\,2}$$

$$\frac{d}{dt}\left(\frac{\partial K}{\partial \dot{\theta}_4}\right) = [I_4 + m_4 (\ell_4 - d_4)^2 + m_5 \ell_4^{\,2}]\ddot{\theta}_4$$
$$+ [m_4 \ell_1 (\ell_4 - d_4) + m_5 \ell_1 \ell_4]\cos(\theta_1 + \theta_4)\ddot{\theta}_1$$
$$+ [m_4 \ell_2 (\ell_4 - d_4) + m_5 \ell_2 \ell_4]\cos(\theta_2 + \theta_4)\ddot{\theta}_2$$
$$+ [m_5 \ell_4 (\ell_5 - d_5)]\cos(\theta_4 - \theta_5)\ddot{\theta}_5$$
$$- [m_4 \ell_1 (\ell_4 - d_4) + m_5 \ell_1 \ell_4]\sin(\theta_1 + \theta_4)\dot{\theta}_1\dot{\theta}_4$$
$$- [m_4 \ell_1 (\ell_4 - d_4) + m_5 \ell_1 \ell_4]\sin(\theta_1 + \theta_4)\dot{\theta}_1^{\,2}$$
$$- [m_4 \ell_2 (\ell_4 - d_4) + m_5 \ell_2 \ell_4]\sin(\theta_2 + \theta_4)\dot{\theta}_2\dot{\theta}_4$$
$$- [m_4 \ell_2 (\ell_4 - d_4) + m_5 \ell_2 \ell_4]\sin(\theta_2 + \theta_4)\dot{\theta}_2^{\,2}$$
$$- [m_5 \ell_4 (\ell_5 - d_5)]\sin(\theta_4 - \theta_5)\dot{\theta}_4\dot{\theta}_5$$
$$+ [m_5 \ell_4 (\ell_5 - d_5)]\sin(\theta_4 - \theta_5)\dot{\theta}_5^{\,2}$$

$$\frac{d}{dt}\left(\frac{\partial K}{\partial \dot{\theta}_5}\right) = [I_5 + m_5(\ell_5 - d_5)^2]\ddot{\theta}_5$$
$$+ [m_5\ell_1(\ell_5 - d_5)]\cos(\theta_1 + \theta_5)\ddot{\theta}_1$$
$$+ [m_5\ell_2(\ell_5 - d_5)]\cos(\theta_2 + \theta\ )\ddot{\theta}_2$$
$$+ [m_5\ell_4(\ell_5 - d_5)]\cos(\theta_4 - \theta_5)\ddot{\theta}_4$$
$$- [m_5\ell_1(\ell_5 - d_5)]\sin(\theta_1 + \theta_5)\dot{\theta}_1\dot{\theta}_5$$
$$- [m_5\ell_1(\ell_5 - d_5)]\sin(\theta_1 + \theta_5)\dot{\theta}_1^2$$
$$- [m_5\ell_2(\ell_5 - d_5)]\sin(\theta_2 + \theta_5)\dot{\theta}_2\dot{\theta}_5$$
$$- [m_5\ell_2(\ell_5 - d_5)]\sin(\theta_2 + \theta_5)\dot{\theta}_2^2$$
$$+ [m_5\ell_4(\ell_5 - d_5)]\sin(\theta_4 - \theta_5)\dot{\theta}_4\dot{\theta}_5$$
$$- [m_5\ell_4(\ell_5 - d_5)]\sin(\theta_4 - \theta_5)\dot{\theta}_4^2$$

$$\frac{\partial K}{\partial \theta_1} = -[m_2\ell_1 d_2 + m_3\ell_1\ell_2 + m_4\ell_1\ell_2 + m_5\ell_1\ell_2]\sin(\theta_1 - \theta_2)\dot{\theta}_1\dot{\theta}_2$$
$$- [m_3\ell_1 d_3]\sin(\theta_1 - \theta_3)\dot{\theta}_1\dot{\theta}_3 - [m_4\ell_1(\ell_4 - d_4) + m_5\ell_1\ell_4]\sin(\theta_1 + \theta_4)\dot{\theta}_1\dot{\theta}_4$$
$$- [m_5\ell_1(\ell_5 - d_5)]\sin(\theta_1 + \theta_5)\dot{\theta}_1\dot{\theta}_5$$

$$\frac{\partial K}{\partial \theta_2} = -[m_2\ell_1 d_2 + m_3\ell_1\ell_2 + m_4\ell_1\ell_2 + m_5\ell_1\ell_2]\sin(\theta_1 - \theta_2)\dot{\theta}_1\dot{\theta}_2$$
$$- [m_3\ell_2 d_3]\sin(\theta_2 - \theta_3)\dot{\theta}_2\dot{\theta}_3 - [m_4\ell_2(\ell_4 - d_4) + m_5\ell_2\ell_4]\sin(\theta_2 + \theta_4)\dot{\theta}_2\dot{\theta}_4$$
$$- [m_5\ell_2(\ell_5 - d_5)]\sin(\theta_2 + \theta_5)\dot{\theta}_2\dot{\theta}_5$$

$$\frac{\partial K}{\partial \theta_3} = -[m_3\ell_1 d_3]\sin(\theta_1 - \theta_3)\dot{\theta}_1\dot{\theta}_3 + [m_3\ell_2 d_3]\sin(\theta_2 - \theta_3)\dot{\theta}_2\dot{\theta}_3$$

$$\frac{\partial K}{\partial \theta_4} = -[m_4\ell_1(\ell_4 - d_4) + m_5\ell_1\ell_4]\sin(\theta_1 + \theta_4)\dot{\theta}_1\dot{\theta}_4$$
$$- [m_4\ell_2(\ell_4 - d_4) + m_5\ell_2\ell_4]\sin(\theta_2 + \theta_4)\dot{\theta}_2\dot{\theta}_4$$
$$- [m_5\ell_4(\ell_5 - d_5)]\sin(\theta_4 - \theta_5)\dot{\theta}_4\dot{\theta}_5$$

$$\frac{\partial K}{\partial \theta_5} = -[m_5\ell_1(\ell_5 - d_5)]\sin(\theta_1 + \theta_5)\dot{\theta}_1\dot{\theta}_5$$
$$- [m_5\ell_2(\ell_5 - d_5)]\sin(\theta_2 + \theta_5)\dot{\theta}_2\dot{\theta}_5$$
$$+ [m_5\ell_4(\ell_5 - d_5)]\sin(\theta_4 - \theta_5)\dot{\theta}_4\dot{\theta}_5$$

$$\frac{\partial P}{\partial \theta_1} = -[m_1 d_1 + m_2 \ell_1 + m_3 \ell_1 + m_4 \ell_1 + m_5 \ell_1] g \sin\theta_1$$

$$\frac{\partial P}{\partial \theta_2} = -[m_2 d_2 + m_3 \ell_2 + m_4 \ell_2 + m_5 \ell_2] g \sin\theta_2$$

$$\frac{\partial P}{\partial \theta_3} = -[m_3 d_3] g \sin\theta_3$$

$$\frac{\partial P}{\partial \theta_4} = [m_4 (\ell_4 - d_4) + m_5 \ell_4] g \sin\theta_4$$

$$\frac{\partial P}{\partial \theta_5} = [m_5 (\ell_5 - d_5)] g \sin\theta_5$$

Appendix II

Transformation of the Dynamic Model

For the control purpose, the equations of motion has to be formulated in terms of the relative angles between links.

$$\underline{D}_q(\underline{q})\ddot{\underline{q}} + \underline{h}_q(\underline{q},\dot{\underline{q}})\dot{\underline{q}} + \underline{G}_q(\underline{q}) = \underline{T}_q$$

where

$$q = [q_0, q_1, q_2, q_3, q_4]^T$$

q_1, q_2, q_3, and q_4 are the relative angle displacements of the corresponding joints with the following relationships,

$$q_0 = \theta_1 \qquad q_1 = \theta_1 - \theta_2 \qquad q_2 = \theta_2 - \theta_3 \qquad q_3 = \theta_3 + \theta_4 \qquad q_4 = \theta_4 - \theta_5$$

The following procedure is used to transform the equations of motion in terms of angles of links with respect to the vertical into equations in terms of relative angles between links.

Since

τ_0: driving torque of the ankle of the support leg

τ_1: driving torque of the knee of the support leg

τ_2: driving torque of the hip of the support leg

τ_3: driving torque of the knee of the swing leg

τ_4: driving torque of the hip of the swing leg

and using the relationship between θ and q (Tzafestas et al. 1996),

$$T_{\theta_i} = \sum_{j=1}^{4} \tau_j \frac{\partial q_j}{\partial \theta_i}$$

The following relation is formed:

$$\underline{T}_\theta = \begin{bmatrix} 1 & 0 & 0 & 0 \\ -1 & 1 & 0 & 0 \\ 0 & -1 & 1 & 0 \\ 0 & 0 & -1 & 1 \\ 0 & 0 & 0 & -1 \end{bmatrix} \begin{bmatrix} \tau_0 \\ \tau_1 \\ \tau_2 \\ \tau_3 \\ \tau_4 \end{bmatrix}$$

The generalized torques $T_{\theta i}$ (i=1,2,...,5) that correspond to the relative angle displacements are $T_{q_i} = \tau_i \quad (i = 1,2,\ldots,5)$ where τ_i are the actual driving torques at the joints. The angle displacement of each link can be expressed in terms of q_i:

$$\theta_1 = q_0$$
$$\theta_2 = q_0 - q_1$$
$$\theta_3 = q_0 - q_1 - q_2$$
$$\theta_4 = -q_0 + q_1 + q_2 + q_3$$
$$\theta_5 = -q_0 + q_1 + q_2 + q_3 - q_4$$

From the relationship (Tzafestas et al. 1996)

$$T_{qi} = \sum_{j=1}^{5} T_{\theta j} \frac{\partial q_j}{\partial q_i} \quad (i = 0,1,\ldots 5)$$

The generalized torque T_{qi} is obtained

$$T_{q0} = T_{\theta 1} + T_{\theta 2} + T_{\theta 3} - T_{\theta 4} - T_{\theta 5}$$
$$T_{q1} = -T_{\theta 2} - T_{\theta 3} + T_{\theta 4} + T_{\theta 5}$$
$$T_{q2} = -T_{\theta 3} + T_{\theta 4} + T_{\theta 5}$$
$$T_{q3} = T_{\theta 4} + T_{\theta 5}$$
$$T_{q4} = -T_{\theta 5}$$

Using the same relationship, the equations of motion are transferred into the following forms:

$$A_{11}\ddot{\theta}_1 + A_{12}\ddot{\theta}_2 + A_{13}\ddot{\theta}_3 + A_{14}\ddot{\theta}_4 + A_{15}\ddot{\theta}_5 + h_{q0} + G_{q0} = 0$$

where

$$A_{1j} = D_{1j} + D_{2j} + D_{3j} - D_{4j} - D_{5j}$$
$$h_{q0} = h_1 + h_2 + h_3 - h_4 - h_5$$
$$G_{q0} = G_1 + G_2 + G_3 - G_4 - G_5$$

$$A_{21}\ddot{\theta}_1 + A_{22}\ddot{\theta}_2 + A_{23}\ddot{\theta}_3 + A_{24}\ddot{\theta}_4 + A_{25}\ddot{\theta}_5 + h_{q1} + G_{q1} = \tau_1$$
where
$A_{2j} = -D_{2j} - D_{3j} + D_{4j} + D_{5j}$
$h_{q1} = -h_2 - h_3 + h_4 + h_5$
$G_{q1} = -G_2 - G_3 + G_4 + G_5$

$$A_{31}\ddot{\theta}_1 + A_{32}\ddot{\theta}_2 + A_{33}\ddot{\theta}_3 + A_{34}\ddot{\theta}_4 + A_{35}\ddot{\theta}_5 + h_{q2} + G_{q2} = \tau_2$$
where
$A_{3j} = -D_{3j} + D_{4j} + D_{5j}$
$h_{q2} = -h_3 + h_4 + h_5$
$G_{q2} = -G_3 + G_4 + G_5$

$$A_{41}\ddot{\theta}_1 + A_{42}\ddot{\theta}_2 + A_{43}\ddot{\theta}_3 + A_{44}\ddot{\theta}_4 + A_{45}\ddot{\theta}_5 + h_{q3} + G_{q3} = \tau_3$$
where
$A_{4j} = D_{4j} + D_{5j}$
$h_{q3} = h_4 + h_5$
$G_{q3} = G_4 + G_5$

$$A_{51}\ddot{\theta}_1 + A_{52}\ddot{\theta}_2 + A_{53}\ddot{\theta}_3 + A_{54}\ddot{\theta}_4 + A_{55}\ddot{\theta}_5 + h_{q4} + G_{q4} = \tau_4$$
where
$A_{5j} = -D_{5j}$
$h_{q4} = -h_5$
$G_{q4} = -G_5$

Again, using the same relations, the equations of motion are finally transformed in terms of the relative angles, as follows:

$$\underline{D}_q(\underline{q})\ddot{\underline{q}} + \underline{h}_q(\underline{q},\dot{\underline{q}})\dot{\underline{q}} + \underline{G}_q(\underline{q}) = \underline{T}_q$$

where

$$\left.\begin{aligned} D_q(i,1) &= A_{i1} + A_{i2} + A_{i3} - A_{i4} - A_{i5} \\ D_q(i,2) &= -A_{i2} - A_{i3} + A_{i4} + A_{i5} \\ D_q(i,3) &= -A_{i3} + A_{i4} + A_{i5} \\ D_q(i,4) &= A_{i4} + A_{i5} \\ D_q(i,5) &= -A_{i5} \end{aligned}\right\} (i = 1,\ldots 5)$$

$$\underline{h}_q\dot{\underline{q}} = [h_{q0}, h_{q1}, h_{q2}, h_{q3}, h_{q4}]^T$$
$$\underline{G}_q = [G_{q0}, G_{q1}, G_{q2}, G_{q3}, G_{q4}]^T$$

and

$$\underline{T}_q = [\tau_0, \tau_1, \tau_2, \tau_3, \tau_4]^T$$

The $D_q(i,j)$ terms are formulated as follows:

$$
\begin{aligned}
D_q(1,1) = {} & [I_1 + m_1 d_1^{\,2} + (m_2 + m_3 + m_4 + m_5)\ell_1^{\,2}] + 2[m_2 \ell_1 d_2 + (m_3 + m_4 + m_5)\ell_1 \ell_2]\cos(q_1) \\
& + 2[m_3 \ell_1 d_3]\cos(q_1 + q_2) - 2[m_4 \ell_1 (\ell_4 - d_4) + m_5 \ell_1 \ell_4]\cos(q_1 + q_2 + q_3) \\
& - 2[m_5 \ell_1 (\ell_5 - d_5)]\cos(q_1 + q_2 + q_3 - q_4) + [I_2 + m_2 d_2^{\,2} + (m_3 + m_4 + m_5)\ell_2^{\,2}] \\
& + 2[m_3 \ell_2 d_3]\cos(q_2) - 2[m_4 \ell_2 (\ell_4 - d_4) + m_5 \ell_2 \ell_4]\cos(q_2 + q_3) \\
& - 2[m_5 \ell_2 (\ell_5 - d_5)]\cos(q_2 + q_3 - q_4) + [I_3 + m_3 d_3^{\,2}] + [I_4 + m_4 (\ell_4 - d_4)^2 + m_5 \ell_4^{\,2}] \\
& + 2[m_5 \ell_4 (\ell_5 - d_5)]\cos(q_4) + [I_5 + m_5 (\ell_5 - d_5)^2]
\end{aligned}
$$

$$
\begin{aligned}
D_q(1,2) = {} & -[m_2 \ell_1 d_2 + (m_3 + m_4 + m_5)\ell_1 \ell_2]\cos(q_1) - [I_2 + m_2 d_2^{\,2} + (m_3 + m_4 + m_5)\ell_2^{\,2}] \\
& - 2[m_3 \ell_2 d_3]\cos(q_2) + 2[m_4 \ell_2 (\ell_4 - d_4) + m_5 \ell_2 \ell_4]\cos(q_2 + q_3) \\
& + 2[m_5 \ell_2 (\ell_5 - d_5)]\cos(q_2 + q_3 - q_4) - [m_3 \ell_1 d_3]\cos(q_1 + q_2) \\
& - [I_3 + m_3 d_3^{\,2}] + [m_4 \ell_1 (\ell_4 - d_4) + m_5 \ell_1 \ell_4]\cos(q_1 + q_2 + q_3) \\
& - [I_4 + m_4 (\ell_4 - d_4)^2 + m_5 \ell_4^{\,2}] + [m_5 \ell_1 (\ell_5 - d_5)]\cos(q_1 + q_2 + q_3 - q_4) \\
& - 2[m_5 \ell_4 (\ell_5 - d_5)]\cos(q_4) - [I_5 + m_5 (\ell_5 - d_5)^2]
\end{aligned}
$$

$$
\begin{aligned}
D_q(1,3) = {} & -[m_1 \ell_1 d_3]\cos(q_1 + q_2) - [m_3 \ell_2 d_3]\cos(q_2) - [I_3 + m_3 d_3^{\,2}] \\
& + [m_4 \ell_1 (\ell_4 - d_4) + m_5 \ell_1 \ell_4]\cos(q_1 + q_2 + q_3) + [m_4 \ell_2 (\ell_4 - d_4) + m_5 \ell_2 \ell_4]\cos(q_2 + q_3) \\
& - [I_4 + m_4 (\ell_4 - d_4)^2 + m_5 \ell_4^{\,2}] - 2[m_5 \ell_4 (\ell_5 - d_5)]\cos(q_4) \\
& + [m_5 \ell_1 (\ell_5 - d_5)]\cos(q_1 + q_2 + q_3 - q_4) + [m_5 \ell_2 (\ell_5 - d_5)]\cos(q_2 + q_3 - q_4) \\
& - [I_5 + m_5 (\ell_5 - d_5)^2]
\end{aligned}
$$

$$
\begin{aligned}
D_q(1,4) = {} & [m_4 \ell_1 (\ell_4 - d_4) + m_5 \ell_1 \ell_4]\cos(q_1 + q_2 + q_3) \\
& + [m_4 \ell_2 (\ell_4 - d_4) + m_5 \ell_2 \ell_4]\cos(q_2 + q_3) \\
& - [I_4 + m_4 (\ell_4 - d_4)^2 + m_5 \ell_4^{\,2}] - 2[m_5 \ell_4 (\ell_5 - d_5)]\cos(q_4) \\
& + [m_5 \ell_1 (\ell_5 - d_5)]\cos(q_1 + q_2 + q_3 - q_4) + [m_5 \ell_2 (\ell_5 - d_5)]\cos(q_2 + q_3 - q_4) \\
& - [I_5 + m_5 (\ell_5 - d_5)^2]
\end{aligned}
$$

$$
\begin{aligned}
D_q(1,5) = {} & -[m_5 \ell_1 (\ell_5 - d_5)]\cos(q_1 + q_2 + q_3 - q_4) - [m_5 \ell_2 (\ell_5 - d_5)]\cos(q_2 + q_3 - q_4) \\
& + [m_5 \ell_4 (\ell_5 - d_5)]\cos(q_4) + [I_5 + m_5 (\ell_5 - d_5)^2]
\end{aligned}
$$

$$D_q(2,1) = D_q(1,2)$$

$$
\begin{aligned}
D_q(2,2) = {} & [I_2 + m_2 d_2^{\,2} + (m_3 + m_4 + m_5)\ell_2^{\,2}] + 2[m_3 \ell_2 d_3]\cos(q_2) \\
& - 2[m_4 \ell_2 (\ell_4 - d_4) + m_5 \ell_2 \ell_4]\cos(q_2 + q_3) - 2[m_5 \ell_2 (\ell_5 - d_5)]\cos(q_2 + q_3 - q_4) \\
& + [I_3 + m_3 d_3^{\,2}] + [I_4 + m_4 (\ell_4 - d_4)^2 + m_5 \ell_4^{\,2}] \\
& + 2[m_5 \ell_4 (\ell_5 - d_5)]\cos(q_4) + [I_5 + m_5 (\ell_5 - d_5)^2]
\end{aligned}
$$

$$
\begin{aligned}
D_q(2,3) = {} & [m_3 \ell_2 d_3]\cos(q_2) + [I_3 + m_3 d_3^{\,2}] - [m_4 \ell_2 (\ell_4 - d_4) + m_5 \ell_2 \ell_4]\cos(q_2 + q_3) \\
& + [I_4 + m_4 (\ell_4 - d_4)^2 + m_5 \ell_4^{\,2}] + 2[m_5 \ell_4 (\ell_5 - d_5)]\cos(q_4) \\
& - [m_5 \ell_2 (\ell_5 - d_5)]\cos(q_2 + q_3 - q_4) + [I_5 + m_5 (\ell_5 - d_5)^2]
\end{aligned}
$$

$$D_q(2,4) = -[m_4\ell_2(\ell_4 - d_4) + m_5\ell_2\ell_4]\cos(q_2 + q_3)$$
$$+ [I_4 + m_4(\ell_4 - d_4)^2 + m_5\ell_4^2] + 2[m_5\ell_4(\ell_5 - d_5)]\cos(q_4)$$
$$- [m_5\ell_2(\ell_5 - d_5)]\cos(q_2 + q_3 - q_4) + [I_5 + m_5(\ell_5 - d_5)^2]$$

$$D_q(2,5) = [m_5\ell_2(\ell_5 - d_5)]\cos(q_2 + q_3 - q_4) - [m_5\ell_4(\ell_5 - d_5)]\cos(q_4)$$
$$- [I_5 + m_5(\ell_5 - d_5)^2]$$

$$D_q(3,1) = D_q(1,3)$$
$$D_q(3,2) = D_q(2,3)$$
$$D_q(3,3) = +[I_3 + m_3 d_3^2] + [I_4 + m_4(\ell_4 - d_4)^2 + m_5\ell_4^2]$$
$$+ 2[m_5\ell_4(\ell_5 - d_5)]\cos(q_4) + [I_5 + m_5(\ell_5 - d_5)^2]$$
$$D_q(3,4) = D_q(3,3)$$
$$D_q(3,5) = -[m_5\ell_4(\ell_5 - d_5)]\cos(q_4) - [I_5 + m_5(\ell_5 - d_5)^2]$$

$$D_q(4,1) = D_q(1,4)$$
$$D_q(4,2) = D_q(2,4)$$
$$D_q(4,3) = D_q(4,4) = D_q(3,4)$$
$$D_q(4,5) = D_q(3,5)$$

$$D_q(5,1) = D_q(1,5)$$
$$D_q(5,2) = D_q(2,5)$$
$$D_q(5,3) = D_q(5,4) = D_q(3,5)$$
$$D_q(5,5) = [I_5 + m_5(\ell_5 - d_5)^2]$$

Appendix III

Derivation of the Five-Link Biped Dynamic Model with Both Legs in the Air

The equations of motion for the impact phase are derived by applying the Lagrangian formulation using the dynamic model with both legs in the air. The Lagranian equation of motion is in the form:

$$\frac{d}{dt}\left\{\frac{\partial K}{\partial \dot{\theta}_{ai}}\right\} - \frac{\partial K}{\partial \theta_{ai}} + \frac{\partial P}{\partial \theta_{ai}} = T_{ai}$$

where $\theta_a = [\theta_1\ \theta_2\ \theta_3\ \theta_4\ \theta_5\ x_b\ y_b]$

Each term in this equation is derived as follows:

$$\begin{aligned}
\frac{d}{dt}\left(\frac{\partial K}{\partial \dot{\theta}_1}\right) &= [I_1 + m_1 d_1^{\,2} + m_2 \ell_1^{\,2} + m_3 \ell_1^{\,2} + m_4 \ell_1^{\,2} + m_5 \ell_1^{\,2}]\ddot{\theta}_1 \\
&+ [m_2 \ell_1 d_2 + m_3 \ell_1 \ell_2 + m_4 \ell_1 \ell_2 + m_5 \ell_1 \ell_2]\cos(\theta_1 - \theta_2)\ddot{\theta}_2 \\
&+ [m_3 \ell_1 d_3]\cos(\theta_1 - \theta_3)\ddot{\theta}_3 \\
&+ [m_4 \ell_1 (\ell_4 - d_4) + m_5 \ell_1 \ell_4]\cos(\theta_1 + \theta_4)\ddot{\theta}_4 \\
&+ [m_5 \ell_1 (\ell_5 - d_5)]\cos(\theta_1 + \theta_5)\ddot{\theta}_5 \\
&- [m_2 \ell_1 d_2 + m_3 \ell_1 \ell_2 + m_4 \ell_1 \ell_2 + m_5 \ell_1 \ell_2]\sin(\theta_1 - \theta_2)\dot{\theta}_1\dot{\theta}_2 \\
&+ [m_2 \ell_1 d_2 + m_3 \ell_1 \ell_2 + m_4 \ell_1 \ell_2 + m_5 \ell_1 \ell_2]\sin(\theta_1 - \theta_2)\dot{\theta}_2^{\,2} \\
&- [m_3 \ell_1 d_3]\sin(\theta_1 - \theta_3)\dot{\theta}_1\dot{\theta}_3 \\
&+ [m_3 \ell_1 d_3]\sin(\theta_1 - \theta_3)\dot{\theta}_3^{\,2} \\
&- [m_4 \ell_1 (\ell_4 - d_4) + m_5 \ell_1 \ell_4]\sin(\theta_1 + \theta_4)\dot{\theta}_1\dot{\theta}_4 \\
&- [m_4 \ell_1 (\ell_4 - d_4) + m_5 \ell_1 \ell_4]\sin(\theta_1 + \theta_4)\dot{\theta}_4^{\,2} \\
&- [m_5 \ell_1 (\ell_5 - d_5)]\sin(\theta_1 + \theta_5)\dot{\theta}_1\dot{\theta}_5 \\
&- [m_5 \ell_1 (\ell_5 - d_5)]\sin(\theta_1 + \theta_5)\dot{\theta}_5^{\,2} \\
&+ m_1 d_1 (\ddot{x}_b \cos\theta_1 - \ddot{y}_b \sin\theta_1 - \dot{x}_b \sin\theta_1\dot{\theta}_1 - \dot{y}_b \cos\theta_1\dot{\theta}_1) \\
&+ (m_2 + m_3 + m_4 + m_5)\ell_1 (\ddot{x}_b \cos\theta_1 - \ddot{y}_b \sin\theta_1 - \dot{x}_b \sin\theta_1\dot{\theta}_1 - \dot{y}_b \cos\theta_1\dot{\theta}_1)
\end{aligned}$$

$$\frac{d}{dt}\left(\frac{\partial K}{\partial \dot{\theta}_2}\right) = [I_2 + m_2 d_2^{\,2} + m_3 \ell_2^{\,2} + m_4 \ell_2^{\,2} + m_5 \ell_2^{\,2}]\ddot{\theta}_2$$
$$+[m_2 \ell_1 d_2 + m_3 \ell_1 \ell_2 + m_4 \ell_1 \ell_2 + m_5 \ell_1 \ell_2]\cos(\theta_1 - \theta_2)\ddot{\theta}_1$$
$$+[m_3 \ell_2 d_3]\cos(\theta_2 - \theta_3)\ddot{\theta}_3$$
$$+[m_4 \ell_2 (\ell_4 - d_4) + m_5 \ell_2 \ell_4]\cos(\theta_2 + \theta_4)\ddot{\theta}_4$$
$$+[m_5 \ell_2 (\ell_5 - d_5)]\cos(\theta_2 + \theta_5)\ddot{\theta}_5$$
$$+[m_2 \ell_1 d_2 + m_3 \ell_1 \ell_2 + m_4 \ell_1 \ell_2 + m_5 \ell_1 \ell_2]\sin(\theta_1 - \theta_2)\dot{\theta}_1\dot{\theta}_2$$
$$-[m_2 \ell_1 d_2 + m_3 \ell_1 \ell_2 + m_4 \ell_1 \ell_2 + m_5 \ell_1 \ell_2]\sin(\theta_1 - \theta_2)\dot{\theta}_2^{\,2}$$
$$-[m_3 \ell_2 d_3]\sin(\theta_2 - \theta_3)\dot{\theta}_2\dot{\theta}_3$$
$$+[m_3 \ell_2 d_3]\sin(\theta_2 - \theta_3)\dot{\theta}_3^{\,2}$$
$$-[m_4 \ell_2 (\ell_4 - d_4) + m_5 \ell_2 \ell_4]\sin(\theta_2 + \theta_4)\dot{\theta}_2\dot{\theta}_4$$
$$-[m_4 \ell_2 (\ell_4 - d_4) + m_5 \ell_2 \ell_4]\sin(\theta_2 + \theta_4)\dot{\theta}_4^{\,2}$$
$$-[m_5 \ell_2 (\ell_5 - d_5)]\sin(\theta_2 + \theta_5)\dot{\theta}_2\dot{\theta}_5$$
$$-[m_5 \ell_2 (\ell_5 - d_5)]\sin(\theta_2 + \theta_5)\dot{\theta}_5^{\,2}$$
$$+ m_2 d_2(\ddot{x}_b \cos\theta_2 - \ddot{y}_b \sin\theta_2 - \dot{x}_b \sin\theta_2\dot{\theta}_2 - \dot{y}_b \cos\theta_2\dot{\theta}_2)$$
$$+ (m_3 + m_4 + m_5)\ell_2(\ddot{x}_b \cos\theta_2 - \ddot{y}_b \sin\theta_2 - \dot{x}_b \sin\theta_2\dot{\theta}_2 - \dot{y}_b \cos\theta_2\dot{\theta}_2)$$

$$\frac{d}{dt}\left(\frac{\partial K}{\partial \dot{\theta}_3}\right) = [I_3 + m_3 d_3^{\,2}]\ddot{\theta}_3$$
$$+[m_3 \ell_1 d_3]\cos(\theta_1 - \theta_3)\ddot{\theta}_1$$
$$+[m_3 \ell_2 d_3]\cos(\theta_2 - \theta_3)\ddot{\theta}_2$$
$$+[m_3 \ell_1 d_3]\sin(\theta_1 - \theta_3)\dot{\theta}_1\dot{\theta}_3$$
$$-[m_3 \ell_1 d_3]\sin(\theta_1 - \theta_3)\dot{\theta}_1^{\,2}$$
$$+[m_3 \ell_2 d_3]\sin(\theta_2 - \theta_3)\dot{\theta}_2\dot{\theta}_3$$
$$-[m_3 \ell_2 d_3]\sin(\theta_2 - \theta_3)\dot{\theta}_2^{\,2}$$
$$+ m_3 d_3(\ddot{x}_b \cos\theta_3 - \ddot{y}_b \sin\theta_3 - \dot{x}_b \sin\theta_3\dot{\theta}_3 - \dot{y}_b \cos\theta_3\dot{\theta}_3$$

$$\frac{d}{dt}\left(\frac{\partial K}{\partial \dot{\theta}_4}\right) = [I_4 + m_4(\ell_4 - d_4)^2 + m_5 \ell_4^{\,2}]\ddot{\theta}_4$$
$$+[m_4 \ell_1 (\ell_4 - d_4) + m_5 \ell_1 \ell_4]\cos(\theta_1 + \theta_4)\ddot{\theta}_1$$
$$+[m_4 \ell_2 (\ell_4 - d_4) + m_5 \ell_2 \ell_4]\cos(\theta_2 + \theta_4)\ddot{\theta}_2$$
$$+[m_5 \ell_4 (\ell_5 - d_5)]\cos(\theta_4 - \theta_5)\ddot{\theta}_5$$
$$-[m_4 \ell_1 (\ell_4 - d_4) + m_5 \ell_1 \ell_4]\sin(\theta_1 + \theta_4)\dot{\theta}_1\dot{\theta}_4$$
$$-[m_4 \ell_1 (\ell_4 - d_4) + m_5 \ell_1 \ell_4]\sin(\theta_1 + \theta_4)\dot{\theta}_1^{\,2}$$
$$-[m_4 \ell_2 (\ell_4 - d_4) + m_5 \ell_2 \ell_4]\sin(\theta_2 + \theta_4)\dot{\theta}_2\dot{\theta}_4$$
$$-[m_4 \ell_2 (\ell_4 - d_4) + m_5 \ell_2 \ell_4]\sin(\theta_2 + \theta_4)\dot{\theta}_2^{\,2}$$
$$-[m_5 \ell_4 (\ell_5 - d_5)]\sin(\theta_4 - \theta_5)\dot{\theta}_4\dot{\theta}_5$$
$$+[m_5 \ell_4 (\ell_5 - d_5)]\sin(\theta_4 - \theta_5)\dot{\theta}_5^{\,2}$$
$$+ m_4(\ell_4 - d_4)(\ddot{x}_b \cos\theta_4 + \ddot{y}_b \sin\theta_4 - \dot{x}_b \sin\theta_4\dot{\theta}_4 + \dot{y}_b \cos\theta_4\dot{\theta}_4)$$
$$+ m_5 \ell_4(\ddot{x}_b \cos\theta_4 + \ddot{y}_b \sin\theta_4 - \dot{x}_b \sin\theta_4\dot{\theta}_4 + \dot{y}_b \cos\theta_4\dot{\theta}_4)$$

$$\frac{d}{dt}\left(\frac{\partial K}{\partial \dot{\theta}_5}\right) = [I_5 + m_5(\ell_5 - d_5)^2]\ddot{\theta}_5$$
$$+[m_5\ell_1(\ell_5 - d_5)]\cos(\theta_1 + \theta_5)\ddot{\theta}_1$$
$$+[m_5\ell_2(\ell_5 - d_5)]\cos(\theta_2 + \theta_5)\ddot{\theta}_2$$
$$+[m_5\ell_4(\ell_5 - d_5)]\cos(\theta_4 - \theta_5)\ddot{\theta}_4$$
$$-[m_5\ell_1(\ell_5 - d_5)]\sin(\theta_1 + \theta_5)\dot{\theta}_1\dot{\theta}_5$$
$$-[m_5\ell_1(\ell_5 - d_5)]\sin(\theta_1 + \theta_5)\dot{\theta}_1^2$$
$$-[m_5\ell_2(\ell_5 - d_5)]\sin(\theta_2 + \theta_5)\dot{\theta}_2\dot{\theta}_5$$
$$-[m_5\ell_2(\ell_5 - d_5)]\sin(\theta_2 + \theta_5)\dot{\theta}_2^2$$
$$+[m_5\ell_4(\ell_5 - d_5)]\sin(\theta_4 - \theta_5)\dot{\theta}_4\dot{\theta}_5$$
$$-[m_5\ell_4(\ell_5 - d_5)]\sin(\theta_4 - \theta_5)\dot{\theta}_4^2$$
$$+m_5(\ell_5 - d_5)(\ddot{x}_b\cos\theta_5 + \ddot{y}_b\sin\theta_5 - \dot{x}_b\sin\theta_5\dot{\theta}_5 + \dot{y}_b\cos\theta_5\dot{\theta}_5)$$

$$\frac{\partial K}{\partial \theta_1} = -[m_2\ell_1 d_2 + m_3\ell_1\ell_2 + m_4\ell_1\ell_2 + m_5\ell_1\ell_2]\sin(\theta_1 - \theta_2)\dot{\theta}_1\dot{\theta}_2$$
$$-[m_3\ell_1 d_3]\sin(\theta_1 - \theta_3)\dot{\theta}_1\dot{\theta}_3 - [m_4\ell_1(\ell_4 - d_4) + m_5\ell_1\ell_4]\sin(\theta_1 + \theta_4)\dot{\theta}_1\dot{\theta}_4$$
$$-[m_5\ell_1(\ell_5 - d_5)]\sin(\theta_1 + \theta_5)\dot{\theta}_1\dot{\theta}_5 + m_1 d_1\dot{\theta}_1(-\dot{x}_b\sin\theta_1 - \dot{y}_b\cos\theta_1)$$
$$+(m_2 + m_3 + m_4 + m_5)\ell_1\dot{\theta}_1(-\dot{x}_b\sin\theta_1 - \dot{y}_b\cos\theta_1)$$

$$\frac{\partial K}{\partial \theta_2} = -[m_2\ell_1 d_2 + m_3\ell_1\ell_2 + m_4\ell_1\ell_2 + m_5\ell_1\ell_2]\sin(\theta_1 - \theta_2)\dot{\theta}_1\dot{\theta}_2$$
$$-[m_3\ell_2 d_3]\sin(\theta_2 - \theta_3)\dot{\theta}_2\dot{\theta}_3 - [m_4\ell_2(\ell_4 - d_4) + m_5\ell_2\ell_4]\sin(\theta_2 + \theta_4)\dot{\theta}_2\dot{\theta}_4$$
$$-[m_5\ell_2(\ell_5 - d_5)]\sin(\theta_2 + \theta_5)\dot{\theta}_2\dot{\theta}_5 + m_2 d_2\dot{\theta}_2(-\dot{x}_b\sin\theta_2 - \dot{y}_b\cos\theta_2)$$
$$+(m_3 + m_4 + m_5)\ell_2\dot{\theta}_2(-\dot{x}_b\sin\theta_2 - \dot{y}_b\cos\theta_2)$$

$$\frac{\partial K}{\partial \theta_3} = -[m_3\ell_1 d_3]\sin(\theta_1 - \theta_3)\dot{\theta}_1\dot{\theta}_3 + [m_3\ell_2 d_3]\sin(\theta_2 - \theta_3)\dot{\theta}_2\dot{\theta}_3$$
$$+m_3 d_3\dot{\theta}_3(-\dot{x}_b\sin\theta_3 - \dot{y}_b\cos\theta_3)$$

$$\frac{\partial K}{\partial \theta_4} = -[m_4\ell_1(\ell_4 - d_4) + m_5\ell_1\ell_4]\sin(\theta_1 + \theta_4)\dot{\theta}_1\dot{\theta}_4$$
$$-[m_4\ell_2(\ell_4 - d_4) + m_5\ell_2\ell_4]\sin(\theta_2 + \theta_4)\dot{\theta}_2\dot{\theta}_4$$
$$-[m_5\ell_4(\ell_5 - d_5)]\sin(\theta_4 - \theta_5)\dot{\theta}_4\dot{\theta}_5$$
$$+m_4(\ell_4 - d_4)\dot{\theta}_4(-\dot{x}_b\sin\theta_4 + \dot{y}_b\cos\theta_4)$$
$$+m_5\ell_4\dot{\theta}_4(-\dot{x}_b\sin\theta_4 + \dot{y}_b\cos\theta_4)$$

$$\frac{\partial K}{\partial \theta_5} = -[m_5\ell_1(\ell_5 - d_5)]\sin(\theta_1 + \theta_5)\dot{\theta}_1\dot{\theta}_5$$
$$-[m_5\ell_2(\ell_5 - d_5)]\sin(\theta_2 + \theta_5)\dot{\theta}_2\dot{\theta}_5$$
$$+[m_5\ell_4(\ell_5 - d_5)]\sin(\theta_4 - \theta_5)\dot{\theta}_4\dot{\theta}_5$$
$$+m_5(\ell_5 - d_5)\dot{\theta}_5(-\dot{x}_b\sin\theta_5 + \dot{y}_b\cos\theta_5)$$

$$\frac{d}{dt}\left(\frac{\partial K}{\partial \dot{x}_b}\right) = (m_1 + m_2 + m_3 + m_4 + m_5)\ddot{x}_b$$
$$+ m_1 d_1 \ddot{\theta}_1 \cos\theta_1 - m_1 d_1 \dot{\theta}_1^{\,2} \sin\theta_1$$
$$+ (m_2 + m_3 + m_4 + m_5)\ell_1 \ddot{\theta}_1 \cos\theta_1$$
$$- (m_2 + m_3 + m_4 + m_5)\ell_1 \dot{\theta}_1^{\,2} \sin\theta_1$$
$$+ m_2 d_2 \ddot{\theta}_2 \cos\theta_2 - m_2 d_2 \dot{\theta}_2^{\,2} \sin\theta_2$$
$$+ (m_3 + m_4 + m_5)\ell_2 \ddot{\theta}_2 \cos\theta_2$$
$$- (m_3 + m_4 + m_5)\ell_2 \dot{\theta}_2^{\,2} \sin\theta_2$$
$$+ m_3 d_3 \ddot{\theta}_3 \cos\theta_3 - m_3 d_3 \dot{\theta}_3^{\,2} \sin\theta_3$$
$$+ m_4(\ell_4 - d_4)\ddot{\theta}_4 \cos\theta_4 - m_4(\ell_4 - d_4)\dot{\theta}_4^{\,2} \sin\theta_4$$
$$+ m_5 \ell_4 \ddot{\theta}_4 \cos\theta_4 - m_5 \ell_4 \dot{\theta}_4^{\,2} \sin\theta_4$$
$$+ m_5(\ell_5 - d_5)\ddot{\theta}_5 \cos\theta_5 - m_5(\ell_5 - d_5)\dot{\theta}_5^{\,2} \sin\theta_5$$

$$\frac{d}{dt}\left(\frac{\partial K}{\partial \dot{y}_b}\right) = (m_1 + m_2 + m_3 + m_4 + m_5)\ddot{y}_b$$
$$- m_1 d_1 \ddot{\theta}_1 \sin\theta_1 - m_1 d_1 \dot{\theta}_1^{\,2} \cos\theta_1$$
$$- (m_2 + m_3 + m_4 + m_5)\ell_1 \ddot{\theta}_1 \sin\theta_1$$
$$- (m_2 + m_3 + m_4 + m_5)\ell_1 \dot{\theta}_1^{\,2} \cos\theta_1$$
$$- m_2 d_2 \ddot{\theta}_2 \sin\theta_2 - m_2 d_2 \dot{\theta}_2^{\,2} \cos\theta_2$$
$$- (m_3 + m_4 + m_5)\ell_2 \ddot{\theta}_2 \sin\theta_2$$
$$- (m_3 + m_4 + m_5)\ell_2 \dot{\theta}_2^{\,2} \cos\theta_2$$
$$- m_3 d_3 \ddot{\theta}_3 \sin\theta_3 - m_3 d_3 \dot{\theta}_3^{\,2} \cos\theta_3$$
$$+ m_4(\ell_4 - d_4)\ddot{\theta}_4 \sin\theta_4 + m_4(\ell_4 - d_4)\dot{\theta}_4^{\,2} \cos\theta_4$$
$$+ m_5 \ell_4 \ddot{\theta}_4 \sin\theta_4 + m_5 \ell_4 \dot{\theta}_4^{\,2} \cos\theta_4$$
$$+ m_5(\ell_5 - d_5)\ddot{\theta}_5 \sin\theta_5 + m_5(\ell_5 - d_5)\dot{\theta}_5^{\,2} \cos\theta_5$$

$$\frac{\partial K}{\partial x_b} = 0 \qquad \frac{\partial K}{\partial y_b} = 0$$

$$\frac{\partial P}{\partial \theta_1} = -[m_1 d_1 + m_2 \ell_1 + m_3 \ell_1 + m_4 \ell_1 + m_5 \ell_1] g \sin\theta_1$$
$$\frac{\partial P}{\partial \theta_2} = -[m_2 d_2 + m_3 \ell_2 + m_4 \ell_2 + m_5 \ell_2] g \sin\theta_2$$
$$\frac{\partial P}{\partial \theta_3} = -[m_3 d_3] g \sin\theta_3$$
$$\frac{\partial P}{\partial \theta_4} = [m_4(\ell_4 - d_4) + m_5 \ell_4] g \sin\theta_4$$
$$\frac{\partial P}{\partial \theta_5} = [m_5(\ell_5 - d_5)] g \sin\theta_5$$
$$\frac{\partial P}{\partial x_b} = 0$$
$$\frac{\partial P}{\partial y_b} = (m_1 + m_2 + m_3 + m_4 + m_5) g$$

Appendix IV

Derivation of Constant Mechanical Energy of the Five-Link Biped Robot

The mechanical energy (V) of the five-link biped robot comprises translational kinetic energy, rotational energy, and potential energy ($V = K + P$). In order to derive a equation representing constant mechanical energy at an instant in time, we have to set

$$\dot{V} = 0$$

where $\dot{V}$ is the time derivative of the mechanical energy

Therefore,

$$\dot{V} = \frac{dV}{dt} = \frac{\partial V}{\partial x_i}\dot{x}_i$$

where

$$x_i = [q_0, q_1, q_2, q_3, q_4, \dot{q}_0, \dot{q}_1, \dot{q}_2, \dot{q}_3, \dot{q}_4]$$

Each term in the above equation is derived as follows:

$$\begin{aligned}\frac{\partial V}{\partial q_0} &= -a_1\sin(q_0) - a_2\sin(q_0 - q_1) - a_3\sin(q_0 - q_1 - q_2) \\ &\quad - a_4\sin(-q_0 + q_1 + q_2 + q_3) - a_5\sin(-q_0 + q_1 + q_2 + q_3 - q_4)\end{aligned}$$

$$\begin{aligned}\frac{\partial V}{\partial q_1} &= a_2\sin(q_0 - q_1) + a_3\sin(q_0 - q_1 - q_2) + a_4\sin(-q_0 + q_1 + q_2 + q_3) \\ &\quad + a_5\sin(-q_0 + q_1 + q_2 + q_3 - q_4) \\ &\quad - b_1\sin(q_1)(\dot{q}_0^{\,2} - \dot{q}_0\dot{q}_1) - b_2\sin(q_1 + q_2)(\dot{q}_0^{\,2} - \dot{q}_0\dot{q}_1 - \dot{q}_0\dot{q}_2) \\ &\quad - b_3\sin(q_1 + q_2 + q_3)(-\dot{q}_0^{\,2} + \dot{q}_0\dot{q}_1 + \dot{q}_0\dot{q}_2 + \dot{q}_0\dot{q}_3) \\ &\quad - b_4\sin(q_1 + q_2 + q_3 - q_4)(-\dot{q}_0^{\,2} + \dot{q}_0\dot{q}_1 + \dot{q}_0\dot{q}_2 + \dot{q}_0\dot{q}_3 - \dot{q}_0\dot{q}_4)\end{aligned}$$

$$\begin{aligned}\frac{\partial V}{\partial q_2} &= a_3\sin(q_0 - q_1 - q_2) + a_4\sin(-q_0 + q_1 + q_2 + q_3) + a_5\sin(-q_0 + q_1 + q_2 + q_3 - q_4) \\ &\quad - b_2\sin(q_1 + q_2)(\dot{q}_0^{\,2} - \dot{q}_0\dot{q}_1 - \dot{q}_0\dot{q}_2) - b_5\sin(q_2)(\dot{q}_0^{\,2} - 2\dot{q}_0\dot{q}_1 - \dot{q}_0\dot{q}_2 + \dot{q}_1^{\,2} + \dot{q}_1\dot{q}_2) \\ &\quad - b_3\sin(q_1 + q_2 + q_3)(-\dot{q}_0^{\,2} + \dot{q}_0\dot{q}_1 + \dot{q}_0\dot{q}_2 + \dot{q}_0\dot{q}_3) \\ &\quad - b_6\sin(q_2 + q_3)(-\dot{q}_0^{\,2} + 2\dot{q}_0\dot{q}_1 + \dot{q}_0\dot{q}_2 + \dot{q}_0\dot{q}_3 - \dot{q}_1^{\,2} - \dot{q}_1\dot{q}_2 - \dot{q}_1\dot{q}_3) \\ &\quad - b_4\sin(q_1 + q_2 + q_3 - q_4)(-\dot{q}_0^{\,2} + \dot{q}_0\dot{q}_1 + \dot{q}_0\dot{q}_2 + \dot{q}_0\dot{q}_3 - \dot{q}_0\dot{q}_4) \\ &\quad - b_7\sin(q_2 + q_3 - q_4)(-\dot{q}_0^{\,2} + 2\dot{q}_0\dot{q}_1 + \dot{q}_0\dot{q}_2 + \dot{q}_0\dot{q}_3 - \dot{q}_0\dot{q}_4 - \dot{q}_1^{\,2} - \dot{q}_1\dot{q}_2 - \dot{q}_1\dot{q}_3 + \dot{q}_1\dot{q}_4)\end{aligned}$$

$$\frac{\partial V}{\partial q_3} = a_4 \sin(-q_0 + q_1 + q_2 + q_3) + a_5 \sin(-q_0 + q_1 + q_2 + q_3 - q_4)$$
$$- b_3 \sin(q_1 + q_2 + q_3)(-\dot{q}_0^{\,2} + \dot{q}_0\dot{q}_1 + \dot{q}_0\dot{q}_2 + \dot{q}_0\dot{q}_3)$$
$$- b_6 \sin(q_2 + q_3)(-\dot{q}_0^{\,2} + 2\dot{q}_0\dot{q}_1 + \dot{q}_0\dot{q}_2 + \dot{q}_0\dot{q}_3 - \dot{q}_1^{\,2} - \dot{q}_1\dot{q}_2 - \dot{q}_1\dot{q}_3)$$
$$- b_4 \sin(q_1 + q_2 + q_3 - q_4)(-\dot{q}_0^{\,2} + \dot{q}_0\dot{q}_1 + \dot{q}_0\dot{q}_2 + \dot{q}_0\dot{q}_3 - \dot{q}_0\dot{q}_4)$$
$$- b_7 \sin(q_2 + q_3 - q_4)(-\dot{q}_0^{\,2} + 2\dot{q}_0\dot{q}_1 + \dot{q}_0\dot{q}_2 + \dot{q}_0\dot{q}_3 - \dot{q}_0\dot{q}_4 - \dot{q}_1^{\,2} - \dot{q}_1\dot{q}_2 - \dot{q}_1\dot{q}_3 + \dot{q}_1\dot{q}_4)$$

$$\frac{\partial V}{\partial q_4} = -a_5 \sin(-q_0 + q_1 + q_2 + q_3 - q_4)$$
$$+ b_4 \sin(q_1 + q_2 + q_3 - q_4)(-\dot{q}_0^{\,2} + \dot{q}_0\dot{q}_1 + \dot{q}_0\dot{q}_2 + \dot{q}_0\dot{q}_3 - \dot{q}_0\dot{q}_4)$$
$$+ b_7 \sin(q_2 + q_3 - q_4)(-\dot{q}_0^{\,2} + 2\dot{q}_0\dot{q}_1 + \dot{q}_0\dot{q}_2 + \dot{q}_0\dot{q}_3 - \dot{q}_0\dot{q}_4 - \dot{q}_1^{\,2} - \dot{q}_1\dot{q}_2 - \dot{q}_1\dot{q}_3 + \dot{q}_1\dot{q}_4)$$
$$- b_8 \sin(q_4)(\dot{q}_0^{\,2} - 2\dot{q}_0\dot{q}_1 - 2\dot{q}_0\dot{q}_2 - 2\dot{q}_0\dot{q}_3 + \dot{q}_0\dot{q}_4 + \dot{q}_1^{\,2} + 2\dot{q}_1\dot{q}_2 + 2\dot{q}_1\dot{q}_3 - \dot{q}_1\dot{q}_4$$
$$+ \dot{q}_2^{\,2} + 2\dot{q}_2\dot{q}_3 - \dot{q}_2\dot{q}_4 + \dot{q}_3^{\,2} - \dot{q}_3\dot{q}_4)$$

$$\frac{\partial V}{\partial \dot{q}_0} = c_1\dot{q}_0 + c_2(\dot{q}_0 - \dot{q}_1) + c_3(\dot{q}_0 - \dot{q}_1 - \dot{q}_2) - c_4(-\dot{q}_0 + \dot{q}_1 + \dot{q}_2 + \dot{q}_3) - c_5(-\dot{q}_0 + \dot{q}_1 + \dot{q}_2 + \dot{q}_3 - \dot{q}_4)$$
$$+ c_6\dot{q}_0 + c_7(\dot{q}_0 - \dot{q}_1) - c_8(-\dot{q}_0 + \dot{q}_1 + \dot{q}_2 + \dot{q}_3)$$
$$+ b_1 \cos(q_1)(2\dot{q}_0 - \dot{q}_1) + b_2 \cos(q_1 + q_2)(2\dot{q}_0 - \dot{q}_1 - \dot{q}_2) + b_5 \cos(q_2)(2\dot{q}_0 - 2\dot{q}_1 - \dot{q}_2)$$
$$+ b_3 \cos(q_1 + q_2 + q_3)(-2\dot{q}_0 + \dot{q}_1 + \dot{q}_2 + \dot{q}_3) + b_6 \cos(q_2 + q_3)(-2\dot{q}_0 + 2\dot{q}_1 + \dot{q}_2 + \dot{q}_3)$$
$$+ b_4 \cos(q_1 + q_2 + q_3 - q_4)(-2\dot{q}_0 + \dot{q}_1 + \dot{q}_2 + \dot{q}_3 - \dot{q}_4)$$
$$+ b_7 \cos(q_2 + q_3 - q_4)(-2\dot{q}_0 + 2\dot{q}_1 + \dot{q}_2 + \dot{q}_3 - \dot{q}_4) + b_8 \cos(q_4)(2\dot{q}_0 - 2\dot{q}_1 - 2\dot{q}_2 - 2\dot{q}_3 + \dot{q}_4)$$

$$\frac{\partial V}{\partial \dot{q}_1} = -c_2(\dot{q}_0 - \dot{q}_1) - c_3(\dot{q}_0 - \dot{q}_1 - \dot{q}_2) + c_4(-\dot{q}_0 + \dot{q}_1 + \dot{q}_2 + \dot{q}_3) + c_5(-\dot{q}_0 + \dot{q}_1 + \dot{q}_2 + \dot{q}_3 - \dot{q}_4)$$
$$- c_7(\dot{q}_0 - \dot{q}_1) + c_8(-\dot{q}_0 + \dot{q}_1 + \dot{q}_2 + \dot{q}_3)$$
$$- b_1 \cos(q_1)(\dot{q}_0) + b_2 \cos(q_1 + q_2)(\dot{q}_0) + b_5 \cos(q_2)(-2\dot{q}_0 + 2\dot{q}_1 + \dot{q}_2)$$
$$+ b_3 \cos(q_1 + q_2 + q_3)(\dot{q}_0) + b_6 \cos(q_2 + q_3)(2\dot{q}_0 - 2\dot{q}_1 - \dot{q}_2 - \dot{q}_3)$$
$$+ b_4 \cos(q_1 + q_2 + q_3 - q_4)(\dot{q}_0) + b_7 \cos(q_2 + q_3 - q_4)(2\dot{q}_0 - 2\dot{q}_1 - \dot{q}_2 - \dot{q}_3 + \dot{q}_4)$$
$$+ b_8 \cos(q_4)(-2\dot{q}_0 + 2\dot{q}_1 + 2\dot{q}_2 + 2\dot{q}_3 - \dot{q}_4)$$

$$\frac{\partial V}{\partial \dot{q}_2} = -c_3(\dot{q}_0 - \dot{q}_1 - \dot{q}_2) + c_4(-\dot{q}_0 + \dot{q}_1 + \dot{q}_2 + \dot{q}_3) + c_5(-\dot{q}_0 + \dot{q}_1 + \dot{q}_2 + \dot{q}_3 - \dot{q}_4)$$
$$+ c_8(-\dot{q}_0 + \dot{q}_1 + \dot{q}_2 + \dot{q}_3)$$
$$- b_2 \cos(q_1 + q_2)(\dot{q}_0) - b_5 \cos(q_2)(\dot{q}_0) + b_3 \cos(q_1 + q_2 + q_3)(\dot{q}_0) + b_6 \cos(q_2 + q_3)(\dot{q}_0 - \dot{q}_1)$$
$$+ b_4 \cos(q_1 + q_2 + q_3 - q_4)(\dot{q}_0) + b_7 \cos(q_2 + q_3 - q_4)(\dot{q}_0 - \dot{q}_1)$$
$$+ b_8 \cos(q_4)(-2\dot{q}_0 + 2\dot{q}_1 + 2\dot{q}_2 + 2\dot{q}_3 - \dot{q}_4)$$

$$\frac{\partial V}{\partial \dot{q}_3} = c_4(-\dot{q}_0 + \dot{q}_1 + \dot{q}_2 + \dot{q}_3) + c_5(-\dot{q}_0 + \dot{q}_1 + \dot{q}_2 + \dot{q}_3 - \dot{q}_4) + c_8(-\dot{q}_0 + \dot{q}_1 + \dot{q}_2 + \dot{q}_3)$$
$$+ b_3 \cos(q_1 + q_2 + q_3)(\dot{q}_0) + b_6 \cos(q_2 + q_3)(\dot{q}_0 - \dot{q}_1) + b_4 \cos(q_1 + q_2 + q_3 - q_4)(\dot{q}_0)$$
$$+ b_7 \cos(q_2 + q_3 - q_4)(\dot{q}_0 - \dot{q}_1) + b_8 \cos(q_4)(-2\dot{q}_0 + 2\dot{q}_1 + 2\dot{q}_2 + 2\dot{q}_3 - \dot{q}_4)$$

$$\frac{\partial V}{\partial \dot{q}_4} = -c_5(-\dot{q}_0 + \dot{q}_1 + \dot{q}_2 + \dot{q}_3 - \dot{q}_4)$$
$$- b_4 \cos(q_1 + q_2 + q_3 - q_4)(\dot{q}_0) - b_7 \cos(q_2 + q_3 - q_4)(\dot{q}_0 - \dot{q}_1) + b_8 \cos(q_4)(\dot{q}_0 - \dot{q}_1 - \dot{q}_2 - \dot{q}_3)$$

where

$$
\begin{aligned}
a_1 &= g(m_1 d_1 + m_2 \ell_1 + m_3 \ell_1 + m_4 \ell_1 + m_5 \ell_1) \\
a_2 &= g(m_2 d_2 + m_3 \ell_2 + m_4 \ell_2 + m_5 \ell_2) \\
a_3 &= g(m_3 d_3) \\
a_4 &= g(m_4(\ell_4 - d_4) + m_5 \ell_4) \\
a_5 &= g m_5(\ell_5 - d_5)
\end{aligned}
$$

$$
\begin{aligned}
b_1 &= m_2 \ell_1 d_2 + m_3 \ell_1 \ell_2 + m_4 \ell_1 \ell_2 + m_5 \ell_1 \ell_2 \\
b_2 &= m_3 \ell_1 d_3 \\
b_3 &= m_4 \ell_1 (\ell_4 - d_4) + m_5 \ell_1 \ell_4 \\
b_4 &= m_5 \ell_1 (\ell_5 - d_5) \\
b_5 &= m_3 \ell_2 d_3 \\
b_6 &= m_4 \ell_2 (\ell_4 - d_4) + m_5 \ell_2 \ell_4 \\
b_7 &= m_5 \ell_2 (\ell_5 - d_5) \\
b_8 &= m_5 \ell_4 (\ell_5 - d_5)
\end{aligned}
$$

$$
\begin{aligned}
c_1 &= I_1 + m_1 d_1^{\,2} \\
c_2 &= I_2 + m_2 d_2^{\,2} \\
c_3 &= I_3 + m_3 d_3^{\,2} \\
c_4 &= I_4 + m_4 (\ell_4 - d_4)^2 \\
c_5 &= I_5 + m_5 (\ell_5 - d_5)^2 \\
c_6 &= (m_2 + m_3 + m_4 + m_5) \ell_1^{\,2} \\
c_7 &= (m_3 + m_4 + m_5) \ell_2^{\,2} \\
c_8 &= m_5 \ell_4^{\,2}
\end{aligned}
$$

Appendix V

Derivation of the Time Derivatives of the First Four Constraint Functions

The time derivatives of the first four constraint functions are derived below. They will be used to generate the joint angle profiles for the five-link biped robot to walk on a flat horizontal surface.

S_1: The erect body posture

$$S_1 = q_0 - q_1 - q_2$$

$$\dot{S}_1 = \dot{q}_0 - \dot{q}_1 - \dot{q}_2$$

$$\ddot{S}_1 = \ddot{q}_0 - \ddot{q}_1 - \ddot{q}_2$$

S_2: The overall progression speed

$$S_2 = \ell_1 \cos(q_0)\dot{q}_0 + \ell_2 \cos(q_0 - q_1)(\dot{q}_0 - \dot{q}_1) + d_3 \cos(q_0 - q_1 - q_2)(\dot{q}_0 - \dot{q}_1 - \dot{q}_2) - V_p$$

$$\int_{t_0}^{t} S_2 dt = \ell_1 \sin(q_0) - \ell_1 \sin(q_0(t_0)) + \ell_2 \sin(q_0 - q_1) - \ell_2 \sin(q_0(t_0) - q_1(t_0)) + d_3 \sin(q_0 - q_1 - q_2) - d_3 \sin(q_0(t_0) - q_1(t_0) - q_2(t_0)) - V_p(t - t_0)$$

$$\dot{S}_2 = \ell_1 \cos(q_0)\ddot{q}_0 - \ell_1 \sin(q_0)\dot{q}_0^2 + \ell_2 \cos(q_0 - q_1)\cdot(\ddot{q}_0 - \ddot{q}_1) - \ell_2 \sin(q_0 - q_1)(\dot{q}_0 - \dot{q}_1)^2 + d_3 \cos(q_0 - q_1 - q_2)(\ddot{q}_0 - \ddot{q}_1 - \ddot{q}_2) - d_3 \cos(q_0 - q_1 - q_2)(\dot{q}_0 - \dot{q}_1 - \dot{q}_2)^2$$

S_3: The bias of the knee of the support leg

$$S_3 = q_1 - \sigma$$

$$\dot{S}_3 = \dot{q}_1$$

$$\ddot{S}_3 = \ddot{q}_1$$

S_4: The coordination of the support leg and swing leg motion

$$S_4 = \ell_1 \sin(q_0) + \ell_2 \sin(q_0 - q_1) + 2d_3 \sin(q_0 - q_1 - q_2) - \ell_4 \sin(-q_0 + q_1 + q_2 + q_3) - \ell_5 \sin(-q_0 + q_1 + q_2 + q_3 - q_4) = 0$$

$$\dot{S}_4 = \ell_1 \cos(q_0)\dot{q}_0 + \ell_2 \cos(q_0 - q_1)(\dot{q}_0 - \dot{q}_1) + 2d_3 \cos(q_0 - q_1 - q_2)(\dot{q}_0 - \dot{q}_1 - \dot{q}_2) - \ell_4 \cos(-q_0 + q_1 + q_2 + q_3)(-\dot{q}_0 + \dot{q}_1 + \dot{q}_2 + \dot{q}_3) - \ell_5 \cos(-q_0 + q_1 + q_2 + q_3 - q_4)(-\dot{q}_0 + \dot{q}_1 + \dot{q}_2 + \dot{q}_3 - \dot{q}_4)$$

$$\begin{aligned}\ddot{S}_4 = {} & \ell_1 \cos(q_0)\ddot{q}_0 - \ell_1 \sin(q_0)\dot{q}_0^{\,2} + \ell_2 \cos(q_0 - q_1)(\ddot{q}_0 - \ddot{q}_1) - \ell_2 \sin(q_0 - q_1)(\dot{q}_0 - \dot{q}_1)^2 \\ & + 2d_3 \cos(q_0 - q_1 - q_2)(\ddot{q}_0 - \ddot{q}_1 - \ddot{q}_2) - 2d_3 \sin(q_0 - q_1 - q_2)(\dot{q}_0 - \dot{q}_1 - \dot{q}_2)^2 \\ & - \ell_4 \cos(-q_0 + q_1 + q_2 + q_3)(-\ddot{q}_0 + \ddot{q}_1 + \ddot{q}_2 + \ddot{q}_3) \\ & + \ell_4 \sin(-q_0 + q_1 + q_2 + q_3)(-\dot{q}_0 + \dot{q}_1 + \dot{q}_2 + \dot{q}_3)^2 \\ & - \ell_5 \cos(-q_0 + q_1 + q_2 + q_3 - q_4)(-\ddot{q}_0 + \ddot{q}_1 + \ddot{q}_2 + \ddot{q}_3 - \ddot{q}_4) \\ & + \ell_5 \sin(-q_0 + q_1 + q_2 + q_3 - q_4)(-\dot{q}_0 + \dot{q}_1 + \dot{q}_2 + \dot{q}_3 - \dot{q}_4)^2\end{aligned}$$